Institut für Wasserbau und Wasserwirtschaft

Technische Universität Darmstadt

MITTEILUNGEN

Heft 149 **2011**

REDA DIAB

Experimental Investigation on Scouring around Piers of different Shape and Alignment in Gravel

Institut für Wasserbau und Wasserwirtschaft

Technische Universität Darmstadt

Experimental Investigation on Scouring around Piers of different Shape and Alignment in Gravel

dem Fachbereich Bauingenieurwesen und Geodäsie
der Technischen Universität Darmstadt
zur Erlangung des akademischen Grades eines
Doktor-Ingenieurs (Dr.-Ing.)
vorgelegte

Dissertation

von

REDA Mahmoud Abd Elaal Ali DIAB
aus El-Mansoura (Ägypten)

Darmstadt im April 2011

D 17

Heft 149 **2011**

Diese Mitteilungsreihe hat zwei Wurzeln:

- die „Wasserbau-Mitteilungen“ (41 Hefte), begründet 1966 on Prof. Dr.-Ing. Friedrich Bassler, später fortgeführt von Prof. Dr.-Ing Josef Mock,
- die „Technischen Berichte über Ingenieurhydrologie und Hydraulik“ (54 Hefte), herausgegeben seit 1965 von Prof. Dr.-Ing. Dr.-Ing. E. h. Otto Kirschmer, später fortgefürt von Prof. Dr.-Ing. Ralph C. M. Schröder und Prof. Dr.-Ing. Manfred Ostrowski.

Mit dem Dienstantritt von Prof. Dr.-Ing. habil. Ulrich C. E. Zanke als Nachfolger von Prof. Mock sind diese beiden Reihen zusammengeführt worden. Die drei Fachgebiete des Instituts für Wasserbau und Wasserwirtschaftung.

- Ingenieurhydrologie und Wasserbewirtschaftung
- Wasserbau

Dokumentieren damit auch nach außen ihre Zusammengehörigkeit. Die neue Nummerierung ergibt sich aus der Summe der Hefte beider Vorgängerreihen.

Die „Mitteilungen des Instituts für Wasserbau und Wasserwirtschaft der Technischen Universität Darmstadt“ erscheinen in unregelmäßiger Folge im Eigenverlag des Instituts für Wasserbau und Wasserwirtschaft. Ein Nachdruck, auch auszugsweise, ist nur mit Genehmigung des Geschäftsführenden Institutsdirektors gestattet.
(ISSN 1430-3434)
ISBN 3-936146-19-5

FG Ingenieurhydrologie
u. Wasserbewirtschaftung
Petersenstraße 13
64287 Darmstadt
Tel.: 0 6151/16 21 43
FAX: 06151/ 16 32 43
e-mail: ostrowski@ihwb.tu-darmstadt.de

FG Wasserbau
Petersenstraße 13
64287 Darmstadt
Tel.: 0 6151/ 16 40 67
FAX: 0 61517 16 32 23
e-mail:wabau@wb.tu-darmstadt.de

Aktuelle Informationen über das Institut und seine Lehrangebote finden Sie im World Wide Web unter: http://wabau.kww.bauing.tu-darmstadt.de

Referent: Prof. Dr.-Ing. habil. Prof. h.c. U.C.E. Zanke
Koreferent: Asst. Prof. Dr.-Ing. Oscar Link

Tag der Einreichung: 15. Dezember 2010
Tag der mündlichen Prüfung: 04. April 2011

Herausgeber:

Prof. Dr.-Ing. habil. Prof. h.c. U.C.E. Zanke (Wasserbau)
Prof. Dr.-Ing. M. Ostrowski (Ingenieurhydrologie und Wasserwirtschaftung)

VORWORT

Brücken über Flüsse und Küstengewässer unterliegen besonderen Gefahren im Bereich der Gründung, da örtliche Erosionen, so genannte Kolke, entstehen können. Diese Kolke werden von den umströmten Brückenfundamenten selbst hervorgerufen, weil die Fundamente in der Strömung als Störkörper. Die Tiefe der Kolke kann an kreiszylindrischen Pfeilern Werte bis zum etwa 2,5-fachen der Pfeilerdurchmesser erreichen. Deswegen und weil der Kolkprozess, wenn er erst einmal einsetzt, sehr schnell vonstatten geht, stürzen auf der gesamten Welt immer wieder Brücken ein, bei denen die Kolkproblematik bei der Planung durch die Brückenbauer falsch eingeschätzt worden war.

Die meisten Forschungen über Pfeilerkolke wurden für kreiszylindrische Pfeiler ausgeführt. Weniger Kenntnisse liegen für die ebenfalls häufig verwendeten quadratischen oder rechteckigen Pfeiler und Gründungskörper vor. Dann kommt noch ein weiterer Parameter hinzu: die Anströmungsrichtung.

Über Kolke an nicht kreiszylindrischen Pfeilern, ggf. auch noch mit Schräganströmung, gibt es relativ wenig veröffentlichte Untersuchungen, oft nur aus Laboruntersuchungen mit verhältnismäßig kleinen Dimensionen.

Vor diesem Hintergrund hat sich Herr Dr.-Ing. Reda Diab in seiner Dissertation mit den vorstehend genannten, offenen Fragen an eckigen Pfeilern auseinandergesetzt und großmaßstäbliche Kolkmessungen durchgeführt. Die Ergebnisse seiner Arbeit sind nicht zuletzt wegen der besonderen, von ihm mitentwickelten Messtechnik und der Systematik eine hervorragende Grundlage für weiterführende Arbeiten zu Kolken an nicht kreiszylindrischen Brückenpfeilern.

Darmstadt, im Mai 2011

Prof. Dr.-Ing. habil. Prof. h.c. Ulrich C. E. Zanke

DEDICATION

For my mother and my family who offered me unconditional love

and support throughout the course of this thesis

To my wife and kids

Ahmed

Mohamed

Basmala

ACKNOWLEDGMENTS

First and foremost, I would to give grace to the Almighty Allah for holding my hand throughout the completion of this work.

I wish to express my sincere appreciation and deep sense of gratitude to my supervisors Prof. Dr.-Ing. habil. Prof. h.c. Ulrich Zanke and Asst. Prof. Dr.-Ing. Oscar Link, for guidance, encouragement and invaluable advice throughout my PhD study. I am heartily thankful to them for sharing their wealth of knowledge from the very beginning to the final level enabling to develop an understanding of the subject.

My sincere acknowledgement also goes to my Advisory Committee remembers for their invaluable and helpful suggestions and guidance in this work

I thankfully acknowledge the financial support provided by the Egyptian Government through a PhD Grant, and by the germen research council, DFG for grant ZA 93/14-1.

All my profound gratitude goes to my Colleagues of the Institute of Hydraulic Engineering of Darmstadt University of Technology for their friendship and helpful during the years of my PhD. Specially gratitude and thankful for Prof. Dr.-Ing. Nicole Saenger, Dr.-Ing. Andreas Wurpts, and Dr.-Ing. Jans Uwe-Wieseman.

Special thanks to Dip.-Ing. Bindernagel, Mr. Dreieicher, Mr. Hahn, Mr. Heiligenthal, Mr. El-masbahi and Mr. Ganzert for their assistance and help throughout the laboratory program.

I would also like to express my gratitude to Mrs. Wicke, Mrs. Huxhorn and Mrs. Zeitler for their assistance throughout this work.

I want to use this opportunity to express my sincere thankfulness to my family members for their all the time love, understanding and support in the course of this program, specially my mother, wife and my son “the best friend” Ahmed.

Lastly, I offer my regards and blessings to all of those who supported me in any respect during the completion of the study.

Institute for Hydraulic and Water Resources Engineering

Darmstadt University of Technology

Experimental Investigation on Scouring around Piers of different Shape and Alignment in Gravel

A Dissertation

Submitted to the Department of Civil Engineering and Geodesy of
Darmstadt University of Technology
in partial fulfillment of the requirements for degree of
''Doktor-Ingenieur (Dr.-Ing.)''

by

REDA Mahmoud Abd Elaal Ali DIAB

from El-Mansoura (Egypt)

Supervisors

Prof. Dr.-Ing. habil. Prof. h.c. U. C. E. Zanke

Asst. Prof. Dr.-Ing. Oscar Link

Darmstadt, April 2011

ABSTRACT

Bridge scour is the leading cause of bridge failure all around the world, affecting significantly on the total construction and maintenance costs. Therefore, scouring around piers and abutments has been extensively studied in the past, focusing on point measurements of scour depth in front of a circular pier in alluvial sand beds. A literature review showed, that there is still a lack of studies on the effects of main scour parameters on the scour hole geometry, and on the mechanism of local scour around piers of different shape and alignment in gravel beds. This thesis attempts to fulfill this gap by experimentally investigating the development of scour holes around piers of different shape and alignment in gravel and sand beds. New non-intrusive, high resolution topography measurements of complete developing and equilibrium scour holes were performed during the experiments with an experimental installation using a laser distance sensor (LDS) and positioning systems. Additionally, the turbulent flow field around a square pier in gravel bed is measured with the acoustic doppler velocimeter (ADV) providing an insight into the complex flow field.

The spatio-temporal variations of the geometric characteristics of developing scour holes are analyzed including the scour hole topography, time-dependent and equilibrium scour depth, scour extent, scour slopes and scoured volume. Firstly, the general observations made for each experiment are presented. All the obtained data are then analyzed in comparisons, as a function of the pier shape, angle of attack and sediment sizes. Empirical equations for the prediction of scour depth, scour radius and scoured volume as well as new pier shape and angle of attack adjustment factors were also obtained. Further, numerous prediction equations of time-dependent and equilibrium scour depths are evaluated. Effect of the pre-estimated experiment time on measuring and predicting the scour depth is also discussed.

The measured situation rather than an assumed inverted scheme of the developing scour hole shape is presented. Scouring starts and progresses fast at the pier sides, and eventually propagates rather rapidly towards the centerline of the pier front. Scoured region surrounds the pier faster at circular than at square piers, faster at square than at rectangular piers, faster at non-aligned than at aligned piers, and also faster in gravels than in sands. The deepest point of the scour hole which is initially located at the pier sides migrates to the centerline of the pier front, during the first hour in gravel bed, and after 1.5 - 2.5 days running time in sand beds.

The time-dependent scour depth develops, in the laboratory dimensions, with different decreasing rates during the first 10 - 30 % of the experiments time (four days), faster at sides than at front of the piers, faster at square and rectangular than at circular piers, faster at non-aligned than aligned piers, and also faster in gravel than in sand bed. Then it

develops with nearly the same rate in all cases to the end of experiments. The highest and lowest scour depths are observed at the square and circular piers respectively. The larger the angle of attack the smaller the scour depth at the square pier is observed.

The shape of the scour hole profiles in different planes remains nearly constant during development, as a nearly uniform slope over a ring shaped portion close to the pier. The average scour side slopes are at the square and rectangular steeper than at the circular piers, and do not exceed the natural repose angle of sediment particles under water. There is only one exception that the steeper slope is observed in the lower part of the profile at the pier front in gravel bed, showing the action of vortex system with different strengths that being lower towards the upper part of the scour hole.

The longitudinal extent and the lateral width of the developing scour hole at the square pier are in average 1.50 and 1.22 times those at the circular pier respectively, and increase with the rectangular pier length to width ratio by 10 - 20% for L/B = 2 and 4. The extent and width of developing scour in gravel bed is about 1.75 - 3.25 and 1.55 - 1.70 times those in coarse and fine/medium sand beds, respectively.

The assumption that there is no effect of sediment coarseness ratio D/d_{50} on the scour depth when it exceeds 25 - 50 does not sound reliable, as shown via the present study. The equilibrium scour depth which firstly increases with the sediment coarseness ratio, decreases again when the ratio exceeds 30, and seems to be unaffected at very higher values of the ratio (values > 500).

The discussion of the definitions of time to equilibrium showed, that variety of equilibrium scour depths can be reached depending on which definition of equilibrium time is adopted. Even though the discussed definitions of equilibrium time indicated that the equilibrium was achieved in the present study, the measured data showed that a truly equilibrium scour state is not attainable.

The volume of developing scour hole is correlated well with the scour time as well as the maximum scour depth at the pier front. Thus, when providing maximum scour depth at the pier front, the obtained correlations can be used to calculate scour-hole.

Laboruntersuchung der Kolkung um Pfeiler mit verschiedenen Formen und Anströmungswinkel in Kies

Kurzfassung

Die lokale Kolkbildung an Pfeilern ist vor allem im Bereich des wasserbaulichen Ingenieurwessens ein wichtiges Thema. Bislang wurden hauptsächlich Laborversuche zur Kolkung an schlanken zylindrischen Pfeilerformen in sandigem Boden durchgeführt. Die meisten dieser Untersuchungen konzentrierten sich auf das Messen und die Vorhersage der zeitlichen Entwicklung und der maximalen Kolktiefe. In der Literatur, z. B. Hoffmans und Verheij (1997) finden sich Korrekturfaktoren zur Anwendung bei nicht kreisförmigen Pfeilerformen oder schräger Pfeileranströmung. Hinweise auf die zeitliche Entwicklung der Kolkgeometrie um Pfeiler sind in der Fachliteratur in nur geringem Umfang vorhanden.

In dieser Forschungsarbeit wird die zeitabhängige Entwicklung der dreidimensionalen Kolkgeometrie an verschiedenen Pfeilerformen und mit variierten Anströmungswinkeln sowohl in Sand als auch in Kies mittels Laborversuchen untersucht und dargestellt. Neue berührungslose und hoch aufgelöste Messungen der vollständigen zeitlichen Entwicklung und der Gleichgewichtphase der Kolkgeometrie werden während der laufenden Versuche mit einen Laser-Distanz-Sensor (LDS), welcher innerhalb des Plexiglaspfeilers installiert ist, durchgeführt. Darüber hinaus wird das turbulente Strömungsfeld um den Pfeiler in Kies mittels einer ADV-Sonde gemessen.

Die zeitliche Entwicklung der Kolkbildung wird analysiert. Dabei werden die Topographie, die Ausdehnung, das Volumen und die Tiefe des Kolks sowohl während der zeitlichen Entwicklung als auch im Gleichgewichtszustand näher betrachtet. Diese Kolkcharakteristika werden in Abhängigkeit der eingebauten Pfeilerform, des eingestellten Anströmungswinkels und des verwendeten Sediments ausgewertet. Neue empirische Formeln zur Vorhersage der Kolktiefe, Kolkausdehnung und des Kolkvolumens sowie neue Korrekturfaktoren für die Pfeilerform und -ausrichtung werden entwickelt. Zu nennen ist insbesondere die Formel von Zanke (1982), für die eine Anpassung an zylindrische and quadratische Pfeiler sowie für Kies als Sediment gegeben werden können. Außerdem werden Gleichungen, die der Vorhersage von Kolktiefen dienen, überprüft und bewertet.

Table of Contents

TABLE OF CONTENTS

Table of Contents

Table of Contents

LIST OF FIGURES

List of Figures

List of Figures

List of Figures

List of Figures

List of Figures

List of Figures

List of Figures

LIST OF TABLES

NOMENCLATURES

B	Pier width
D	Pier diameter
$d_{15.9}$	Grain size for which 16% by weight of the sediment is finer
d_{50}	Median size of sediment particle
$d_{84.1}$	Grain size for which 84% by weight of the sediment is finer
d_*	Sedimentologic diameter of sediment particle $= d_{50}\left[\Delta g/\upsilon^2\right]^{1/3}$
$D*$	Effective diameter of the pier
Fr_1	Froude number of flow $= u/\sqrt{gh}$
F_d	Densimetric Froude number $= u/\left(\Delta g\, d_{50}\right)^{1/2}$
g	Gravitational acceleration
g'	Reduced gravitational acceleration $= \{(\rho_s - \rho)/\rho\}g$
h	Section-average flow depth
K	Bottom width of a scour hole
k_d	Sediment size factor
k_I	Flow intensity factor
k_h	Flow shallowness factor
k_{sh}	Pier shape factor
k_t	Time factor
$k_{\alpha,L/B}$	Flow angle of attack factor
L	Pier length
L_R	Reference length $= b^{\alpha}h^{\beta}$, and $\alpha + \beta = 1.0$
N	Pier shape factor (1.0 for circular and 1.25 for square piers)
R	Radius of a scour hole at a single point on its surface
R^2	Determination coefficient
t	Scour time
t_1	Time at which scour depth equal to pier width
t_e	Time to equilibrium scour
T	Total test duration

Nomenclatures

T_d	Dimensionless scour time $= t / t_R = \left\{ \left(\Delta \mathrm{g}\, d_{50} \right)^{1/2} / L_R \right\} t$
u	Section-average velocity at the undisturbed bed
u_{cr}	Critical flow velocity
u^*	Shear velocity
w_s	Settling velocity of sediment particles
W	Top width of a scour hole $= y_s (K + \cot \phi)$
x, y	Variables
y_s	Scour depth
Z	Depth of a scour hole at a single point on its surface
Z_t	Maximum developing depth of scour at any time
Z_{eq}	Maximum scour depth at the end of the given time duration
γ	Coefficient (0.20 -0.40)
$\forall$	Scour volume
Δ	Relative density $= (\rho_s - \rho) / \rho$
ρ	Water density
υ	Kinematic viscosity
g	Gravity acceleration
σ_s	Geometric standard deviation of sediment size distribution $= \sqrt{d_{84.1} / d_{15.9}}$
θ	Angle of azimuthal half-plane with the principle flow direction
ϕ	Natural repose angle of sediment particles
α	Flow angle of attack
ω	The effect velocity increase due to the turbulence

CHAPTER 1
INTRODUCTION

1.1 BACKGROUND

Scour is a natural phenomenon, caused by the erosive action of flowing water over alluvial beds in rivers and streams (Breusers et al. 1977, Barbhuiya and Dey 2004). It occurs when the critical condition for initiation of sediment transport is exceeded locally. This might happen as a result of natural flow or man-induced flow acceleration due to water works. Scour at bridge elements (piers and abutments) is one of the common examples of the effect of human river interference.

Bridge scour is the leading cause of bridge failure all around the world. It also has the major effect on the total construction and maintenance costs. About 383 bridge failures in the United States are caused by 25% pier scour and 75% abutment scour (Richardson and Davis 2001). It is estimated that an optimization potential of bridge costs up to 40% when scour depth is accurately taken into account (Dumas and Krolack 2002). Therefore, a good understanding of the scour process and better estimation of scour dimensions are of utmost importance in civil engineering.

Local pier scour is a complex three dimensional phenomenon, which occurs as a result of the strong flow-sediment-pier interaction. The scour mechanism and the flow field in sand beds have been extensively studied in the past (Muzzammil and Gangadhariah 2003, Unger and Hager 2007, Dey and Raikar 2007, Kirkil et al. 2008, Gobert et al. 2010). However, less information is available on scour in gravel beds (Ettema 1980). Raikar and Dey (2005a, 2005b) presented experimental results on scour in uniform gravel, analyzing the effect of gravel size and gradation on the equilibrium scour depth. In their work, authors concluded that significant differences in scour are expected depending on the sediment type i.e. sand or gravel.

Several numerical and laboratory investigations have been conducted to quantify the maximum scour depth at bridge piers. Most of the studies have been focused on equilibrium scour depth in alluvial sand beds, such as Breusers et al. (1977) and Melville and Sutherland (1988). Work on the estimation of time dependent scour depth has been conducted by many researchers, such as Zanke (1982a), Dey (1999) and Oliveto and Hager (2002). Most of these experimental researches are devoted to point-measurements of scour depth in front of a circular pier, resulting in a lot of empirical prediction equations for both time dependent and equilibrium scour depths. Methods for estimating the scour depth at other pier shapes and alignments (Hoffmans and Verheij 1997, Melville and Chiew 1999, Richardson and Davis 2001) are based on the knowledge of local scour at circular ones and correction factors. Different shape factors were suggested

based on few laboratory researches (Tison 1940, Chabert and Engeldinger 1956, Laursen and Toch 1956), and used as multiplying correction factors in almost all prediction methods. Moreover, there is only one design curve suggested by Laursen and Toch (1956) to account the effect of angle of attack. This curve is suitable for rectangular piers with a pier length to width ratio between 2 and 16. However, no systematic studies on the effect of pier shape and alignment on local scour are conducted since then.

Furthermore, investigations on the geometric properties of scour holes, as known to the author, are rarely found in the specialized literature (Dargahi 1987, Yanmaz and Köse 2007, Link et al. 2008b). Hoffmans and Verheij (1997) presented sketches of scour hole topography for equilibrium scour holes based on few available references. The knowledge of geometric features of the scour hole provides useful information for the design of the bridge foundation size and for the selection of the appropriate scour countermeasures.

1.2 OBJECTIVES AND SCOPE OF WORK

The general objective of this thesis is to investigate experimentally the spatio-temporal variation of scour hole around piers of different shape and alignment in both sand and gravel beds. Consequently, the specific objectives are:

- Development and application of an experimental installation for the measurement of scour development,
- Measurement and characterization of the scour hole development around piers,
- Measurements and characterization of the flow field at a square pier,
- Quantification of the effect of sediment size on scouring in sand and gravel beds,
- Quantification of the effect of pier shapes on scour development, and
- Quantification of the effect of flow angle of attack on scour at piers.

In order to achieve these objectives, series of experiments were conducted at the Hydraulic Laboratory of the Institute for Hydraulic and Water Resources Engineering, Darmstadt University of Technology, (Germany). In chapter 2, the background and current state of the knowledge of local scour and literature related to the thesis objectives are presented. In chapter 3, experimentation including dimensional analysis, experimental setup and measuring techniques is presented. Chapter 4 shows the results of clear-water scour experiments with piers of different shape and alignment, including a description of the topography of the developing and equilibrium scour holes, of the side slopes of the scour hole, of the developing and equilibrium scour hole depth and of the scoured volume as well as the measured flow field around the square pier. Analysis and discussion of the time development of maximum scour hole depth, radius, slopes and volume are covered

in chapter 5. Finally, chapter 6 presents the principle conclusions drawn from the results of the study and recommendations for future works.

The author has already published partial results of the current work in international indexed journals, conferences, symposiums and workshops. Among the seven published papers, five summarise specific results on the time development of scour holes geometry in gravel and sand beds around square and circular piers under clear water conditions (Diab et al. 2008a, 2008b, 2008c, 2010a, 2010c). Remaining two papers, account for the experimental measurement and characterization of the 3D turbulent flow field around a square pier in both a fixed and a mobile gravel bed under the clear water condition (Diab et al. 2009, Diab et al. 2010b).

CHAPTER 2
BACKGROUND: STATE OF THE ART

Many papers have been published on scouring around bridge piers founded in cohesionless sediment beds. This chapter attempts to present a review of relevant literature. The chapter begins with general speaking on bridge scour definitions, types and regimes. The local scour process and flow velocity field around piers are reviewed and some of related studies are summarized. Local scour parameters are presented in brief. The effects of pier shape and angle of attack on local scour are discussed. Next, developing and equilibrium scour depth definitions and formulas are included. Finally, the present understanding of the geometry of scour hole bridge piers is presented.

2.1 STATE OF THE ART

2.1.1 Bridge Scour Definition, Types and Regimes

Scour Definition

Scouring at bridges is defined as the lowering of the stream bed at its piers and abutments as a result of the erosive action of flowing water (BSC 2005, Richardson and Richardson 2008). Scour can be caused by either base-flow or by flood events, when the bed shear stress at the pier foundation exceeds the critical bed shear stress. Usually the scouring rate is much higher during flood events.

Scour Types

Types of scour at bridges consist of long-term aggradation and degradation, general scour, contraction scour and local scour. In addition, bed form propagation through the bridge site may play a role resulting in an increase of the scour (Melville and Coleman 2000, BSM2005, Richardson and Richardson 2008).

Long-term aggradation or degradation are the deposition or the erosion of sediment material in the bridge reach, as a part of an overall rising or lowering of the stream bed over long times due to natural or man-induced causes.

General scour refers to the lowering of the stream bed due to instability of flow through river meanders or at tidal inlets. In river meandering, the flow depth and velocity are higher at the outside than at the inside of a bend. This results in scour at the outer part and deposition at the inner part of the bend. Thus, an overall rising or lowering of the stream bed should be considered if the bridge foundation is located in meanders. Tidal inlet instability is similar to meanders but the temporal variation of scouring differs and also

tidal flows reverse often its direction (FHWA No. 20, HEC-20). General scour is different from long-term degradation because it may be cyclic and/or related to a flood event.

Contraction scour is the erosion of the sediment from the stream bed and banks as a result of increased velocities and shear stresses due to a reduction in the flow cross-section area at the bridge sites. It may occur under clear water or live bed conditions.

Local scour refers to the erosion of the sediment from the vicinity of the bridge piers or abutments. The increased turbulences, pressures and velocities and the induced secondary flow in form of vortices and downflow are considered as the main cause of local scour. It can be either clear water or live bed scour.

Bed form propagation through the bridge site, may also play a role. Bed forms refer to the pattern of regular or irregular waves that may result from water flow over a sediment bed. These forms may propagate either in the same or in the opposite direction of the flow and may increase or decrease the total scour at bridges.

The combined sum of the previous components of scouring in addition to bed forms propagation effect determines the total scour at a bridge pier or abutment.

Scour Regimes

Local scour regimes are divided into two categories (Chabert and Engeldinger 1956): (i) clear water scour that occurs when there is no sediment feeding from upstream of the bridge into the scour hole, and (ii) live bed scour when there is continuous feeding with sediment from upstream. The velocity or bed shear stress is used as indicator for clear water scour or live bed scour conditions. If the mean flow velocity or the average bed shear stress upstream of the bridge is less than the critical flow velocity or the critical bed shear stress of the median diameter of the bed material, then clear water scour conditions are achieved.

2.1.2 Local Scour Process and Flow Field around Piers

The flow field at a bridge pier is a complex three dimensional turbulent phenomenon resulting from strong flow-pier-sediment interaction. The basic mechanism causing local scour at piers is the increased turbulence and the induced secondary flow in form of vortices and downflow around a pier (Shen et al. 1969, Melville 1975, Breusers and Raudkivi 1991, Hoffmans and Verheij 1997, Muzzamil et al. 2004). Flowing towards the pier, the flow velocity goes to zero on the upstream face of the pier, called stagnation point. This causes an increase of the pressure at the pier. As the flow velocity decreases from the surface to the bed, the pressure on the pier face decreases accordingly. The downward pressure gradient forces the flow down the pier face. The resulting downflow

impinges on the bed and creates a hole in the vicinity of the pier base. The downflow rolls up again as it continues to create a hole and by interaction with the coming flow forms a complex vortex system, called horseshoe vortex. This develops as a result of flow separation at the upstream face of the scour hole. The horseshoe vortex is very effective in transporting sediment particles away from the pier. As the scour depth increases, the strength of the horseshoe vortex diminishes, leading to a reduction of the scouring rate. At the downstream face of the pier a wake vortex system is formed due to the separation of the flow on the pier sides. Both the horseshoe and the wake vortices erode sediment from the base region around the pier. The wake vortex intensity reduces with the distance and as a result the eroded sediment deposits downstream the pier. Figure 2.1 shows sketch of features of flow around a circular pier.

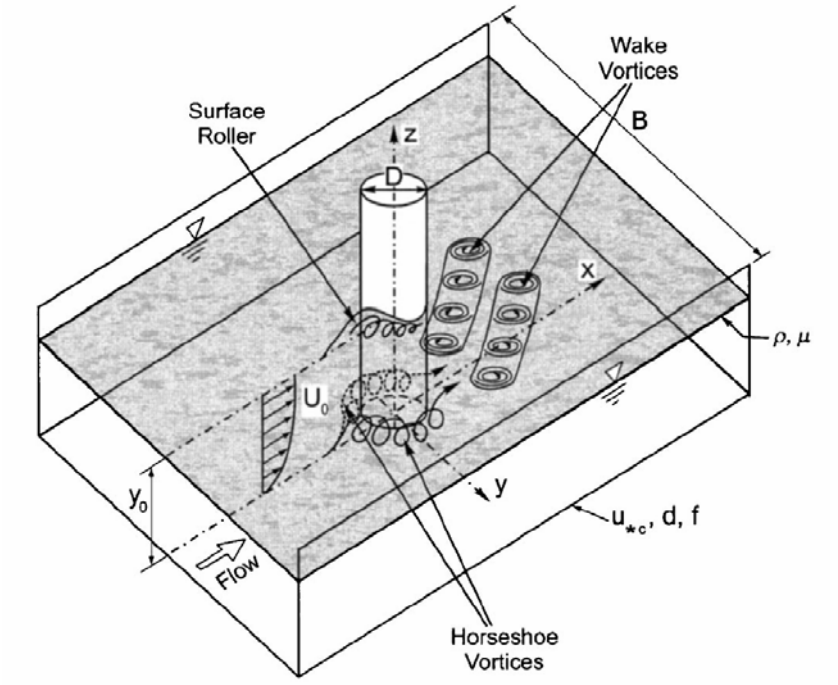

Figure 2.1. Flow field features around a circular pier (Ettema et al. 2006)

Many studies investigating experimentally and numerically the flow field around the bridge piers have been carried out, such as Dargahi (1987), Muzzammil and Gangadhariah (2003), Unger and Hager (2007), Dey and Raikar (2007), Kirkil et al. (2008), Link et al. (2008a), and Gobert et al. (2010). Flow field has been investigated with different experimental techniques, e.g. hydrogen-bubble flow visualization technique, acoustic doppler velocimeters (ADV), acoustic Doppler velocity profilers (ADVP), and particle image velocimetry (PIV) and numerical techniques in both plane and scoured beds under clear-water and live-bed conditions at circular piers.

In 1987, 1989, and 1990, Dargahi presented laboratory experiments where the horseshoe vortex was visualized at the front of a circular pier in the symmetry plane using the hydrogen bubble technique. Different experiments were carried out with pier Reynolds numbers $Re_{pier} = u\ D\ /v$ =8400, 20000, 39000 and 46000, where u is the section-averaged flow velocity, D is the cylinder diameter and v is the kinematic viscosity of the fluid. It is found that the vortex structure at the pier front is linked to the scour profiles in fine sand.
Sarker (1998) performed measurements of instant point velocities around a cylinder in a scoured sand bed with the ADV. Although the researcher presented time-average flow field, he did not mention anything about the turbulent characteristics of the flow.
In 1998, Graf and Yulistiyanto performed measurements of the flow field around a cylinder in a fixed plane bed with the ADVP, registering time averaged velocity field, turbulent velocity fluctuations as well as determining turbulent flow field properties, i.e. Reynolds stresses, turbulent kinetic energy distribution, and vorticity. They concluded that at the front of the cylinder the horseshoe vortex is confined to 15% of the flow depth.
Graf and Istiarto (2002) applied the same methodology as Graf and Yulistiyanto (1998) in order to measure the flow field around a cylinder in a scoured sand bed. Results showed time averaged and turbulent-fluctuating characteristics of flow.
Muzzammil and Gangadhariah (2003) visualised the horseshoe vortex in front of a circular pier founded in sand bed (d_{50} = 0.16 and 0.60 mm) by injecting a benthonite solution into the flow. They observed an elliptic form of the horseshoe vortex, determined its geometry as well as the tangential velocity of the vortex. However, the accuracy of this flow visualization method is questionable, as discussed by Unger and Hager (2005).
Muzzammil et al. (2004) investigated experimentally the features of horseshoe vortices around a circular pier embedded in a sand bed during scouring. The mudflow visualisation technique was used to visualise the horseshoe vortex in front of the pier. Results show that the shape of the vortex, i.e. circular or elliptical, is dependent on the pier Reynolds number. The horizontal dimension of the vortex has been found to be a function of the pier form.
Later, Unger and Hager (2007) studied the characteristics of downflow and horseshoe vortex at the vertical plane at the front of a wall-side attached half cylinder by using the PIV. Two sediment sizes were used, a uniform sand with d_{50} = 1.14 mm and σ = 1.18 as well as a non-uniform sand mixture with d_{50} = 5.00 mm and σ = 2.29. The obtained data provided an experimental data bases for numerical simulation.
Dey and Raikar (2007) presented spatial characteristics of horseshoe vortex in developing scour holes in different azimuthal planes around a cylinder using an ADV. Their results added valuable knowledge on time variation of the flow field during scour in a non cohesive soil.

A numerical experiment was presented by Kirkil et al. (2008), using the large eddy simulation technique (LES) on the horseshoe vortex system around a circular pier on equilibrium scoured sand bed. Results for two cases with relative small Reynolds numbers were discussed.
Link et al. (2008a) studied the instantaneous flow field around a circular cylinder in sand scoured beds using the model proposed by Manhart (2004). Link (2008b) presented detailed measurements on spatio-temporal development of scour around a circular pier in coarse sand, linking slopes of the scour hole to the horseshoe vortex system.
Tseng et al. (2000) simulated numerically the three dimensional turbulent flow field around circular and square cylinders. The results showed that the downflow strength and the domain of the high bed shear stress were greater in the case of the square pier.
Raikar and Dey (2005a and b) presented experimental results of scour around circular and square piers in uniform gravel, analyzing the effect of gravel size and gradation on equilibrium scour depth. In both mentioned studies, it was concluded that significant differences in scouring are expected depending on the sediment type i.e. sand or gravel.
Recently, Diab et al. (2009) and (2010b) investigated experimentally the turbulent flow field around a square pier in plane and scoured gravel beds using an ADV. The measurements were carried out under clear water conditions in different azimuthal half-planes with θ = 0, 45, 90, 135 and 180º around the pier. The results showed the spatial distribution of time-averaged velocity components, velocity vector and absolute velocity as well as turbulence intensities and turbulent kinetic energy. Their results are useful for calibration and validation of the advanced numerical models.

2.1.3 Local Pier Scour Parameters

The following discussion of local scour factors is limited to scouring at piers founded in cohesionless sediment and under current action. According to Breusers et al. (1977), Raudkivi and Ettema (1983), Breusers and Raudkivi (1991), Hoffmans and Verheij (1997), Melville and Coleman (2000), Richardson and Davis (2001) and BSC 2005 the local pier scour parameters are given as follows:

- Fluid parameters: water density (ρ), kinematics viscosity (υ) and gravity acceleration (g),
- Flow parameters: approaching flow depth (h), mean flow velocity (u) and critical flow velocity (u_{cr}),
- Sediment parameters: density (ρ_s), grain size ($d_{84.1}, d_{50}, d_{15.9}$), grain form, gradations ($\sigma_s = \sqrt{d_{84.1} / d_{15.9}}$) and angle of repose ($\phi$),

- Pier parameters: shape in horizontal section (circular, squared, rectangular and other shapes), size (diameter D, width B and length L), and alignment (the angle of flow attack; α), and
- Time parameter, t, which is added by Dey (1997).

The local scour depth and its dependent parameters can be related mathematically as:

$$f\left\{\overbrace{Z}^{Scour depth},\underbrace{h,u,u_{cr}}_{Flow},\overbrace{\rho,g,\upsilon}^{fluid},\underbrace{\rho_s,d_{50},\sigma_s,\phi}_{Sediment},\overbrace{D,B,L,\alpha}^{Pier},\underbrace{t}_{time}\right\}=0 \qquad [2.1]$$

Where: f *is* a general function and Z is the maximum depth in the scour hole.

According to dimensional analysis technique and π-Buckingham theorem, equation [2.1] can be rewritten in dimensionless form as (assuming constant relative density and no viscous effect):

$$f\left\{\frac{Z}{D},\frac{Z}{h},\frac{h}{D},\frac{u}{u_{cr}},\frac{D}{d_{50}},\frac{d_{50}}{h},\sigma_s,k_{\alpha,L/B},k_{sh},\frac{ut}{D},\frac{t}{T}\right\}=0 \qquad [2.2]$$

Where: The flow depth to pier diameter or width ratio h/D or h/B is termed the flow shallowness. The ratio between approach and critical flow velocities u/u_{cr} is called flow intensity and controls the scour condition, i.e. clear-water or live-bed conditions. The pier diameter or width to sediment size ratio D/d_{50} is named sediment coarseness. The sediment gradation is characterized by using the geometric standard deviation $\sigma_s=\sqrt{d_{84.1}/d_{15.9}}$. The size and gradation of the sediment material affect on the time required to reach the equilibrium scour and if the armouring will occurs or not. The two parameters $k_{\alpha,L/B},k_{sh}$ are correction factors for the shape and alignment of noncircular piers. The last two parameters ut/D and t/T provide the time effect, where T is the time required to reach the maximum equilibrium local scour depth. A brief summery of the effect of the mentioned scour parameters is given below.

Flow intensity effect, u/u_{cr}

Flow intensity u/u_{cr}, defined as the ratio of the mean approach flow velocity to the critical velocity (threshold velocity for the motion of the sediment in the approaching flow), is used extensively as indicator of scour conditions (Raudkivi and Ettema 1983, Breusers and Raudkivi 1991, Hoffmans and Verheij 1997). For uniform sediment material, clear water scour occurs for flow intensity up to unity, for which there is no sediment supply from the upstream to the scour hole. Live bed scour occurs when flow intensity exceeds the unity. For non-uniform sediment, the limiting armouring velocity

u_a controls scour conditions in addition to the flow intensity (Melville and Sutherland 1988). For non uniform sediment material, clear water scour conditions exist when $[u-(u_a-u_{cr})]/u_{cr}<1$ and live-bed scour occurs when $u/u_a>1$.

For clear-water scour conditions, the equilibrium scour depth in uniform sediment increases almost linearly with the flow velocity to a maximum at the critical velocity which is called as threshold peak, see figure 2.2. As the mean flow velocity exceeds the critical velocity, the average scour depth first decreases and then increases again to a second peak which is called the live-bed peak. This second peak occurs at the transition flat bed conditions and does not exceed the threshold peak. Other investigators noted that the live-bed peak may exceed the threshold peak at higher velocities.

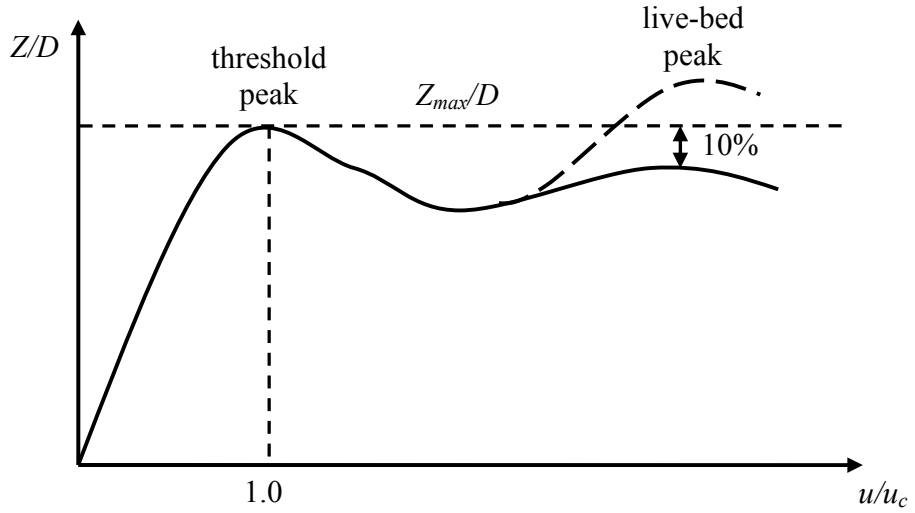

Figure 2.2. Local pier scour depth versus flow intensity
(Modified after Breusers and Raudkivi 1991)

Flow shallowness effect, h/D

The flow depth to pier diameter (or pier width) ratio *h/D* is known as flow shallowness and represents the effect of flow depth on local scour. Many researchers have been investigated the effect of flow depth on the local scour depth at piers, such as Laursen and Toch (1956), Breusers (1977), Ettema (1980), and Chiew (1984). They concluded that the scour depth increases with the flow depth up to a limiting value for the flow shallowness ratio. This value is about 2.6 according to Melville and Sutherland (1988). Beyond this value, the local scour depth becomes independent of the flow depth. Figure 2.3 shows the relative local scour depth versus flow shallowness. Melville and Coleman (2000) present a useful classification of scour processes at bridge piers depending on the flow shallowness as shown in table 2.1. The interference between the two rollers which are the

horseshoe vortex at the base of the pier and the surface bow wave help to understand the effect of flow depth. For narrow pier class or deep flow, there is no interference between the two rollers and the scour depth depends only on the pier width. While at wide piers, the interference between the bow wave and the horseshoe vortex which rotates in opposite direction reduces the capability of the horseshoe vortex to entrain sediment from the scour hole. That results in a decrease of the scour depth with a decrease in the flow depth. For intermediate width class, the scour depth depends on both parameters flow depth and pier width.

Table 2.1. Classification of local scour processes at bridge piers.

Class	D/h	Local scour dependence
Narrow pier	$D/h < 0.70$	$z \propto D$
Intermediate width pier	$0.70 < D/h < 5.0$	$z \propto \sqrt{hD}$
Wide pier	$D/h > 5.0$	$z \propto h$

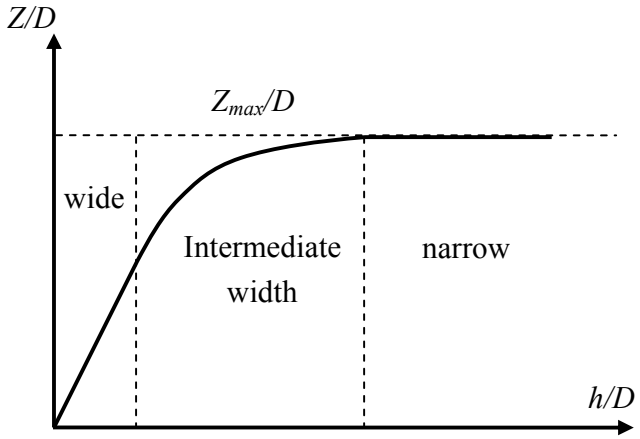

Figure 2.3. Local pier scour depth versus flow shallowness (Melville and Coleman 2000)

Sediment size, coarseness and gradation effect

Sediment size in sand size range has little effect on scour depth but will affect the time required to reach the equilibrium (Hoffmans and Verheij 1997). Raudkivi and Ettema (1977a, b) investigated experimentally the effect of sand size on the scour depth at circular pier. They concluded that a flat bed, i.e. clear water scour, can not be maintained in the laboratory near the threshold conditions when the grain size d_{50} <0.70mm. The ripples are expected to develop when the flow velocity exceeds 60% of the threshold velocity. Breusers and Raudkivi (1991) give the same conclusion for ripples formation

with an exception: clear water scour conditions can be maintained when the geometric standard deviation of the sand is between 1.30 and 1.50.

Relative Sediment Coarseness

The ratio of the pier width to the mean grain size of the sediment material is defined as relative sediment coarseness D/d_{50}. Figure 2.4 shows the scour depth versus the sediment coarseness ratio. As shown, the scour depth increases with sediment coarseness up to a maximum at D/d_{50} = 25 - 50, and seemingly becomes independent when D/d_{50} ratio exceeds 50 (Raudkivi 1986, Breusers and Raudkivi 1991, Melville and Sutherland 1998). Ettema (1980) found that the effect of sediment coarseness ratio was significant up to D/d_{50} = 20 – 25, and for higher values of sediment coarseness, the scour depth became independent of D/d_{50}, see figure 2.5. However, Sheppard et al. (1995) and (2004) investigated local scour at a circular pier in a large flume and concluded that the sediment coarseness ratio with very large values may decrease the scour depth. Recently, Lee and Strum (2009) studied the effect of sediment size on local scour depending on laboratory and field data. Their results showed that after the scour depth reached a peak value at D/d_{50} = 25, it decreased again as the sediment coarseness increased, see figure 2.5.

The model scale, the sediment size range, or the experiment time length might be the reason for the differences in results of the sediment size effect. Further researches on pier scour with large sediment size and with large scale models are needed to clear this effect.

Sediment gradation

Sediment gradation is characterized by the geometric standard deviation of the sediment grain size $\sigma_s = \sqrt{d_{84.1} / d_{15.9}}$. For natural river sand, σ_s is about 1.80 while for uniform sand σ_s is about 1.30 (Hoffmans and Verheij 1997). The effect of sediment gradation on local scour was investigated by many researchers, such as Ettema (1980), Chiew (1984), Dey (1995) and Molinas (2003). The general conclusion was that both the scour rate and the scour depth decrease as the geometric standard deviation increases. At a higher value of σ_s (i.e. for non-uniform sediment), armouring occurs on the upstream bed and at the bottom of the scour hole near the threshold conditions (i.e. $u/u_{cr} \approx 1$), resulting in a considerable reduction of the scour depth. For high flow intensity, the sediment non-uniformity has little effect on the scour depth. Figure 2.6 shows the coefficient K_σ versus σ_s, where K_σ is the ratio of maximum scour depth in non-uniform sediment and maximum scour depth in uniform sediments (σ_s=1.50 – 2.00) under clear water scour conditions. Dey et al. (1995) divided the sediment material into uniform sediment (σ_s < 1.40) and non-uniform sediment (σ_s >1.40).

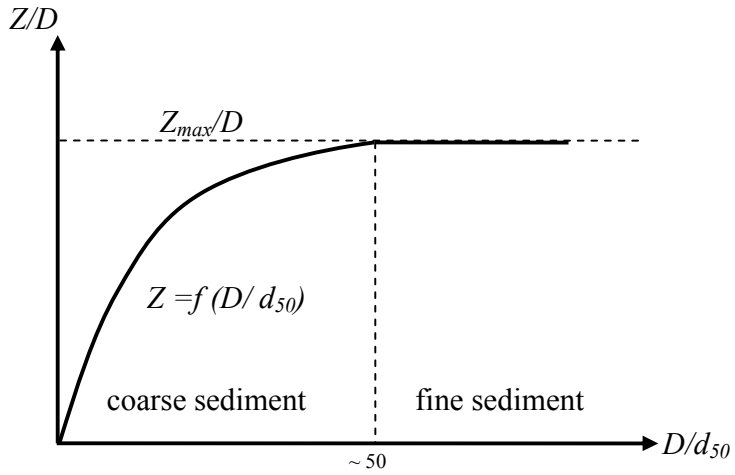

Figure 2.4. Local pier scour depth versus sediment coarseness (Melville and Coleman 2000)

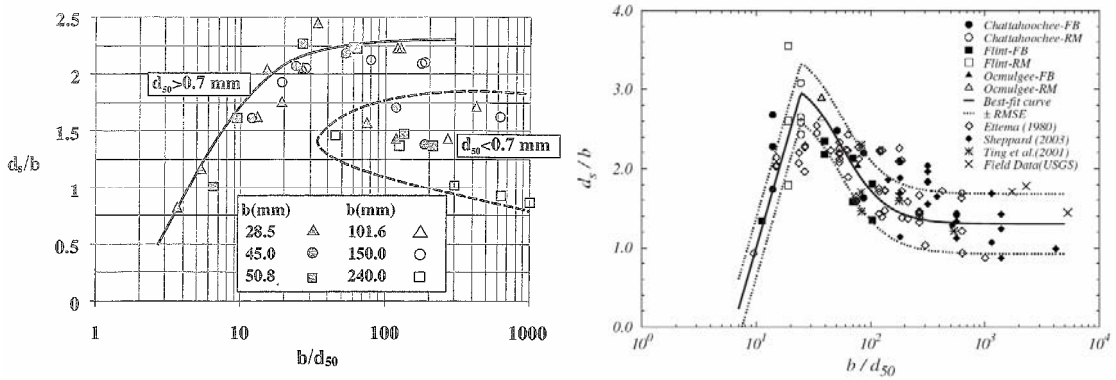

Figure 2.5. Scour depth versus sediment coarseness: laboratory data of Ettema (1980) (left) and Lee & Strum (2009) (right), *(d_s = Z and b = D)*

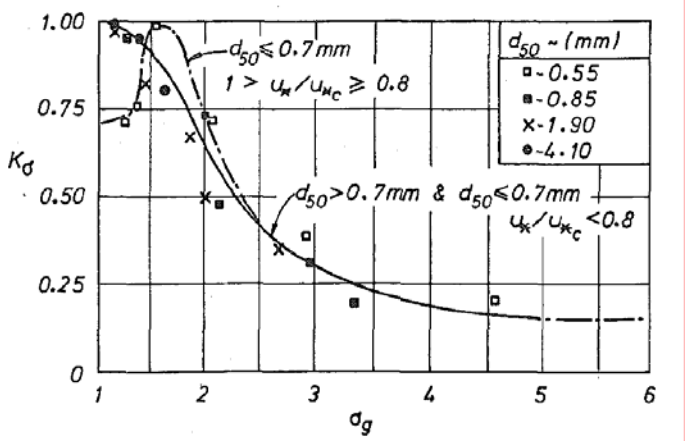

Figure 2.6. Coefficient K_σ versus sediment gradation (Raudkivi and Ettema 1983)

Pier shape and alignment effect, $k_{\alpha,L/B}, k_{sh}$

Bridge piers are constructed of various shapes and aligned with different angles with the flow direction. The most common used shapes are circular, square, rectangular with different nose, oblong and streamline. Almost all current methods predicting scour depth at piers are depending on studies focusing on local scour at circular piers in sand bed. The effect of pier shape and alignment are often accounted by using correction factors. Regarding the objective of this thesis, the effect of pier shape and alignment is discussed in detail in section 2.4.

Time Effect

Development of local pier scour is dependent on time and scour conditions. Under clear-water conditions, scour depth develops gradually in time following a first order exponential relation towards the equilibrium clear-water scour depth. For live-bed conditions, scour depth increases rapidly with the time reaching a maximum value in short duration. Then scour depth fluctuates over time around a mean value called equilibrium live-bed scour depth (Chabert and Engeldinger 1956, Raudkivi 1976, Melville and Chiew 1999). The equilibrium scour depth under live-bed is about 10% less than under clear-water conditions (Graf 1996). Figure 2.7 shows the time development of scour depth. For clear-water conditions, the known relations for predicting the equilibrium scour depth were developed through laboratory models. The time required to achieve the equilibrium depends on the scale of these experiments. This is a very important point because the results obtained after short run time may give scour depths smaller than the equilibrium scour depth. The data obtained in small-scale laboratory experiments after short run time of 10 to 12 hours can lead to scour depths less than 50% of the equilibrium depth of scour (Melville and Chiew 1999). Therefore, it is necessary to run experiments for several days. For live-bed conditions, the equilibrium scour depth (clear-water) is appropriate. During flood events, live-bed scour occurs during the flood duration. The hydrograph and duration of the flood help to determine if the equilibrium live-bed scour will develop. During the duration of recession flow, clear water conditions may prevail and induce additional scour (Breusers et al. 1977). More details about time and scour will be presented in the following section.

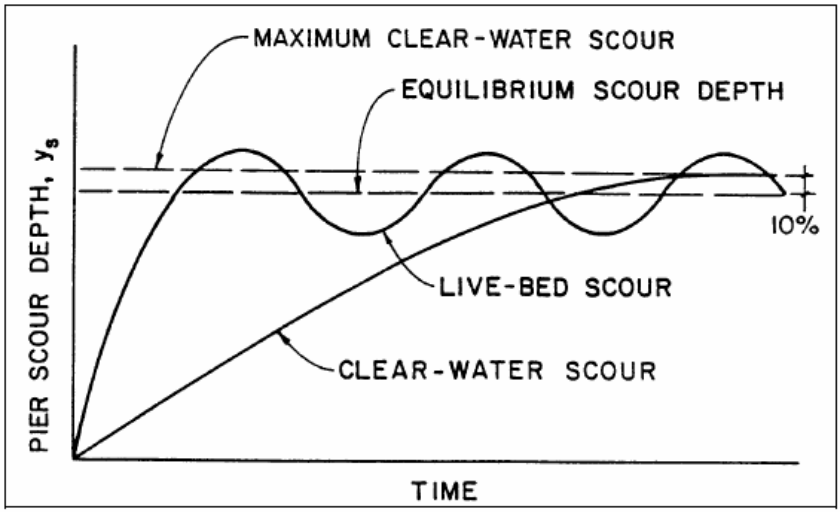

Figure 2.7. Scour depth as a function of time (Breusers and Raudkivi 1991)

2.1.4 Scouring around Piers of different Shape and Alignment

Pier geometry is defined to be the size and shape of the pier in the horizontal and in the vertical cross-sections. In elevation, piers take a prismatic (constant) shape or increased or decreased width upwards. Hoffmans and Verheij (1997) concluded that maximum scour depth at a pier of narrowing width upwards is smaller than at a pier of prismatic shape, and higher than at a pier of broadening width upwards. In this thesis, only the prismatic shapes are considered. Figure 2.8 shows a schematic illustration of the most common pier shapes.

The effect of pier size has been discussed by Shen et al. (1969), Breusers et al. (1977) and others. They concluded that the horseshoe vortex shape and strength which is the main cause of scouring is a function of the pier size. Shen et al. (1969) observed that the horseshoe vortex is proportional to the pier Reynolds's number that is a function of the pier width ($\mathrm{Re}_{pier} = uD/v$). Breusers et al. (1977) related the scour depth to the pier size. Hoffmans and Verheij (1997) reported that scour depth increases with the increase of the pier width when the ratio of pier width to water depth is less than unity ($D/h<1$). Breusers and Raudkivi (1991) concluded that the pier size influences the time required to reach the equilibrium as well as the volume of the upstream part of the scour hole.

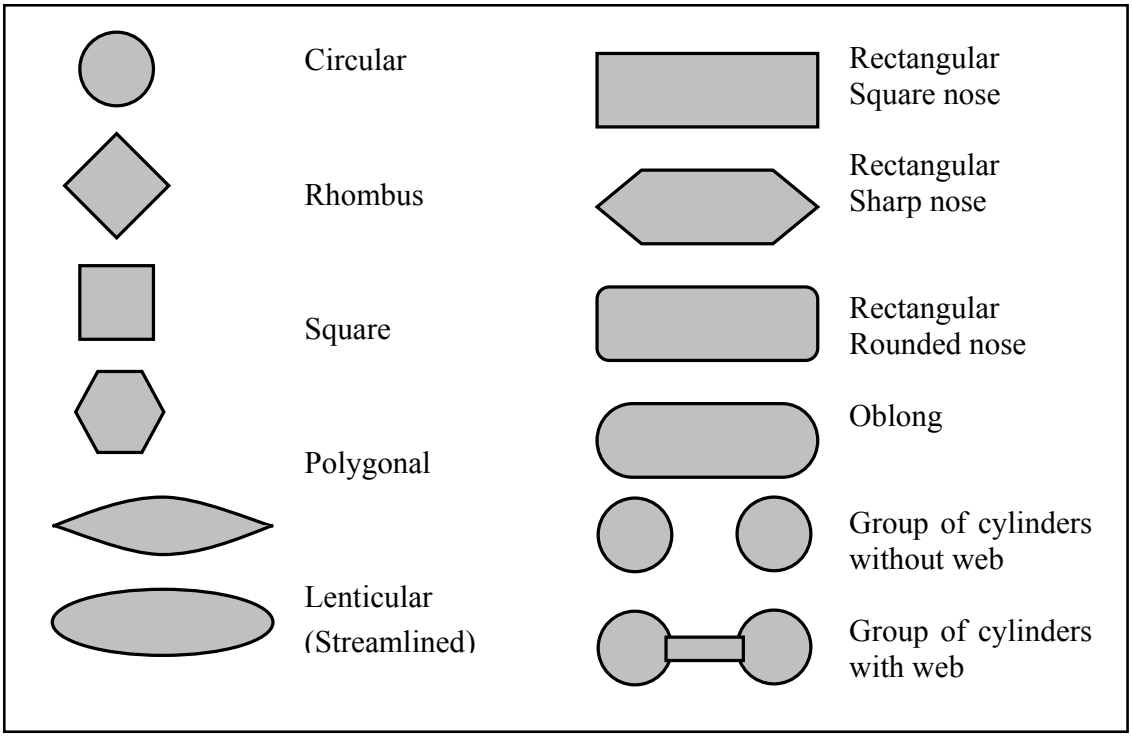

Figure 2.8. Schematic of common pier shapes

The effect of pier shape and alignment (angle of attack) has been studied by few researchers (e.g. Tison 1940, Chabert and Engeldinger 1956, Laursen and Toch 1956, Neil 1973, Dietz 1972, Melville 1975, Breusers et al. 1977). The angle of flow attack refers to the angle between the direction of flow and the direction of pier (Hoffmans and Verheij 1997). General conclusions are: (1) the blunter shapes induce the deeper scour, (2) the local scour is sensible to the alignment or orientation of the pier to the flow, and (3) the effect of pier shape and alignment are often accounted by correction factor.

Flamant (1900) [from Breusers et al. 1977] compared the relative scour depth around three different pier shapes namely circular, square and triangular. The highest and lowest scour depths were observed at the square and triangular piers, respectively.

Tison (1940 and 1961) tested the effect of pier shape and alignment on scouring in sand with d_{50} = 0.48mm. The deeper scour was observed at the rectangular pier shape. No effect of the rectangular pier length on scour depth was observed when the pier was aligned with the flow. It was also concluded that streamlining the pier with zero angle of attack may minimise the scour depth.

The most established research on the effect of pier shape and alignment was carried out by Laursen and Toch (1956). Figure 2.9 shows some of the pier shapes used in their study.

Iowa pier models consisted of two circular or square shafts (circular or square) with and without connecting web. Tested angles of attack ranged from 0 to 90º. The experiments were carried out in two flumes; each was 10.6 m (35 ft) long and 1.50 m (5 ft) wide at the laboratory of the Iowa Institute of Hydraulic Research. The two flumes can be used as one wide flume (3 m wide) by removing the wall between them. The bed material was sand with d_{50} = 0.58 mm. Horizontal layers of coloured sand with a diameter of 3 mm (0.01 ft) thick were placed at intervals of 0.03 m (0.10 ft) below the original sand surface to observe the development of the scour depth. During the experiments, the time of appearance of each red layer was noted. After three hours running time, the water was drained out and standard photographs were taken. In the study of basic pier shapes, which was conducted by Schneidle 1951, the running time was reduced to only 60 minutes. The model of Texas pile pier which has battered piles extended up from the river bed to low water level was tested in the next step. Two different levels (3 and 6 cm) of pile tops above the bed level and four different flow angles of attack (0, 15, 30 and 45º) were tested. The results show the effect of pier shape and alignment on the relative scour depth, not the maximum scour depth. For Iowa pier models, the scour depth was observed at the upstream shaft for small angles of attack (0 - 10º) while it moved to the downstream shaft with the increase of the angle of attack. The effect of rounded and rectangular shafts was clear for small attack angles, the scour depth around the rectangular shafts was 15% higher. The pier shape and the existence of the web have no effect on scour when the pier was aligned with the flow. As the angle of attack increased, the relative scour depth at angle of 30 and 45º were about 2 and 2.5 times that at angle of 0º. The results of basic geometrical pier shapes tests showed, that the use of streamlined shapes decreased the scour depth when the angle of attack equal to 0º. This effect diminishes while increasing the angle of attack. Scour depth at Texas pile pier increased with the angle of attack and the setting of the pier at the bed level.

Finally, Laursen and Toch (1956) give a design curve to predict the scour depth at rectangular piers of zero angle of attack depending on the relative flow depth, which was expressed by Neil (1964) (quoted from Breusers et al. 1977) as:

$$\frac{Z}{B} = 1.50\left(\frac{h}{B}\right)^{0.30} \qquad [2.3]$$

For other pier shapes or if the pier is skewed to the flow direction, the predicted value of scour depth from equation (2.3) should be multiplied by a correction factor for the pier shape k_{sh} [Table 2.2], or for the angle of attack $k_{\alpha,L/B}$ [Figure 2.10]. It should be noted that the two correction factors must not be used together.

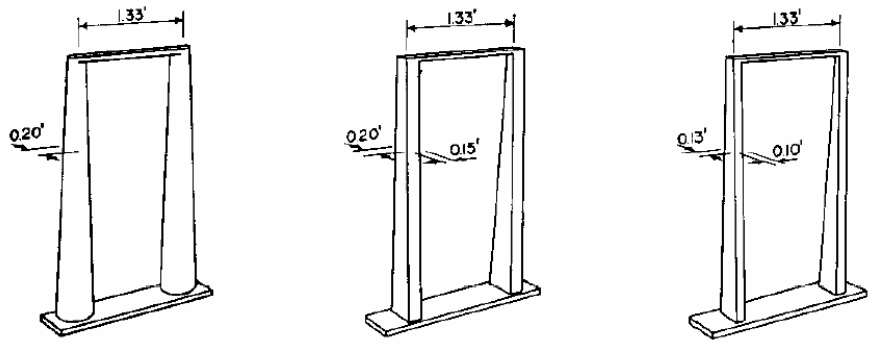

Model IV Model V Model VI

Models of typical Iowa piers

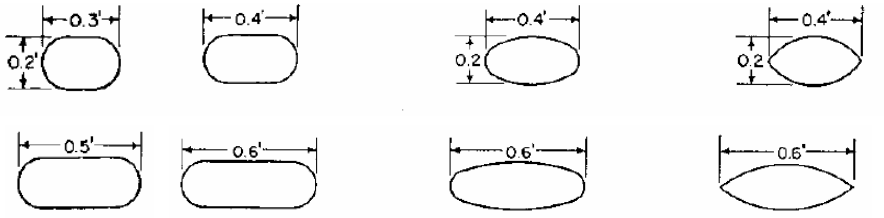

Basic pier shapes

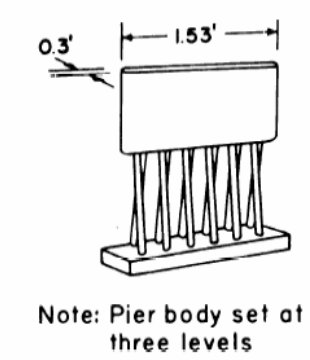

Model of Texas pie pier

Figure 2.9. Used pier shapes by Laursen and Toch (1956)

Richardson and Davis (2001) gave the following expression for $k_{\alpha,L/B}$, depending on The design curve of Laursen and Toch:

$$k_{\alpha,L/B} = \left(\cos\alpha + \frac{L}{B}\sin\alpha \right)^{0.65} \qquad [2.4]$$

According to Richardson and Davis (2001) $k_{\alpha,L/B}$ should be used if the angle of attack is higher than 5 degrees and for the rectangular pier with L/B ranged between 2 and 16.

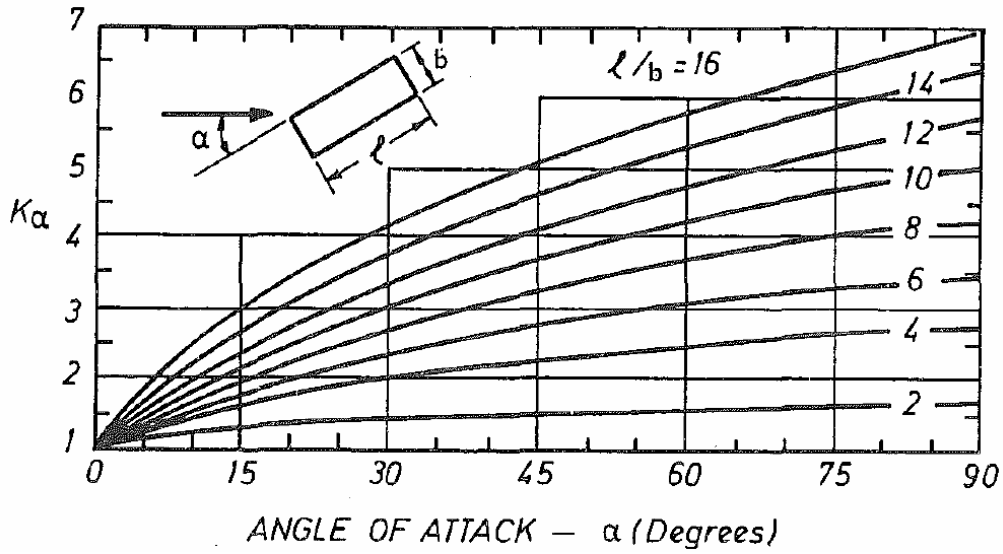

Figure 2.10. Design factor for piers not aligned with flow. (Laursen and Toch 1956)

A variety correction factors for pier shape were suggested by different researchers depending on limited experimental data (Tison 1940, Laursen and Toch 1956, Chabert and Engeldinger 1956, Breusers et al. 1977, Richardson et al. 1993, Mostafa 1994, Melville 1997, Hoffmans and Verheij 1997, Richardson and Davis 2001, Oliveto and Hager 2002). Table 2.2 presents some recommended values for the pier shape effect regarding to the circular pier shape.

Table 2.2. Some segmentations of pier shape factor.

Pier shape	**Reference**								
	Tison (1940)	Laursen and Toch (1956)	Chabert and Engeldinger (1956)	Breusers et al. (1977)	Mostafa (1994)	Melville (1997)	Hoffmans and Verheij (1997)	Richardson et al. (1993), Richardson and Davis (2001)	Oliveto and Hager (2002)
Circular	1.00	0.90	1.00	1.00	1.00	1.00	1.00	1.00	1.00
Rectangular	1.40	1.00	1.11	1.30	1.29	1.00	1.00 - 1.20	1.10	1.20
Rounded-nosed	-	0.90	-	-	1.07	1.00	0.90	1.00	-
Stream-lined pier	0.67 - 0.41	0.70 - 0.80	0.73	0.75	-		0.70 - 0.80	-	-
Sharpe-nosed	-	-	-	-	-	0.90	0.65 - 0.76	0.90	-
Elliptic	- -	0.75-0.8	- -	-	-	-	0.60 - 0.80	-	-

In summary: the angle of attack factor developed by Laursen and Toch (1956) is almost used in all methods predicting the local scour depth at piers. To the best of the author knowledge, no systematic studies are done on the effect of angle of flow attack on local scour other than Laursen and Toch (1956). Therefore, improving and updating the angle of attack factor is essential. There is also a need to extend the curve of $k_{\alpha,L/B}$ for square piers, i.e. when L/B =1. Furthermore, laboratory measurements to improve the knowledge of the pier shape effect on local scour are required. Wide range of values is suggested for the pier shape factor by different authors as shown in table 2.2.

2.1.5 Scouring of Gravel Beds around Bridge Piers

Scouring around bridge piers has been extensively studied in the past. Nevertheless, most of the past studies focused on scour in alluvial sand beds. Only few studies concentrate on scouring in gravel bed were found such as Ettema (1980). Raikar and Dey (2005a) conducted an experimental study on scour in uniform and non-uniform gravel at bridge piers, analyzing the effect of sediment gradation on the equilibrium scour depth. Raikar and Dey (2005b) presented experimental results on scour in uniform gravels, analysing the effect of gravel size on the scour depth at bridge piers and abutments. In both mentioned studies, it was concluded that significant differences in scour are expected depending on the sediment type i.e. sand or gravel. The time required to reach the equilibrium scour depth in gravel is longer than in sand beds. The equilibrium scour depth increases with the increase of gravel size. Recently, Diab et al. (2008b) and (2008c) performed experimental investigations on scour at circular and square piers in uniform gravel bed. The results showed the time variation of scour hole dimensions, i.e. scour hole depth, radius and slopes. The need for further efforts to understand the unexplored scour process in gravel is evident.

2.2 DEVELOPING AND EQUILIBRIUM SCOUR DEFINITIONS AND FORMULAS

Local pier scour process is time dependent. The equilibrium scour depth is rapidly attained under live-bed conditions, but more slowly under clear-water conditions. The maximum scour depth attained in a given time t, is called here the developing scour depth (Z_t)**.** When the rate of scouring becomes insignificant with time, the scour reaches the equilibrium and the maximum scour depth is called here the equilibrium scour depth (Z_{eq}).

The local scour process at bridge piers can be divided into several phases, namely initial phase, development phase, stabilization phase and equilibrium phase (Ettema 1980, Dey 1997 and 1999, Melville and Chiew 1999, Hoffmann and Verheij 1997, BSM 2005, Link and Zanke 2006). In the initial phase, the erosion capacity is most severe. The scour depth changes considerably but the shape of the scour hole does not change during the development phase. During the stabilization phase, the rate of scour development decreases. The equilibrium phase is achieved when the change of the scour hole dimension is insignificant. The time to equilibrium increases with flow intensity for clear-water conditions up to a maximum value at the threshold conditions of sediment transport, then at higher live-bed scour the time is expected to rapidly decrease again (Melville and Chiew 1999).

Regarding the time required to reach the equilibrium scour phase, several researchers have developed different definitions of time to equilibrium scour for piers in uniform sands under clear-water conditions (Shen et al 1969, Dietz 1972, Nakagawa and Suzuki 1976, Franzetti et al. 1982, Melville and Coleman 2000, Sheppard et al. 2004). Ettema (1980) defined the time at which the change of scour depth is no more than 1 mm in a timeframe of 4 hours as the equilibrium time. Raudkivi (1986) noted that equilibrium scour can be attained in the laboratory after a test duration of 50 hrs. Melville and Chiew (1999) defined the time to equilibrium as the time at which the rate of change of scour depth does not exceed 5 % of the pier diameter in the succeeding 24 hours period. Equation (2.5) can be used to compute the equilibrium scour time at a circular pier in sand bed without ripples when $u/u_{cr} = 1$ and h/D > 6.

$$t_e(days) = 28.96\frac{D}{u} \qquad [2.5]$$

Where t_e is the equilibrium time, D is the pier diameter [m] and u is the approach flow velocity [m/s].

Mia and Nago (2003) concluded that the bed shear velocity decreased with time as the scour hole increased and the equilibrium scour occurred when the approach bed-shear velocity was nearly equal to the critical bed-shear velocity. Jones and Sheppard (2000) noted that the duration for many experiments reported in the literature was insufficient to reach the equilibrium conditions, so that a lot of the data reported therein are questionable. Therefore, the whole concept of an experimental equilibrium scour condition warrants further investigations.

Some formulas predicting the developing and equilibrium scour depths are presented in sections 2.6.1 and 2.6.2.

2.2.1 Developing Scour Depth formulas

The time development of local scour has attracted the attention of many researchers (e.g. Shen et al. 1969, Ettema 1980, Kothyari et al .1992, Melville and Chiew 1999, Dey 1999, Oliveto and Hager 2005). Table 2.3 presents some prediction equations of developing scour depth.

Franzetti et al. (1982) studied the influence of test duration on the equilibrium scour depth, using the data of Chabert and Engeldinger (1956) and Franzetti et al. (1981) which were obtained from long-duration (ranging between 410000-842000s) experimental tests on scour at circular piers in mobile beds (sand bed and light synthetic material). The evaluation of scour in time leads to an exponential expression (equation 2.6).

Zanke (1982a) derived semi-analytically equation 2.7 from the continuity equation of mass and the balance of the acting forces during scouring in non-cohesive sediment bed. The equation was also calibrated by using laboratory data, which were obtained from scour experiments under both current and wave actions.

The developing scour depth at slender piers can be described by equation 2.8 which is suggested by Hoffmans and Verheij (1997). As shown, the relation between Z_t and t is reduced when the scour depth is less than the pier width.

Melville and Chiew (1999) conducted several series of experiments to clarify the effect of time on development of scour depth at cylindrical piers in uniform sand beds under clear water conditions. They combined their results with data from Ettema (1980) and Graf (1995) developing a relation for predicting the developing scour depth as well as the time to equilibrium (equation 2.9). Additional data on time development of scour depth around circular and non circular piers was obtained by Barkdoll (2000). The gained data was compared with the data of Melville and Chiew (1999). The data for circular piers from Barkdoll showed close agreement with those from Melville and Chiew. However, Melville and Chiew's equation (eqn. 2.9) seems to overpredict scour depth at a given time. With some scatter in the data for noncircular piers from Barkdoll, there is no significant difference with Melville and Chiew's equation. A modified form of Melville and Chiew's equation was produced by Barkdoll based on a curve fitting for all his experimental data, resulting in a new equation (2.10).

Oliveto and Hager (2002) proposed equation 2.11 for temporal scour depth prediction in clear water scour around cylindrical piers in uniform and non-uniform sediment. They calibrated their equation by using their extensive laboratory data of scour at bridge elements as well as the available literature data. They found that the principle parameter affecting the scour process at bridge elements is the densimetric Froude number, $F_d = u/\sqrt{\Delta g d_{50}}$, where $\Delta = (\rho_s - \rho)/\rho$.

Table 2.3. Summery of some time-development local pier scour formulas

Author & Reference and Formula	Note	Eq.
Franzetti et al. (1982): $\frac{Z_t}{Z_{eq}} = 1 - \exp\left[- B\left(\frac{ut}{D}\right)^{1/3} \right]$	0.021<B<0<0.042 B (average) = 0.028	2.6
Zanke (1982a): $t = \frac{1.94 z_t^2}{\left(\frac{d_*}{w_s}\right)^4 \upsilon \left\{ \left[\left(\left(\frac{u\omega}{1+\frac{z_t}{D}} \right)^2 - u_{cr}^2 \right) \frac{u}{u_{cr}} \right]^2 - \left(u^2 - u_{cr}^2\right)^2 \right\}}$	$d_* = d_{50}\left[\Delta g / \upsilon^2\right]^{1/3}$ w_s = settling velocity $\Delta = (\rho_s - \rho)/\rho$ validation: $0.40 < u/u_{cr} < 8.8$	2.7
Hoffmans and Verheij (1997): $\frac{Z_t}{D} = \left(\frac{t}{t_1}\right)^{\gamma}$, $t < t_1$ $\frac{Z_t}{Z_{eq}} = 1 - \exp\left\{ \ln\left[1 - D/Z_{eq}\right] \left[t/t_1\right]^{\gamma} \right\}$, $t > t_1$	γ = coefficient 0.2-0.4 t_1 = time at which $Z_t = D$ validation: slender pier D/h <1.0 & $Z_{eq} > D$	2.8
Melville and Chiew (1999): $Z_t = k_I k_h k_d k_{sh} k_{\alpha,L/B} k_t$ $k_t = \frac{Z_t}{Z_{eq}} = \exp\left\{ -0.03 \left| \frac{u_{cr}}{u} \ln\left(\frac{t}{t_e}\right) \right|^{1.6} \right\}$, for clear-water conditions $t_e(days) = \begin{cases} 48.26 \frac{D}{u}\left(\frac{u}{u_{cr}} - 0.4\right) & , h/D > 6 \\ 30.89 \frac{D}{u}\left(\frac{u}{u_{cr}} - 0.4\right)\left(\frac{h}{D}\right)^{0.25} & , h/D \le 6 \end{cases}$	k_t = 1.0 for live-bed validation: $\sigma_s < 1.30$	2.9
Barkdoll (2000): $\frac{Z_t}{Z_{eq}} = \exp\left\{ -0.154 \left| \frac{u_{cr}}{u} \ln\left(\frac{t}{t_e}\right) \right| \right\}$		2.10
Oliveto and Hager (2002): $Z_t = 0.068 L_R N \sigma_s^{-0.50} F_d^{1.50} \log(T_d)$ $L_R = D^{\alpha} h^{\beta}$, $\alpha + \beta = 1$ $F_d = u/\left(\Delta g\, d_{50}\right)^{1/2}$, $T_d = t/t_R = \left\{ \left(\Delta g\, d_{50}\right)^{1/2} / L_R \right\} t$	N=1.0 for circular pier =1.25 for rect. pier *α=2/3 and β=1/3, in Oliveto & Hager 2002* validation: $u<u_{cr}$ & $F_d > F_{di}$	2.11

Some of the listed equations (2.6, 2.9 and 2.10) depend on the knowledge of equilibrium scour depth and/or the equilibrium time, which are difficult to achieve in the laboratory. Other researchers overcome these difficulties by proposing expressions (equations 2.7 and 2.11) that do not include the equilibrium scour depth. Comparison between the equations will be presented in the discussion chapter.

2.2.2 Equilibrium Scour Depth Formulas

Numerous equations are available in the literature predicting equilibrium scour depth near bridge piers (Tison 1940, Chabert and Engeldinger 1956, Laursen and Toch 1956, Jain & Fischer 1980, Melville & Sutherland 1988, Johnsons 1992, Richardson and Davis 2001, Yanmaz and Ciceckdag 2002). Table 2.4 summarizes some of the most commonly used and cited local pier scour equations.

Neill (1964) suggested the expression for the design curve of rectangular pier with zero angle of attack of Laursen and Toch (1956) (eqn. 2.12). For other pier shapes and alignments, Laursen and Toch's correction factors for shape or angle of attack should be used. While Breusers et al. (1977) suggested his equation 2.13 depending on several conclusions of many previous efforts on expressing local pier scour. The constant was taken as 2.00 instead of 1.50 to be on the safe side. The pier shape factor is only used when the pier is aligned with the flow. It is considered that there is no scour when the approaching flow velocity is smaller than half of the critical flow velocity.

Zanke (1982a) conducted experimental investigation on local scour around cylindrical pier under current, wave and current-wave interaction. Two different pier diameters (0.065 and 0.09 m) were embedded in sand (d_{50} = 0.24 mm, density = 2650 kg/m^3) and in a light weight material (Hostyrene, d_{50} = 2.4 mm, density 1035 kg/m^3). Equation 2.14 was rearranged analytically from Zanke's (1978) formula for bed load to a general equation to predict scour at bridge piers and tested using the laboratory results. The effective velocity ω measures the influence of secondary flow on the rate of erosion. The values of ω increases due to the increment of turbulence and should be determined experimentally. The measurements of vertical velocity at 5mm above the bed of Ettema (1980) showed that ω is depended on the ratio of vertical velocity near the scour hole bed to the approach flow velocity.

Equation 2.15 was suggested by Melville (1997) following Melville and Sutherland (1988). It was based on laboratory data that was derived from experiments with cylindrical piers. As shown, the effects of pier shape or alignment are account as multiplying correction factors. Note that there is no deference in the values of scour depth around circular, round nosed or sharp nosed piers.

Hoffmans and Verheij (1997) expressed equations (2.16) for local scour depth at bridge piers based on the data of Laursen and Toch (1956) and Breusers et al. (1977).
The Colorado State University's (CSU) equation was recommended by Richardson et al. (2001). It was based on Richardson et al. (1975) for both live-bed and clear-water scour. In Richardson and Davis (2001), an equation based on CSU equation with adding multiplying correction factor for bed conditions and armoring by sediment size is given. The maximum recommended value of scour depth for round nose pier aligned with the flow is 2.4 and 3 times the pier width when $Fr \leq 0.80$ and $Fr > 0.80$, respectively. Recently, the Bridge Scour Manual (BSM 2005) recommends equation 2.18 to calculate the equilibrium clear-water local scour depth, depending on the results of Sheppard and his graduate students at the University of Florida.
Many researchers presented comparisons of these equations (Mueller 1996, Link 2006, Richardson et al. 2001, Richardson and Davis 2001). Depending on laboratory data and limited field data, the comparisons showed wide differences in the predicted values for scour depth at simple circular piers with sand beds. Accordingly, there is a need for laboratory data with non-circular pier as well as in gravel beds to verify the current used equations for scour depth.

Table 2.4. Summery of some equilibrium local scour pier formulas

Author & Reference and Formula	Note	Eq.
Neill (1964): $\frac{Z_{eq}}{D} = 1.50\left(\frac{h}{D}\right)^{0.30}$	validation: rectangular pier with zero angle of flow attack	2.12
Breusers et al. (1977): $\frac{Z_{eq}}{D} = \begin{cases} 2.0\left(2\frac{u}{u_{cr}}-1\right)\left[\tanh\left(\frac{h}{D}\right)\right].k_{sh}.k_{\alpha,L/B}, & 0.5 \le u/u_{cr} \le 1.00 \\ \left[2.0\tanh\left(\frac{h}{D}\right)\right].k_{sh}.k_{\alpha,L/B}, & u/u_{cr} \ge 1.00 \end{cases}$	k_{sh} = from table 2.2 $k_{\alpha,L/B}$ = from fig. 2.10 validation: 1.0 < h/D < 4.0 $u/u_{cr} > 0.5$	2.13
Zanke (1982a,b): $\frac{Z_{eq}}{D} = \begin{cases} \left[\frac{u}{u_{cr}}\omega - 1\right], & u/u_{cr} < 1.00 \\ \frac{\omega}{\left(\frac{u_{cr}}{u} + \frac{u_{cr}^2}{u^2} + \frac{u_{cr}^3}{u^3}\right)^{0.50}} - 1, & u/u_{cr} > 1.00 \end{cases}$	ω = the effective velocity increase due to the turbulence. validation: $0.40 < u/u_{cr} < 8.8$	2.14
Melville (1997): $Z_{eq} = k_I k_h k_d k_{sh} k_{\alpha,L/B}$ $k_I = \begin{cases} 1.00, & u/u_{cr} > 1.0 \\ u/u_{cr}, & u/u_{cr} < 1.0 \end{cases}$ $k_h = \begin{cases} 2.4D, & h/D < 0.7 \\ 2.0\sqrt{hD}, & 0.7 < h/D < 5.0 \\ 4.50h, & h/D > 5.0 \end{cases}$ $k_d = \begin{cases} 0.57\log(2.24D/d_{50}), & D/d_{50} < 25 \\ 1.0, & D/d_{50} > 25 \end{cases}$	k_{sh} = from table 2.2 $k_{\alpha,L/B}$ = from fig. 2.10 $k_h \rightarrow$ Kandasamy (1989) $k_d \rightarrow$ Ettema (1980) & Chiew (1984) validation: $\sigma_s < 1.40$	2.15
Hoffmans and Verheij (1997): $\frac{Z_{eq}}{D} = 1.35 k_{sh}.k_{\alpha,L/B}.k_{\sigma}.h^{0.30}$	Basing on data of Laursen and Toch (1956) and Breusers et al. (1977)	2.16
CSU' Equation, (Richardson et al. 1975) : $\frac{Z_{eq}}{h} = 2.0 k_{sh}.k_{\alpha,L/B}\left[\frac{D}{h}\right]^{0.65}\left(\frac{u}{\sqrt{gh}}\right)^{0.43}$	k_{sh} = from table 2.2 $k_{\alpha,L/B}$ from equation 2.4	2.17
Sheppard D. M. and Miller W. Jr. (2004) (from BSM 2005): $\frac{Z_{eq}}{D^*} = 2.5\tanh\left[\left(\frac{h}{D^*}\right)^{0.4}\right]\left\{1 - 1.75\left[\ln\left(\frac{u}{u_{cr}}\right)\right]^2\right\}\left[\frac{D^*/d_{50}}{0.4(D^*/d_{50})^{1.2} + 10.6(D^*/d_{50})^{-0.13}}\right]$ D^* is the effective pier diameter		2.18

2.3 DEVELOPING AND EQUILIBRIUM SCOUR HOLES GEOMETRY

Studies of developing and equilibrium maximum depth of scour at bridge piers has received considerable attention by different researchers. However less information is available on the time variation of scour hole geometry, which includes not only the maximum scour depths but also the scour extension, maximum scour radius, scour-side-slopes, hole-surface area and scoured-volume. The knowledge of the dimensions of scour holes around bridge piers is needed to select the required degree and extension of scour countermeasures.

Laursen and Toch (1956) gave an idea about scour contours around pier and abutment models depending on photographs that were taken after 3 hours run time. The results showed that the scour hole has the form of an inverted cone with side slopes equal to the repose angle of sand for all pier shapes. Dargahi (1987) described the slopes of a scour hole based on experiments with sand.

Yanmaz and Altinbilek (1991) conducted experiments to study the development of scour hole at bridge piers in uniform sands under clear water conditions. The duration time of the experiments were kept constant for around 6 hours, during which the final equilibrium scour was not achieved. The experiments were stopped after durations of 5 min, 20 min, 60 min, 100 min and 150 min to measure the scour hole contours around the pier. They concluded that the shape of the scour hole remains almost unchanged with time. The observed average side slope of the scour hole was 33º which was approximately the angle of repose of the used sand. The following expressions to calculate the volume of scour hole were given by assuming that the scour hole takes the shape of an inverted cone having square or circular bases depending on the pier shape:

$$\forall = \frac{\pi}{3\tan\phi}\left(\frac{d_s^3}{\tan\phi} + \frac{3bd_s^2}{2}\right) \quad \text{...for cirular pier} \qquad [2.19]$$

$$\forall = \frac{d_s}{3}\left[\pi\left(\frac{\mathrm{d_s}}{\tan\phi} + \frac{b}{2}\right)^2 + \left(\frac{2d_s b}{\tan\phi} + b^2\right)\ln\tan\left(\frac{3\pi}{8}\right) - 2b^2\right] \quad \text{...for square pier} \qquad [2.20]$$

Where: $\mathrm{d_s}$ is the scour depth, b is the pier diameter or width and Φ is the scour hole side slopes.

Yanmaz and Altinbilek (1991) also noted that for a known time-to-peak value of a flood hydrograph, smaller scour depths may be obtained, which reduce the total cost of construction. In their comprehensive review of the important studies on scour at piers, Hoffmans and Verheij (1997) presented sketches of scour hole topography for

equilibrium scour holes. Yanmaz and Köse (2007) performed experiments to investigate the time variation of scour holes at circular and square piers and at vertical-wall abutments in uniform sand bed under clear-water conditions. The tests durations were limited by 6 hours that was not enough to reach the equilibrium. Dimensionless empirical expressions were given for time-dependent scour hole surface area and volume.

Recently, Link et al. (2008b) conducted detailed measurements of developing scour holes in sand. Gobert et *al.* (2010) used this experimental data to characterize the interaction between the horseshoe vortex and the scour slopes through advanced numerical large eddy simulations, LES.

Diab et al. (2010a) presented experimental results on the geometry of developing and equilibrium scour holes at circular and square piers under clear water conditions with uniform gravel. The time development of scour hole radius, depths and slopes at different azimuthal half-planes around the pier were discussed. An empirical formula to compute the developing scour hole volume depending on the knowledge of scour depth in front of the pier is suggested. Also, Diab et al. (2010c) discussed the geometric characteristics of scour holes at square pier in uniform sand and compared the experimental results with some known formulas of scour depth.

Regarding the top width of scour holes, Richardson et al. (1993) suggested a value of 2.80 times the maximum scour depth as a general estimate of the scour hole top width, while Butch (1996) depending on field data found that the width of the scour hole being 4.70 time the scour depth. Richardson et al. (2001) (HEC 6) based on Richardson and Abed (1999) calculated the top width of scour holes with the following equation:

$$W = y_s(K + \cot\phi) \qquad [2.21]$$

Where: W is the scour hole top width from each side of the pier footing (m), y_s is the scour depth (m), K is the bottom width of the scour hole as a fraction of scour depth, and ϕ the repose angle which ranges between 30-44º.

Numerical simulations of scour at sediment-embedded cylinders lack experimental data on developing scour hole characteristics (Olsen and Melaaen 1993, Olsen and Kjellesvic 1998, Yen et al. 2001, Ali and Karim 2002, Salahedin et al. 2004, Roulund et al. 2005, Kirkil et al. 2008). Spatial information of scour hole is useful for testing numerical simulation models of loose boundary hydraulics.

Therefore, more investigations to characterize the geometry of developing and equilibrium scour holes at bridge piers are needed to predict the possible dimensions of a scour hole satisfactorily.

CHAPTER 3
EXPERIMENTATION

3.1 INTRODUCTION

In the following sections the developed experimental installation, measuring techniques, and experimental procedures and series are described. The experimental set-up provided all necessary tools for investigation of the time-variation of the geometric characteristics of scour holes around piers of different shape and alignment in gravel and sand beds through a set of laboratory experiments. Additionally, the time-averaged flow velocity field and turbulence features around a square pier were measured and analyzed to improve understanding of tturbulence and induced secondary flow field interaction.

3.2 EXPERIMENTAL SETUP

Experiments were conducted in a large flume at the laboratory of the Institute for Hydraulic and Water Resources Engineering of the Darmstadt University of Technology, Germany. The flume is part of a closed system formed by a pump station, elevated tank, main flume, and an in-floor recirculation channel. Figure 3.1 shows a schematic illustration of the experimental set-up.

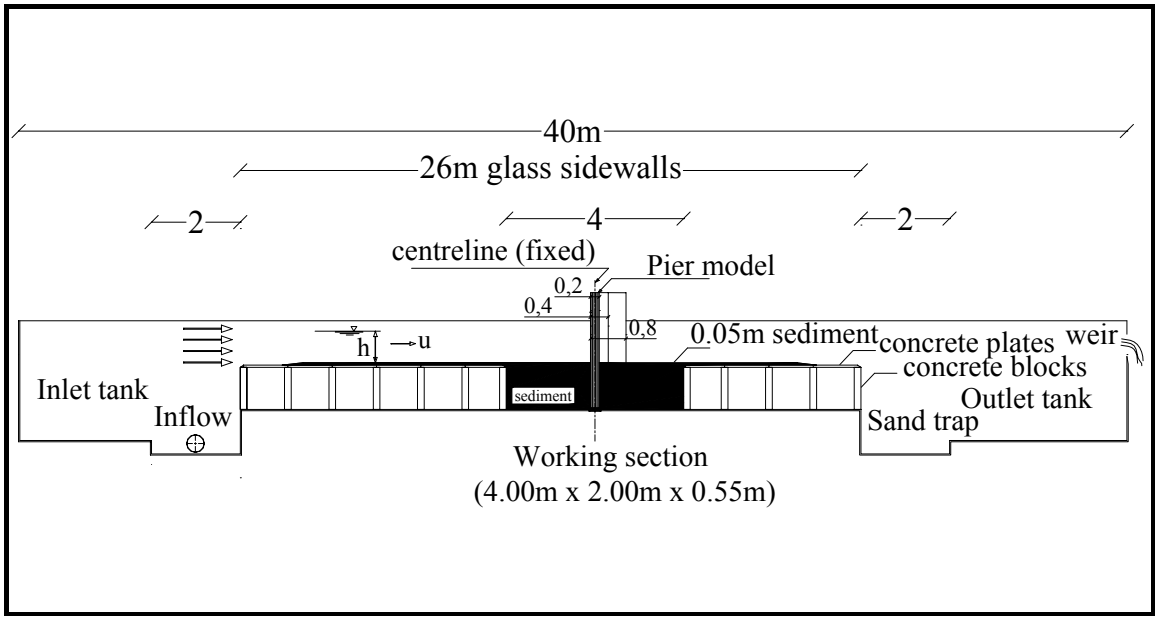

Figure 3.1. Experimental, setup schematic

The main flume was rectangular with 40m overall long, 2 m wide and 1 m deep. The flume has 26 m long glass side-walls which help to monitoring and observation of the flow and sediment transport. During experiments, the required discharge was pumped from the ground reservoir through the elevated tank into the inlet of the main flume using two parallel-operated pumps that can serve up to 800 lit/s. The inflow was controlled by a magnetic inductive discharge flow-meter (Fischer Porter Model D10) and regulated by an electronic inlet valve (fluctuation ±0.05 Lit/s). The flow depth was adjusted by tailgate and controlled by ultrasonic distance sensors (UDS) (Wehrhahn, P8000) with a precision of ± 0.50mm.

Measurements were performed in the middle of a working section located 16 m downstream of the flume entrance and having a length of 4 m, width of 2 m and depth of 0.55 m. A false bottom made of concrete plates was installed to avoid the filling of the whole flume with sediment material. The plates rested on bricks, 0.5 m above the original flume bottom. Over the false concrete bed, a 5 cm uniform thickness layer was made from the used bed material to have the same boundary condition. This layer extended 9.0 m upstream and 4.0 m downstream the location of the pier models. To smooth the flow at the upstream, a wooden mesh was installed over the water surface at the flume inlet. To avoid secondary flows, the sides of the working section were coated with absorbing material. A sand trap was installed before the flume outlet.

Pier Shape

Four different piers were fabricated and used in the scouring tests, (1) 0.20 m diameter circular cylinder, (2) 0.20 m width square cylinder, (3) 0.20 x 0.40 m rectangular pier, and (4) 0.20 x 0.80 m rectangular pier. Piers were made of plexiglass or glass, depending on the required rigidity. The transparency of models was necessary to facilitate the measurement of the scour hole dimensions from inside the pier by using a Laser Distance Sensor. Two rings made of PVC or aluminium was fixed at the top and the bottom of the piers in order to support the measuring system and attach the pier on the flume bottom. Figure 3.2 shows photographs of the piers.

In each case, the pier was placed on the centreline of the flume and at a certain longitudinal location, keeping the coordinates of the pier centreline constant for all the conducted experiments. This was important for inter-comparison of measured contour profiles.

Figure 3.2. Experimental piers. Circular (up-left), Square (up-right), Rectangular 0.20x0.40 (down-left) and Rectangular 0.20x0.80 (down-right)

Pier Alignment

The square pier was installed with four different angles of attack; namely α = 0, 15, 30 and 45º with the principle flow direction, in order to investigate the effect of square pier alignment on scouring.

Sediment Material

The used bed materials were tested and characterized in the laboratory of Hydraulics of the Darmstadt University of Technology. The soil tests carried out included a mechanical sieve analysis and a specific gravity tests. Figure 3.3 gives the plots of the particle size distribution (sieve analysis) tests.

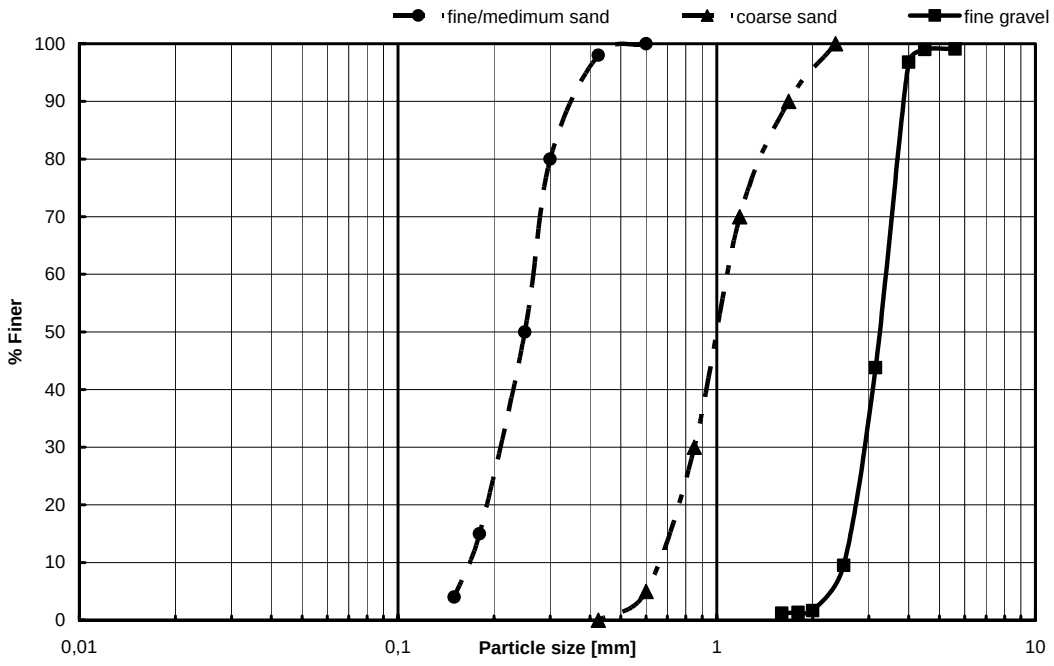

Figure 3.3. Results of the sieve analysis test

Three different sediment were used; the first was fine gravel that was the standard bed material for the series R1 and R2 of pier shape and pier alignment tests. The other two bed material were coarse and fine/medium sand that were employed in the series of bed material effect on scour at square pier. The geometric standard deviations of the particle size which is defined as $\sigma_g = \sqrt{d_{84.1}/d_{15.9}}$ was less than 1.50 for all used bed materials, therefore the sediment were considered to be uniform bed (Dey et al. 1995). The angle of repose of the bed materials (ϕ) was measured from shear box tests. The section-

averaged critical velocity for the initiation of motion of isolated sediment particle (u_{cr}) was firstly obtained from the Hjulström diagram (Zanke 2002) then checked in the experiment. All experiments were performed under clear-water scour conditions near the threshold velocity with bed shear stress about 95% of the critical bed shear stress (τ_{cr}) for the initiation of sediment motion at the plane sediment bed, see table 3.1.

3.3 MEASURING TECHNIQUES

Scour topography

Experimental installations using a laser distance sensor LDS (Baumer Electronic, OADM 13U6480/S35A) and positioning systems (precision step motors and linear units of the firma ISEL) were developed to measure developing and equilibrium scour holes topography during running experiments from the pier inside. The laser distance sensor OADM13 has a compact housing (13.4 x 40 x 48.2 mm) and a measuring distance ranged from 50 up to 550 mm in air (under water up to 750mm) with an accuracy of ± 0.30mm. The sensor works on the triangulation principle to provide a precise output signal which is proportional to the measured distance (here: scour hole radius) between the transmitter and the surface of reflection (here: scour hole surface).

For circular and square piers the sensor was driven in the vertical direction by a step motor with a precision of ± 0.02 mm allowing the recording of vertical profiles in the scour hole. In the radial direction, the vertical positioning system was driven by a second step motor with a precision of ± 0.01º, allowing the sensor to turn around in the scour hole, taking various vertical profiles in different azimuthal half-planes. Figure 3.4 shows the installation of the measuring system for square and circular piers.

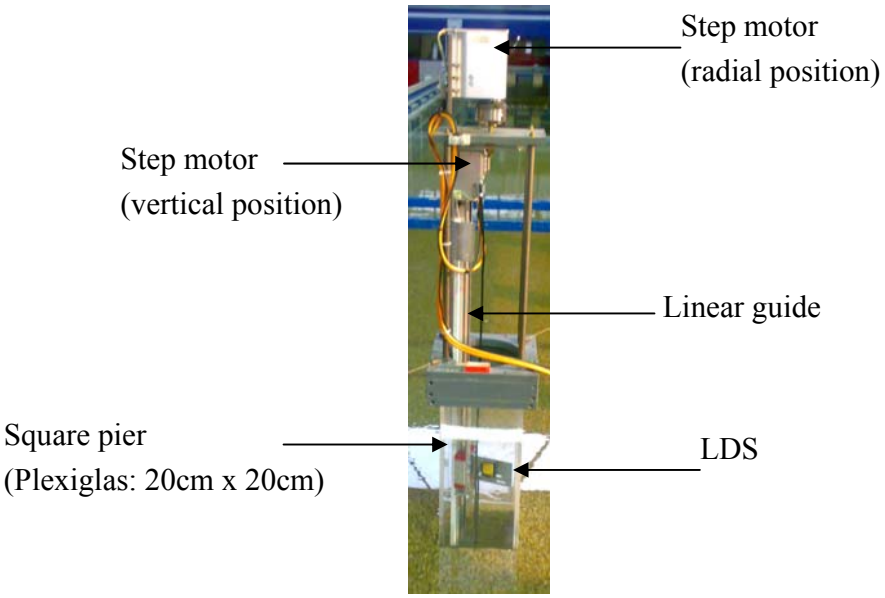

Figure 3.4. Installation of LDS measuring system for square pier**.**

For rectangular piers, the moving system was improved and modified to able to move the sensor in the longitudinal direction too. Two new linear units of the firma ISEL were used for the vertical and the longitudinal directions and one step motor for the radial direction. The sensor was mounted together with the step motor for radial direction on the lower end of the first linear unit (Model: LES 6 with Spindle Drive, KG-trieb16x5 & L1690mm) which was attached vertically on the other linear unit (Model: LES 5 with Spindle Drive, KG-Trieb16x5 & L1090mm), that was supported horizontally in the longitudinal direction over two lateral carriers on the top of the flume sides. Figure 3.5 shows the experimtal pier for the rectangular case.

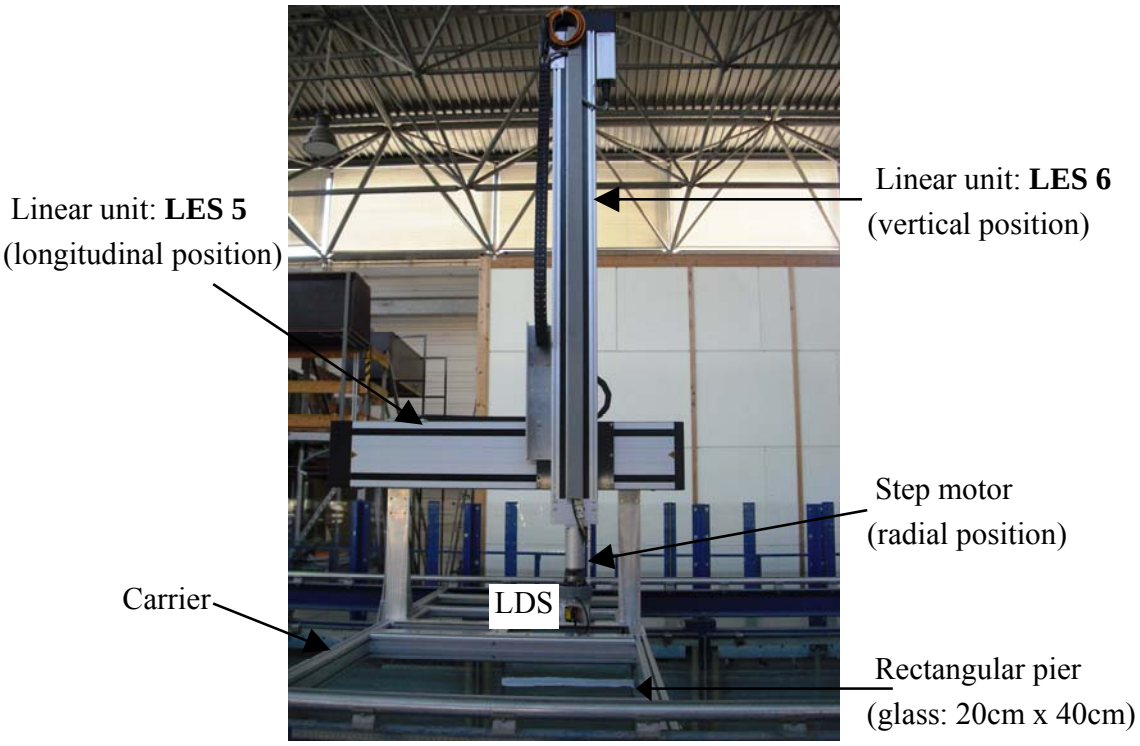

Figure 3.5. Installation of LDS measuring system for rectangular piers**.**

Figure 3.6 shows the used coordinates systems for the flow and bed topography measurements.

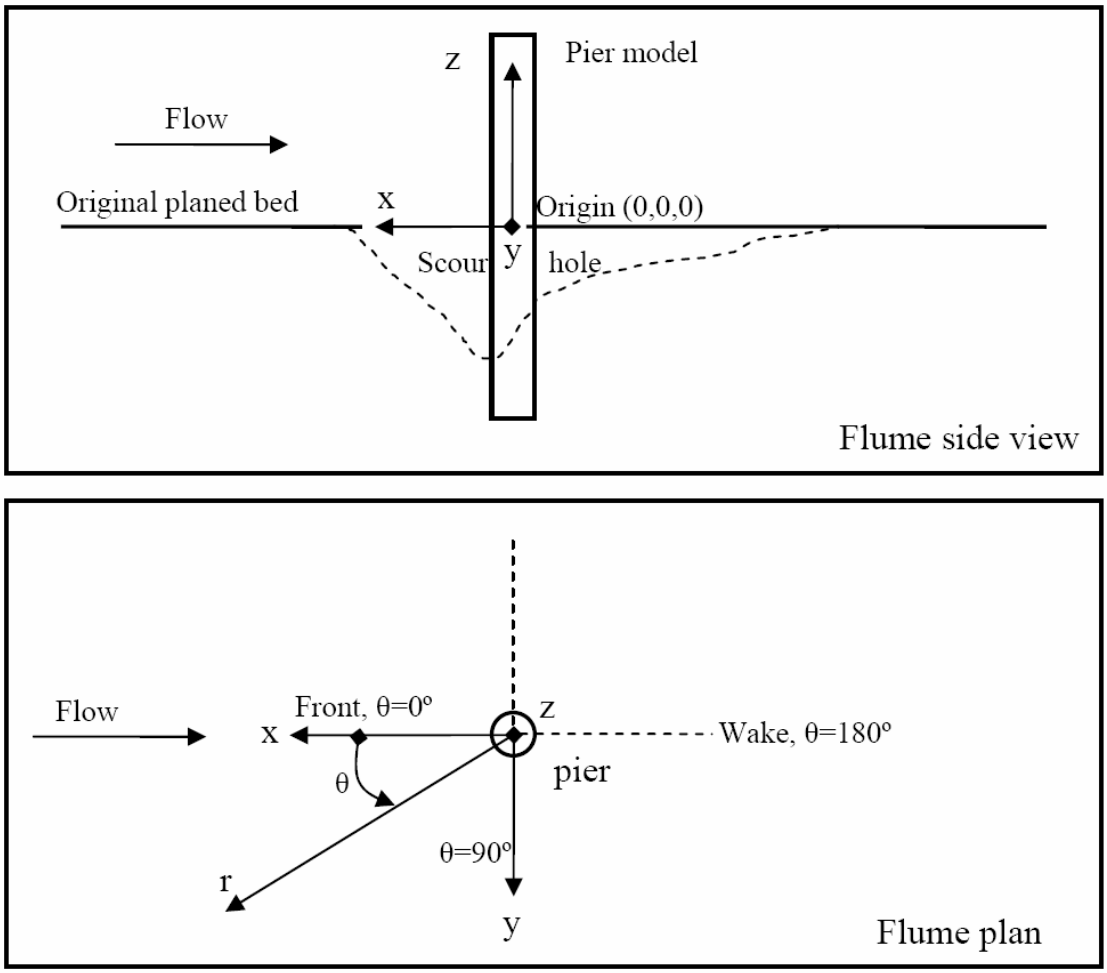

Figure 3.6. Coordinates systems for flow and bed topography measurements

Analogue signals of distance sensor, step motors and linear units control systems were electronically filtered and transformed into digital format using a real-time data acquisition system. Real-time data acquisition and digital record were addressed by using an Adwin-L16 card with L16-CO1. Acquisition programs were written using real-time developing-tool AD-basic. Data was recorded at a Personal Computer using a FIFO strategy, registering time and Cartesian coordinates (x, y, and z) of measured points in the scour hole.

Using one of the both positioning systems, the distance sensor was located in the pier model and aligned in the horizontal, vertical and radial directions to measure the scour hole radius at any point on the surface of the scour hole. Calibration curves for different radial directions around the pier were taken to determine the relations between the sensor signals and the measured radial distances. For square and rectangular pier, the effect of

refraction was taken in consideration when the laser beam being not perpendicular to the pier surface using a new calibration curve for each measuring direction.

Vertical profiles were taken in different azimuthal half-planes by turning the distance sensor in step of 15º in case of circular and square piers. The system was translated along the rectangular pier with steps of 0.05m in the longitudinal direction. Scour at the edges of square and rectangular piers in azimuthal half-plane with θ = 45, 135, 225 and 315º were interpolated from measurements at θ = (43 & 47), (133 & 137), (223 & 227) and (313 & 315º), respectively where θ is the angle of azimuthal plane with the principal flow direction. Up to 30 radius values per measured point were recorded. Measured radius, vertical and longitudinal sensor positions were registered at a frequency of 70 Hz, allowing a very fast measurements of the scour hole. Measurements were performed continuously during running experiments. A measurement of the complete scour hole with vertical profiles containing about 10-60 points took about 30 and 60 seconds at the beginning of the experiment and about 180 and 360 seconds at the end of the experiments, depending on the bed material, sand or gravel. Therefore in the present study the measurements are considered to be instantaneous and the measuring technique is a non-intrusive high resolution system.

The visualization and analysis of the measured data were carried out using much software such as Active Perl, MATLAB, Excel, Surfer and Tec Plot.

Flow Velocity Field

An Acoustic Doppler Velocimeter ADV, developed by SonTek (5cm down-looking and sampling rate up to 50 Hz) was mounted together with a vertical positioning on carriage in order to measure the three dimensional velocity components as well as the turbulence intensities. This instrument carriage was mounted on rails on the top of the flume sides allowing the movement of ADV in both longitudinal and transverse direction of the flume. Scales were fitted in the flume wherever necessary to provide a reference datum. The installation of the velocity measurement system as well as the pier model and the used axes are shown in Figure 3.7.

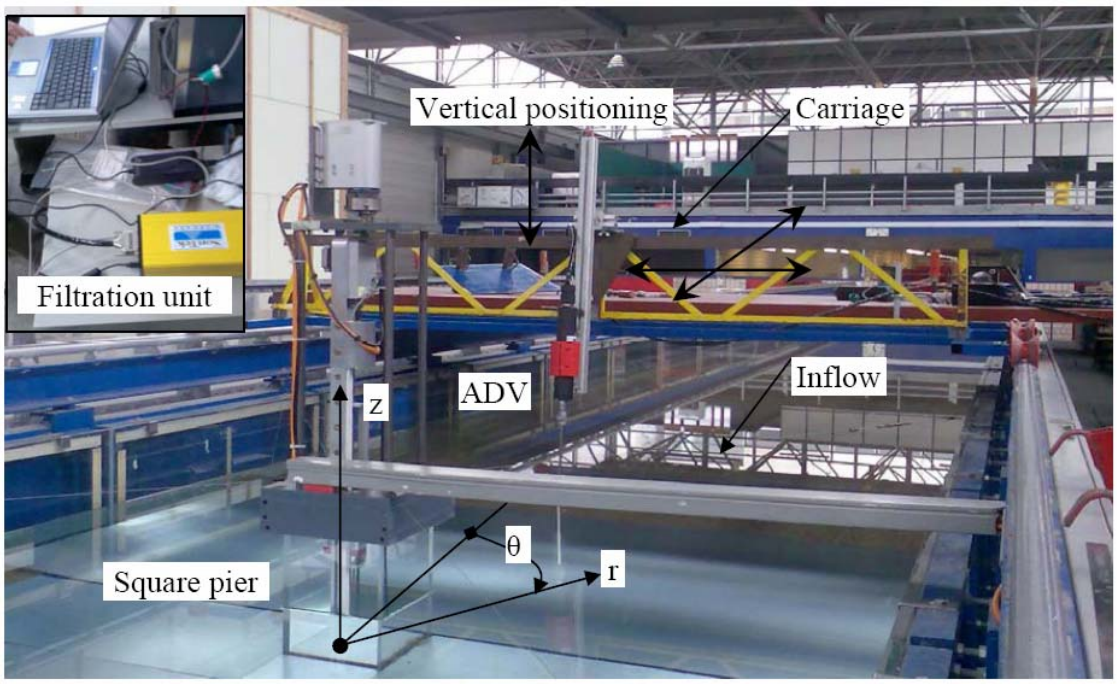

Figure 3.7. Installation of velocity measurement system

The cylindrical polar coordinates system (θ, r, z) were used to represent the flow velocity field. Here, the time-averaged velocity components in (θ, r, z) were represented by (u, v, w) and their fluctuations were (u', v', w') respectively. The set-up of distances from the bed, sampling durations at each point, sampling rates, and file names were provided with a PC-Software named HORIZON. The lowest possible point of ADV reading was 1 cm above the bed. The sample durations were between 3-5 minutes depending on the turbulence to obtain statically time independent average-velocities. The output data of ADV was filtered using an algorithmic filtration unit. Velocity components and turbulence intensities were plotted in rz planes using MATLAB, EXCEL and TECPLOT programs.

3.4 EXPERIMENTAL PROCEDURES AND DATA ACQUISITION

In order to achieve the planed series, a strict experimental procedure was followed during the tests. The procedure which was divided to before, during and after the runs can be summarized as follows:

Preparation of experiment:

1. The pier shape, alignment or sediment material was changed between the experimental series. The circular pier was first embedded in uniform gravel. Then the square pier (alignment with the flow) was installed and tested with three different bed materials. This was followed by installing of the square pier with different angle of attack, 15, 30 and 45 degrees in gravel bed. Finally, the square pier was replaced with two rectangular piers one after the other that were tested also with the standard bed material, i.e. gravel,
2. The laser distance sensor LDS and its positioning system were installed inside and above the pier model. The LDS was recalibrated between the pier shape or alignment experiments. Also the ultrasonic distance sensors UDS for water level as well as the ADV were mounted.
3. Before each run, the bed was carefully leveled throughout its length especially in the working section in the vicinity of the pier using a trowel with screed. This trowel with screed is of the same width as the flume and can be dragged along the flume rails. Some measurements to check the leveling of the bed were taken randomly using the ultrasonic distance sensors.
4. Photographic documentation was taken.
5. The flume was very slowly filled with water from the two flume ends to the required water depth, taking care for escaping of the air bubbles from the bed and extra care for the sediment movement. The tailgate was kept fully closed during the filling with water.
6. Finally, all instrumentations were checked.

During-experiment:

1. After filling the flume slowly to the required water depth, the pump was turned on and its speed was slowly increased until the required flow rate. Concurrent with speeding the pump, the tailgate was adjusted to maintain the required water depth in the flume.

2. After the desired flow conditions were established, two velocity profiles at the centerline of the flume at a distance of 8m upstream and of 4m downstream the pier were measured using the ADV to check and control the desired velocity.
3. The water depth was measured and controlled with UDS along the flume.
4. The measurement of the geometric properties of developing scour holes proceeds as follows: the sensor LDS was firstly positioned at the centerline of the pier front at the original bed level. There, radius was measured by the LDS. After the performed measurement, LDS descend a given step in the vertical and another radius was registered continuing so until the bottom of scour hole was reached by the sensor. A vertical profile at an azimuthal plane was measured. Next, the LDS was driven up to the original bed level, and the vertical system was turned one step (i.e. 15 degrees), to get the next profile. In case of rectangular piers, the sensor was also moved along the pier sides by step of 5cm. After measurement of the complete scour hole, sensor was returned to the first position to start another measurement. The measured radius (its x and y components), the vertical distance from the original bed level (z) and the value of azimuthal half-plane angle (θ) were recorded.
5. The measurement of the flow velocity field around the square pier in gravel bed using the ADV before scour started (planed bed) and after the equilibrium reached. Vertical profiles of the instantaneous three dimensional velocity components were measured at different distance from the original bed level along a length of 1 meter from the pier face. The measurements were carried out at five different azimuthal half-planes with θ = 0, 45, 90, 135 and 180º, where θ is the angle of the azimuthal plane and the principle flow direction. The output data from the ADV was filtered using a spike removal algorithm.
6. Using an external video camera, flow field as well as sediment movement around the pier was monitored through the glass sidewalls of the flume.
7. The tests were conducted until negligible scour rate, i.e. when maximum scour depth deepens less or equal to d_{50} per hour. Since no general sediment transport was achieved during the experiments. Then the pump was gradually stopped and the tailgate was fully closed to allow the flume to slowly drain through two hosepipes without disturbing the scour topography.

Post-experiment:

1. Post-experiment photographs of the scour hole around the pier were taken.
2. Recorded data was analyzed as in the next part.
3. The above procedures were repeated for each test run.

Data processing, presentation and analysis

After experimentation, automatic data analysis and white noise filter application for suppression of measurement errors was carried out. Programs were written in MATLAB. For characterization of scour holes and flow velocity fields, tables containing time and Cartesian coordinates were elaborated. Vertical profiles in different azimuthal half-planes were plotted for different times. Isolines showing scour hole shape for several time points, as well as time-averaged and instantaneous flow velocity fields, streamlines, and turbulent kinetic energy in different azimuthal planes were plotted using several software such as SURFER, TECPLOT and EXCEL. Average side slopes of scour hole were determined. Curves plotting scour depth, scour radius at different azimuthal planes, scour volume, and scour rate on time were created. Similarly, curves plotting scour depth at different azimuthal planes, scour radius at different azimuthal planes, scour volume, and scour rate on maximum scour depth at the front of the cylinder were plotted. These figures constitute the basis for data analysis.

Existent scour formulas were used for calculation of the experimentally obtained scour depths, testing their performance. A new scour formula was proposed, applying dimensional analysis and using the experimental data for determination of formula coefficients and validation.

3.5 EXPERIMENT SERIES

To achieve the goals of the study, the experimental program was divided into three series of tests as follows:

The first series of tests (Series R1) was designed to investigate the time development of the geometric characteristics of scour holes around piers of different shape in gravel bed. The used shapes were circular, square, rhombus and two rectangular piers with different lengths. Only clear water scour conditions with a flat bed were studied.

The second series of tests (Series R2) was conducted to study the effect of angle of attack on local scouring around square piers. As my knowledge, the effect of angle of attack were tested and reported only for rectangular piers having pier width to length ratio from 2 to 16 (see Laursen and Toch 1956). Four different angles of flow attack, α =0, 15, 30 and 45º was tested also under clear water conditions near the threshold velocity in gravel bed.

The third series of tests (Series R3) was preformed to evaluate the effect of sediment median grain size on the temporal variation of scour holes around square piers. Three different uniform bed materials, two sands in addition to the gravel one, were used with

the specific weight of 2.65 t/m^3, the mean particle size of 0.25mm, 0.97mm and 3.25mm with geometric standard deviation σ_g = 1.37, 1.43 and 1.20, respectively.

In addition to these three series, the flow field was measured around the square pier aligned with the flow in gravel in planed and scoured beds.

A summery of the experimental series and conditions is shown in table 3.1

Table 3.1. Summery of experimental series and conditions

Run	Pier shape	*D* or *B* [cm]	*L* [cm]	α [º]	d_{50} [mm]	σ_g [-]	ϕ [º]	u_{cr} [m/s]	u/u_{cr} [-]	*h/D* [-]
Investigation of pier shape; Series R1										
R1-VP1	circular	20	-	0	3.25	1.20	35.5	0.65	0.95	1.50
R1-VP2	square	20	20	0	3.25	1.20	35.5	0.65	0.95	1.50
R1-VP3	rhombus	20	20	0	3.25	1.20	35.5	0.65	0.95	1.50
R1-VP4	rectangular	20	40	0	3.25	1.20	35.5	0.65	0.95	1.50
R1-VP5	rectangular	20	80	0	3.25	1.20	35.5	0.65	0.95	1.50
Investigation of angle of attack; Series R2										
R2-VA1	square	20	20	0	3.25	1.20	35.5	0.65	0.95	1.50
R2-VA2	square	20	20	15	3.25	1.20	35.5	0.65	0.95	1.50
R2-VA3	square	20	20	30	3.25	1.20	35.5	0.65	0.95	1.50
R2-VA4	square	20	20	45	3.25	1.20	35.5	0.65	0.95	1.50
Investigation of bed material; Series R3										
R3-VS1	square	20	20	0	0.25	1.37	30.0	0.26	0.94	1.34
R3-VS2	square	20	20	0	0.97	1.43	29.0	0.32	0.95	1.50
R3-VS3	square	20	20	0	3.25	1.20	35.5	0.65	0.95	1.5
Measurements of flow field										
R*	square	20	20	0	3.25	1.20	35.5	0.65	0.95	1.5

Where *D* is the diameter/ of the circular/square pier, *L* and *B* are the length and the width of the rectangular pier, α is the angle of flow attack (the angle between the axis of the pier and the principle flow direction), d_{50} and σ_g the median particle size and the geometric standard deviation of the sediment, h and *u* is the mean approach flow depth and velocity, respectively and u_{cr} is the critical mean flow velocity. For proposed experimental investigation, there were no measurable effect for the flume sidewalls on local pier scour, knowing that the maximum ratio of pier width to flume width was approximately 14% when the square pier aligned α = 45º with the flow direction that was lesser than (1: 6.25) ~ 16% (Raudkivi and Ettema 1983).

CHAPTER 4
EXPERIMENTAL RESULTS

Results obtained from all conducted scour experiments are presented. The general observations made of each experiment are discussed, including the time development of scour hole topography, depth, radius, slopes and volumes. Additionally, the turbulent flow field around the square pier is presented and discussed, in order to provide an insight on the complex flow field.

4.1 SCOURING AROUND SQUARE PIER IN GRAVEL: REFERENCE CASE

The previous studies concerned mostly on measurement and prediction of maximum local scour depths at a single circular pier in sand beds (e.g. Ettema 1980, Zanke 1982a, Richardson 1987, Melville and Chiew 1999, Dey 1999, Richardson and Davis 2001, Mia and Nago 2003, Oliveto and Hager 2005, Ataie-Ashtiani and Beheshti 2006). Scour manuals as e.g. Hoffmans and Verheij (1997) incorporate the effect of pier shapes different to the circular cylinder. Studies on the temporal variation of scour around piers have been carried out by e.g. Oliveto and Hager 2002, 2005, Link 2006, Dey and Raikar 2005, 2007, and Yanmaz and Köse 2007. Nevertheless, scarce references are found in the specialized literature on the spatio-temporal variation of the scour hole shape around a square pier in a gravel bed. In this section, the experimental results corresponding to a local scour experiment at a square pier in fine gravel are presented.

Experiments were carried out in a relative large flume under clear water scour conditions with constant water depth of 0.30 m (i.e. h/D = 1.50) and approach flow velocity of 0.62 m/s (i.e. u/u_{cr} = 0.95). A 0.20x0.20m Plexiglas square pier (side facing the approaching flow) was mounted in the middle of the working section. The used bed material was uniform gravel with grain sizes ranging between 2.25 and 4.00 mm and having a median grain size, d_{50} of 3.25 mm and geometric standard deviation σ_g of 1.20.

The test was conducted for more than 4 days, in order to reach almost the equilibrium conditions. However, an equilibrium scour condition was not achieved until the duration of 100 hours. The test was stopped because the scour was nearly reaching the bottom and sides of the flume. Notwithstanding the equilibrium condition did not occur, the scouring rate became very small. The achieved scour rate was just 0.47 mm/hr at the end of test. Moreover, the change in the measured maximum scour depth was only about 13 mm on the last day of the test. In this study, the obtained final scour depth after 100 hours is considered as the equilibrium scour depth, and the corresponding time is therefore taken as the reference time. This point is discussed more extensively in chapter 5.

4.1.1 Maximum Scour Depth

In figure 4.1.1, the time development of maximum depths in the scour hole in azimuthal half-planes with θ = 0, 45, 90, 135, 180, 225, 270 and 315° are presented. During the first 3000s, maximum scour depth in the scour hole moved from the azimuthal half-planes with θ = ± 45° and ± 315° to the centerline of the pier front at the plane with θ = 0°. At the pier wake, scouring was delayed and started at the plane with θ = 180° after 3240s, when the maximum scour depth at the pier front reached 0.21m. At the end of experiment, the maximum final scour depth, Z_{eq} observed at the plane with θ = 0° was 0.458m (~2.29D). The maximum scour depths observed at the pier sides at θ = 90° and wake at θ = 180° were 0.384m (~ 0.84 Z_{eq}) and 0.30m (~ 0.66 Z_{eq}), respectively.

Note that scouring progressed with different velocities around the pier, i.e. at the pier front, sides and wake during the first 20% of the experimentation time. Then curves become parallel and scour progressed in all planes with same velocity.

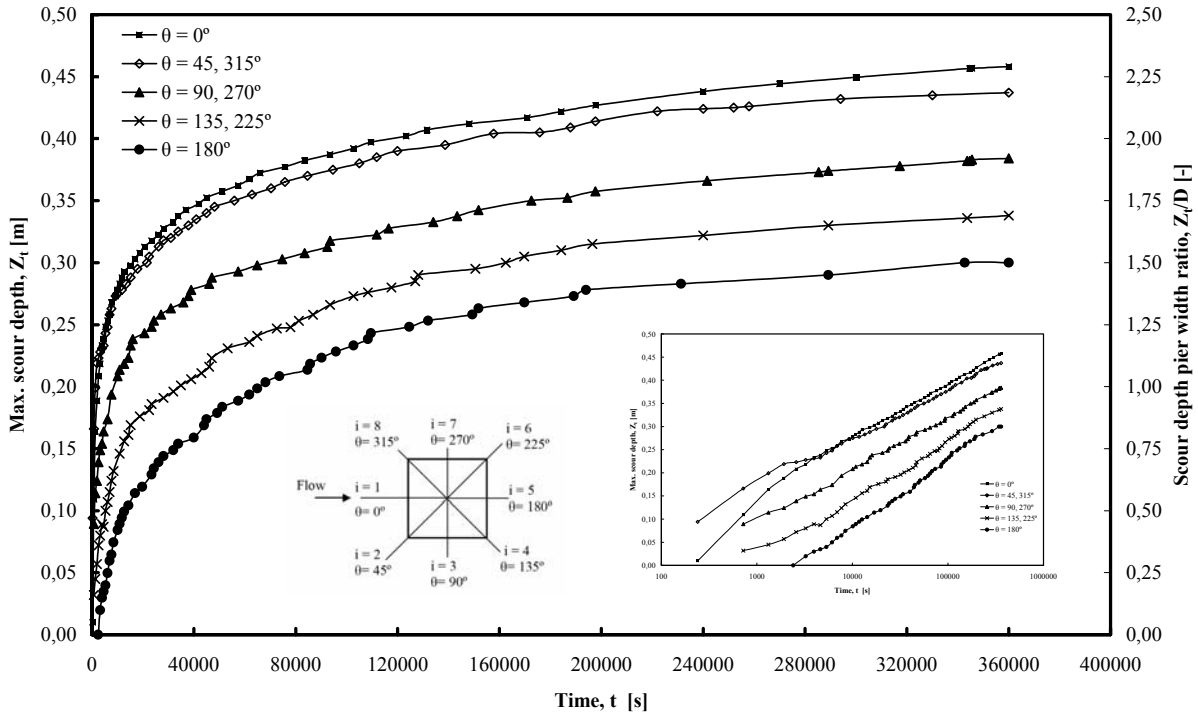

Figure 4.1.1. Time development of maximum scour depth in azimuthal half-planes with θ = 0, 45, 90, 135 and 180° at a square pier [d_{50} = 3.25mm, h/D =1.50 and u/u_{cr} = 0.95].

Figure 4.1.2 shows the maximum scour depth inside the scour hole and the corresponding scour rate (upper), as well as the rates of scouring in different azimuthal half-planes around the square pier (lower).

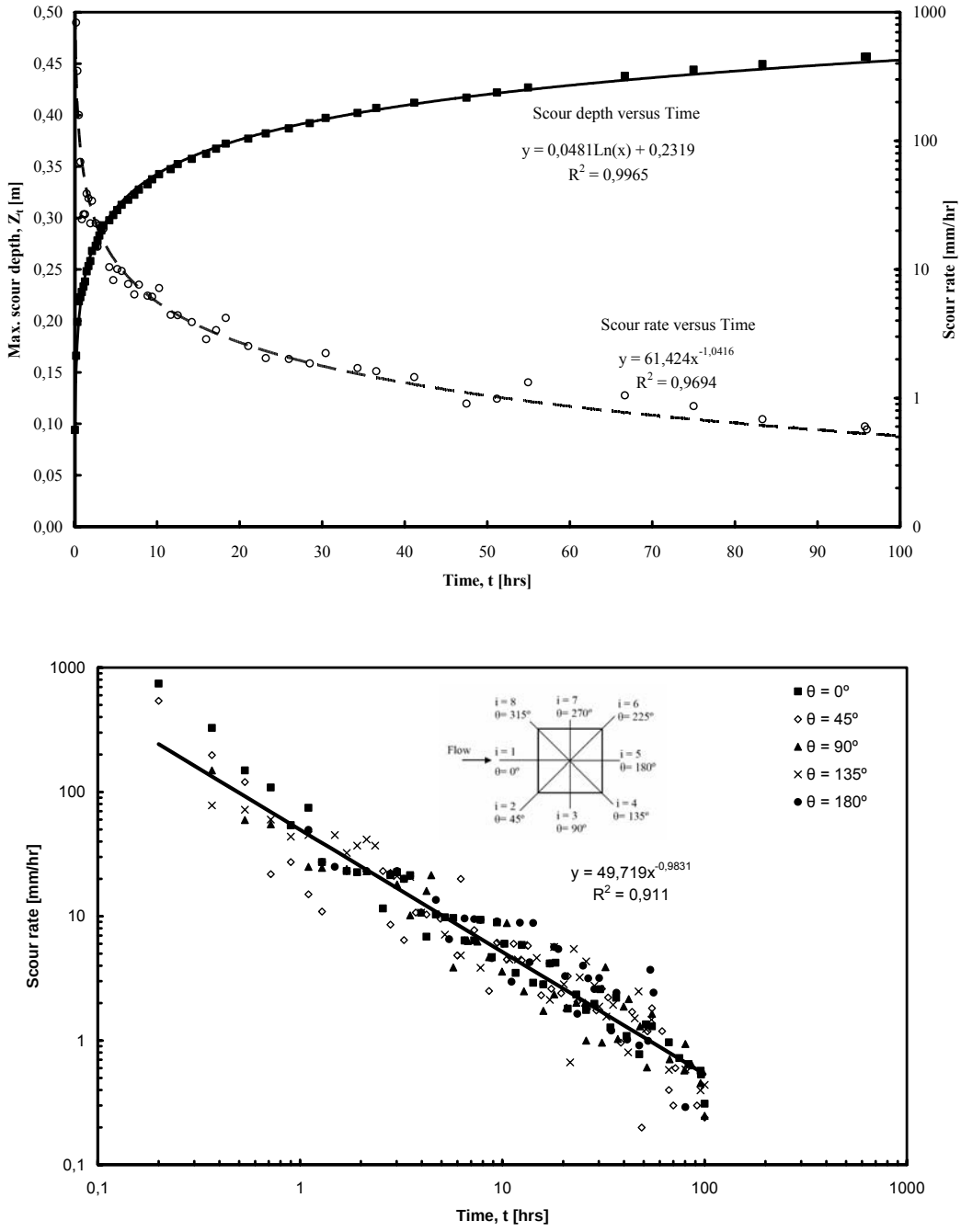

Figure 4.1.2. Maximum scour depth and corresponding scour rate (upper) and scour rates in different planes (lower) at the square pier over time [d_{50} = 3.25mm, h/D =1.50 and u/u_{cr} = 0.95].

As shown, scour progressed with decreasing rate, so that the obtained scour depth during the first hour was nearly as deep as in the following about 4 days. About 75% of the final scour depth was attained within the first 10 hours (10% of experiment time). The maximum scour depth at square pier in gravel bed was fitted well following equation [4.1] with a determination coefficient of $R^2 = 0.9965$.

$$Z_t = 0.0481 \ln(t) + 0.2319 \quad [4.1]$$

Where: Z_t is the maximum scour depth obtained at the end of the given time duration t.

The scour rate is defined as the change in scour depth per change in time (mm/hr). As shown in figure 4.1.2, the rate of scour which was 830 and 350 mm/hr during the first 12 and 22 minutes respectively, was drastically reduced to 10 mm/hr after 5 hours to about 0.47 mm/hr at the end.

The figure also shows the rates of scouring in different azimuthal planes around the pier as well as the tendency line. The negative slope of the fitted straight line which was 0.983 denotes that the scour developed with decreasing rate with the time.

4.1.2 Scour Geometry

Figure 4.1.3 shows the development of scour hole topography around the square pier in gravel bed after 720, 5340, 11760, 35880, 144600 and 360060s. Scouring was noticed immediately after starting the test at the corners of the pier front at θ = ± 45 and ± 315°. Eventually scour propagated rather rapidly around the pier perimeter from both corners toward the centerline of the pier front with θ = 0°. The deepest point was firstly observed at the planes with θ = 45 and 315° during the first 3000s. Later, scour depth at the plane with θ = 0° approached maximum scour depth inside the scour hole. In this stage, a mound of the eroded sediment from the scour hole was firstly deposited close to the pier wake, and found to be moving downstream with time. Then the scoured region surrounded the pier after 3240s.

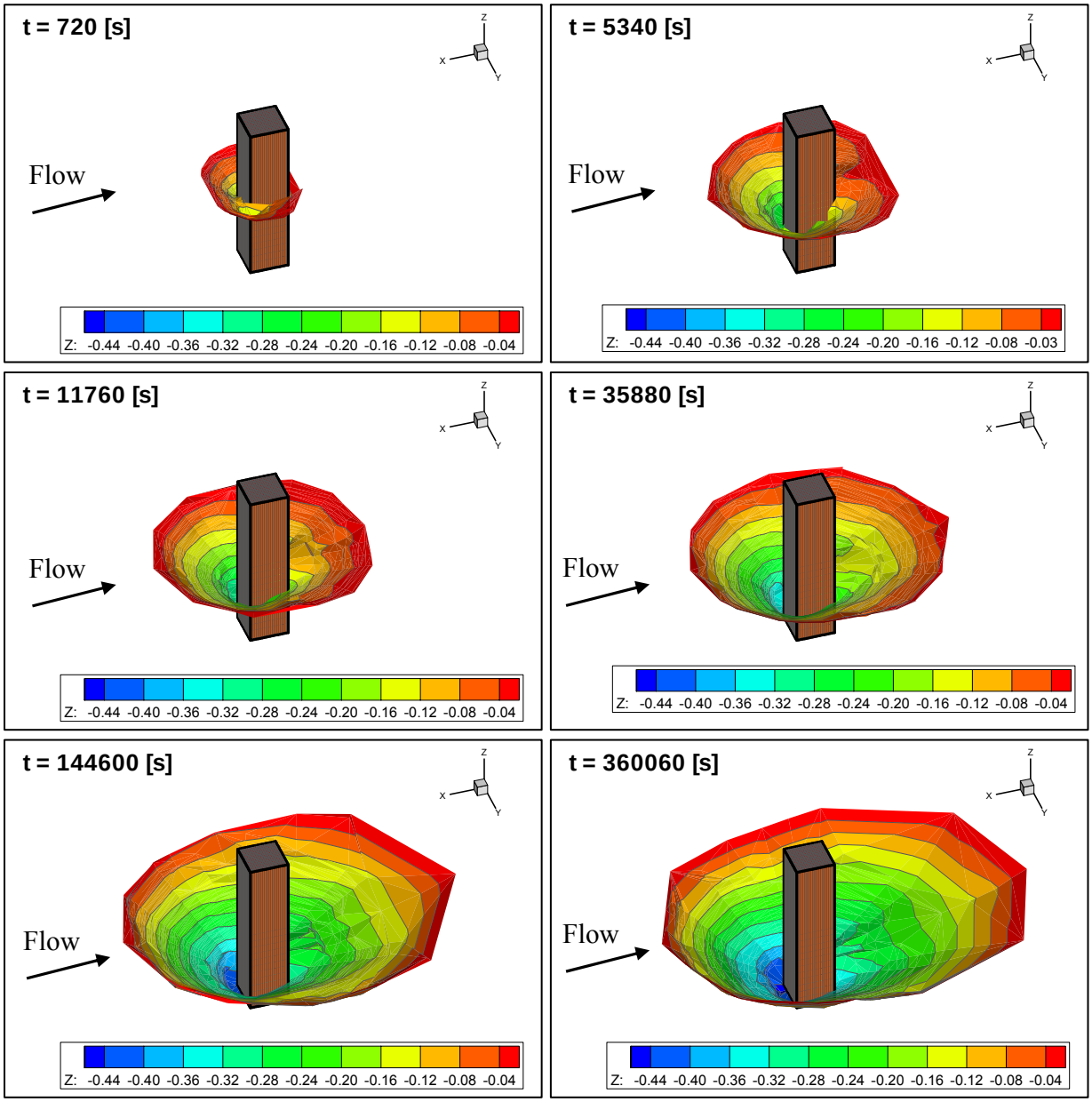

Figure 4.1.3. Developing scour hole topography at a square pier after 720, 5340, 11760, 35880, 144600 and 360060s [d_{50} = 3.25mm, h/D =1.50 and u/u_{cr} = 0.95].

Figure 4.1.4 presents maximum scour depths at different azimuthal half-planes for given times. At the upstream side of the pier between θ = 315, 0 and 45º, the gradient of scour hole bottom shows declination with time. The observed difference in maximum scour depth at planes with θ = 0 and 45º decreased from 26% at t =720s to 4.6% at the end of the test. At the downstream, flat region between azimuthal planes with θ = 210, 150 and 180° was identified. In other words, the bottom of the scour hole looked like two nearly flat region at the pier front and wake, and two gradients on the pier sides.

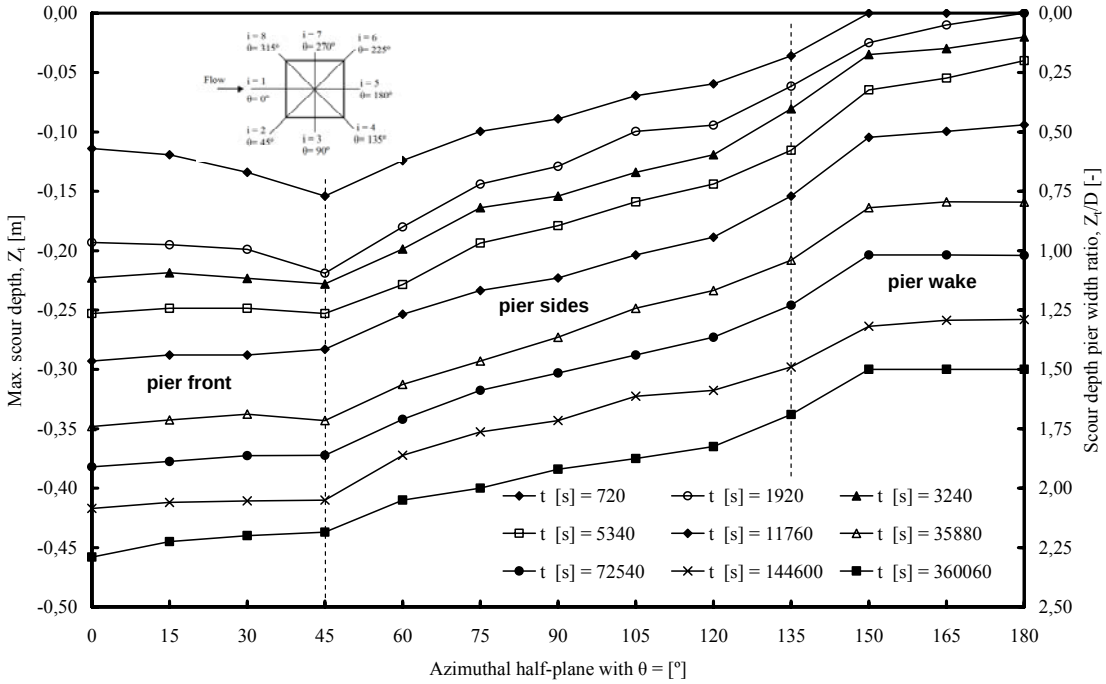

Figure 4.1.4. Maximum scour depth in azimuthal half-planes with θ = 0, 15, 30, 45, 60, 75, 90, 105, 120, 135, 150, 160 and 180° over time around a square pier [d_{50} = 3.25mm, h/D =1.50 and u/u_{cr} = 0.95].

Figure 4.1.5 presents the measured scour-slopes over time at the square pier front, sides and wake in planes with θ = 0, 45, 90, 135 and 180°. The plot corresponding to azimuthal half-plane with θ =135° contains data measured at the planes with θ =133 and 137°, and the tendency line. Scour hole shape remained nearly constant during the development of scouring. Close to the pier front, at θ = 0 and 45°, a flat ring shaped portion was observed. Over the ring, two uniform slopes were identified. The lower slope was steeper than the upper one. At the pier sides with θ = 90º, a nearly uniform slope over the ring shape portion was identified. A second concave slope located in the upper part of the profile at the pier wake with θ = 135 and 180º was observed. The radius of this concave slopes was approximately 1.05 and 1.15 m at θ = 135 and 180º, respectively. Average slope of the scour hole sides diminished with θ, changing from an average of 36 to 16° at planes with θ = 0 and 180°.

Average inclination of scour slopes in gravel did not exceed the natural repose angle significantly. Only one exception was the lower slope at the pier front that was about 48º. Scour hole shape and slope break suggest the action of three main vortices with different strength that being lower to the upper part of the scour hole. Counterclockwise vortex rotation contributes to side stabilization, explaining the existence of sides with a higher inclination than the natural repose angle.

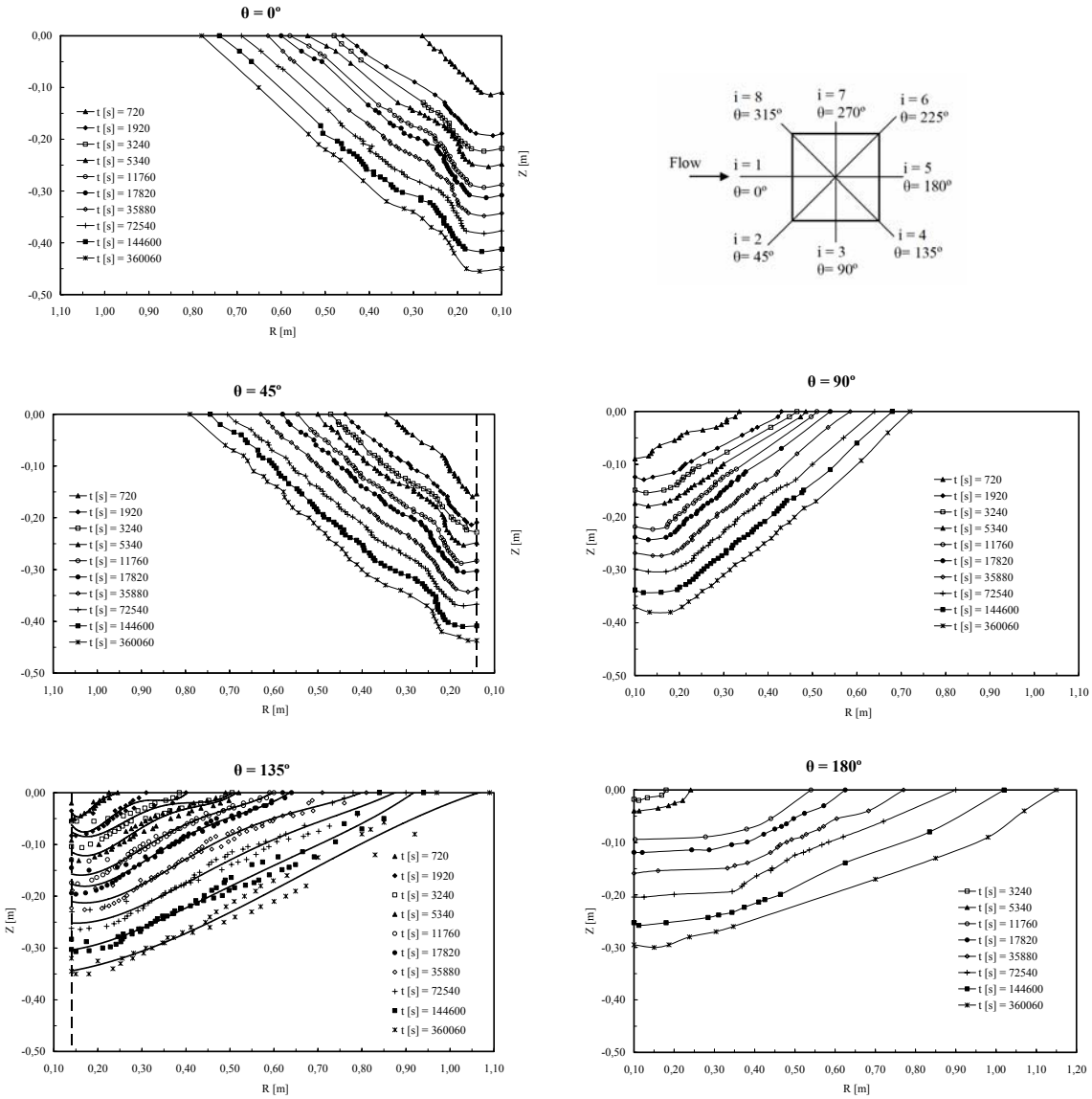

Figure 4.1.5. Measured scour-slopes in azimuthal half-planes with θ = 0, 45, 90, 135, and 180º over time at a square pier [d_{50} = 3.25mm, h/D =1.50 and u/u_{cr} = 0.95].

Figure 4.1.6 relates between non-dimensional maximum scour radius ($R_{m,\theta}/D$) at azimuthal half-planes with θ = 0, 45, 90, 135, and 180º and non-dimensional maximum scour depth ($Z_{m,\theta\ =\ 0^o}/D$) in front of the pier with θ = 0º. The maximum scour radius correlated linearly well with maximum scour depth at the pier front, determination coefficient R^2 between 0.93 and 0.99. The maximum scour hole radius for all azimuthal half-planes always exceeded the corresponding maximum scour depth in front of the pier with θ = 0º during the running time. The developing maximum scour radius (or the scour extent) increased from the upstream to the downstream with θ, reaching about 3.90D and

5.75D at the planes with θ = 0 and 180º at the end of the experiment, respectively. The obtained correlations can be used to estimate maximum scour radius, and then the scour hole surface area.

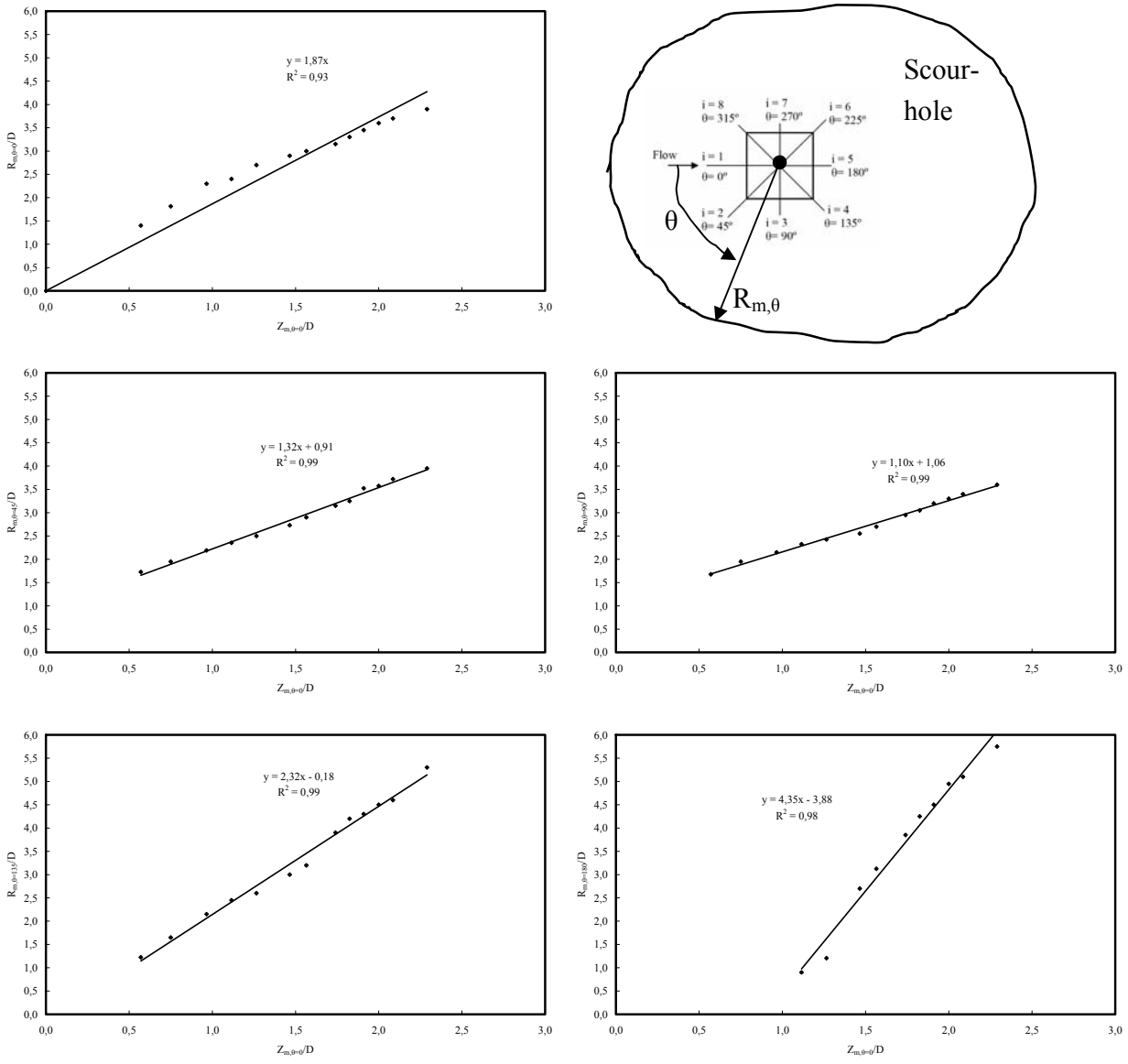

Figure 4.1.6. Non-dimensional maximum scour radius in azimuthal half-planes with θ = 0, 45, 90, 135, and 180º over non-dimensional maximum scour depth at azimuthal half-plane with θ = 0º at a square pier [d_{50} = 3.25mm, h/D =1.50 and u/u_{cr} = 0.95].

4.1.3 Scour Volume

Figure 4.1.7 shows non-dimensional volume of developing scour holes on non-dimensional scour time, and on non-dimensional maximum scour depth in front of the pier with θ = 0º. Since scour started at the pier's front corners, scoured volume was recorded before maximum scour depth at the plane with θ = 0º was larger than zero. After the scour reached the pier's front, the general tendency of the scoured volume was to correlate well with the maximum scour depth in front of the pier following a parabola with a determination coefficient of 0.97. Thus, when providing maximum scour depth at the pier front, the obtained correlations can be used to calculate scour hole volume.

The plotted curve between scour volume and time showed that the scour developed at a decreasing rate over time. About 75% of the maximum scour hole volume was obtained in the first 35% of the experiment time.

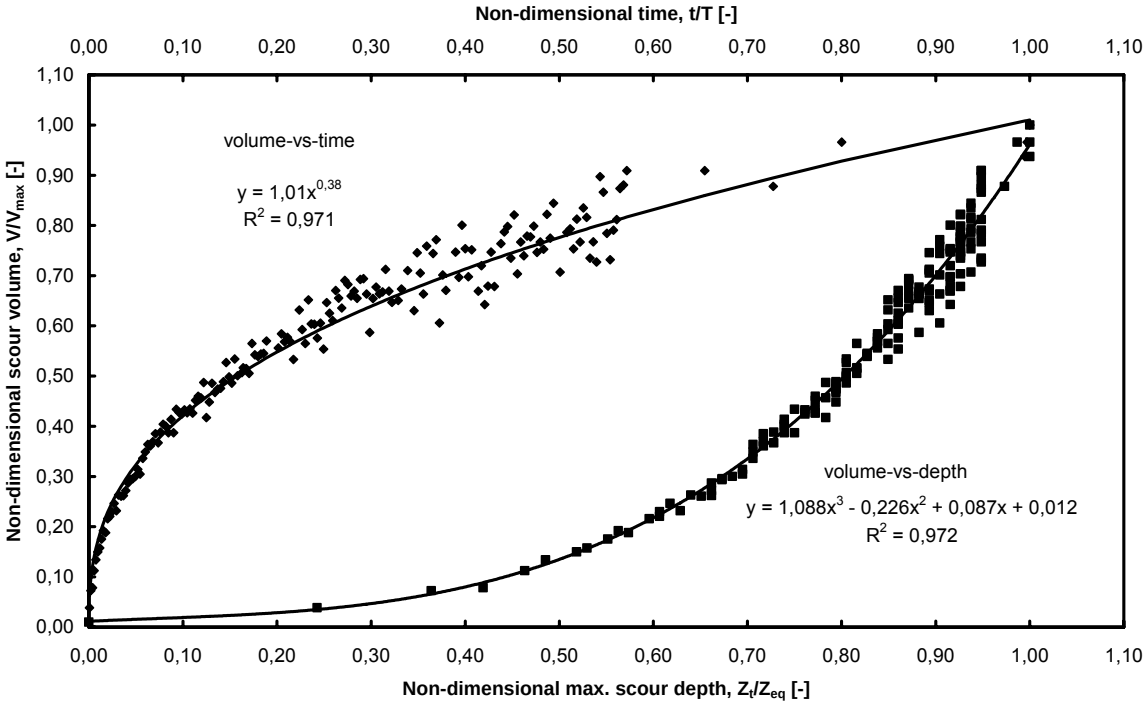

Figure 4.1.7. Non-dimensional volume of developing scour holes on non-dimensional maximum scour depth (bottom) and on non-dimensional time (upper) at a square pier [d_{50} = 3.25mm, h/D =1.50 and u/u_{cr} = 0.95].

4.1.4 Flow Field

Bridge piers in a flow induce turbulence and vorticity that increase the risk of sediment bed scouring. Experimental investigation of the three dimensional turbulent flow field around a square pier (side facing the approaching flow) embedded in uniform gravel bed (d_{50} = 3.25mm & σ_g=1.20) is presented. Point flow velocities and turbulent intensities were measured with the acoustic doppler velocimeter (ADV). Measurements were carried out at the pier front, corners, sides and wake in azimuthal half-planes with θ =0, 45, 90, 135 and 180º. Clear water scour experiments were conducted over 100 hours with section-averaged flow depth of 0.30 m and velocity of 0.616 m/s which was 95% of the critical velocity for initiation of sediment motion at an undisturbed plane bed. Two experiments were conducted, namely (1) with a plane sediment bed and (2) in an equilibrium scour hole. Figure 4.1.8 shows the coordinate system for the velocity measurements. Results show the spatial distribution of time-averaged velocity components, flow vectors and time-absolute velocity as well as turbulence intensities components and turbulent kinetic energy.

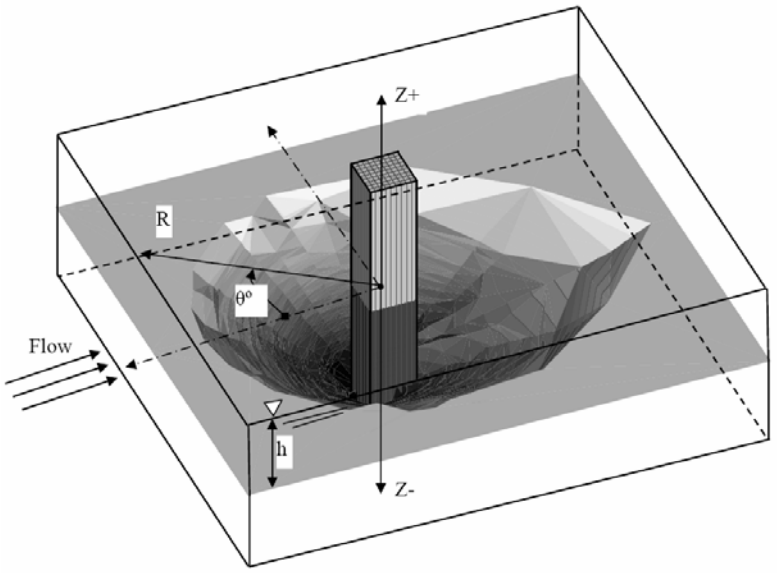

Figure 4.1.8. Coordinate system (Z = 0 at bed surface and θ = 0º at pier longitudinal axis)

Velocity measurements

Figure 4.1.9 shows the patterns of the time-average tangential velocity component *u* (in cm/s) at azimuthal planes with θ = 0, 45, 90, 135 and 180º plane bed (left) and equilibrium scour hole (right). At pier front with θ = 0º, the time-average tangential velocity component *u* was relatively small, and increased with θ, becoming a maximum at pier sides with θ = 90º. At the pier wake from 90 to 180º, it diminished with θ. The

magnitude of u increased with the distance to the bed and decreased with the distance to the pier. The maximum observed values were 78.87 and 61.85 cm/s with θ = 90º (1.28 and 1.004 U_m) for plane bed and equilibrium scour hole, respectively. General speaking, higher velocities were observed around the pier in a plane bed. At the pier front with θ = 0º, differences of 15% were observed. At pier wake with θ = 180º, the existence of wake due to the flow separation results in a reversible flow (negative values).

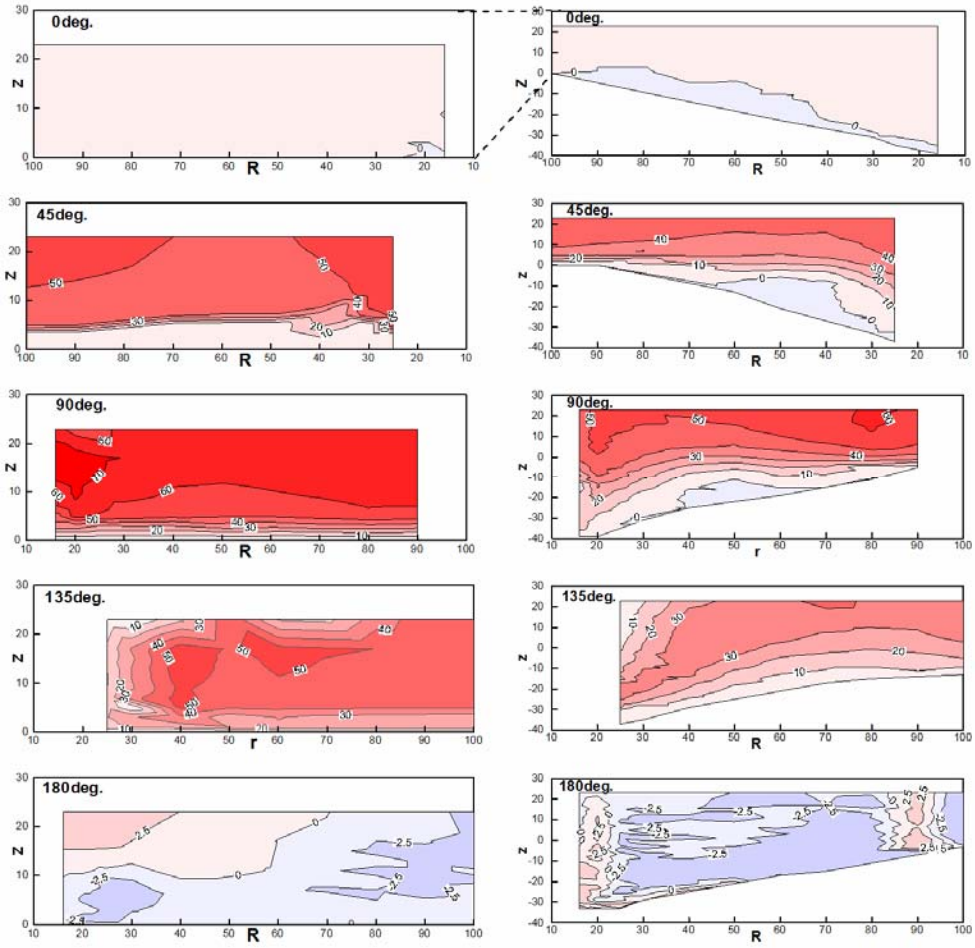

Figure 4.1.9. Contours of time-averaged tangential velocity u (in cm/s) at azimuthal planes with θ = 0, 45, 90, 135 and 180º for plane (left) and scoured (right) beds.

In figure 4.1.10, the contours of the time-average radial velocity component v (in cm/s) at azimuthal planes with θ = 0, 45, 90, 135 and 180º for the plane bed (left) and equilibrium scour hole (right) are shown. At pier front, flow separation was evident at the scour hole edge resulting in a reversal flow inside the scour hole. The imaginary line of separation where v = 0 was observed at a depth 0.45-0.75 times the local scour depth inside the scour hole. The maximum reversal v-value was 14.212 cm/s (0.23 U_m) at θ = 45º. It confirmed that a strong horseshoe vortex existed inside the scour hole in front of the pier.

At pier sides with θ = 90º, the flow separation existed inside the scour hole with small v-values than at the pier front. The reversal flow velocity at pier sides was about 20% less than it at pier front. At plane with θ = 135º, v-component was towards downstream and increased with increase in the vertical and radial distances with maximum value of 66.4 cm/s (1.08 U_m). At pier wake with θ = 180º, it showed reversal flow above the scour hole at R < 60cm (3D) because of the backflow and the flow separations. The v- component decreased with the decrease of the radial distance because of the vertical solid boundary (pier). It also decreased with increasing θ.

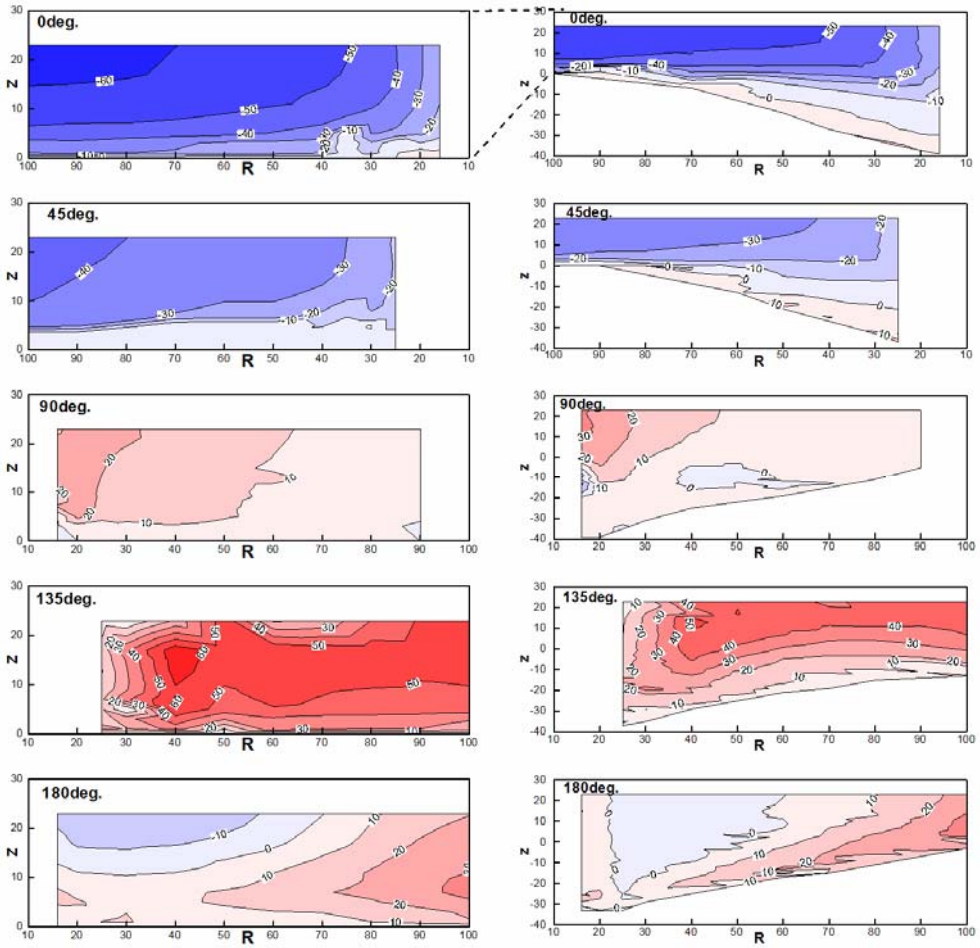

Figure 4.1.10. Contours of time-averaged radial velocity v (in cm/s) at azimuthal planes with θ = 0, 45, 90, 135 and 180º for plane (left) and scoured (right) beds

Figure 4.1.11 presents contours of the time-average vertical velocity component w (in cm/s) at azimuthal planes with θ = 0, 45, 90, 135 and 180º for the plane bed (left) and equilibrium scour hole (right). At pier front and sides, distribution of w was mostly downward (negative) in the flow zone and it was upward (positive) near the bed. At pier wake with θ = 180º, w became upward (positive) as a result of the existing of suction

that helps to remove the sediment material. The magnitude of w for the experiment in an equilibrium scour hole was greater than at the plane bed. The downward flow increased and the upward flow decreased with decrease in θ and radial distance R. The magnitude of w grows clearly in zone $R < 2D$. The maximum measured value of w was -30.43 cm/s (0.49 U_m) to downward at θ = 0º and 22.75 cm/s (0.37 U_m) upward at θ = 180º at the equilibrium state. A core with a maximum w occurred near the pier inside the scour hole at a depth of 0.25 times the local scour depth at the pier front and sides. The separation of flow was clearly evident below the edge of the scour hole at the pier front and sides between θ = 0 and 90º as a result of the natural reversal of w-component at the bed. The imaginary line of separation with w = 0 was a curved line intersecting the scoured bed at the edge of the scour hole and near its base.

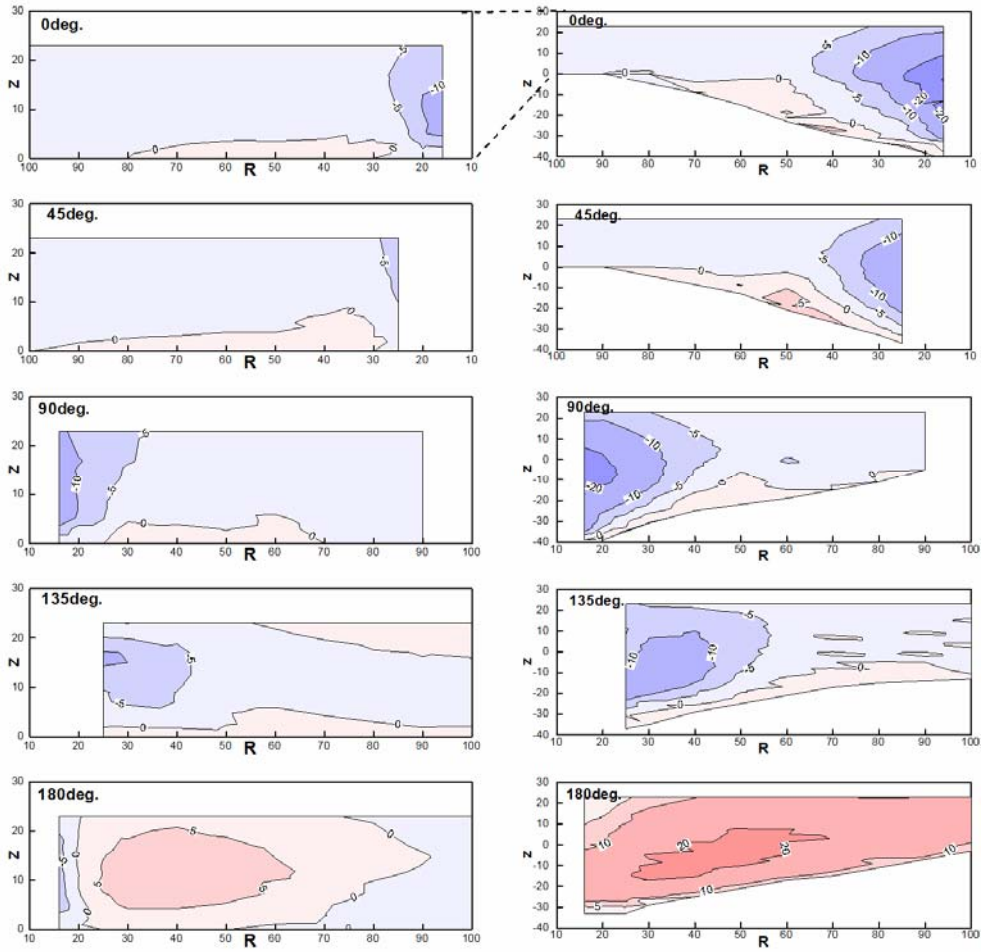

Figure 4.1.11. Contours of time-averaged vertical velocity w (in cm/s) at azimuthal planes with θ = 0, 45, 90, 135 and 180º for plane (left) and scoured (right) beds

The contours of the time-average vertical velocity vector $\sqrt{v^2 + w^2}$ (in cm/s) at azimuthal planes with θ = 0, 45, 90, 135 and 180º for plane bed (left) and equilibrium scour hole (right) are shown in figure 4.1.12. The characteristics of the horseshoe vortex and the strong downflow inside the scour hole at the pier front and sides with θ = 0 to 60º were evident. The flow was horizontal above the scour hole for R >2D for the solid bed and R > 3D for the equilibrium phase between θ = 0 to 45º. Then the flow gradually curved down towards the pier. At θ = 90 and 135º, the flow became outwards the pier above the scour hole with low circulation motion. At θ = 180º, it showed a swirl motion near the pier with R < 2D, and then the flow became gradually outwards the pier over the flow depth in the solid bed case. For the solid bed, the horseshoe vortex was not distinct while it became strong at the pier front for the equilibrium phase and decreased with increase θ.

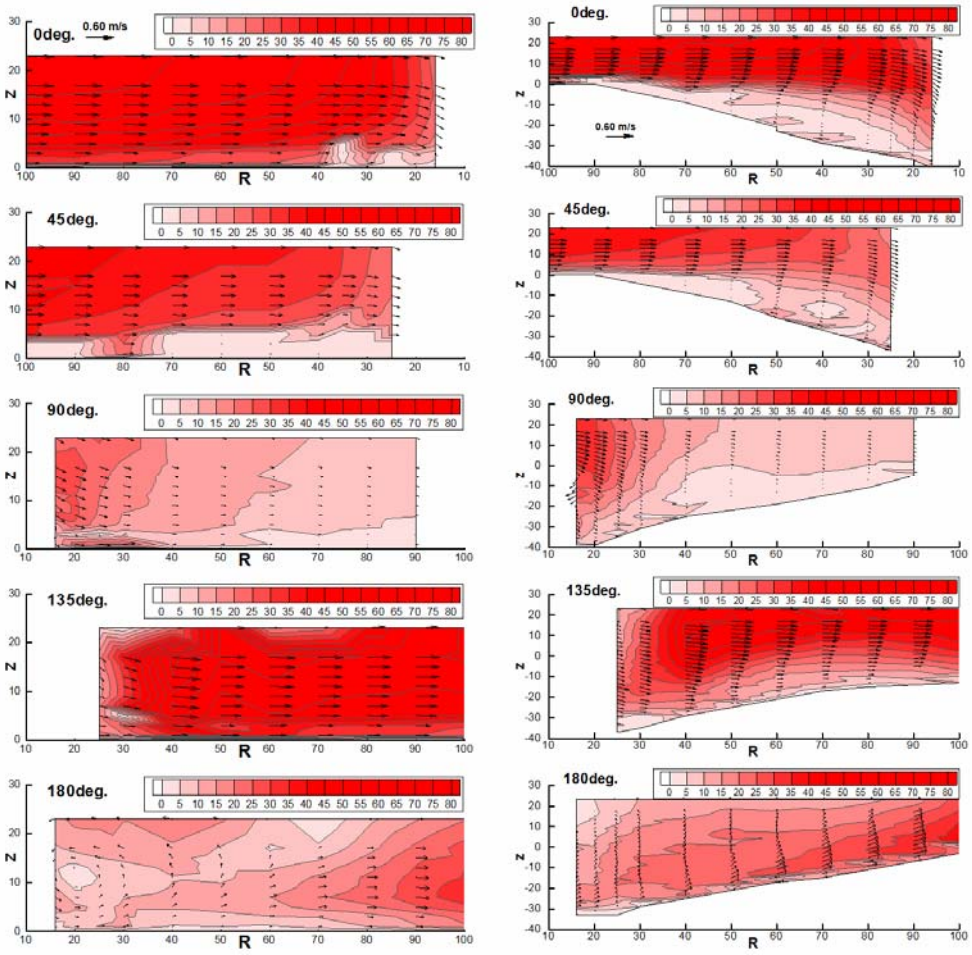

Figure 4.1.12. Velocity vector $\sqrt{v^2 + w^2}$ (in cm/s) at azimuthal planes with θ = 0, 45, 90, 135 and 180º for plane (left) and scoured (right) beds.

Figure 4.1.13 shows the contours of the time-average absolute velocity $U_{total} = \sqrt{u^2 + v^2 + w^2}$ (in cm/s) at azimuthal-half planes with θ = 0, 45, 90, 135 and 180º for plane bed (left) and equilibrium scour hole (right). U_{total} is a scalar quantity which represents the intensity of the total velocity. For the plane bed, the magnitude of U_{total} increased with increasing θ from 0 to 135º then diminished towards the pier wake with θ = 180º. At θ = 45º, the existence of flow separation due to the pier edge cause smaller values of U_{total}. A region of rapid changing in U_{total} near the bed was clear from the concentration of contour lines. In the equilibrium scour hole, U_{total} values were smaller than those over the plane bed. At θ = 0º, the vertical flow component and the absence of the tangential velocity u was evident. At θ = 90º, the tangential velocity u was a predominant flow feature. While the vertical flow and the tangential velocity together characterized the flow at θ = 135º. At the pier wake with θ = 180º, the lower values of U_{total} was observed near the pier face due to the back flow and the lower values of the radial velocity and it grow toward the downstream.

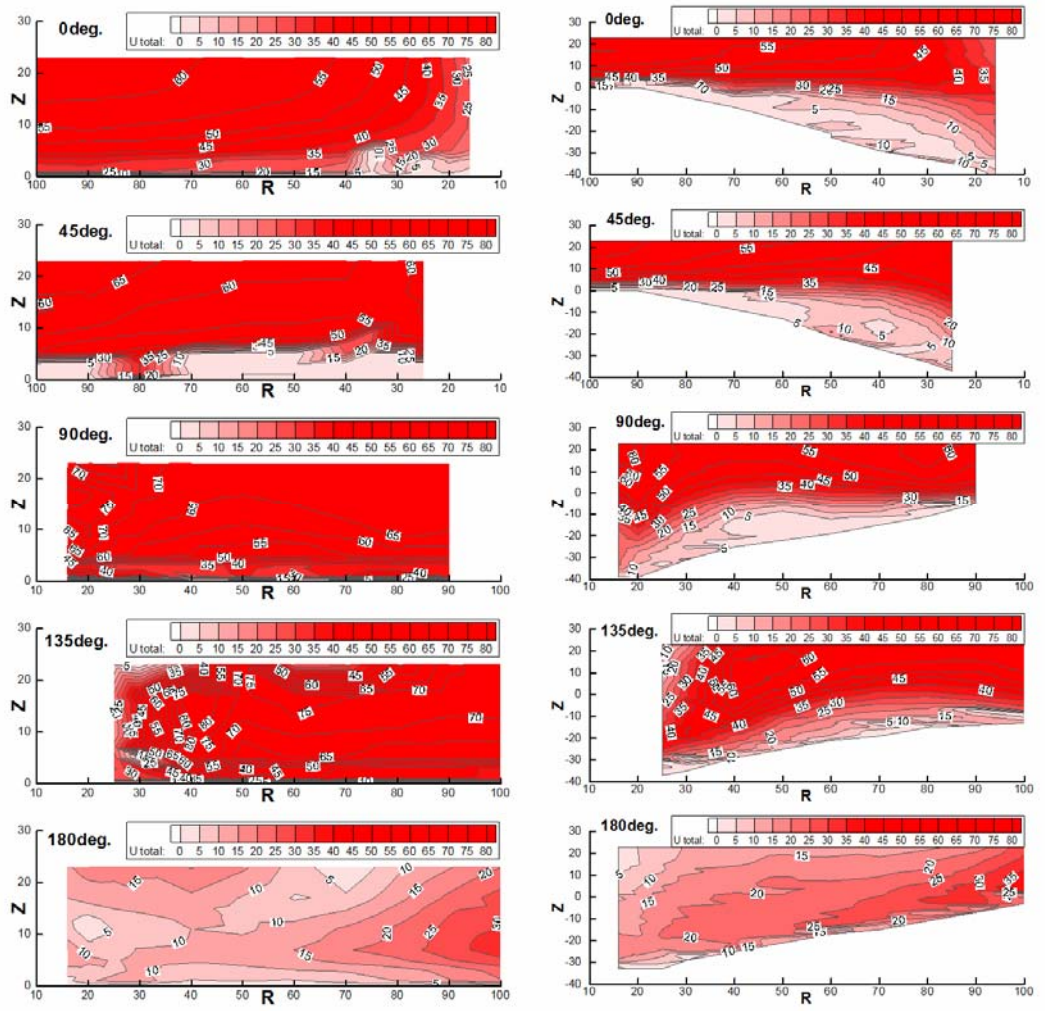

Figure 4.1.13. Contours of time-averaged absolute velocity $U_{total} = \sqrt{u^2 + v^2 + w^2}$ (in cm/s) at planes with θ = 0, 45, 90, 135 and 180º for plane (left) and scoured (right) beds.

Turbulent Field

The pattern of turbulence intensities, $\sqrt{u'u'}$, $\sqrt{v'v'}$, and $\sqrt{w'w'}$ (in cm/s) at azimuthal half-planes with θ =0, 90 and 180º for plane bed (left) and for scoured bed (right) are shown in figures 4.1.14, 4.1.15 and 4.1.16. The distributions of the turbulent intensities at different azimuthal planes were identical. The radial and tangential components of turbulent intensities were larger than the vertical one. At the pier front and sides, with θ = 0 and 90º, the magnitudes $\sqrt{u'u'}$, $\sqrt{v'v'}$, and $\sqrt{w'w'}$ decreased with the vertical distance from the bed. At θ = 180º on the scoured bed, the turbulent intensities first increased with z until an imaginary line of separation at a depth of 0.45-0.75 times the local scour depth inside the scour hole, then decreased again vertically, forming a core of high turbulent intensity over whole of the scour hole. At planes with θ = 0 and 90º, the turbulence intensities increased with decreasing distance to the pier when R < 2D due to the downflow and flow separation. The maximum turbulent intensity was found as a core at the upstream pier face.

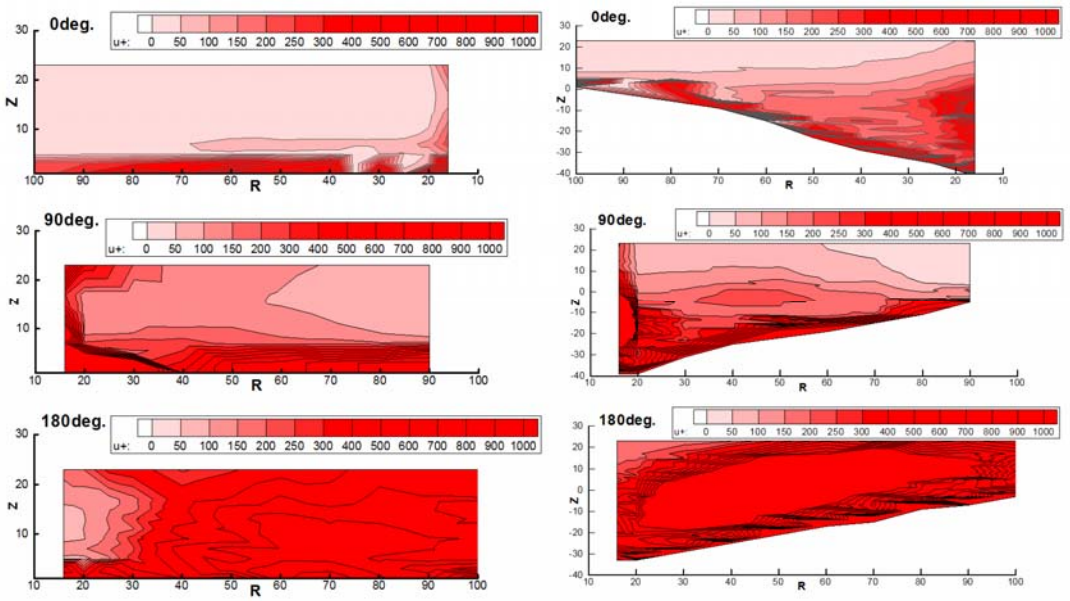

Figure 4.1.14. Contours of tangential turbulence intensity $\sqrt{u'u'}$ (in cm/s) at azimuthal planes with θ = 0, 90 and 180º for plane (left) and scoured (right) beds

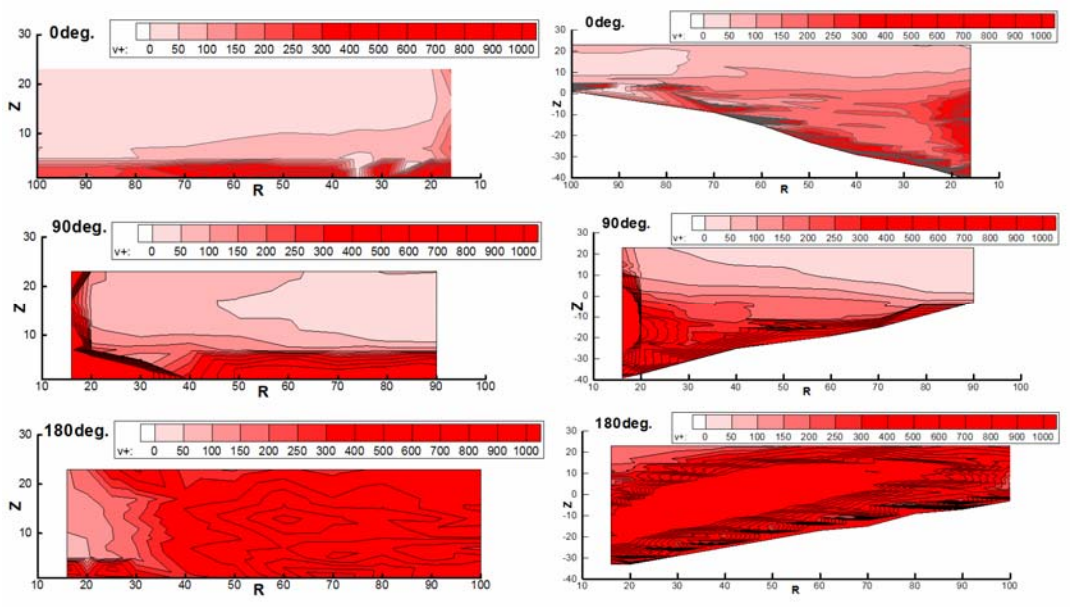

Figure 4.1.15. Contours of radial turbulence intensity $\sqrt{v'v'}$ (in cm/s) at azimuthal planes with θ = 0, 90 and 180º for plane (left) and scoured (right) beds

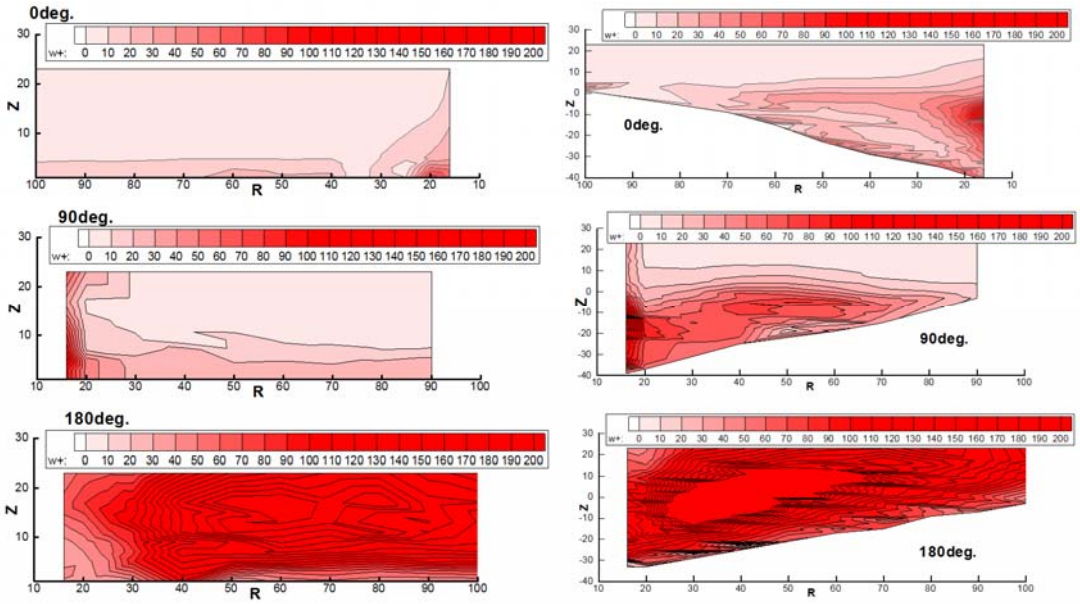

Figure 4.1.16. Contours of vertical turbulence intensity $\sqrt{w'w'}$ (in cm/s) at azimuthal planes with θ = 0, 90 and 180º for plane (left) and scoured (right) beds

The contours of the turbulent kinetic energy *TKE* [$=0.50(\overline{u'u'}+\overline{v'v'}+\overline{w'w'})$] at the pier front, sides and wake with θ = 0, 90 and 180º for plane and scoured beds are plotted in figure 4.1.17. The distribution of *TKE* was similar to that of the turbulent intensity components. *TKE* values increased with θ and with decreasing *r* and *z*. The effect of turbulence lead to much more scouring in front of the pier than at the pier wake where up flow occurred.

Unfortunately- to the best of our knowledge- very few researches on scouring and flow field around square pier in gravel beds are available for comparison of the presented results. Nevertheless the results of Dey and Raikar (2007) show a similar trend.

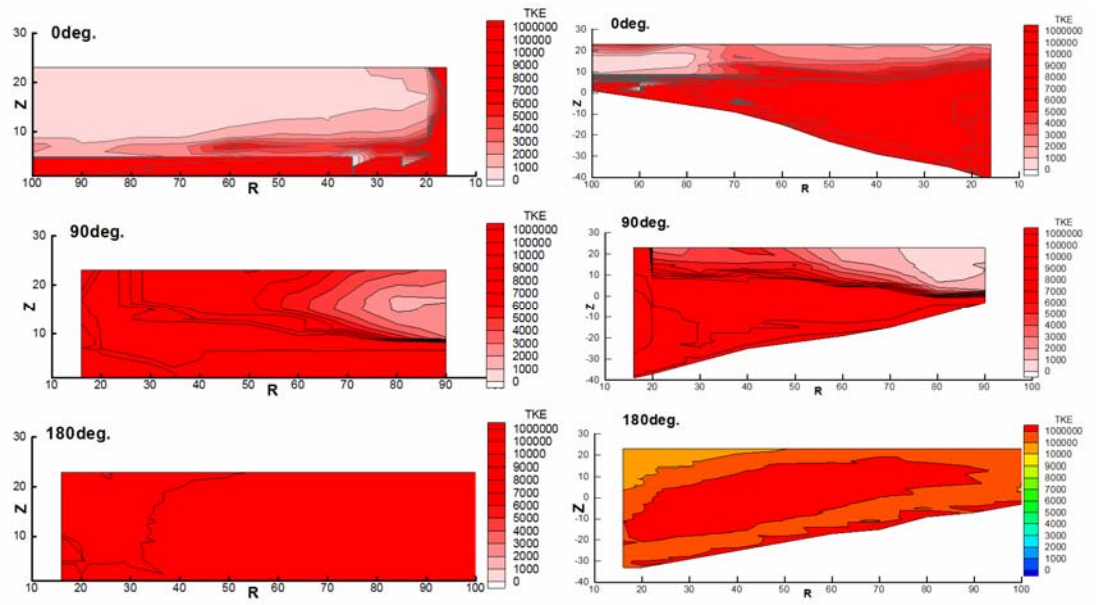

Figure 4.1.17. Contours of turbulent kinetic energy *TKE* (in cm^2/s^2) at azimuthal planes with θ = 0, 90 and 180º for plane (left) and scoured (right) beds.

4.2 EFFECT OF PIER SHAPE ON SCOURING IN GRAVEL

The effect of pier shape on developing scour hole geometry was investigated using circular and two rectangular (with L/B = 2 and 4) piers, in addition to the square pier. The present section is devoted to discuss the general observations of each case, comparing to the reference case (square pier in gravel bed).

4.2.1 Scouring around Circular Pier

Time development of scour hole around a circular pier (0.20m diameter) in gravel bed is presented. Clear water scour experiment was performed with h/D = 1.50 and u/u_{cr} = 0.95. The test was performed for more than 48 hours until the change in the scour depth became very small and insignificant. At the end of the test, the achieved erosion rate was 0.98 mm per hour. Figure 4.2.1 shows photographs of the experimental set-up as well as the final scour hole. It has been seen that scour hole is symmetric around the longitudinal axis of the pier.

Figure 4.2.1. Circular shape at plane (left) and scoured (right) beds
[d_{50} = 3.25mm, h/D =1.50 and u/u_{cr} = 0.95].

Figure 4.2.2 shows the development of maximum depths in the scour hole over time in azimuthal half-planes with θ = 0, 45, 90, 135, 180, 225, 270 and 315º. During the first 10% of experimentation, different decreasing rates of scouring in different azimuthal half-planes around the pier were observed. Later, scour depths in all planes increased with time by nearly the same rate. During the first 3600s, maximum depth in the scour hole moved from azimuthal half-plane with θ = 45º to plane with θ = 0º. Scour was delayed at the azimuthal plane with θ = 180º and started when scour depth with θ = 0º

reached 0.11m (~ 0.50D). The maximum final scour depth Z_{eq} was 0.313m (~1.57 D) at the plane with θ = 0º. About 75% of Z_{eq} was achieved during the first 14% of the test time. The maximum observed scour depth at θ = 90 and 180º were $0.90\,Z_{eq}$ (0.283m) and $0.66\,Z_{eq}$ (0.208m), respectively.

Maximum scour depth inside the scour hole was fitted well following the logarithmic equation 4.2, with determination coefficient of $R^2 = 0.99$.

$$Z_t = 0.0383\ln(t) - 0.145 \qquad [4.2]$$

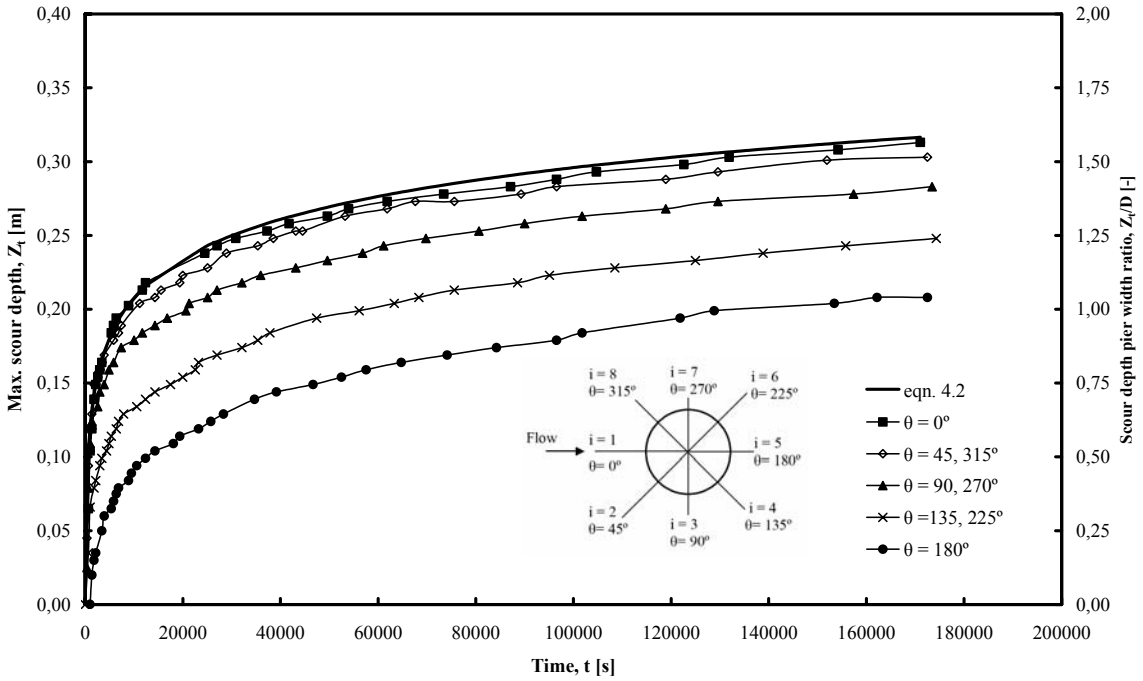

Figure 4.2.2. Time development of maximum scour depth in azimuthal half-planes with θ = 0, 45, 90, 135 and 180° at a circular pier [d_{50} = 3.25mm, h/D =1.50 and u/u_{cr} = 0.95].

Figure 4.2.3 shows developing of scour holes topography at the circular pier after 660, 1020, 3900, 18060, 72000 and 174300s. The scour started and progressed fast at the pier sides between planes with θ = 45 and 90º. The deepest point was found at θ = 45º during the first 3600s. Later, maximum scour depth inside the scour hole was located at the centerline of pier front with θ = 0º to the experiment end. At the pier wake, a deposition area was observed during the first 900s. Then the pier was surrounded with the scour.

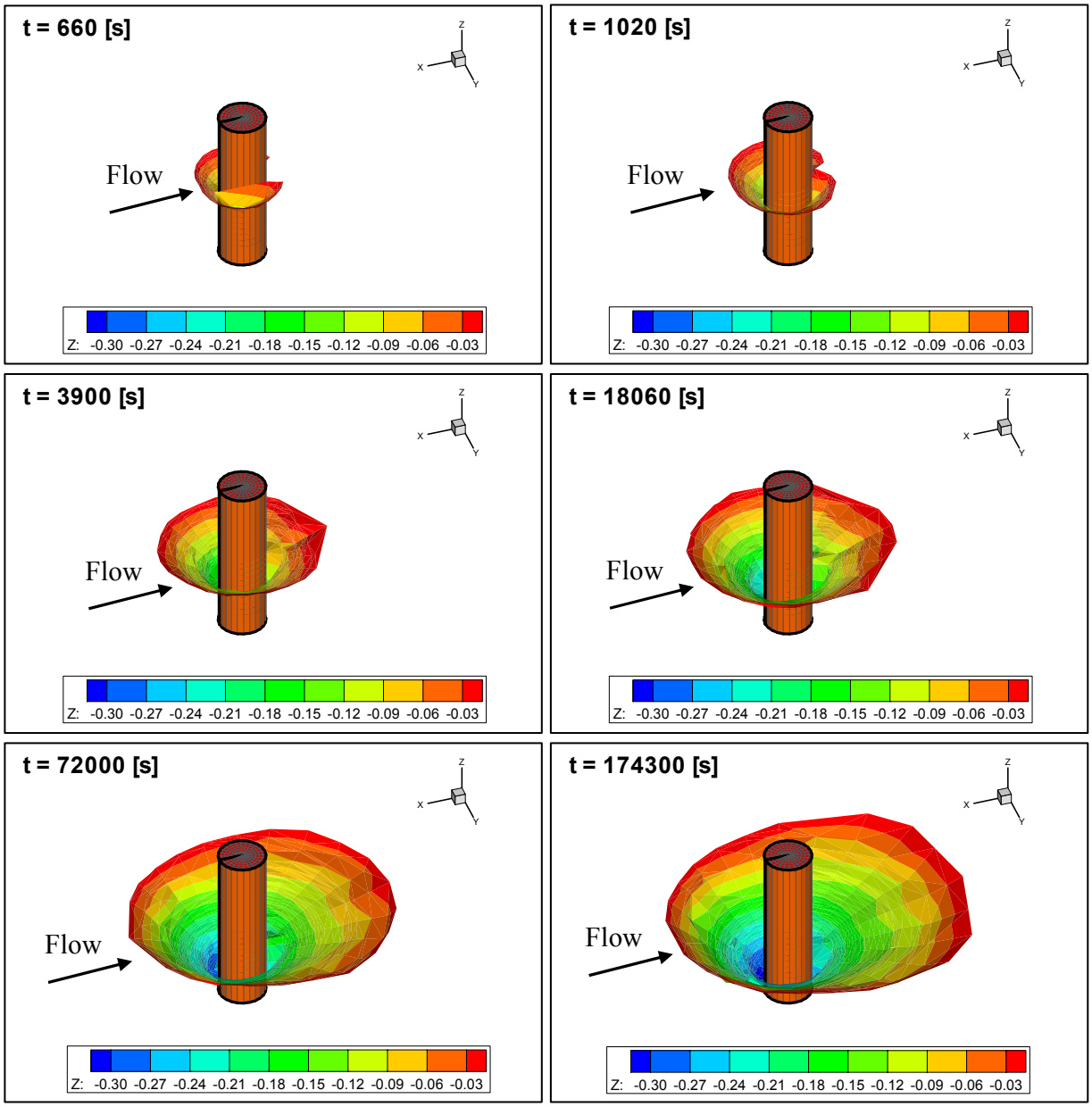

Figure 4.2.3. Developing scour hole topography at a circular pier after 660, 1020, 3900, 8880, 18060, 36600, 72000 and 173460s [d_{50} = 3.25mm, h/D =1.50 and u/u_{cr} = 0.95].

Figure 4.2.4 shows the maximum scour depths in azimuthal half-planes with θ = 0, 15, 30, 45, 60, 75, 90, 105, 120, 135, 150 and 180° at the circular pier for given times. The gradient of the scour hole bottom diminished with time. A flat region between azimuthal half-planes with θ = 165 and 180º was observed. Remarkably, the gradient of the scour bottom at circular was lower than at the square pier.

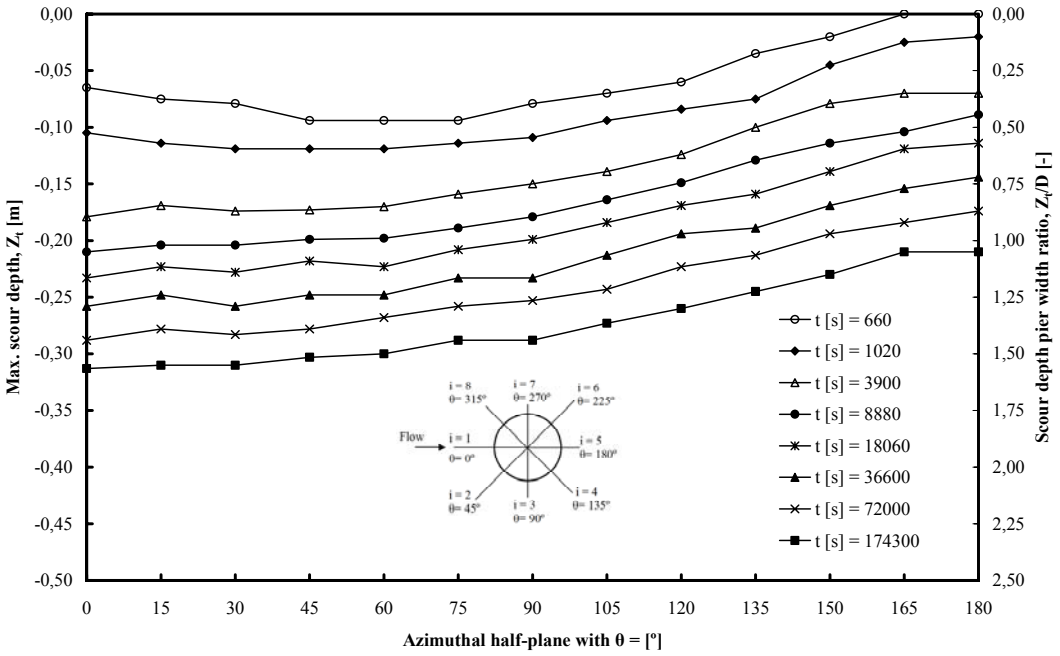

Figure 4.2.4. Maximum scour depth in different azimuthal half-planes around a circular pier over time [d_{50} = 3.25mm, h/D =1.50 and u/u_{cr} = 0.95].

Figure 4.2.5 illustrates the development of scour-slopes in azimuthal half-planes with θ = 0, 45, 90, 135, and 180º at circular pier with time. Similar to square pier, the shape of the scour hole remained nearly constant during the scour process. Close to the pier, a ring shaped groove was identified. The width of the ring at the circular pier was about 70-85% of the ring at the square pier. Over the ring, a nearly uniform slope was observed at the pier front and sides. At the pier wake, a second concave slope located in the upper part of the scour hole was observed. This radius of concave slope was about 3.75 the pier width. Average scour hole slopes diminished with θ, changing from an average of 38º to 19º at planes with θ = 0º and 180º. Note that scour slopes at the circular pier were milder than at the square pier.

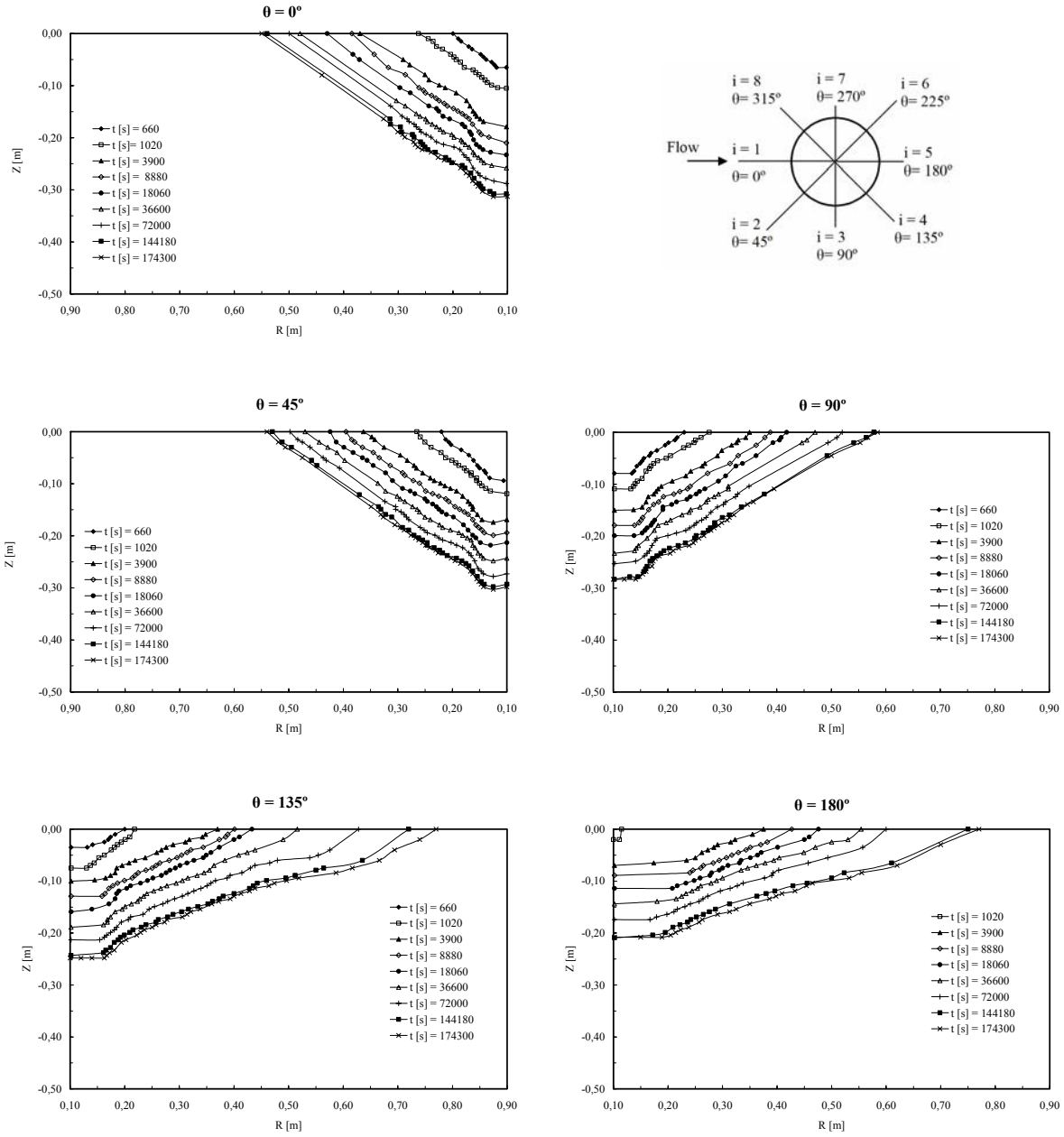

Figure 4.2.5. Measured scour-slopes in azimuthal half-planes with θ = 0, 45, 90, 135, and 180º at a circular pier over time [d_{50} = 3.25mm, h/D =1.50 and u/u_{cr} = 0.95].

Figure 4.2.6 shows non-dimensional volume of developing scour hole on non-dimensional maximum scour depth in front of the pier at θ = 0º over time. Since scour started at the pier's sides, scoured volume was recorded before scour reached the pier front. After the scour reached the pier front, the general tendency of the scoured volume was correlated well with maximum scour depth in front of the pier following a parabola as shown in the fig. 4.2.6 with a determination coefficient R^2= 0.972. The suggested formula might be used to calculate the scour hole volume depending on the knowledge of maximum scour depth at θ = 0º.

The figure shows also the relation between scoured volume and scour time. About 75% of the maximum scour hole volume was obtained during the first 43% of the experiment time. The obtained scoured volume at the circular pier was smaller than at the square pier during experimentation.

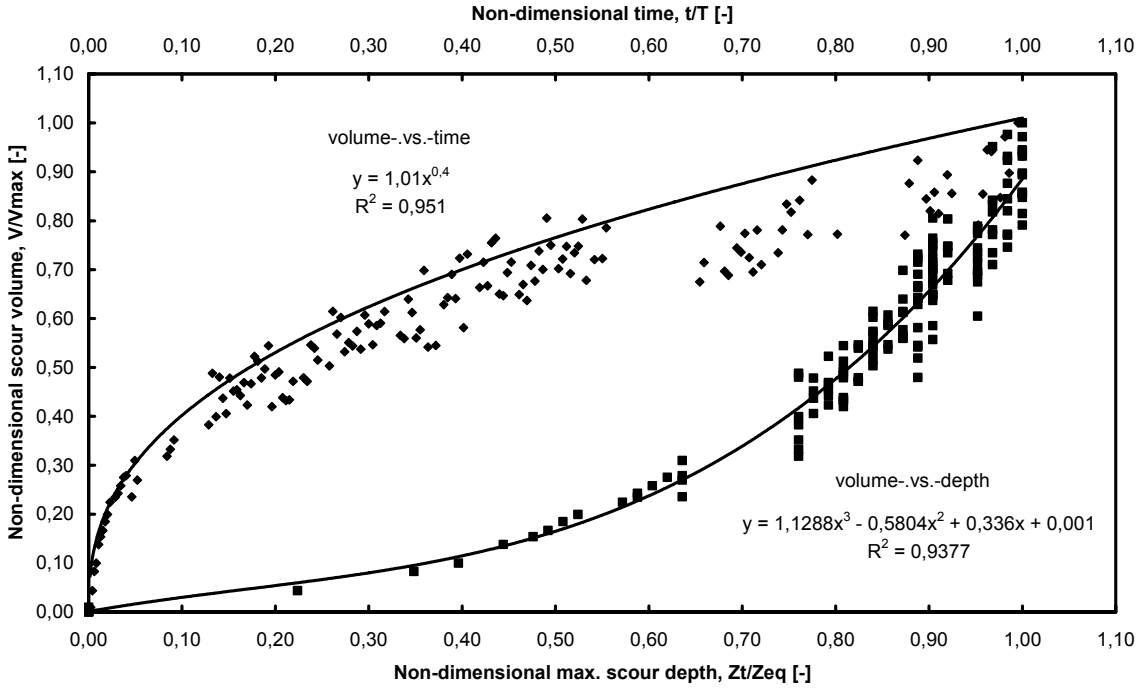

Figure 4.2.6. Volume of developing scour hole over time (upper), and over max scour depth (bottom) at a circular pier [d_{50} = 3.25mm, h/D =1.50 and u/u_{cr} = 0.95].

4.2.2 Scouring around Rectangular Pier with L/B = 2

Clear water scour experiment was conducted using a rectangular pier with L/B = 2 founded in the reference gravel bed (d_{50} =3.25m). The same flow conditions of the reference case test were performed (h/B = 1.5 and u/u_{cr} = 0.95). The LDS system, showed in figure 2.5, was installed to measure the topography of scour hole over time. With this new positioning system, LDS can be driven in the vertical and radial direction and also can be shifted along the rectangular pier. Vertical profiles were taken in 32 different azimuthal planes at the pier by turning the LDS in step of 15 degrees around the pier front and wake and by shifting the LDS in step of 5 cm in the longitudinal direction.
The experiment was conducted for more than 100 hours until the equilibrium conditions were achieved. The achieved erosion rate was about 0.37 mm/hr. The change in the maximum scour depth on the last day of the experiment was less than 10mm (0.05B) (Melville and Chiew1999). Figure 4.2.7 shows upstream and downstream views of the scoured bed at the rectangular pier at the end of the experiment. As shown, the scour hole was symmetric to the longitudinal axis of the pier.

Figure 4.2.7. Upstream (left) and downstream (right) views of the equilibrium scour hole at a rectangular pier with L/B = 2 [d_{50}= 3.25mm, h/B=1.50 and u/u_{cr} = 0.95].

Figure 4.2.8 shows the time development of maximum scour depth in two planes with θ = 0 and 45º at the pier front, three planes with θ = 90º each 10 cm along the pier sides, and two planes with θ = 135 and 180º at the pier wake. At pier front, scour depths were observed immediately after the test started at the planes with θ = 0, 45 and 90º (x = 0). During the first 2280s, maximum scour depth in the scour hole was moved from azimuthal half-plane with θ = 45º to plane with θ = 0º. At pier wake with θ = 180º, scour

was delayed and started after 14100s when the maximum scour depth at θ = 0º reached 0.28 m. At the end of the experiment, the equilibrium maximum scour depth Z_{eq} was 0.42 m (~2.10 the pier width) at the centreline of pier front. At pier wake with θ = 180º, the final observed scour depth was 0.21 m.

The obtained maximum scour depth at planes with θ = 0 and 180º at the rectangular pier were about 9% and 30% smaller than at the square pier at the end of experiments.

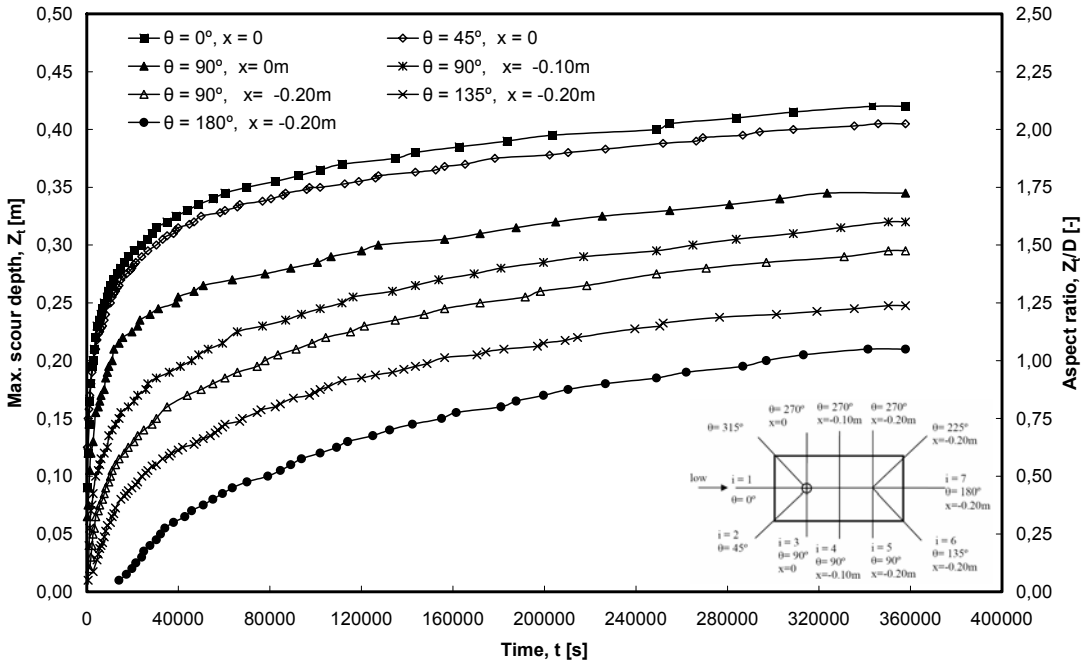

Figure 4.2.8. Time development of maximum scour depth in different azimuthal half-planes at a rectangular pier with L/B = 2 [d_{50} = 3.25mm, h/B =1.50 and u/u_{cr} = 0.95].

In figure 4.2.9, developing scour holes topography at rectangular pier with L/B = 2 after 240, 3300, 9600, 174420 and 357840s are presented. Scour was noticed immediately upon starting the test around the pier's corners with θ = 45º and 315º. Eventually scour propagated rather rapidly around the pier perimeter from both corners toward the center line of the pier front with θ = 0º. At this stage, the scour hole shape was a ring-like groove formed by the scouring process around the upstream face of the pier, and mound of the eroded sediment from the scour hole on the sides and wake of the pier. This mound of sediment was found to be moving to the downstream with time. Scoured region surrounded the rectangular pier after 14100s, which was about 4 times longer than at the square pier. The deepest point of the scour hole moved from plane with θ = 45º to the centerline of the pier front with θ = 0º during the first 2280s.

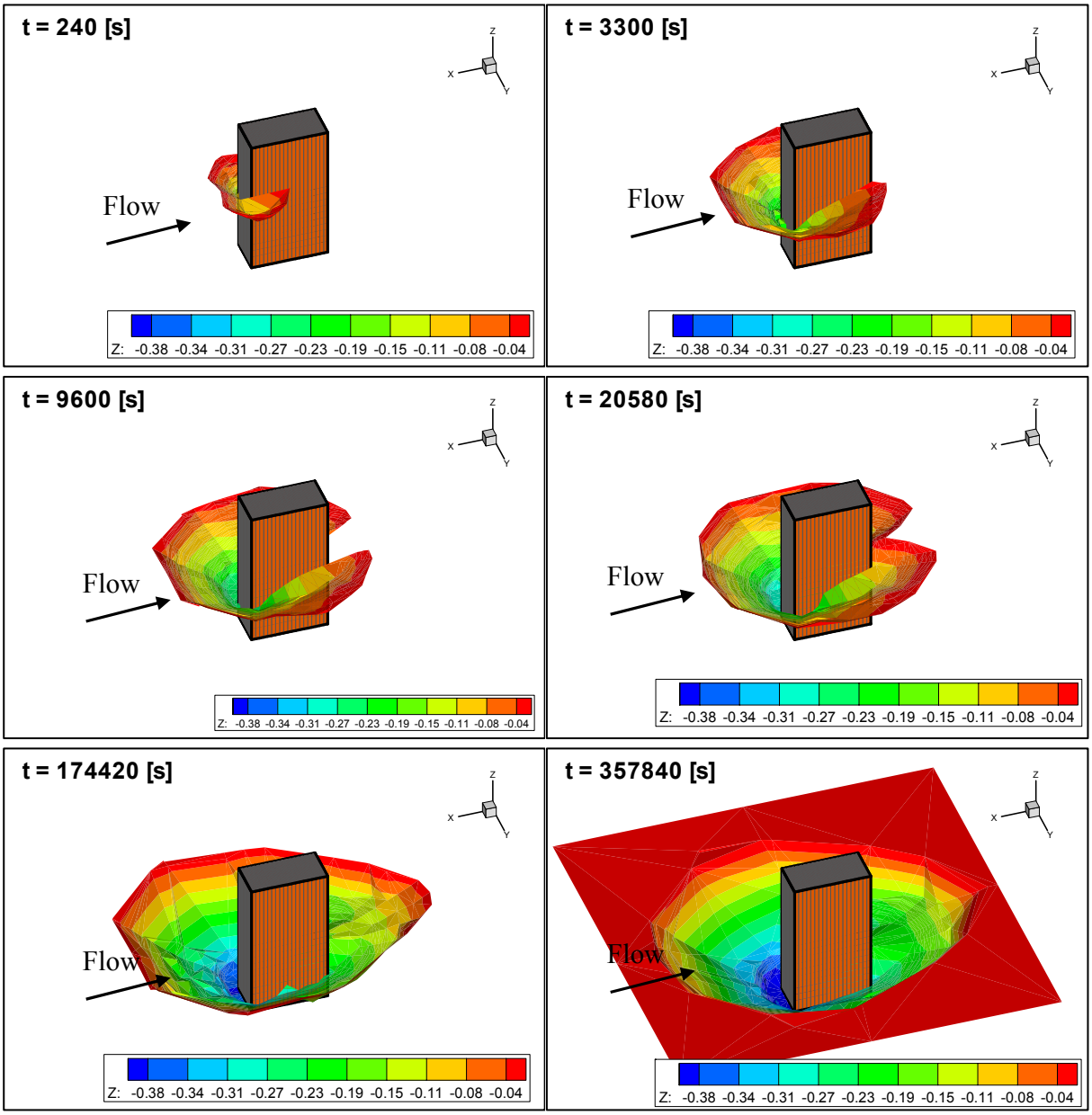

Figure 4.2.9. Developing scour hole topography at a rectangular pier with L/B = 2 after 240, 3300, 9600, 20580, 174420 and 357840s [d_{50}= 3.25mm, h/B=1.50 and u/u_{cr} = 0.95].

Figure 4.2.10 shows maximum depths of the scour hole in different azimuthal half-planes around the rectangular pier L/B = 2 for given times. In pier front, the gradient of scour hole bottom diminished with time, reaching a nearly flat bed at the experiment end with a difference of only 3.6% in scour depths at θ = 0 and 45º. A flat region observed initially downstream the plane with θ = 90º and x = -0.10 m, reduced to be only in the pier wake between planes with θ = 150 and 180º.

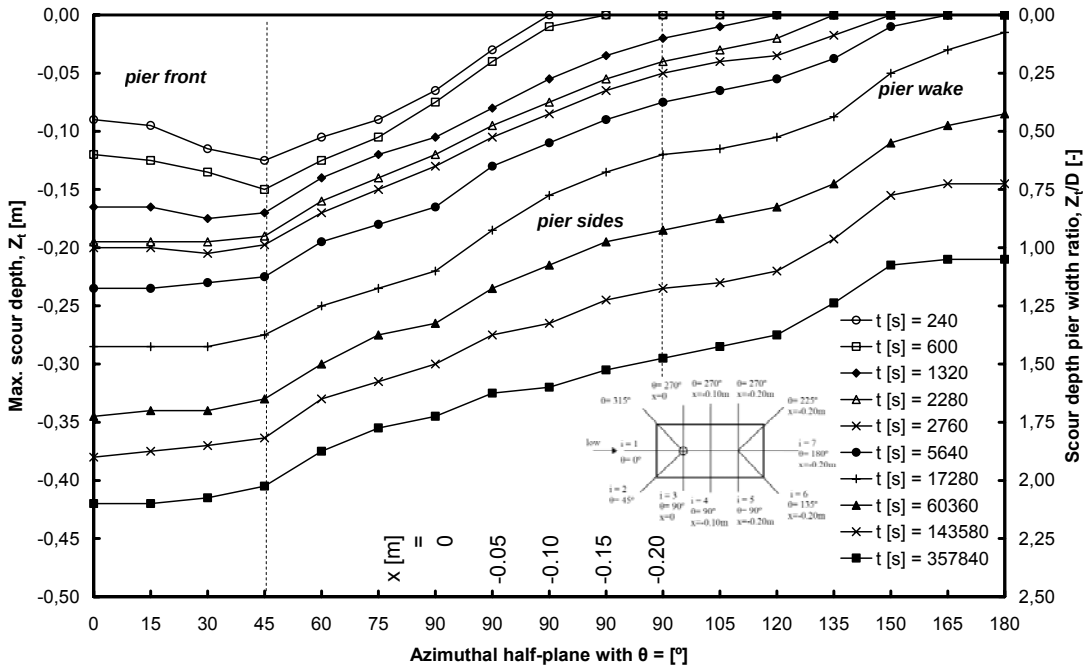

Figure 4.2.10. Maximum scour depth in different azimuthal half-planes at a rectangular pier with L/B = 2 over time [d_{50}= 3.25mm, h/B=1.50 and u/u_{cr} = 0.95].

Figure 4.2.11 presents the measured scour hole profiles at azimuthal planes with θ = 0, 45, 90 (for x=0 and -0.20m), 135 and 180º. The plot corresponding to plane with θ =135º contains data measured at θ =133 and 137º and the tendency line. The shape of the scour hole remained nearly constant during the experiment. Average slopes over a flat ring shaped portion close to the pier were observed. At the pier front with θ = 0º, two concave slopes similar to those at the square pier were observed. The lower slope was also steeper than the upper one. At the plane with θ =45º, two average slopes initially observed at the beginning of the test, was reduced to only one uniform slope at the end of the test. At the pier sides at planes with θ =90º, a second concave slope in the upper part of the profile was identified. A flat slope in the middle part of profile at θ =90º and x = 0.20 was observed. Average slopes of the scour hole diminished with θ, changing from an average slope of 36 to 21º at planes with θ = 0 and 180º respectively. The width of the ring portions at the square and rectangular piers was nearly the same in front of the pier, but it was wider at the wake of the rectangular pier.

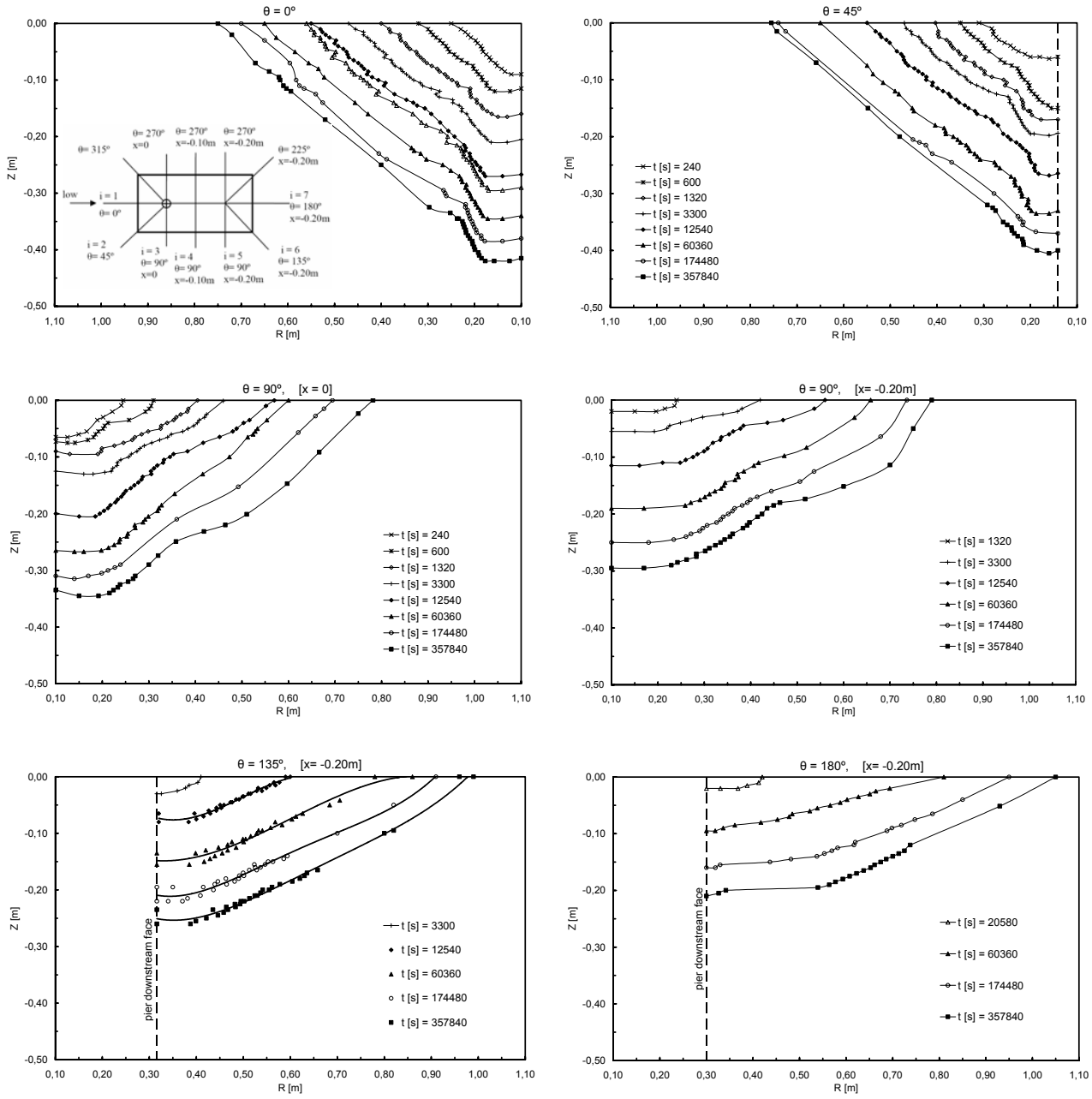

Figure 4.2.11. Measured scour-slopes in azimuthal half-planes with θ = 0, 45, 90 (x = 0 & -0.20m), 135, and 180º at a rectangular pier with L/B = 2 for given times [d_{50} = 3.25mm, h/B =1.50 and u/u_{cr} = 0.95].

4.2.3 Scouring around Rectangular Pier with L/B = 4

The geometric properties of scour holes around a glass rectangular pier with L/B = 4 (20cmx80cm) are presented. Clear water experiment was conducted with approaching flow velocity equal to 95% of the critical flow velocity (u/u_{cr} = 0.95) and approach flow depth equal to 1.50 time the pier width (h/B=1.50). The reference sediment bed of uniform gravel was used. Vertical profiles of the scour hole were taken in 36 different azimuthal half-planes around the pier. In the radial direction, the LDS was turned in step of 15º around the pier front and wake. In the longitudinal direction, the sensor was shifted it in step of 10cm. The experiment was conducted for more than 4 days until the equilibrium was achieved. The achieved scour rate was 0.48mm/hr (less than d_{50}) (Link et al. 2008). The rate of change of scour depth on the last experimentation day was less than 0.05B (10mm) (Melville and Chiew 1999).

Figure 4.2.12 presents views of the scour hole at the beginning of the run, after three hours and at the experiment end. As shown, a mound of the eroded sediment from the scour hole, which was firstly observed on the pier sides, found to be moving downstream.

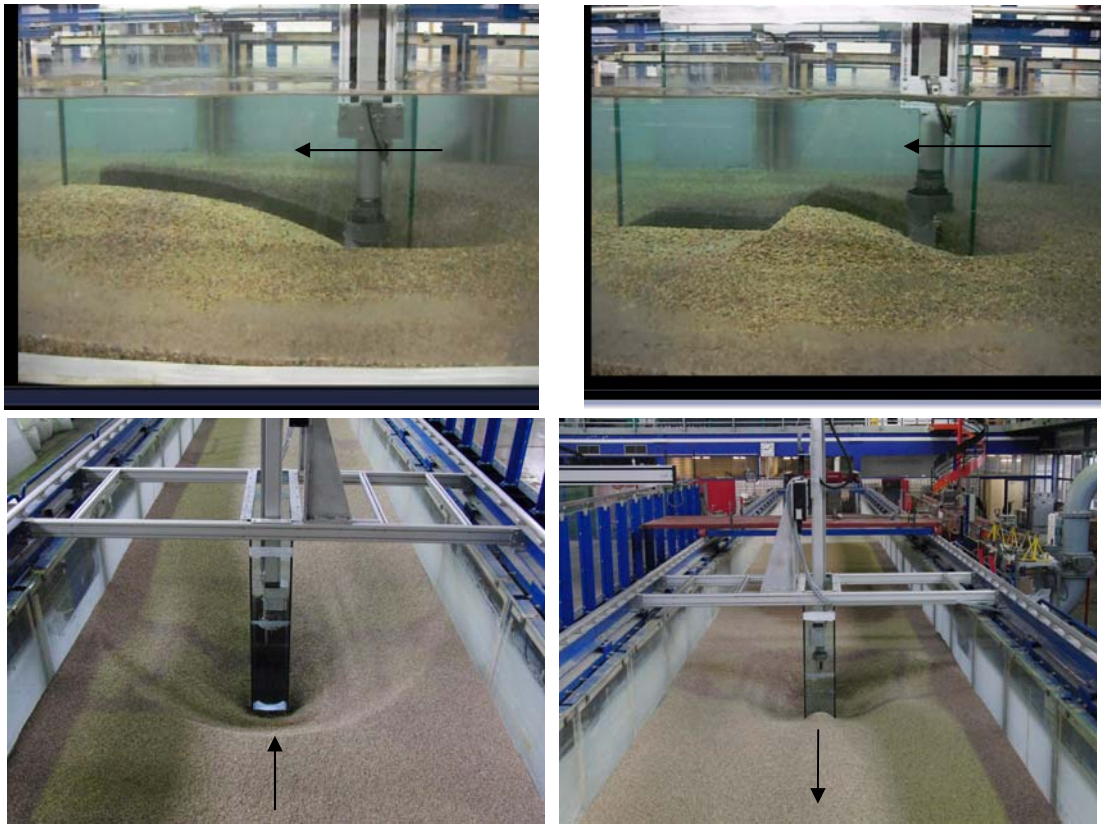

Figure 4.2.12. Propagation of eroded sediment during the beginning of the test (upper), and upstream (down-left) and downstream (down-right) views of equilibrium scour hole at a rectangular pier [d_{50} = 3.25mm, h/B =1.50 and u/u_{cr} = 0.95].

In figure 4.2.13, the development of maximum scour depths with time for different azimuthal half-planes around the rectangular pier, L/B = 4 are presented. In a duration shorter than at the square pier, the maximum scour depth in the scour hole was moved from the plane with θ = 45º to the centerline of the pier front with θ = 0º during the first 1620s. Scouring progressed slowly towards the downstream of the pier, reaching azimuthal half-plane with θ = 180º after 16500s, when scour depth at plane with θ = 0º was 0.275m. To the end of test, maximum scour depth which observed at θ = 180º was about 25% of that at θ = 0º. The ratio of maximum scour depths observed at the pier sides at θ = 90º with x = 0 and -0.60m was 0.54. The maximum clear-water equilibrium scour depth, Z_{eq} which observed at θ = 0º was 0.415m (2.075 B).

The observed equilibrium scour depth at the rectangular pier with L/B = 4 was about 90% of that observed at the square pier shape. For the tested rectangular piers, no significant effect of the tested pier length-width ratio (L/B = 2 and 4) was observed. The current results distinguish between the developing and equilibrium scour depths at square and rectangular piers, which are not taken into account in Laursen and Toch (1956).

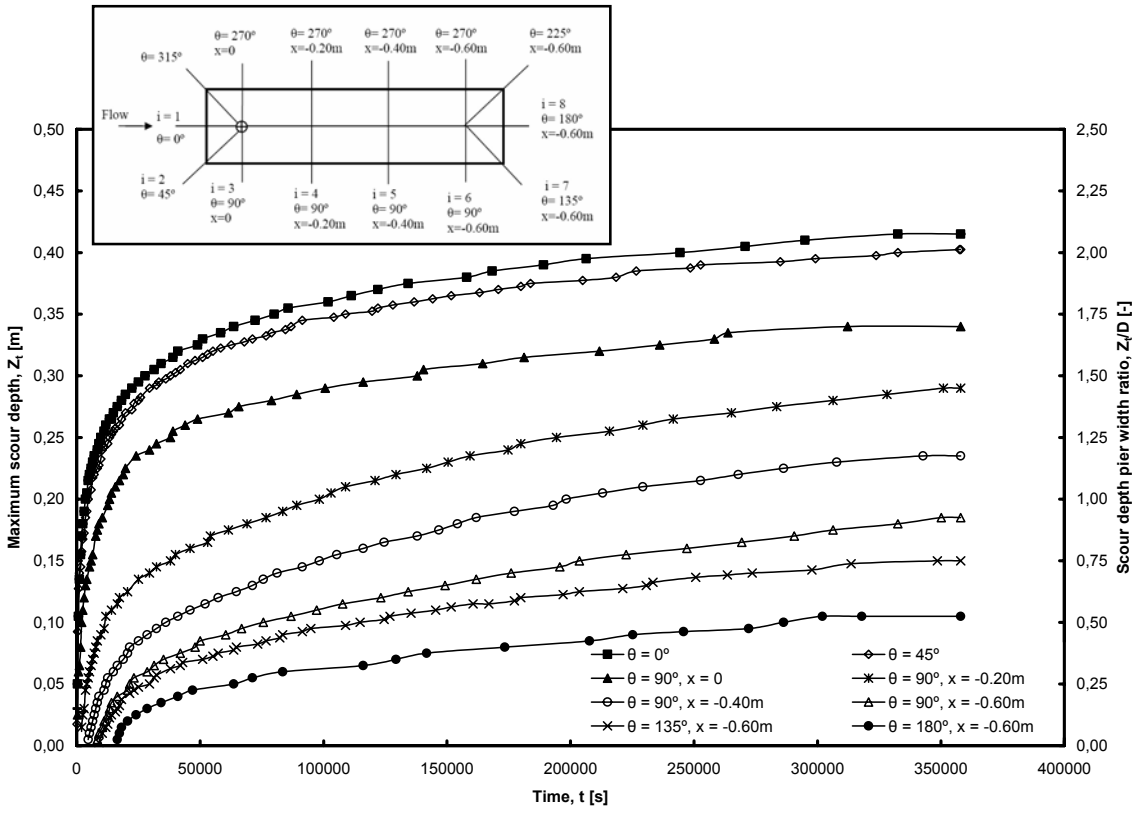

Figure 4.2.13. Time development of maximum scour depth in different azimuthal half-planes at a rectangular pier with L/B = 4 [d_{50} = 3.25mm, h/B =1.50 and u/u_{cr} = 0.95].

Figure 4.2.14 shows the measured scour patterns after 420, 2040, 9060, 17340, 174720 and 357960s at rectangular pier (L/B = 4) in gravel bed. Scour was noticed immediately after starting the test around the corners of the pier front with θ =45º. Eventually scour propagated rather rapidly from both corners toward the pier front with θ =0º. During the first 1620s, the deepest point in the scour hole was moved from plane with θ = 45º to the centerline of the pier front with θ = 0º. At this stage, scour hole shape was a ring-like groove formed by the scour process around the upstream face of the pier. A mound of the eroded sediment from the scour hole was accumulated at the pier sides, reaching the plane with θ = 135º during the first 10800s (three hours). This sediment mound, which was firstly observed on the pier sides and wake, found to be moving to the downstream, and scour surrounded the pier after 16500s (4.50 hrs). The extent of the scour hole at the rectangular pier with L/B = 4 was larger than at the square pier, but its depth was smaller.

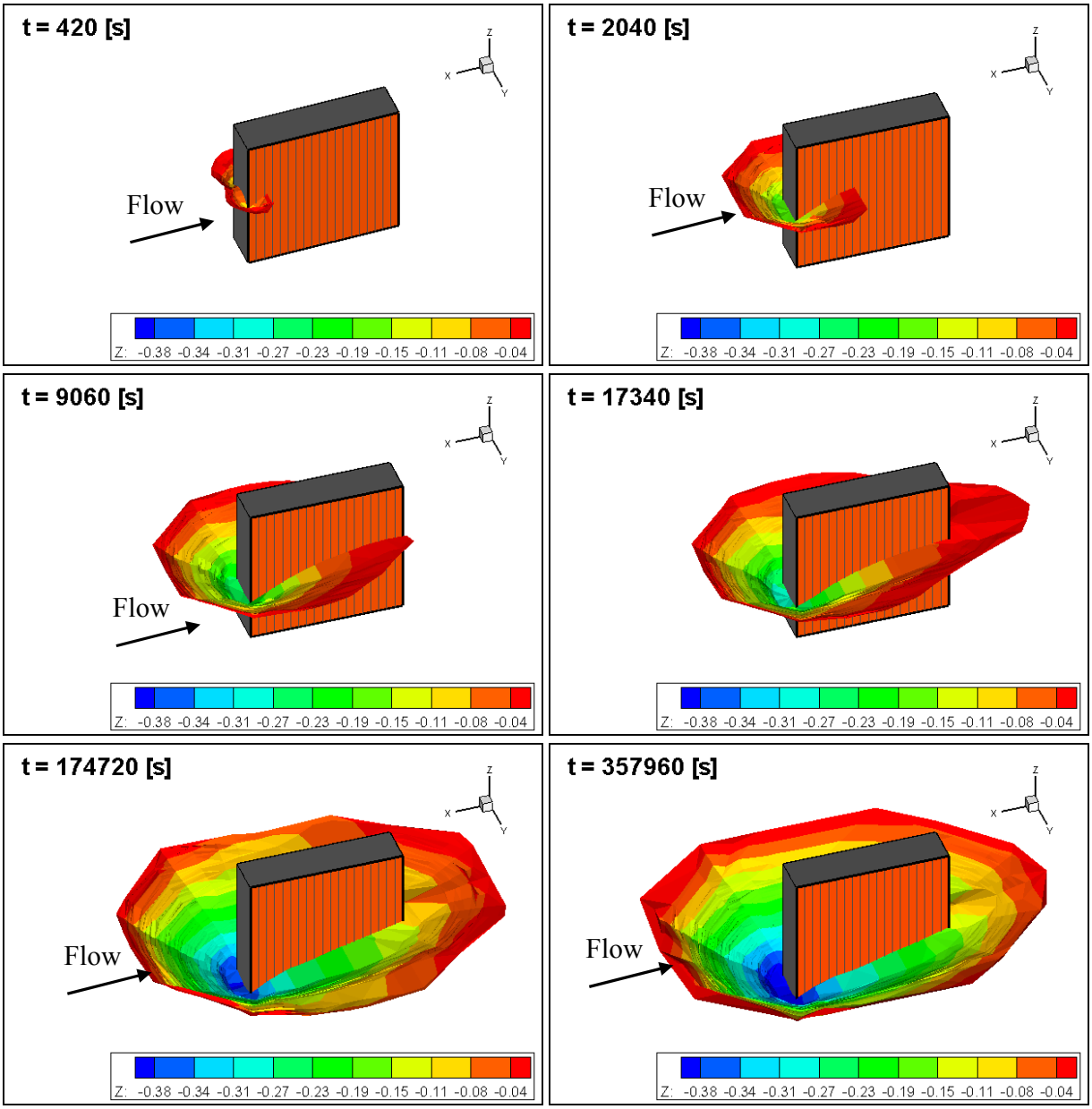

Figure 4.2.14. Developing scour hole topography at a rectangular pier with L/B = 4, after 420, 2040, 9060, 17340, 174720 and 357960s [d_{50} = 3.25mm, h/B =1.50 and u/u_{cr} = 0.95].

Figure 4.2.15 shows maximum depths inside the scour hole in different planes around the rectangular pier with L/B = 4 over time. At the pier front, the gradient of the scour bottom diminished with time. The difference in maximum scour depths at θ = 0 and 45º decreased from 45% at t = 420s to less than 3% at the experiment end. A flat region was observed between the planes with θ = 150 and 180º at the end of the test. The gradient of the scour bottom at the rectangular pier is remarkably higher than at the square pier.

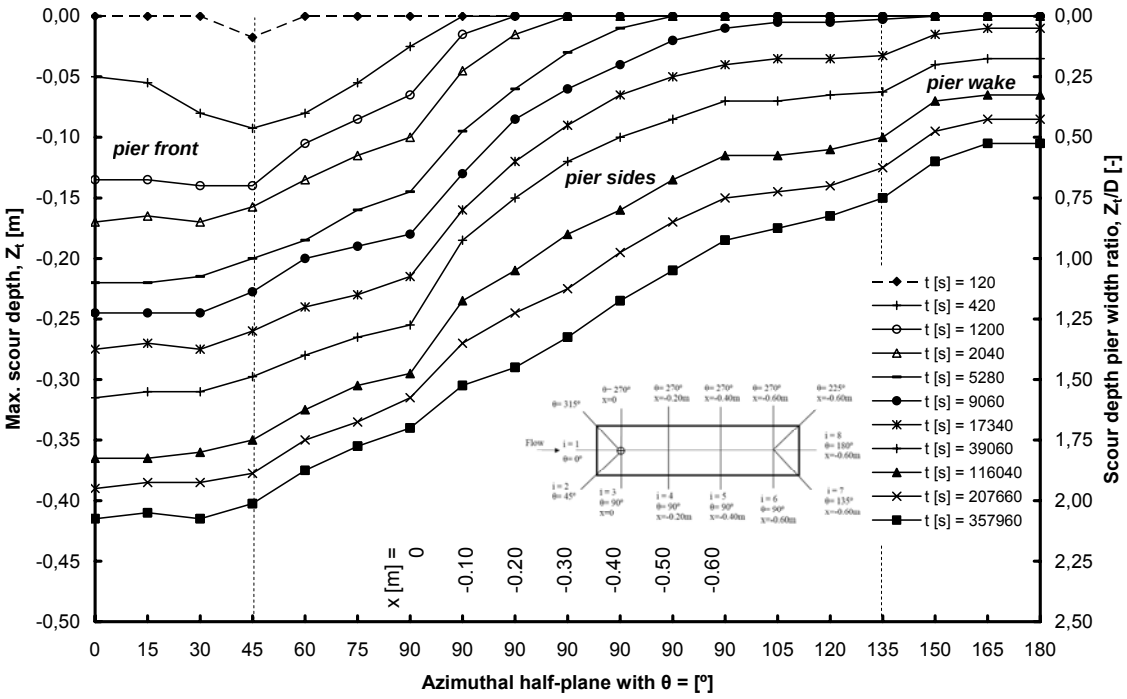

Figure 4.2.15. Maximum scour depth in different azimuthal half-planes around a rectangular pier with L/B = 4 over time [d_{50} = 3.25mm, h/B =1.50 and u/u_{cr} = 0.95].

Figure 4.2.16 shows the measured scour-slopes in azimuthal half-planes with θ = 0, 45, 90 (x = 0), 90 (x = -0.20 m), 90 (x = -0.40 m), 90 (x = -0.60 m), 135, and 180º for given times. At the pier front with θ = 0 and 45º, the shape of the scour hole was similar to that observed at the square pier. A nearly uniform slope and a ring shaped portion close to the pier were observed. Also, a steeper slope at the lower part of the profile was identified. The inclination of this lower slope was smaller than at the square pier. At pier sides with θ = 90º and x = 0, -0.20 and -0.40 m, milder slope in the middle part of the profile followed by a second concave slope was observed, and at x = -0.60 m the slope became nearly uniform. The width and depth of the scour decreased to the downstream significantly. At the pier wake with θ = 135 and 180º, the radius of the scour hole was smaller than at the square pier.

Average slopes of the scour hole diminished with θ, changing from an average slope of 36 to 12º for the planes with θ =0 and 180º, respectively. The extent of scour hole at rectangular pier with L/B = 4 is 10% larger than at the square pier.

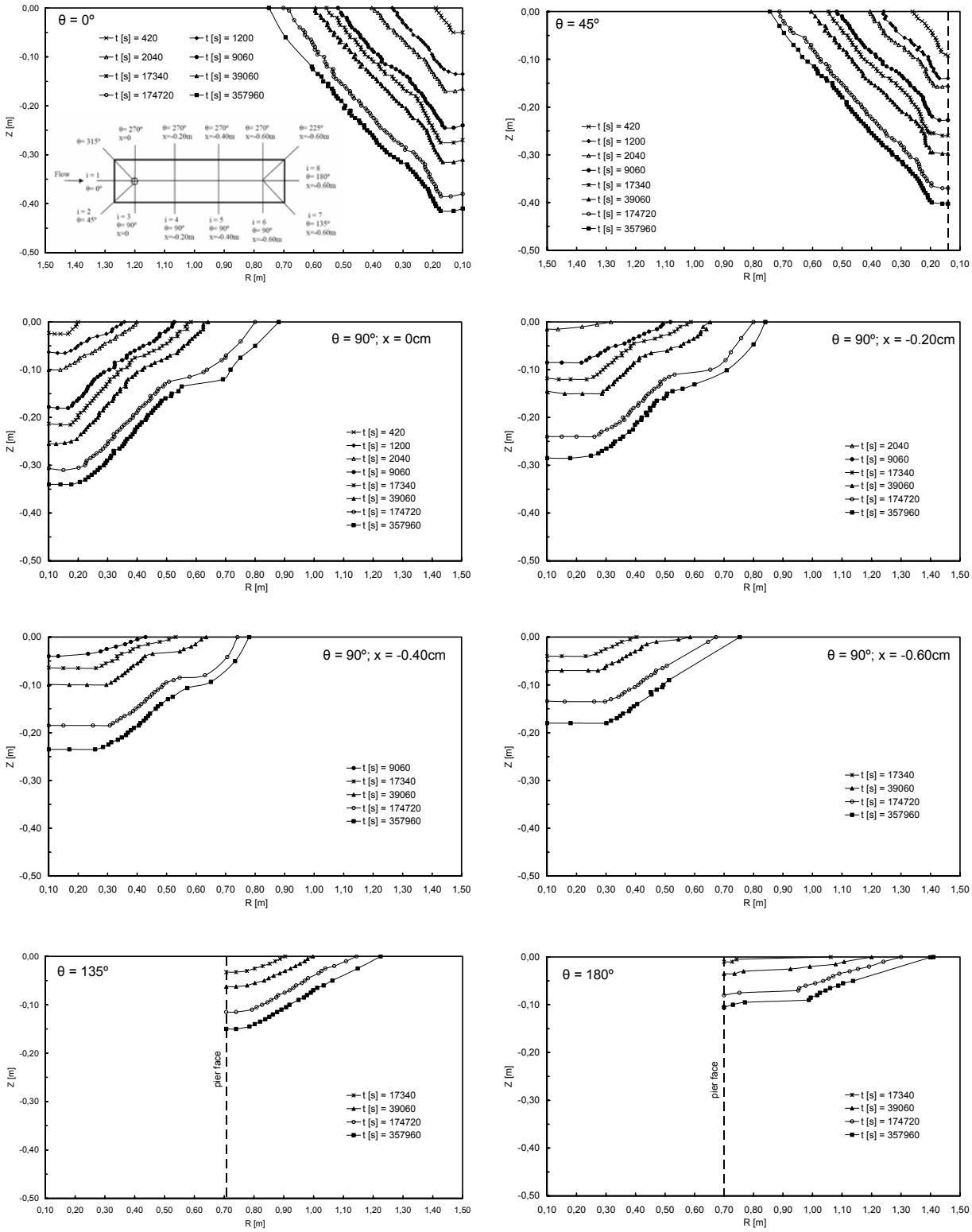

Figure 4.2.16. Measured scour-slopes in different azimuthal half-planes at a rectangular pier with L/B = 4 for given times [d_{50} = 3.25mm, h/B =1.50 and u/u_{cr} = 0.95].

4.3 EFFECT OF ALIGNMENT ON SCOURING AT SQUARE PIER IN GRAVEL

The square pier was aligned with four different angles of attack α = 0, 15, 30 and 45º, in order to account the effect of square pier alignment on scour development. The experiments were performed during 4 days or more under the same flow and bed conditions as the reference case. The obtained experimental results are presented in the current part of thesis.

4.3.1 Scouring around Scour Pier with α = 15º

The first non alignment of the square pier was at angle of attack of α = 15º with the principle flow direction. The experiment was conducted under clear water scour conditions with h/D =1.50 and u/u_{cr} = 0.95 over 100 hours, trying to achieve the equilibrium state when the erosion rate becomes less than d_{50} per hour. The achieved scour rate was 0.42 mm/ hour. Figure 4.3.1 shows the upstream and downstream views of the equilibrium scour hole. The asymmetry of the scour hole was evident.

Figure 4.3.1. Upstream (left) and downstream (right) views of equilibrium scour hole at a square pier with α =15º [d_{50} = 3.25mm, h/D =1.50 and u/u_{cr} = 0.95].

Figure 4.3.2 shows the time development of maximum scour depths at square pier aligned with in α = 15º, for azimuthal planes for θ = 0, 15, 45, 90, 133, 180, 195, 225, 270 and 315°. During the first 20% of experimentation, scour progressed with difference rates in different azimuthal planes, faster at planes with θ = 315 and 270º than at planes with θ = 45 and 90º respectively. Later, scour propagated on all planes with nearly the same erosion rate. During the first 35400s, maximum scour depth inside the scour hole moved from the plane with θ = 315º to the main flow direction with θ =15º. At planes with θ =0 and 15º, negligible difference in the measured maximum scour depths was found. At the

pier wake θ =195º, scour was delayed and started after 2760s when maximum scour depth at θ = 315º reached about 0.23 m.

The maximum clear-water equilibrium scour depth, Z_{eq} was 0.4268 m (2.13D) and located at the main flow direction with θ =15º. The maximum depths observed at planes with θ = 90, 270 and 180º were 0.3523, 0.3722 and 0.283 m.

As shown, the maximum scour depth decreased when the square pier aligned with $\alpha \neq 0$. The scour surrounded the non-aligned faster than at the aligned square pier. At non aligned pier, the migration of the point of maximum scour depth to the main flow direction required much longer time, about 10 times longer than at the aligned pier.

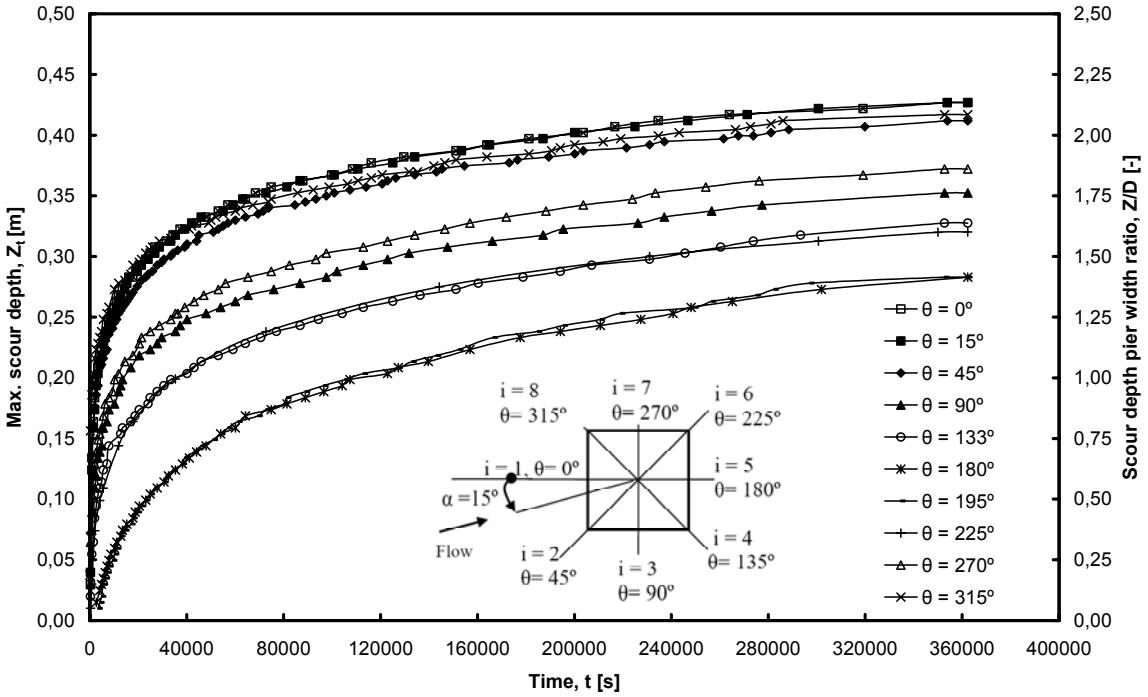

Figure 4.3.2. Time development of maximum scour depth in different azimuthal half-plane at a square pier with α =15º [d_{50} = 3.25mm, h/D =1.50 and u/u_{cr} = 0.95].

Figure 4.3.3 presents the patterns of temporary and equilibrium scour holes at square pier with α =15º for given time and at the end of the experiment. Scour started and progressed fast at the corners of pier front at planes with θ =45 and 315º. The deepest point was found at θ =315º during the first 10 % of experimentation. Later, maximum depth inside the scour hole was observed at the main flow direction, with θ = α =15º. At the wake region, a mound of the eroded sediment was observed between planes with θ =180 and 195º, and found to be moving to the downstream. The pier was surrounded with the scour after less than 1 % of the experiment time.

The asymmetry of the scour hole increased when the pier not aligned with the flow direction. The scour hole topography was turned around the pier with the flow direction. The extent and depth of the scour hole at the planes with θ =315 and 270º were approximately 5% larger than at planes with θ =45 and 90º.

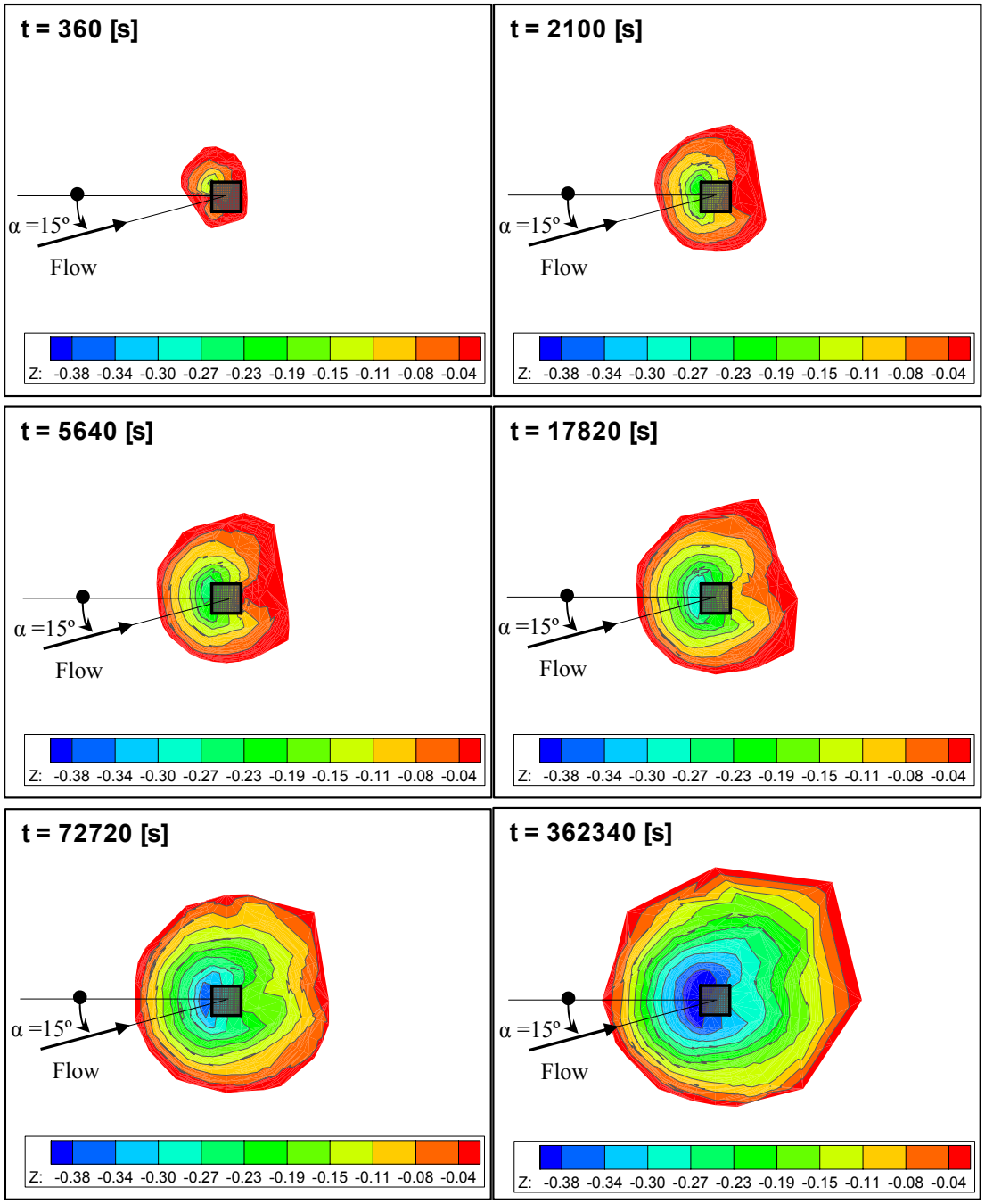

Figure 4.3.3. Developing scour hole topography at a square pier with α =15º after 360, 2100, 5640, 17820, 72720 and 362340s [d_{50} = 3.25mm, h/D =1.50 and u/u_{cr} = 0.95].

Figure 4.3.4 shows the maximum scour depths in different azimuthal half-planes with time, for square pier with α =15º. The bottom of the scour hole can be described as flat levels in front and wake regions linked together with gradient. The gradient of the scour bottom decreased and the width of the flat bottoms increased with time. At the end of the experiment, flat regions were identified between planes with θ = 30 and 330º at the pier front, and between planes with θ = 150 and 210º at the pier wake.

The gradient of scour hole bottom at square pier with α =15º was higher than at the square pier with α = 0º.

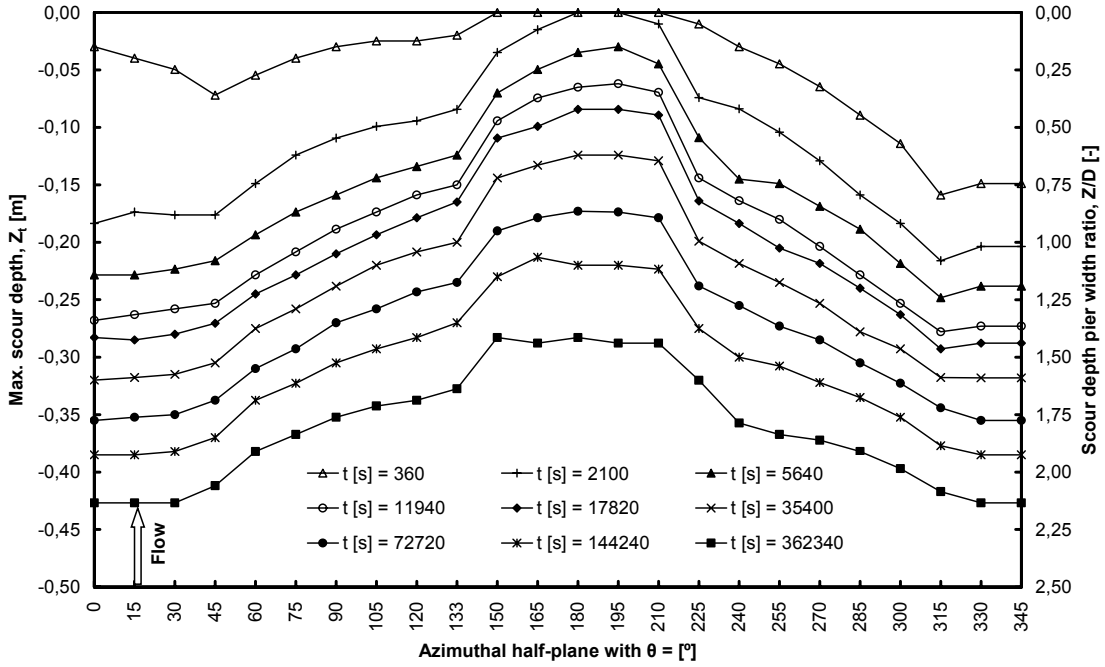

Figure 4.3.4. Maximum scour depth in different azimuthal half-planes around a square pier with α =15º for given times [d_{50} = 3.25mm, h/D =1.50 and u/u_{cr} = 0.95].

Figure 4.3.5 presents the measured data as well as the tendency lines of non-dimensional volume of developing scour holes on non-dimensional maximum scour depth and time. The scoured volume correlated well to the maximum scour depth as well as to the scour time. The suggested scoured volume-depth formula can be used to estimate the scour hole volume depending on the knowledge of maximum scour depth with a determination factor R^2= 0.97.

The curve of scoured volume-scour time showed that about 75 % of the maximum scour hole volume was obtained after 51% of experimentation.

The increase of the angle of attack from α = 0 to 15º resulted in a decrease in the scoured volume. For square pier with α = 15º, the volume of the equilibrium scour hole was about 15% smaller than at the square pier with α =0º.

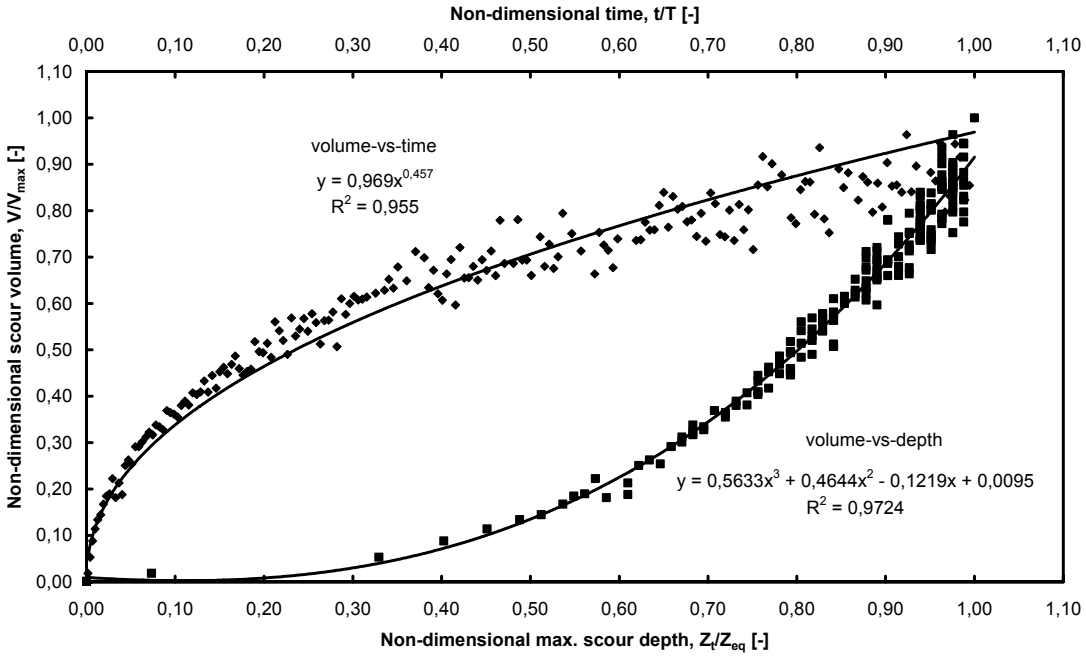

Figure 4.3.5. Non-dimensional volume of developing scour holes on non-dimensional maximum scour depth (bottom) and on non-dimensional time (upper) at a square pier with α =15º [d_{50} = 3.25mm, h/D =1.50 and u/u_{cr} = 0.95].

4.3.2 Scouring around Scour Pier with α = 30º

A clear-water scour experiment at square pier aligned with α = 30º was conducted. After 100 hours running time, scouring reached the equilibrium with scour rate of 0.27 mm/hr which was less than d_{50}.
Views of the equilibrium scour hole were presented in figure 4.3.6.

Figure 4.3.6. Upstream (left) and downstream (right) views of equilibrium scour hole at a square pier with α = 30º [d_{50} = 3.25mm, h/D =1.50 and u/u_{cr} = 0.95].

The time development of maximum scour depth in different azimuthal planes around the pier is presented in figure 4.3.7. During the first 109860s, maximum depth in the scour hole was moved from azimuthal plane with θ = 317º to planes with θ = 30º with a negligible difference of about 1.2% with θ = 0º at the end of the experiment. The maximum scour depths observed at planes with θ = 270 and 228º were initially greater than that observed at planes with θ = 135 and 180º. After 40500s, the scour depths at θ = 270 and 135º as well as at θ = 228 and 180º were nearly the same. The maximum clear water equilibrium scour depth, Z_e observed at the pier front was 0.4158 m (2.08D). Noted that the equilibrium scour depth at square pier aligned at α =15º is about 90% of that observed at square pier aligned with α = 0º.

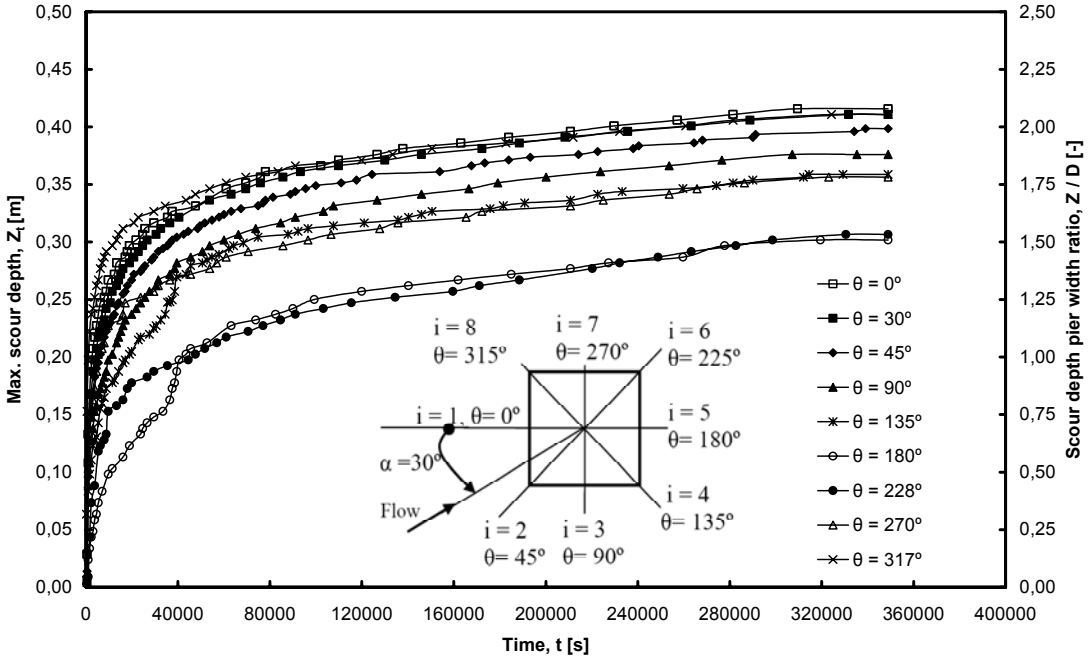

Figure 4.3.7. Time development of maximum scour depth in different azimuthal half-planes at a square pier with α = 30º [d_{50} = 3.25mm, h/D =1.50 and u/u_{cr} = 0.95].

Figure 4.3.8 gives an idea about the topography of developing scour holes at square pier aligned with α = 30º. Scouring started and progressed very fast around the pier perimeter between planes with θ = 255º- 30º. For a very short period, a deposition region was observed between planes with θ = 165-210º, then scouring surrounded the pier after 960s. During the first 31% of experimentation, the deepest point in the scour hole was located at plane with θ = 317º. Later, maximum depth in the scour hole was shifted to the main flow direction at θ = α = 30º, with small difference of 1.10 % and 3.0 % with those at planes with θ = 317 and 45º respectively. The depth of the scour hole at the pier front between θ = 315 and 45º was 25% deeper than at the pier side between θ = 60 and 120º, and 10% deeper than at the pier wake between θ = 180 and 210º.

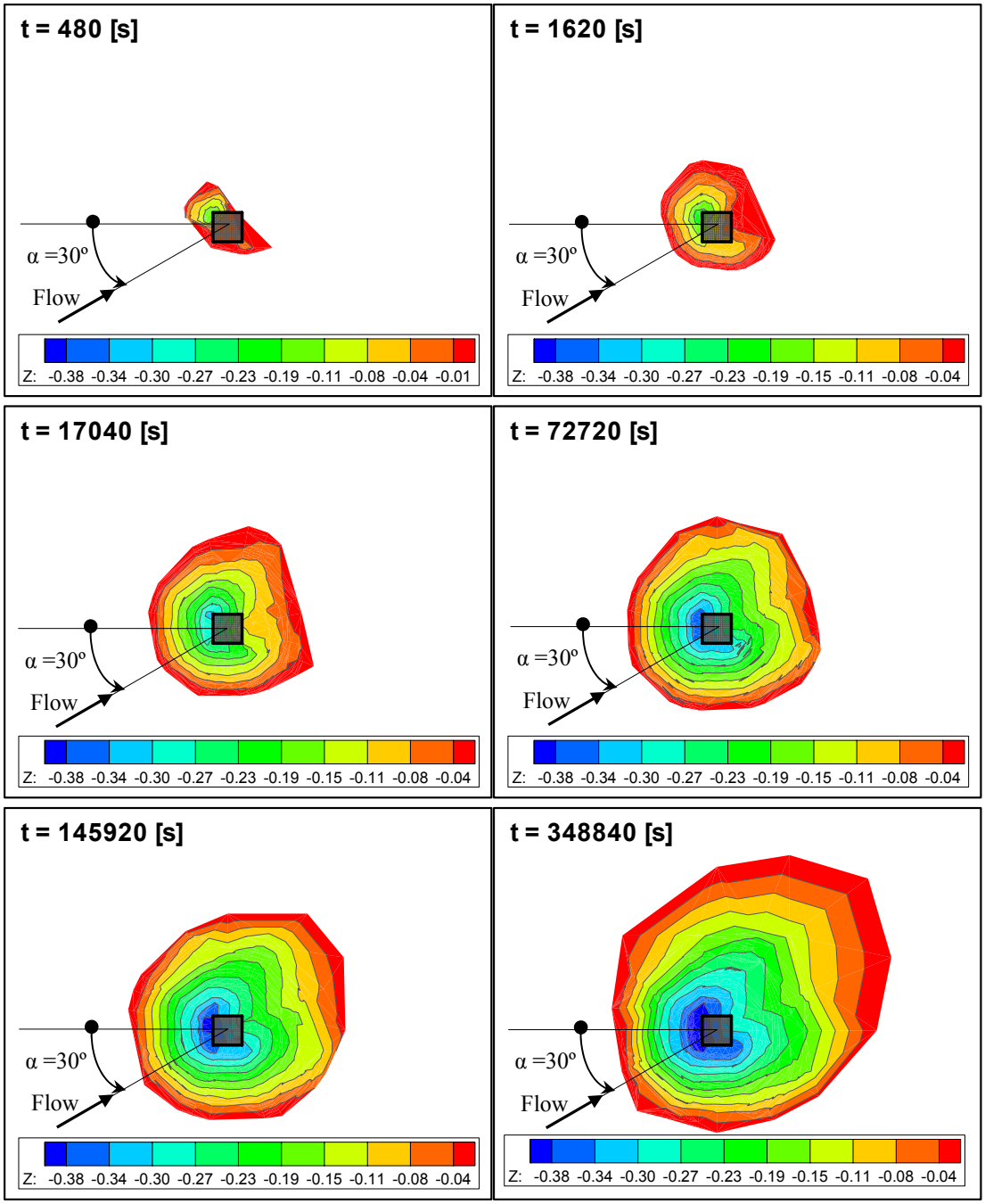

Figure 4.3.8. Developing scour hole topography at a square pier with α =30º after 480, 1620, 17040, 72720, 145920 and 348840s [d_{50} = 3.25mm, h/D =1.50 and u/u_{cr} = 0.95].

Figure 4.3.9 shows maximum scour in different azimuthal half-planes at square pier aligned with α =30º for given times. Two flat regions at the upstream were observed, one was deeper and located between planes with θ = 315 and 45º and the other was between θ = 60 and 120º. While two gradients between θ = 135 and 180º and between θ = 315 and 210º were observed at the downstream of the pier.

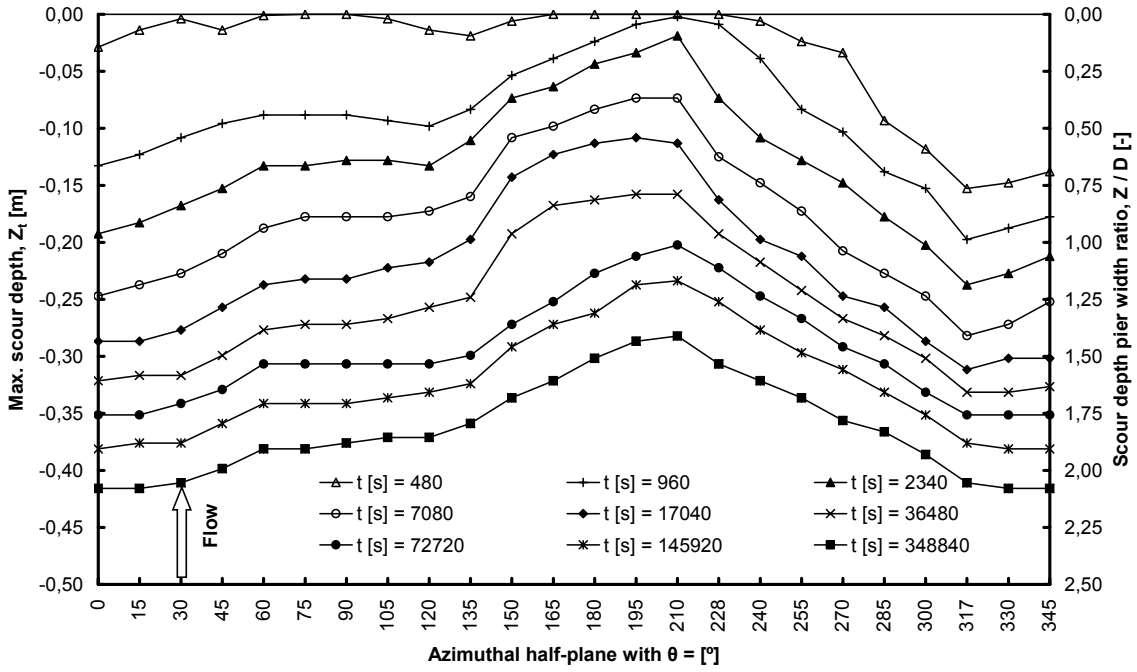

Figure 4.3.9. Maximum scour depth in different azimuthal half-plane at square pier with α = 30º for given times [d_{50} = 3.25mm, h/D =1.50 and u/u_{cr} = 0.95].

Figure 4.3.10 relates between the non-dimensional scour hole volume of developing scour hole and the non-dimensional scour hole depth as well as with the non-dimensional time. The volume of developing scour hole correlated well to the scour depth. Depending on the knowledge of maximum scour depth, the scoured volume might be estimate using the suggested parabolic formula with $R_2 = 0.94$.

The figures showed also that about 75% of the maximum scour hole volume was obtained during the first 46% of the experimentation time.

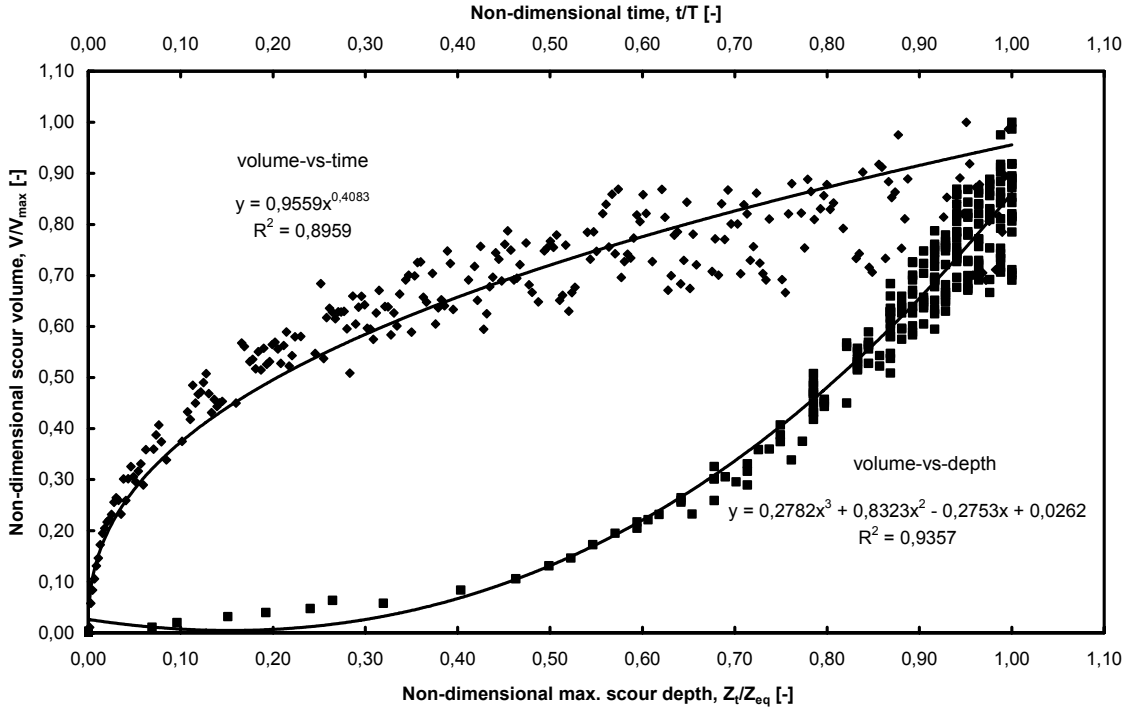

Figure 4.3.10. Non-dimensional volume of developing scour holes on non-dimensional maximum scour depth (bottom) and on non-dimensional time (upper), for square pier with $\alpha = 30º$ [$d_{50} = 3.25$mm, h/D =1.50 and $u/u_{cr} = 0.95$].

4.3.3 Scouring around Scour Pier with α = 45º

A 100 hours clear water scour experiment was carried out using square pier aligned 45º with the principle flow direction. The test was stopped after 100 hours because the scour hole was nearly reaching the sides of the flume. The achieved scour rate was 0.58 mm/hour. Figure 4.3.11 shows the upstream and the downstream views of the final scour hole at the end of the experiment. The symmetric of the scour hole is apparent.

Figure 4.3.11. Upstream (left) and downstream (right) views of the final scour hole at a square pier with α = 45º [d_{50} = 3.25mm, h/D =1.50 and u/u_{cr} = 0.95].

Figure 4.3.12 explain the development of maximum scour hole depths in different azimuthal planes with θ = 0, 45, 90, 135, 180, 225, 270 and 315º around the pier during the test. During the first 101940s, maximum scour depth in the scour hole moved from azimuthal plane with θ = 135 and 315º to azimuthal plane with θ = 0º. Observed difference between the measured maximum depth of scour at planes with θ = 0 and 45º (the flow direction) decreased from 35 % at t = 480s to 5 % at the end of the experiment. Scouring advanced to the pier wake at plane with θ = 225º after only 480s. The maximum observed scour depths at planes with θ = 135 and 225º were about 83% and 68% of that at θ = 0º. The maximum final scour depth Z_{eq} observed at planes with θ = 0 and 90º was 0.402m (~2.0D), i.e. about 88% of that observed at square pier with α = 0º.

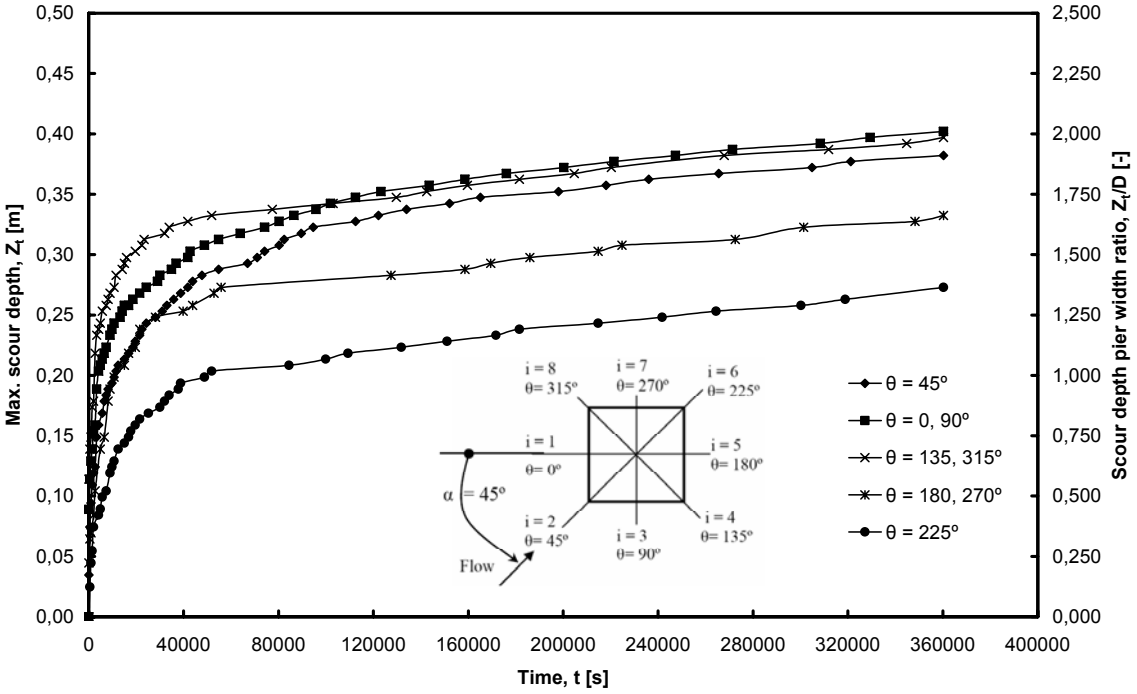

Figure 4.3.12. Time development of maximum scour depth in different azimuthal half-planes at a square pier with α = 45º [d_{50} = 3.25mm, h/D =1.50 and u/u_{cr} = 0.95].

Figure 4.3.13 shows developing scour hole topography after given time at a square pier aligned with α = 45º in gravels. Scouring was noticed immediately upon starting the run at azimuthal planes with θ = 135 and 315º and eventually propagated rather rapidly around the pier from both sides toward the pier front with θ = 45º. At the wake region between θ = 210-225-240º, a deposition region was observed during the first 0.10% of the experimentation. Then scoured region surrounded the pier perimeter. The deepest point was always observed on the upstream sides of the pier, firstly at planes with θ = 135 and 314º during the first 30% of the experiment time. Then scour depth at planes with θ = 0 and 90º approached the maximum scour depth inside the scour hole with a small difference of 5% with the scour depth at θ = 45º at the end of the experiment.

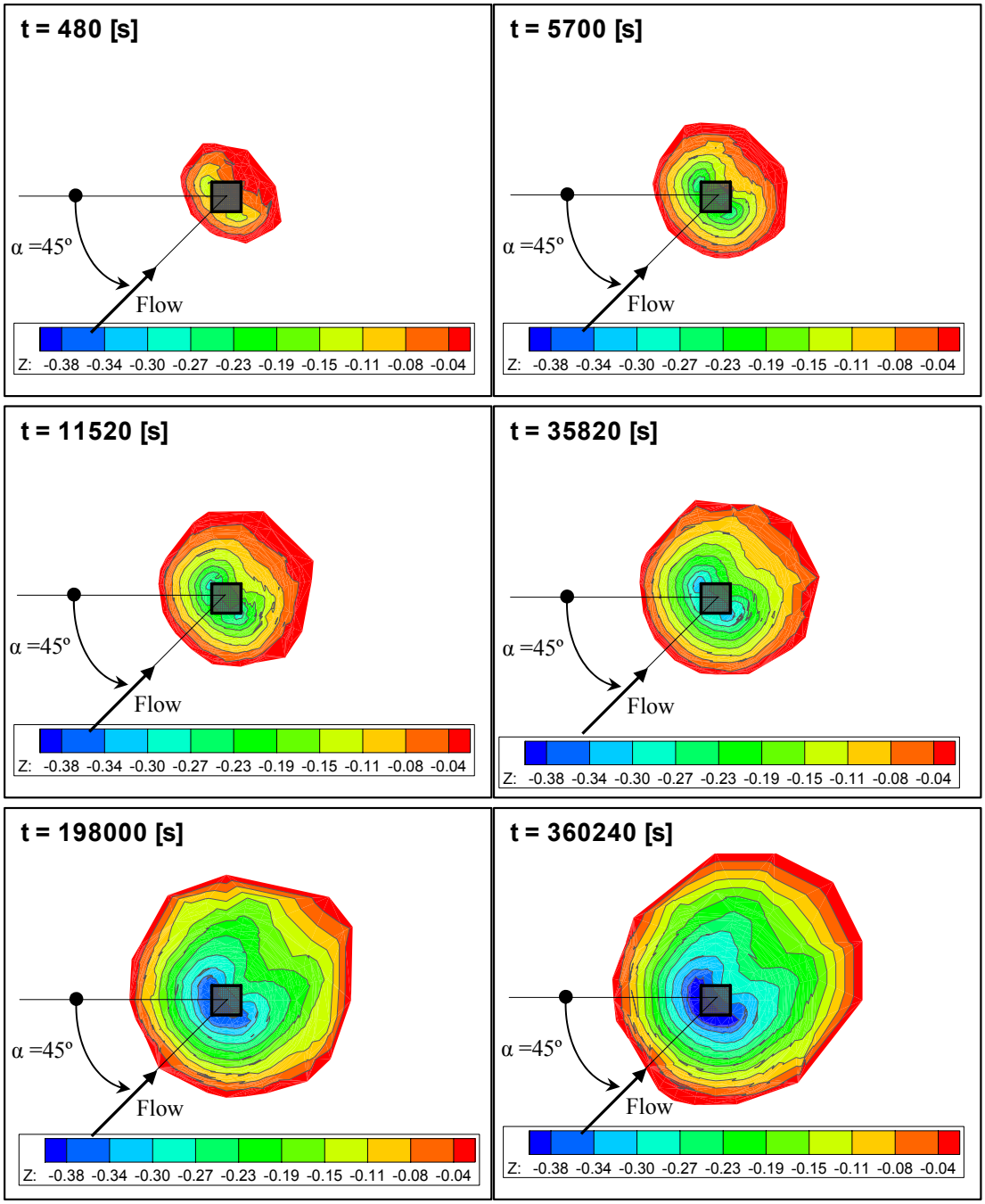

Figure 4.3.13. Developing scour hole topography at a square pier with α = 45º after 480, 5700, 11520, 35820, 198000 and 360240s [d_{50} = 3.25mm, h/D =1.50 and u/u_{cr} = 0.95].

In figure 4.3.14, the measured maximum scour depths in the scour hole in azimuthal planes at the square pier with α =45º for t = 240, 480, 960, 2040, 5700, 11540, 35820, 198000 and 360240 seconds are presented. The gradient of the scour hole found to be decreased with time. At the upstream between θ = 315-0-45-90-135º, a nearly flat bottom of the scour hole was observed at the end of the experiment.

The gradient of the scour hole bottom at the square pier aligned with α = 0º was higher than at the square pier with α =45º.

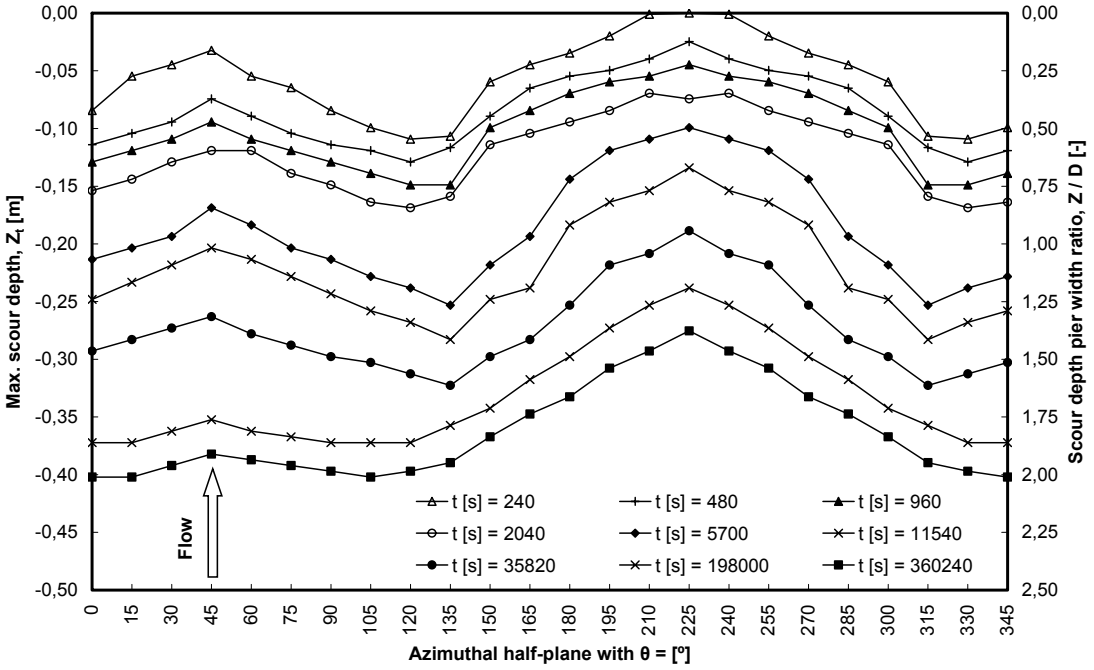

Figure 4.3.14. Maximum scour depth in different azimuthal half-planes around a square pier with α = 45º for given times [d_{50} = 3.25mm, h/D =1.50 and u/u_{cr} = 0.95].

Figure 4.3.15 shows the relation between non dimensional scour hole volume and depth of developing scour hole over time. The volume of scour hole was correlated well following the suggested parabolic formula with a good determination factor of 0.95.
About 75 % of the maximum scour hole volume was obtained during the first 60% of experimentation.

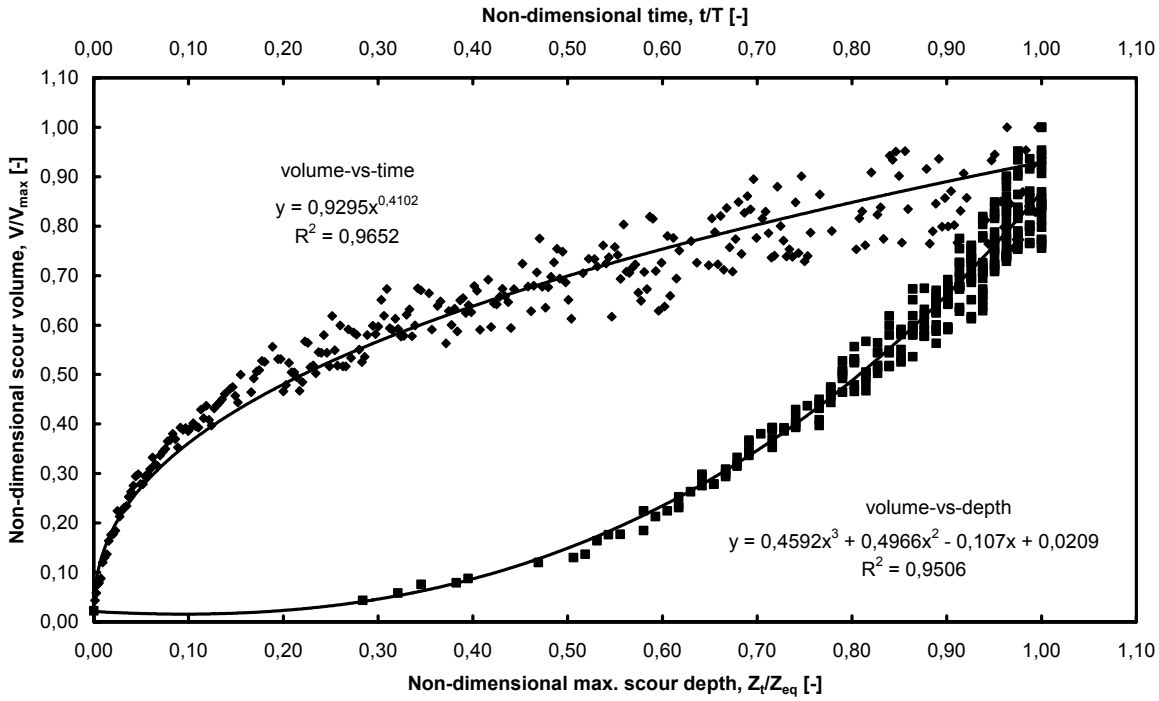

Figure 4.3.15. Non-dimensional volume of developing scour holes on non-dimensional maximum scour depth (bottom) and on non-dimensional time (upper), for square pier with $\alpha = 45^{o}$ [$d_{50} = 3.25$mm, h/D =1.50 and $u/u_{cr} = 0.95$].

4.4 EFFECT OF SEDIMENT SIZE ON SCOURING AROUND SQUARE PIER

Additionally to the standard fine gravel two sediment sizes, namely fine/medium sand and coarse sand were tested under the clear water scour conditions, in order to account the effect of sediment size on scouring.

4.4.1 Scouring around Square Pier in Fine/Medium Sand

The time-dependent scour hole geometry at a square pier founded in fine to medium sand bed with d_{50} = 0.25 mm and σ_g = 1.20 is presented. In literatures, it is written that the probability to maintain a plane bed (i.e. clear water conditions) near the threshold conditions is very low for ripple forming sediment d_{50} < 0.70mm (Raudkivi and Ettema 1983, Breusers and Raudkivi 1991). The given reason was that the ripples are expected to develop when $u > 0.60\ u_{cr.}$ However, clear water conditions were achieved in the present test with approaching flow intensity $u/u_{cr} \approx 0.94$ and flow depth-width ratio h/D = 1.35, when the filling of flume and the starting of the test were good controlled. A flat bed was observed in the upstream for more than 2 days running time, as shown in figure 4.4.1.
Figure 4.4.1 shows also upstream view of the final scour hole at the end of the experiment. Scour hole topography, which was symmetric around the longitudinal axis of the pier, consisted of a hole in front of the pier and an alternate formation of depressions and ripples in the wake region.

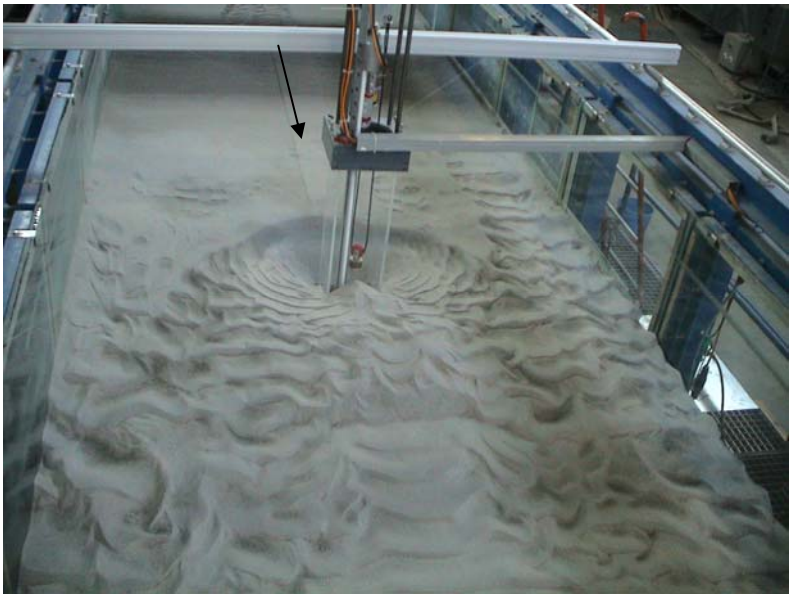

Figure 4.4.1. Upstream view of the final scour hole at a square pier
[d_{50} = 0.25mm, h/D =1.35 and u/u_{cr} = 0.94].

Figure 4.4.2 shows the development of maximum depth in the scour hole with time in azimuthal half-planes with θ = 0, 45, 90, 135, 180, 225, 270 and 315º. The scour started to develop fast at the plane with θ = 45º after the test started. While at the pier front with θ = 0º, the scour delayed and started after about 780s. Although scour reached the planes with θ = 90 and 135º during the first 1380s and 6420s respectively, no scour at the pier wake with θ = 180º was recorded during about 90% of the running time (165000s) at the pier wake with θ = 180º. The maximum depth of the scour hole was observed at the corner of the pier front with θ = 45º during the first 114840s. Later, it moved to the centerline of the pier front with θ = 0º with a negligible difference of about 2% with the depth at θ = 45º. At the end of the experiment, the maximum clear water scour depth observed at θ = 0º was 0.165m (0.825D). The maximum scour depths observed at the planes with θ = 90 and 180º were 0.1314m (80% that at θ = 0º) and 0.0232m (0.14% of that at θ = 0º).

The maximum depth in the scour hole over time was fitted well following equation 4.3 with determination coefficient $R^2 = 0.98$:

$$Z_t = 0.017\ln(t) - 0.038 \qquad [4.3]$$

Note that the observed maximum scour depths at the pier front and wake in fine/medium sand bed were about 40% and 9% of those at the same planes when the bed was gravel.

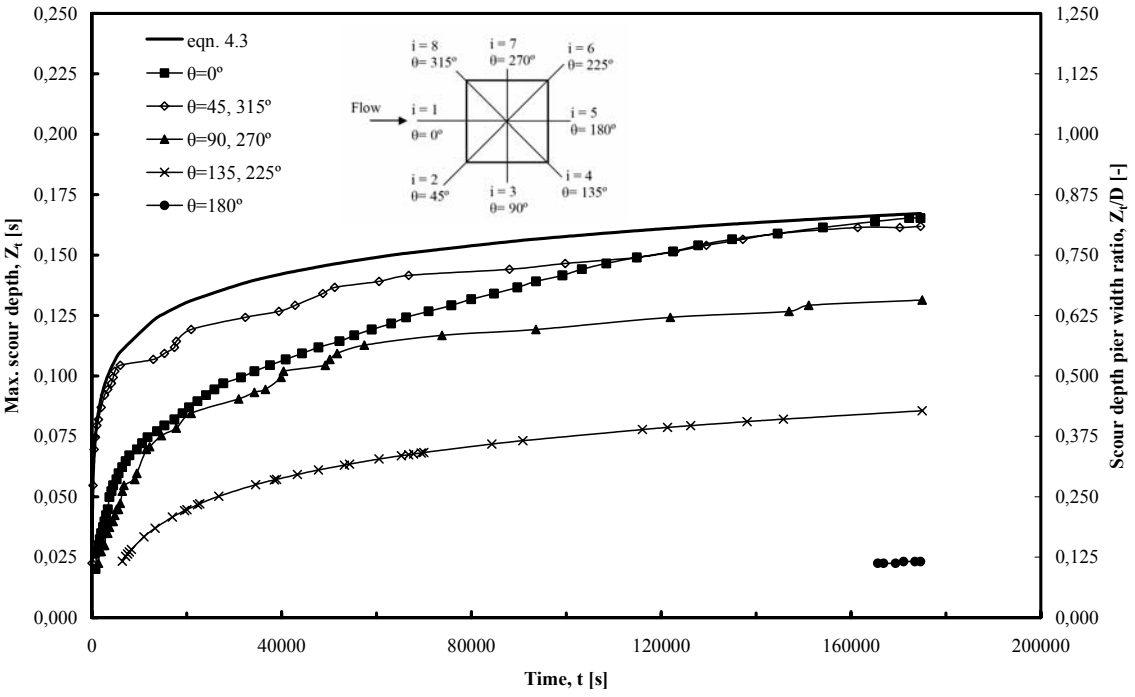

Figure 4.4.2. Time development of maximum scour depth in different azimuthal half-planes around a square pier [d_{50} = 0.25mm, h/D =1.35 and u/u_{cr} = 0.94].

In figure 4.4.3, developing scour hole topography after 780, 3720, 9480, 17820, 72060 and 174660s at a square pier in fine/medium sand are presented. The removal of sand in the vicinity of the pier was noticed immediately after the test started. Scouring started and progressed fast at the corners of pier front at θ = 45 and 315º, where also the deepest point of the scour hole was initially observed. Then scour propagated rather towards the centerline of the pier front reaching the plane with θ = 0º after 780s. In this stage, ripple formations were observed at the wake region. The deepest point of the scour hole which was firstly found at the plane with θ = 45º, migrated to the plane with θ = 0º during the first 114840s. In front of the pier, the difference in scour depths at planes with θ = 0 and 45° decreases from 73% at 780s to negligible value of 2% at the test end. Scour propagated slowly to the pier wake and surrounded the pier after about 165000s.

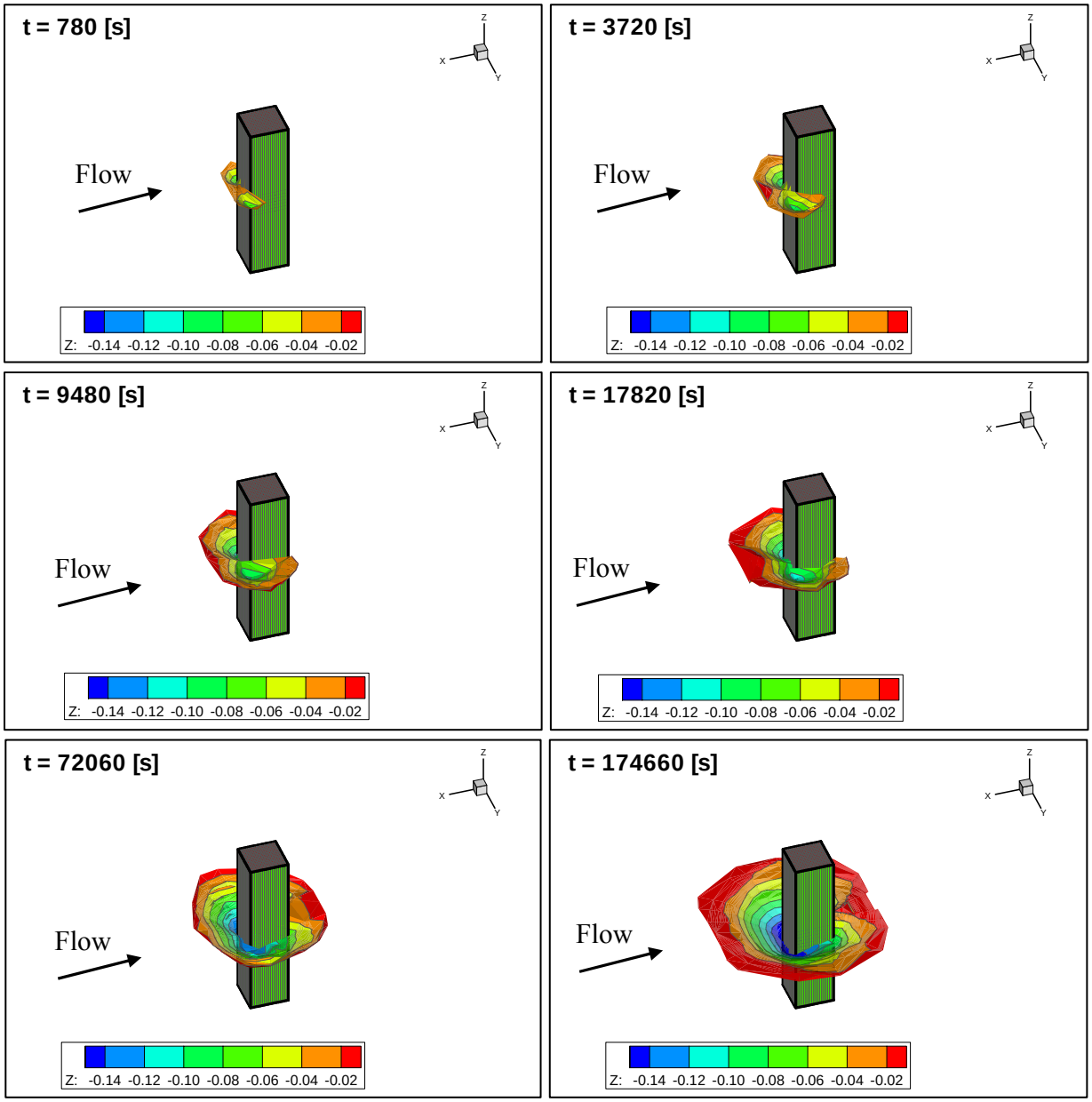

Figure 4.4.3. Developing scour hole topography at a square pier after 780, 3720, 9480, 17820, 72060 and 174660s [d_{50} = 0.25mm, h/D =1.35 and u/u_{cr} = 0.94].

Figure 4.4.4 shows the measured scour hole slopes for given times for azimuthal half-planes with θ = 0, 45, 90, 135, and 180º at the square pier. The shape of scour hole remained nearly the same during experimentation. A ring shaped portion close to the pier and a nearly uniform slope over it were observed. The width of the ring increased and the average side-slopes decreased with the increase of θ. The observed side slopes which were about 30 and 24º at the planes with θ = 0 and 90º, never exceeded the natural angle of repose. At the pier front, the width of the ring portion in fine/medium sand was about

60% smaller than in gravel bed. At the pier wake, an inclination with ripples was identified. At the end of test, the extent of the scour hole in fine/medium sand was nearly half the extent in gravel bed, being approximately two times the pier width.

The shape and slopes of the scour hole showed that the strength of horseshoe vortex in fine/medium sand is lower and the size of vortex is smaller than in the gravel bed.

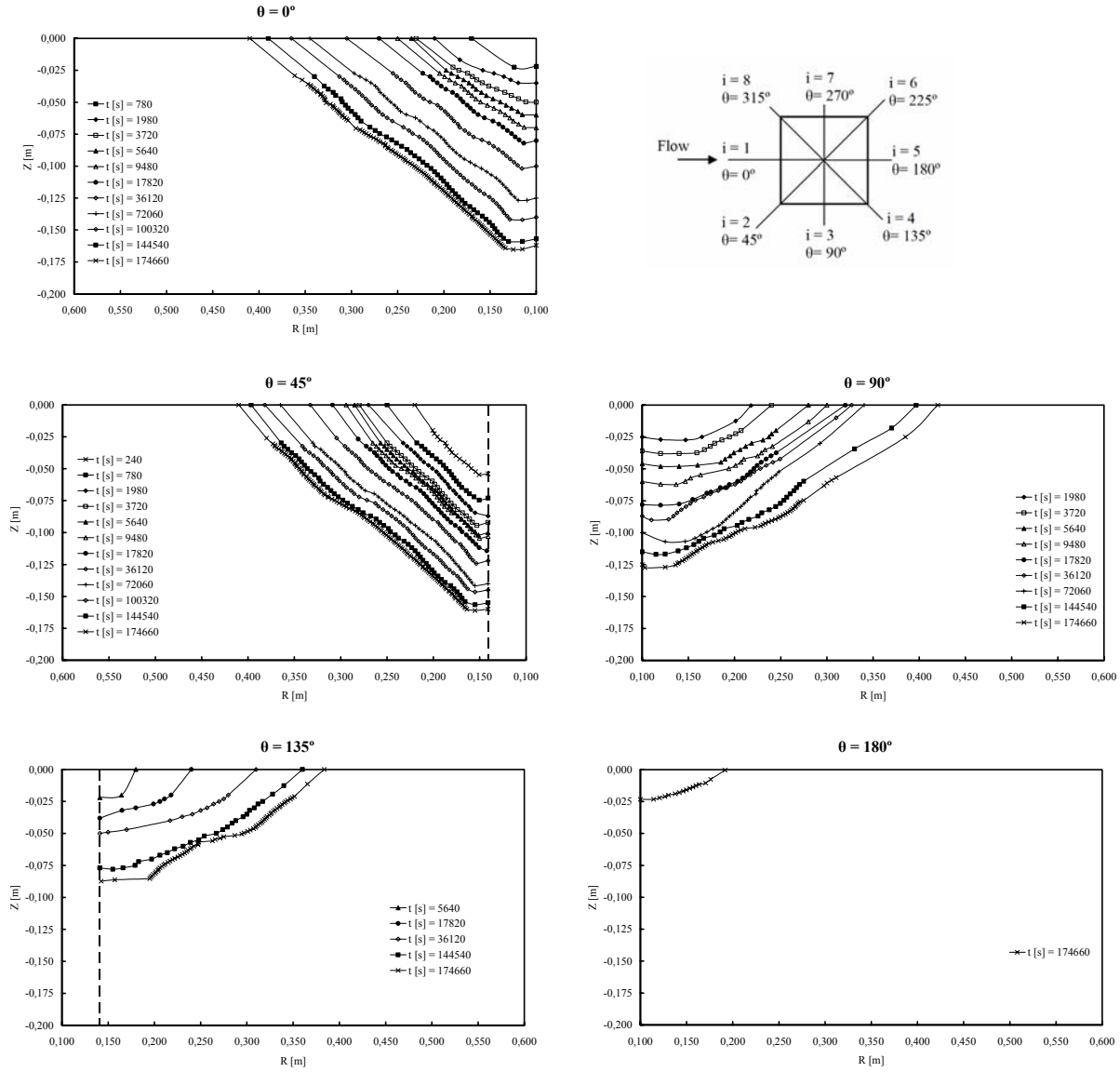

Figure 4.4.4. Measured scour-slopes in different azimuthal half-planes at a square pier [d_{50} = 0.25mm, h/D =1.35 and u/u_{cr} = 0.94].

Figure 4.4.5 relates between non-dimensional scour hole volume and non dimensional maximum scour depth in front of the pier over time. The general trend of scour hole volume in fine/medium sand was nearly the same trend of the reference case (in gravel). The pronounced difference was in the obtained values of scoured volume in the same time. Scour volume correlated well with maximum scour depth at pier front following a parabola with determination coefficient of $R^2 = 0.972$. The given formula might be used to calculate the scour hole volume depending on knowledge of scour depth in front of the pier.

The volume-time-curve showed that 75% of the maximum scour hole volume was achieved in the first 55% of the experiment time. The erosion intensity at the scour hole in fine/medium sand was lesser than in gavel bed.

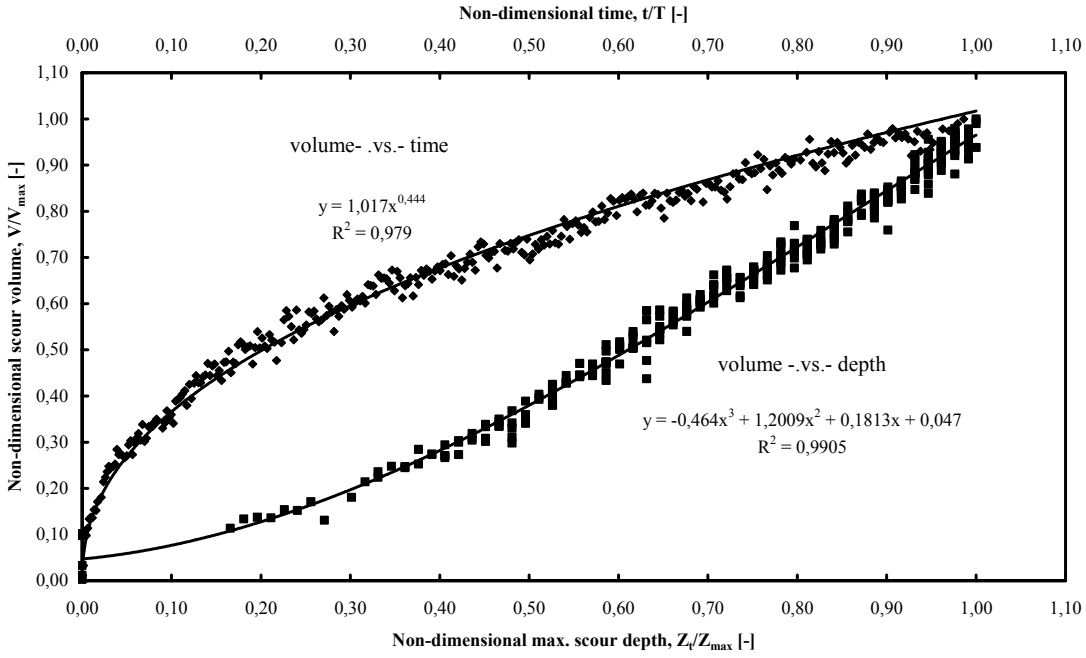

Figure 4.4.5. Volume of developing scour hole over time (upper) and maximum scour depth (bottom), for a square pier [$d_{50} = 0.25$mm, h/D =1.35 and $u/u_{cr} = 0.94$].

4.4.2 Scouring around Square Pier in Coarse Sand

The time variations of scour holes around a square pier embedded in uniform coarse sand bed with d_{50} = 0.97mm are presented. Experiment was conducted under clear water scour conditions with Flow intensity ratio u/u_{cr} = 95% and with flow depth to pier width ratio h/D =1.50. The experiment was performed during 70 hours. However the equilibrium scour conditions did not achieved, the scour rate became very small. The achieved scour rate was 0.82 mm/hr.

Figure 4.4.6 shows upstream and downstream views of the final scour hole. As shown, the scour hole was symmetric around the longitudinal axis of the pier. A mound of the eroded sediment from the scour hole was observed at the downstream.

Figure 4.4.6. Upstream (left) and downstream (right) views of the final scour hole at a square pier [d_{50} = 0.97mm, h/D =1.50 and u/u_{cr} = 0.95].

In figure 4.4.7, maximum scour depths in different azimuthal half-planes around the pier during the experiment are presented. Similar to gravel bed, scouring started and progressed fast at the pier front corners with θ = 45º. Eventually scour propagated with different velocities toward the front and wake of the pier, reaching the planes with θ = 0 and 135º during the first 360s and 2600s, respectively. At θ = 180º, scour was delayed and started after 24780s when the maximum scour depth at the pier front reached 0.16m. During the experiment, the maximum depth inside the scour hole was always observed at the upstream face of the pier, initially at θ = 45º during the first 198800s (80% of the experiment time). Later, it moved to the plane with θ = 0º with a negligible difference of 1.1% with the depth at θ = 45º at the end of the experiment.

The maximum final scour depth, Z_{eq} observed at θ = 0º was 0.231m (1.16 D) at the end of test. The maximum observed scour depths at the sides and wake of the pier with θ = 90 and 180º were 0.194 m (0.84 Z_{eq}) and 0.104m (0.45 Z_{eq}), respectively.

Maximum scour depth inside the scour hole at square pier in coarse sand bed follows the logarithmic equation 4.4 with determination coefficient of R^2= 0.993:

$$Z_t = 0.0289\ln(t) - 0.1266 \qquad [4.4]$$

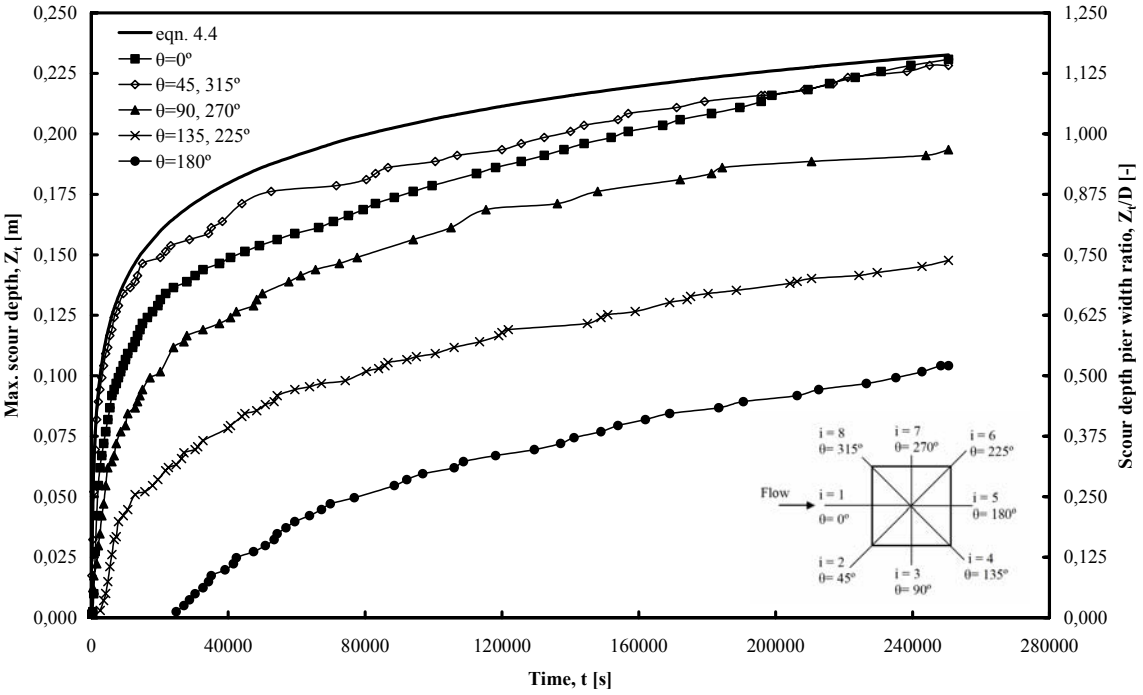

Figure 4.4.7. Time development of maximum scour depth in different azimuthal half-planes at a square pier [d_{50} = 0.97mm, h/D =1.50 and u/u_{cr} = 0.95].

Figure 4.4.8 shows development of the scour patterns at square pier in coarse sand bed after 720, 2040, 5400, 35880, 72480 and 250500s. Scour started and progressed fast at the corners of the pier front with θ = 45º, and eventually propagated during the first 360s from the both corners toward the pier front with θ = 0°. At this stage, the upstream half of the scour hole was a ring-like groove formed by scouring process and a mound of the eroded sediment was observed close to the pier pack. The accumulated sediment mound found to be moving to the downstream with time, and the scoured region surrounded the pier after 24780s. The point of maximum depth in the scour hole was initially observed at plane with θ = 45º and migrated to the plane with θ = 0° during the first 198800s with small difference with θ = 45º.

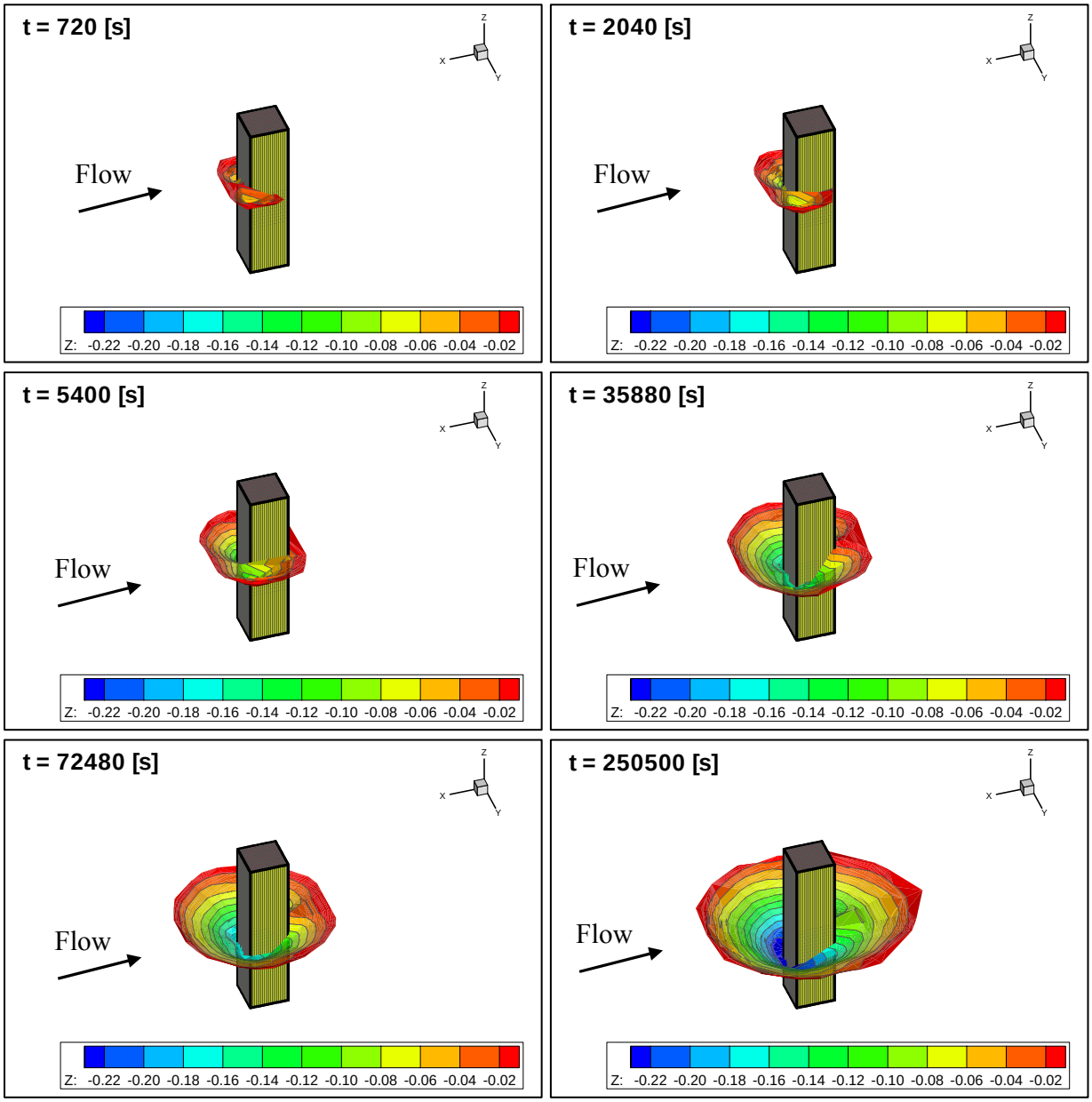

Figure 4.4.8. Developing scour hole topography at a square pier after 720, 2040, 5400, 35880, 72480 and 250500s [d_{50} = 0.97mm, h/D =1.50 and u/u_{cr} = 0.95].

Figure 4.4.9 gives the measured scour-slopes in azimuthal half-planes with θ = 0, 45, 90, 135, and 180º at the square pier in coarse sand. After scouring surrounded the pier, scour hole has taken a constant shape during the scour process. Flat ring shaped portion was identified close to the pier. At pier front, the width of the ring increased with time reaching about 32% of the radius of the scour hole at the end if the experiment. Over this ring a nearly uniform slope was observed. Average scour-slope diminished with θ, changing from 31 to 12º at the planes with θ = 0 and 180º respectively. At the end of the

test, the longitudinal extent of the scour hole in coarse sand was 40% smaller than in gravel bed.

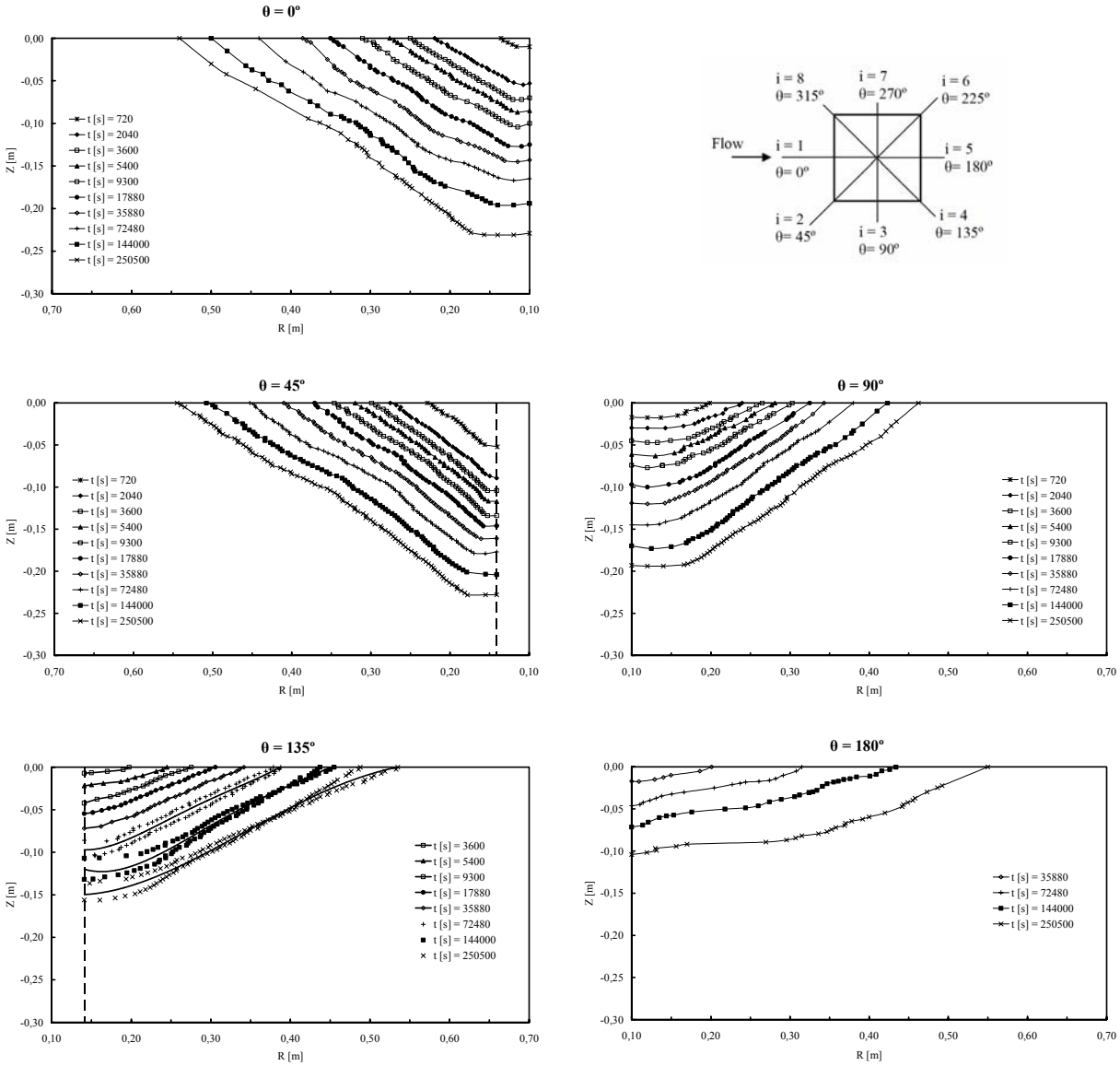

Figure 4.4.9. Measured scour-slopes in different azimuthal half-planes over time at a square pier [d_{50} = 0.97mm, h/D =1.50 and u/u_{cr} = 0.95].

Figure 4.4.10 shows the volume of the scour hole versus the maximum scour depth at θ =0º and scour time, in dimensionless form. After 10% of the running time when the pier was surrounded by the scour, scoured volume correlated well with maximum scour depth in front of the pier following a parabola with determination factor of 0.985. The obtained scour volume after 60% of the experimentation time was 75% of that obtained at the end.

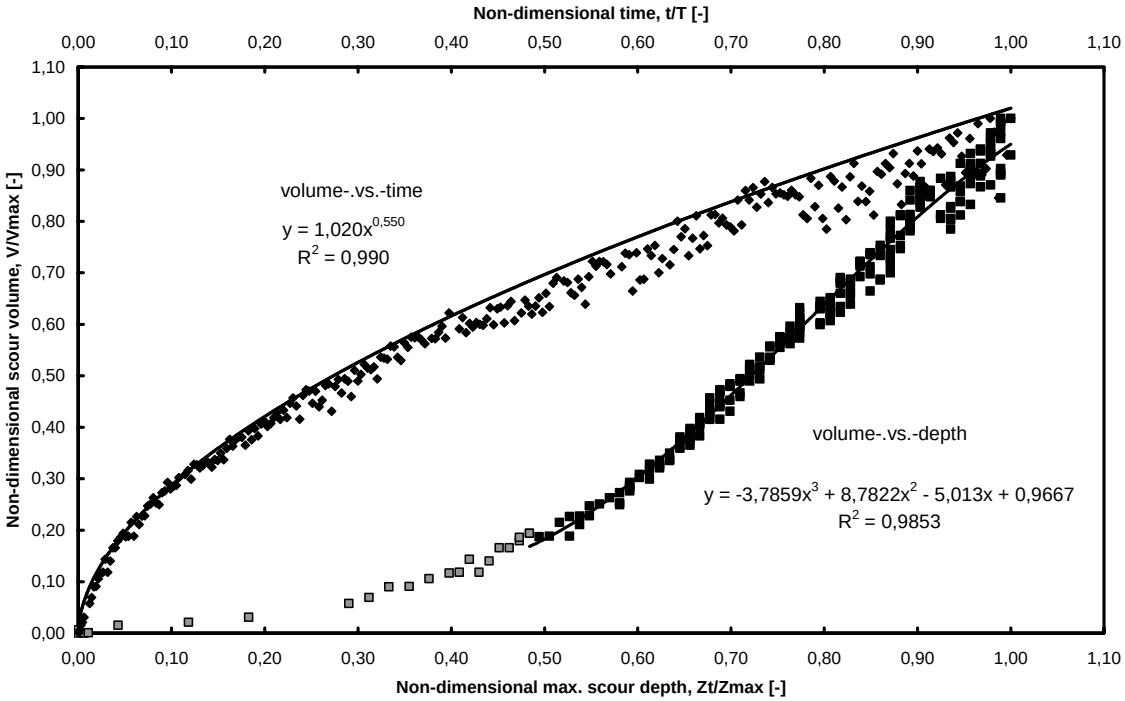

Figure 4.4.10. Volume of developing scour hole over time (upper) and maximum scour depth (bottom) at square pier [d_{50} = 0.97mm, h/D =1.50 and u/u_{cr} = 0.95].

CHAPTER 5
ANALYSIS OF THE RESULTS

In this chapter, all the obtained results are analysed in comparison. First, evaluation of the scour hole shape in case of circular, square, and rectangular with L/B = 2 and 4 piers as well as in case of square pier with different attack angles and in different sediment are presented. Second, the effect of pier shape, alignment and sediment size on the maximum scour depth on time is analysed. Third, the measured and computed time-dependent maximum scour depth around circular and square cylinders is discussed. Fourth, the development of scour profiles in the longitudinal and lateral directions with time as a function of pier shape and sediment size is analysed. Next, the effect of pier shape, alignment and sediment size is taken into account for the prediction of equilibrium scour depth. Finally, the time-dependent scour volume is presented. When possible, results obtained in the current study have also been compared with previous work of other researchers.

5.1 DEVELOPMENT OF SCOUR HOLE SHAPE

Figure 5.1.1 shows the measured situation rather than an inverted scheme of the scour hole shape, for circular and square piers in gravel after dimensionless scour time t/T = 0.001, 0.003, 0.01, 0.10 and 1.00. The scour hole is symmetric respect to the plane with θ = 0º during the experiments. Scouring was observed immediately after the test started at the sides of the circular pier between the planes with θ =45 - 90º and around the front corners of the square pier with θ = ± 45º. Eventually, scour propagated rather rapidly around the pier perimeter from both sides toward the centreline of the pier front with θ = 0º. In this stage, the shape of the upstream half of the scour hole was initially like two holes on the pier sides that come together fast and form a ring-like groove, and a mound of the eroded sediment from the scour hole was observed in the wake region. The mound of deposited sediment which was initially noticed very close to the pier pack, found to be moving downstream while running the test. Scoured region surrounded the circular pier [after t/T = 0.0025] faster than the square pier [after t/T = 0.01], when the relative maximum scour depth Z/D reached 0.60 and 1.15 at the circular and square piers, respectively. In due course, the deepest point in the scour hole which was initially observed at the plane with θ = ± 45º, migrated to the centreline of the pier front with θ = 0º during the first 3600s [t/T = 0.01] and 3000s [t/T = 0.008] when Z/D = 0.80 and 1.20 at the circular and square piers, respectively. After scour surrounded the pier and deepest point moved to the pier front, the scour hole enlarged with nearly the same shape to the end of experiments.

Developing scour holes at the equivalent square pier were about 25 - 40% larger than those at the circular pier, probably because of the increased downflow at the upstream face of the square pier due to the perpendicular attack of the incoming flow and the existence of spiral edge vortex due to the flow separations at the corners of the square.

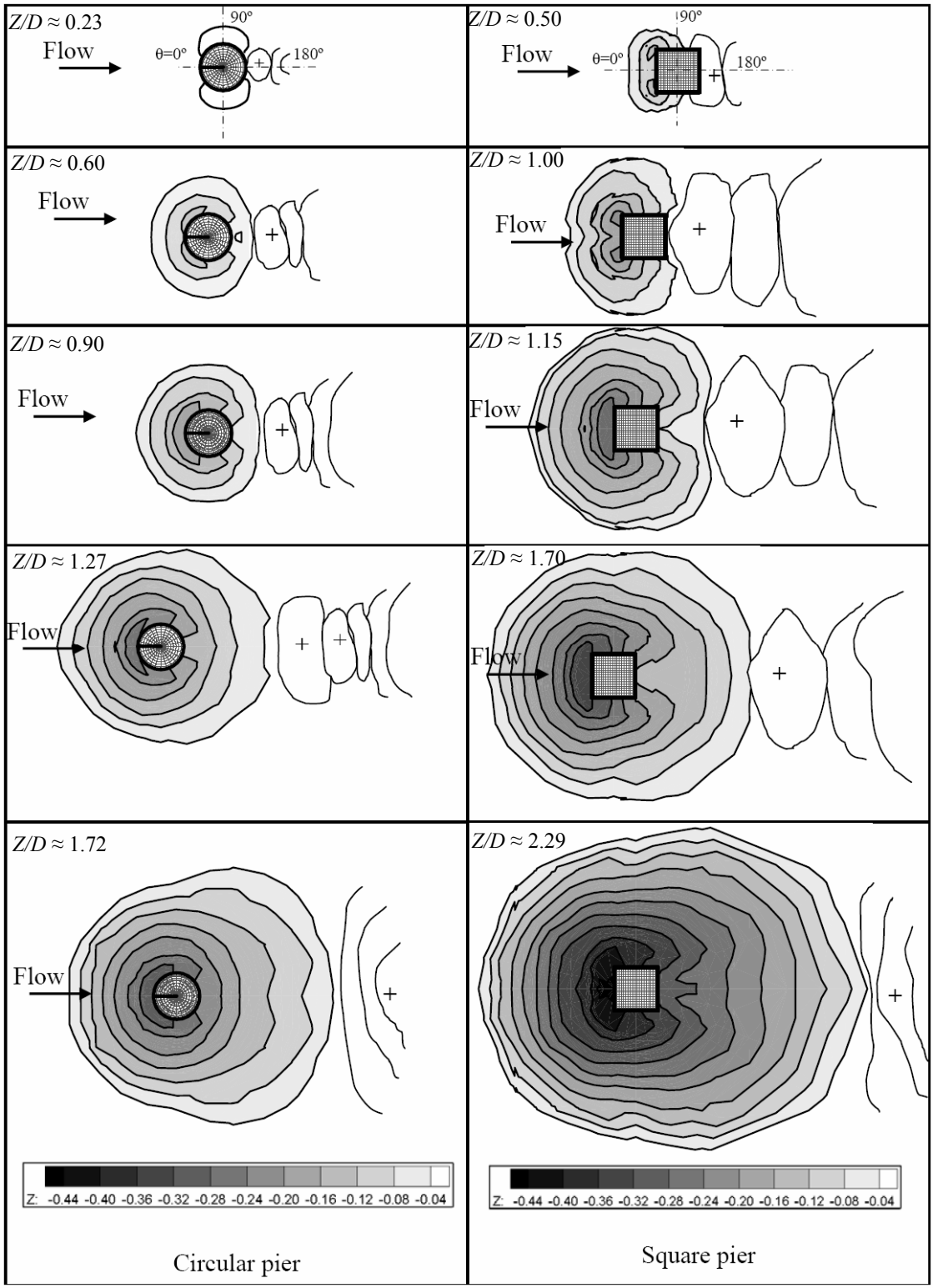

Figure 5.1.1. Scour hole development at circular (left) and square (right) piers in gravel after dimensionless experimentation time t/T = 0.001, 0.003, 0.01, 0.10 and 1.00.

In figure 5.1.2, development of scour hole topography at rectangular piers with L/B = 2 and 4 after dimensionless time t/T = 0.001, 0.01, 0.05, 0.10 and 1.00 is represented. Similar to the case of square pier, scouring started around the pier front corners at azimuthal half planes with $\theta = \pm 45^{o}$, where the deepest point of the scour hole was also observed during the first 2280-1620s [t/T = 0.006-0.0045] for rectangles with L/B = 2 and 4, respectively. The deepest point was moved to the centreline of the pier front when Z/D reached about 1.00 and 0.80 at rectangles with L/B = 2 and 4 respectively. In this stage, the shape of the scour hole was also a ring-like groove formed by the scouring process around the upstream face of the pier and two small mounds of the eroded sediment on the pier sides. With the time, more sediment accumulated on the sides of the pier, reaching the azimuthal half plane with $\theta = 135^{o}$ after only 2760s [t/T = 0.008] at rectangular pier with L/B = 2, while a time of 10800s [t/T = 0.03] was needed in the case of rectangular with L/B = 4. Scour surrounded the piers when Z/D = 1.40 after 14100 and 16500s for piers with L/B = 2 and 4, respectively.
Note that the interference between the spiral edge vortex and the wake vortex at the square pier decreases with increasing pier length-width ratio, resulting in smaller scour rates and depths at the rectangular piers.

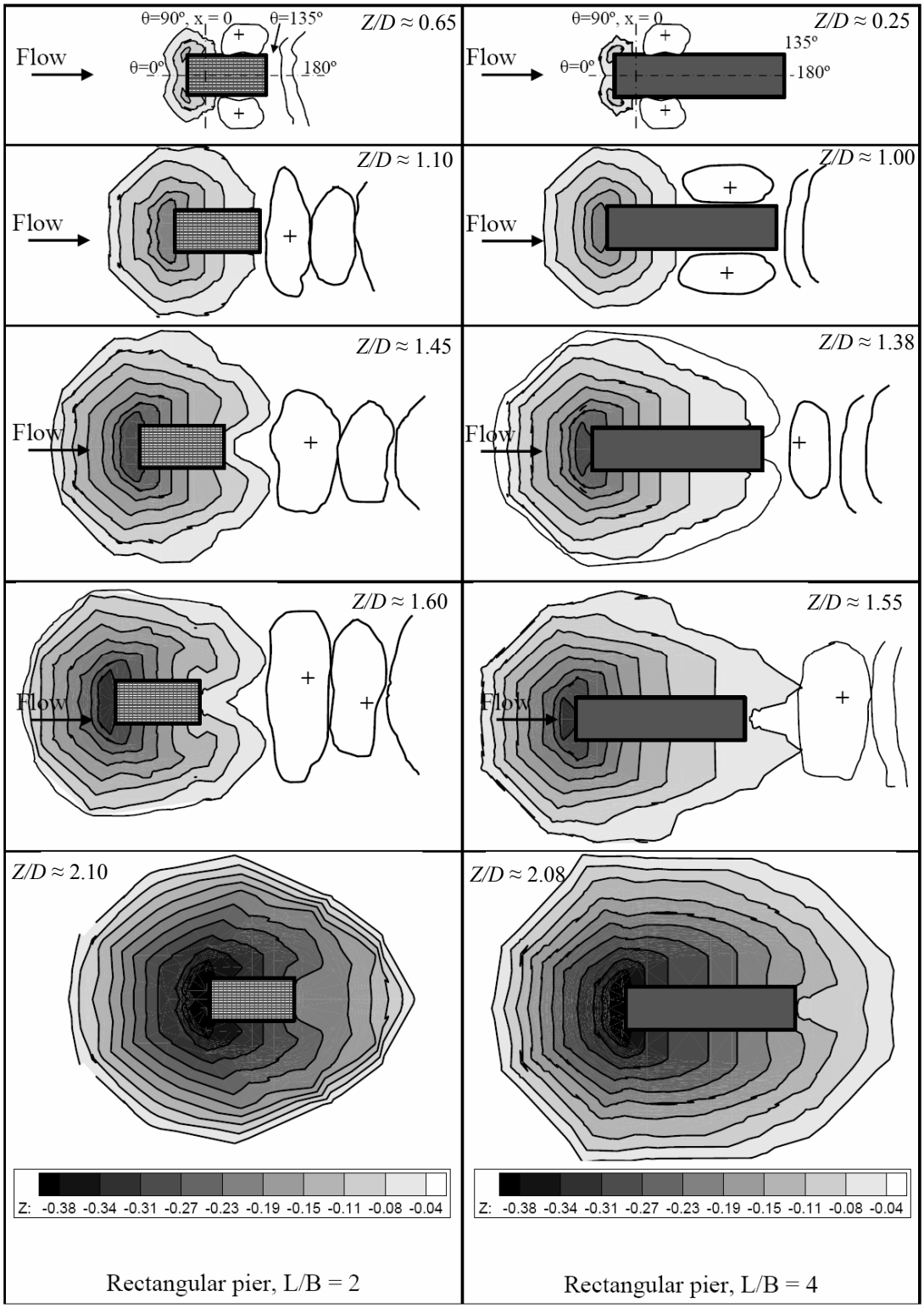

Figure 5.1.2. Scour hole development at rectangular piers with L/B = 2 and 4 in gravel after dimensionless experimentation time t/T = 0.001, 0.01, 0.05, 0.10 and 1.00.

Figure 5.1.3 shows the measured scour pattern at a square pier as a function of angle of flow attack α = 0, 15, 30, and 45º, after dimensionless experimentation time t/T = 0.001, 0.01, 0.10 and 1, respectively. Scour pattern varies significantly with the angle of attack. The plots show that asymmetry of scour hole was zero when the pier is aligned with the flow, and increased with the angle of attack. Scour started and progressed immediately after the test started around the corners of the upstream side of the pier, faster at the corner away from the flow direction (i.e. with θ = 315º). Then scour propagated rather from both corners toward the main flow direction. The deepest point in the scour hole which was initially located at the far corner of the upstream side of the pier at the plane with θ = 315º, migrated to the main flow direction when Z/D = 1.20 – 1.70 after dimensionless time t/T = 0.01 to 0.30, increasing with the angle of attack. On the contrary, scour progressed to the downstream slower around the pier aligned with the flow, surrounded the piers after 3240s, 2760s, 960s and 480s for attack angles α = 0, 15, 30, and 45º, respectively.

To the end of the tests, the bottom of the final scour hole can be described as flat regions upstream and downstream the pier, connecting together with gradients. The overall extension of the scour hole was nearly constant in all cases with different angles of attack. The maximum depth in the scour hole decreased from 2.29D to 2.01D with increasing the angle of attack from 0 to 45º. That may be because the strength of the spiral edge vortex and the downflow decreased with the angle of attack.

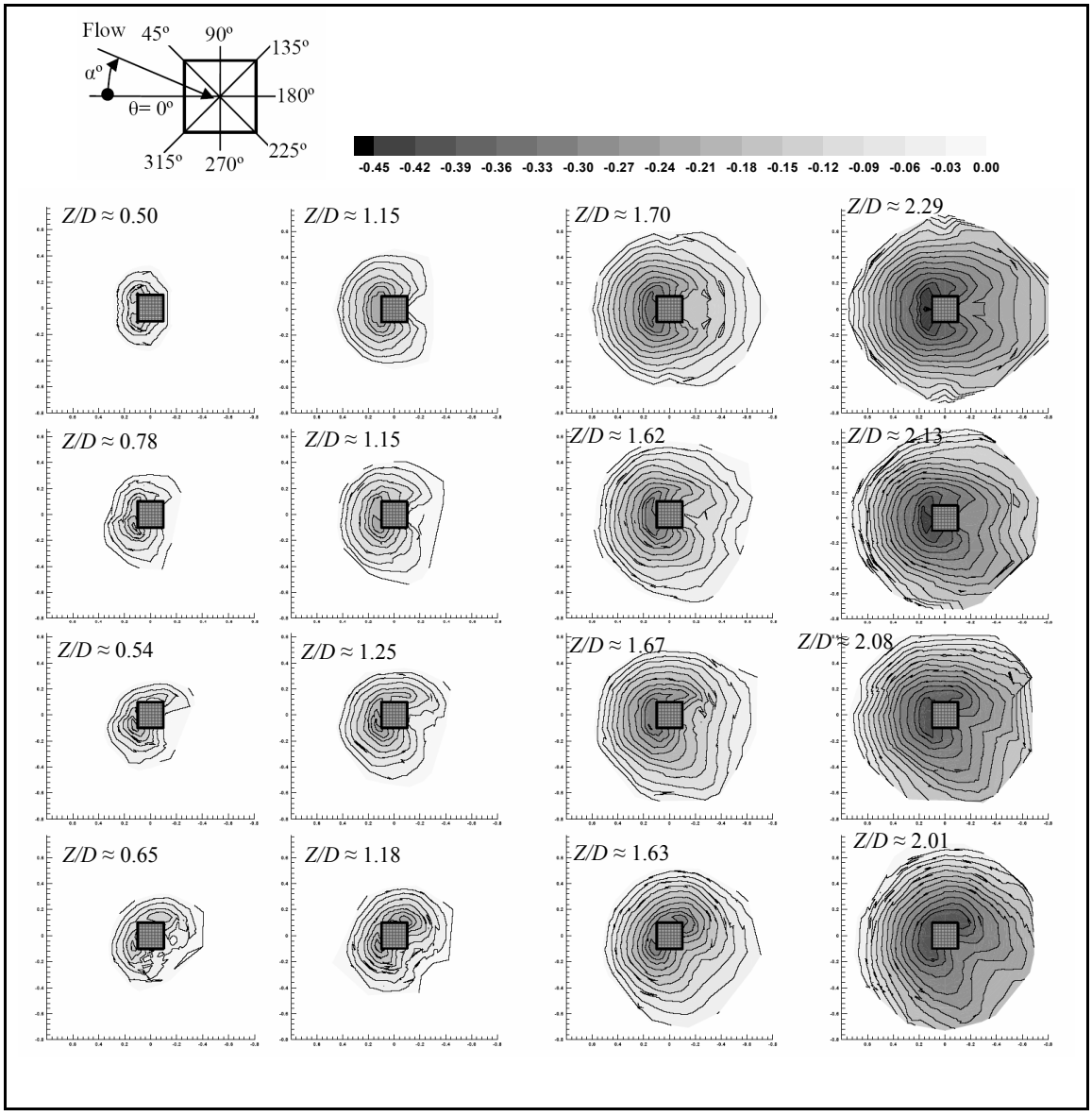

Figure 5.1.3. Scour pattern at a square pier with angle of attack α = 0, 15, 30, and 45º after dimensionless experimentation time t/T = 0.001, 0.01, 0.10 and 1.00, respectively.

The results of sediment size study show that the development of scour holes in sand size range is slower than in gravel. Figurer 5.1.4 presents the development of scour holes at a square pier founded in fine gravel, coarse and fine/medium sands under clear-water scour conditions. Scouring started and progressed also fast around the pier front corners with θ = ± 45º. Slower than in gravel, scour propagated rather towards the centreline of the pier front, reaching the plane with θ = 0º after 360 and 780s in coarse and fine/medium sands, respectively. During this phase, ripple formations were noticed downstream the pier in fine/medium sand, while mound of the eroded sediment from the scour hole was deposited close to the pack of the pier founded in coarse sand. Scour progressed slower toward the downstream face of the pier, reaching the pier wake with θ =180º when Z/D = 0.75 - 0.80, after 24780s (about 7 hours) in coarse sand and when Z/D = after 165000s (ca. 2 days) in fine/medium sand. During most of the experimentation time, the deepest point in the scour hole was observed at the corners of the upstream face of the pier at θ = ± 45º, and migrated to the centreline of the pier front at the plane with θ = 0º after 198800s (when Z/D = 1.10 in coarse sand) and 114840s (when Z/D = 0.75 in fine/medium sand) with a negligible difference of 2% with the depth at θ = ± 45º.

Time variation of the scour hole topography around piers is highly dependent on the pier shape and alignment as well as on the sediment size. Scouring in gravel progressed faster to the wake of the circular and square piers than at the rectangular piers. On the contrary, the deepest point in the scour hole migrated faster to the front of the rectangular piers. The extension of the scour holes at rectangular piers was larger than those at the square and circular piers.

The time required for migrating the deepest point in the scour hole from the far corner of the pier upstream side to the main flow direction increased significantly with the variation of the attack angle from 0 to 45º. Scoured region surrounded the pier faster with the attack angle.

Scouring in sand size range progressed to the front and wake of the square pier slower than in gravel, surrounding the pier after t/T = 0.01, 0.07 and 0.50 when Z/D = 1.15, 0.75 and 0.80 in fine gravel, coarse and fine/medium sands respectively. The overall extent and width of scour holes in the here used sand sizes were approximately 30 - 65% of those observed in the gravel bed of this test series.

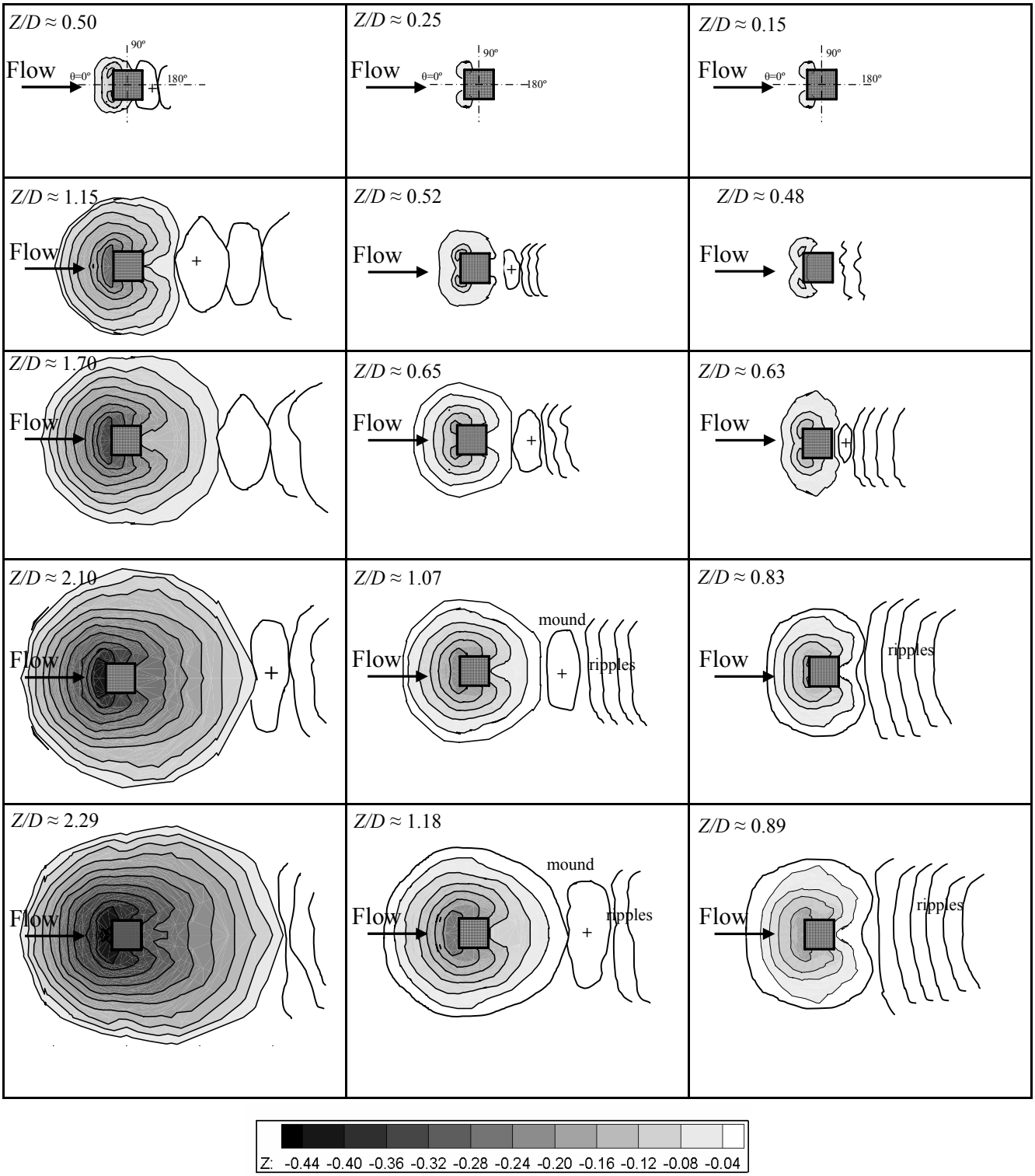

Figure 5.1.4. Scour hole development at a square pier in fine gravel (left), coarse sand (middle) and fine/medium sand (right) after t/T = 0.001, 0.01, 0.10, 0.50 and 1.00.

5.2 TIME-DEPENDENT MAXIMUM SCOUR DEPTH: LABORATORY DATA

The time-dependent maximum scour depth in uniform sand and gravel is presented, showing the effect of pier shape, angle of attack and sediment size. All experiments were conducted near the threshold velocity (h/D = 1.50 and u/u_{cr} = 0.95). Almost all experiments were conducted during 4 days or longer, in order to ensure a condition at least very close to the equilibrium. The experimentation time (100hours) is taken as the reference time, T.

Effect of pier shape

Figure 5.2.1 shows time-dependent maximum scour depth, Z_t / D over scour time t/T for different pier shapes in gravel.

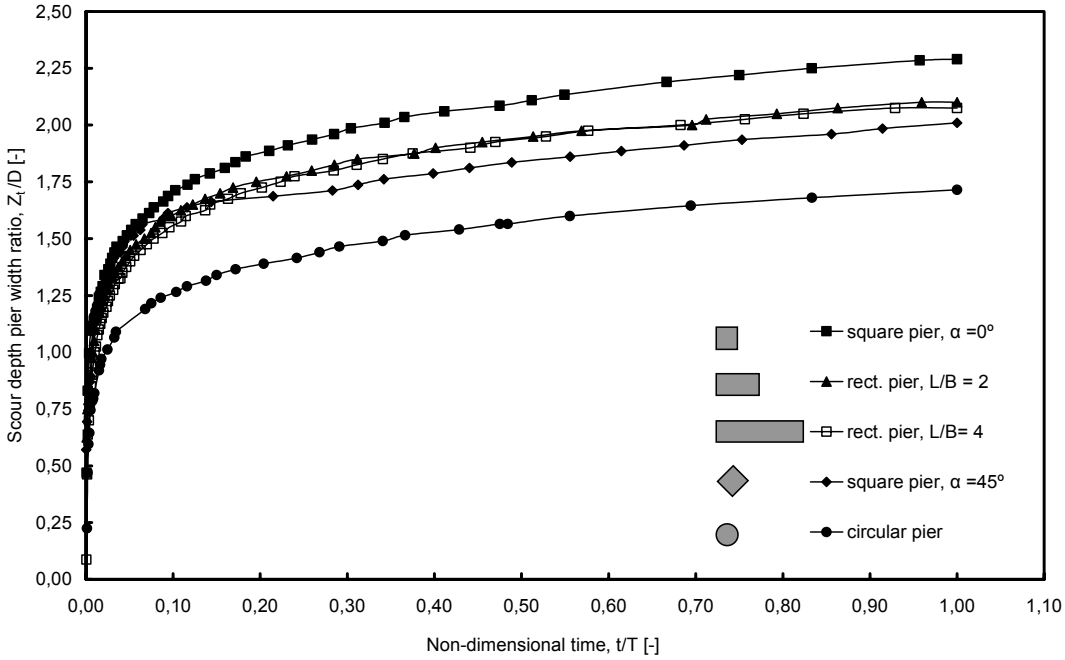

Figure 5.2.1. Effect of pier shape on time-dependent maximum scour depth.
[d_{50} =3.25mm, h/D = 1.50 & u/u_{cr} = 0.95]

Scour depth developed with different decreasing scour rates at different pier shapes during the first 25% of the running time, and then progressed around all shapes with the same rating. The achieved average scour rate was 0.47mm/hr. Results indicated that 50% of the final scour depths are attained in a time varying from 0.01 - 0.02 of the experimentation time (100 hours). And 70% of Z_{eq} is attained within a time variation of 0.03 to 0.08 of the experimentation time, while time of 0.60 - 0.70 of the experimentation

time was needed to develop 95% of the final scour depth. In the case of square pier aligned 45º with the flow direction, about 85% of Z_{eq} is attained only during the first 15% of the experimentation time. This explains the significant effect of the time on measuring and predicting the scour depth. Wrong conclusion may be reached if the tests were stopped short of an equilibrium state.

The highest and the lowest values of the time-dependent maximum scour depth were always observed around the square (aligned with the flow) and circular piers, respectively. The ratio between time-dependent maximum scour depths at square (aligned with the flow) and circular piers diminishes from 1.60 at the beginning of the tests to the average of about 1.34 for all measurements that were taken after 10% of the experimentation time. Changing the alignment of the square pier from 0 to 45º with respect to the flow direction decreases the values of the time-dependent maximum scour depths for about 14%. For rectangular piers, there is no significant effect of the pier length-width ratio L/B on the values of the scour depth. To the end of experiments, the obtained Z_t / D were 1.72 (circular), 2.01 (Square aligned 45º), 2.10 (rectangular) and 2.30 (square aligned with the flow).

The time-dependent maximum scour depth was first observed at the square and rectangular pier front corners and at the circular pier sides during the first 0.005T - 0.01T. Later, it located at the centreline of the pier's front. An exception case was the square pier aligned at 45º where the shifting of maximum scour depth to the pier front was needed a long time of about 0.30T.

The observed scour depths at square and rectangular piers are greater than at the circular one, possibly due to the existence of the spiral edge vortex at the front corner of square and rectangular piers which increases the ejection of sediment from the bed. The interference between this spiral edge vortex and the wake vortex may be the main cause of the deepest scour which observed around the square pier. In the case of rectangular piers, this interference diminishes with the increase of the pier length and also the vorticity of the wake vortex decreases.

Effect of pier alignment

Figure 5.2.2 shows the measured time-dependent maximum scour depth Z_t / D over scour time t/T for square pier aligned with different angles of attack together with that for circular pier. For different attack angles, scour depth at the square pier initially progressed with different rates during the first 30% of the experimentation time. Then scour depth developed with the same velocity for all the 4 different angles of attack. The achieved average scour rate was 0.44 mm/hr.

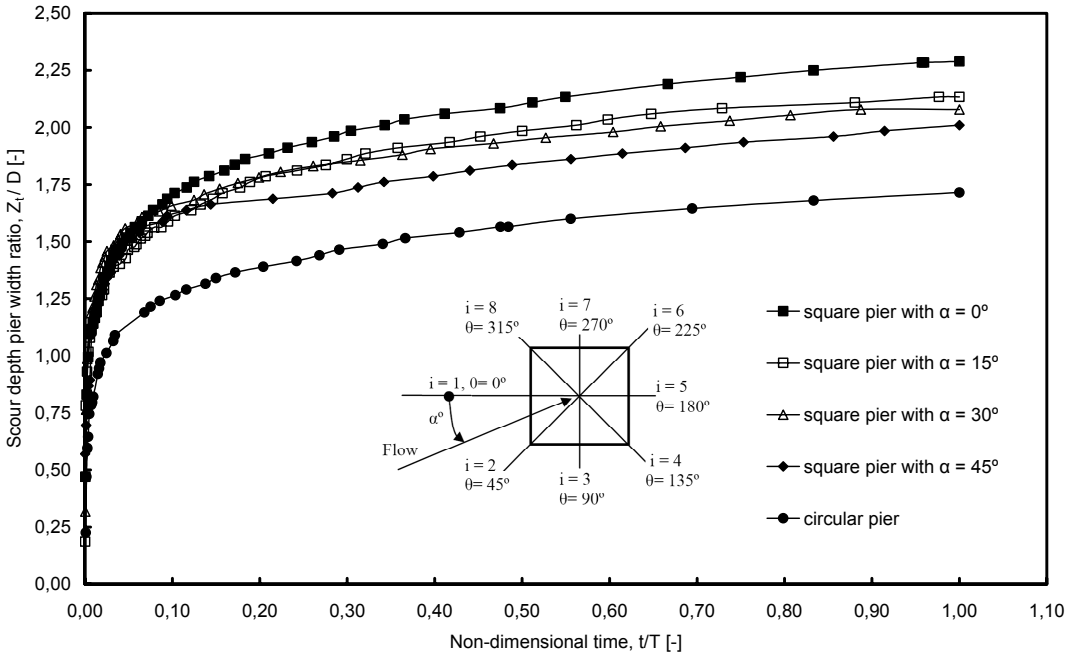

Figure 5.2.2. Effect of angle of attack on time-dependent maximum scour depth. [square pier, d_{50} =3.25mm, h/D = 1.50 & u/u_{cr} = 0.95]

During the first 0.01T (for α = 0 and 15º) or 0.30T (for α = 30 and 45º), the point of maximum scour depth in the scour hole which was initially located at the pier's front corner with θ = 315º, migrated to the main flow direction. During the first 10% and 15% of the time of tests, the measured scour depths at square pier with α = 30 and 45º were higher than that observed at the square pier with α = 0º, respectively. About 50 - 70% of the final scour depth was attained during the first 0.003 - 0.01 and 0.03 - 0.07 of the experimentation time respectively, while a time variation of 0.55 - 0.70 of the experimentation time was required to develop 95% of the final scour depth. That confirms the major effect of time on the prediction of scour depths.

The magnitude of time-dependent maximum scour depth decreases with the angle of attack. Excluding the first 30% of experimentation, the position of developing maximum scour depth was always observed on the main flow direction. The observed scour depth at the circular pier was significantly smaller than that at the square pier with all attack angles. To the end of experiments, the values of Z_t / D were about 1.72 (circular), 2.01 (square aligned 45º), 2.08 (square aligned 30º), 2.13 (square aligned 15º) and 2.30 (square aligned with the flow).

Effect of sediment size

Time-dependent maximum scour depth at circular and square piers founded in three different uniform cohesionless sediment materials; namely fine gravel, coarse and fine/medium sands was studied. In addition to the data of present study, the local scour data for circular pier in coarse and fine/medium sands obtained by Link (2006b) and Link et al. (2008b) was employed. Since some of the tests were conducted shorter than the others, a regression analysis was performed in order to independently compare the data. In figure 5.2.3, typical time evolution trends for maximum scour depth is shown.

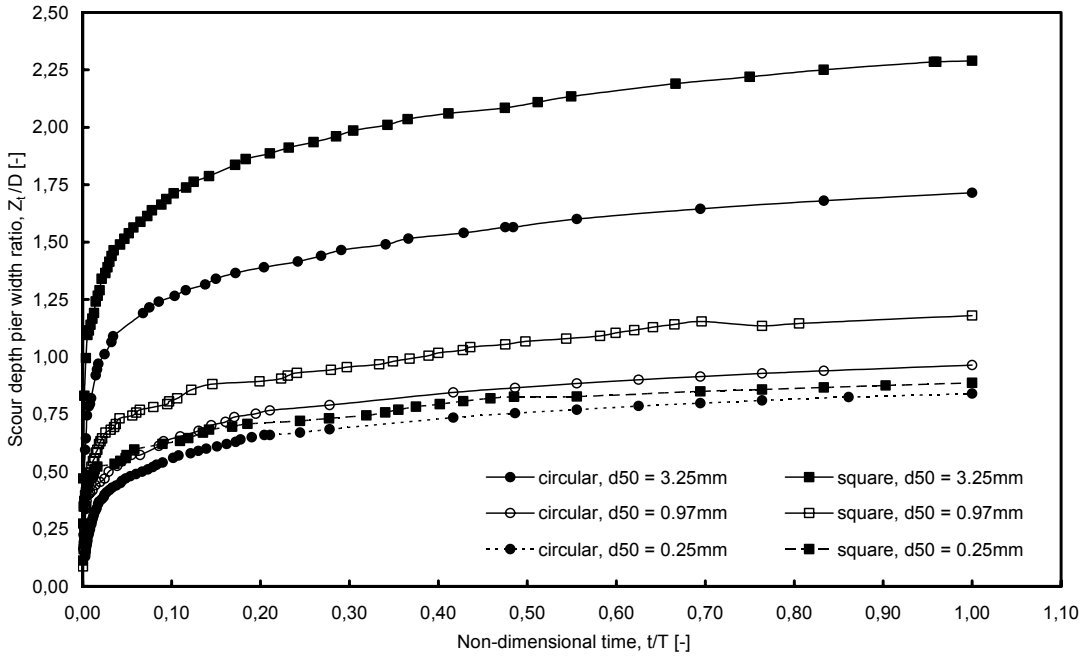

Figure 5.2.3. Effect of sediment size on time-dependent maximum scour depth.
[circular and square piers, h/D = 1.50 & u/u_{cr} = 0.95]

Scouring developed at a decreasing rate; so that the obtained scour depth during the first 0.01-0.03 of experimentation was approximately as much as in the following days until the end of the experiments. Scour depth increases with increasing the median grain size, i.e. with decreasing the sediment coarseness D/d_{50}. The observed scour depth in coarse sand was 15 - 23% larger than in fine/medium sand for circular and square piers, respectively. Changing the bed material from sand to gravel increases significantly the scour depth, the observed scour depth in gravel (d_{50}=3.25mm) was about 1.80-2.00 times that in coarse sand (d_{50}=0.97mm) in the cases of circular and square piers, respectively.

The point of maximum scour depth in the scour hole around the square pier was moved from the pier's front corners to the pier centreline after 0.01T in gravel size and 0.30T - 0.55T in sand size range. Note that the effect of sediment size is noticeable nevertheless the sediment coarseness ratio D/d_{50} is more than 50.

Empirical equation of time-dependent scour depth

All the laboratory data of the present study as well as the data from Link (2006b) and Link et al. (2008b) are plotted in figure 5.2.4, as non-dimensional scour depth over non-dimensional scour time. The final maximum scour depths and the experimentation time (100hours) were used as the equilibrium scour depth Z_{eq} and the reference time, T. All results are well represented by the following equation which is also plotted in figure 5.2.4.

$$\frac{Z_t}{Z_{eq}} = 0.1098 \ln\left(\frac{t}{T}\right) + 0.9896 \qquad [5.1]$$

As shown, all the laboratory data are within ± 15% and ± 5% of equation [5.1] before and after t/T = 0.25, respectively. The obtained determination coefficient is 0.93.

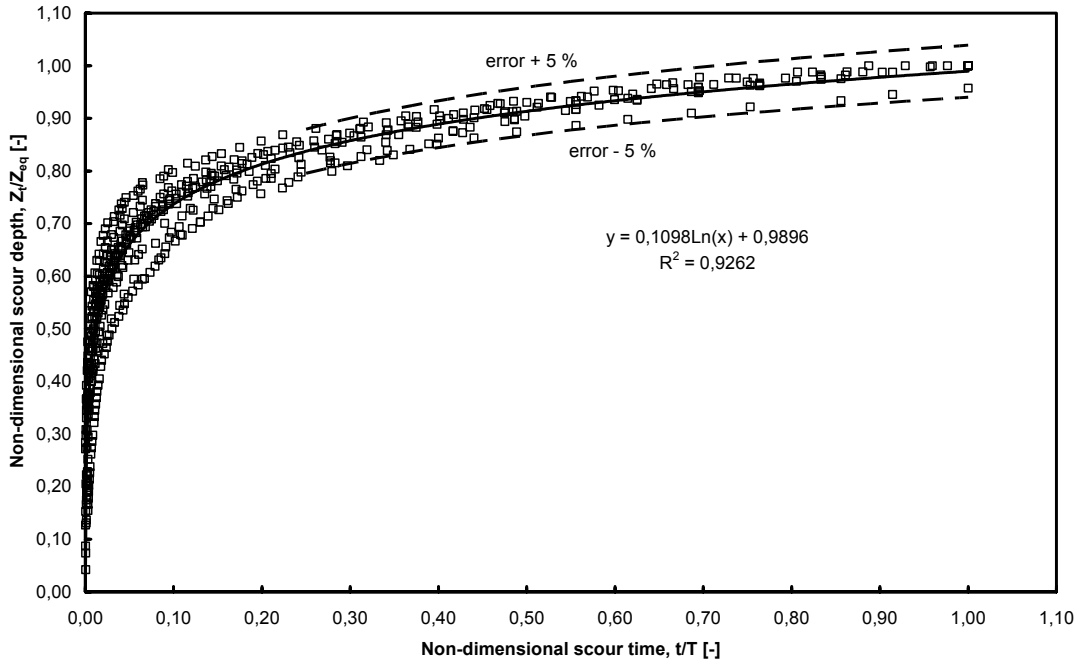

Figure 5.2.4. Non-dimensional scour depth versus non-dimensional scour time

5.3 TIME-DEPENDENT MAXIMUM SCOUR DEPTH: FORMULAS COMPARISON

The present section is devoted on the comparing of the laboratory data and equation [5.1] with some of the scour formulas listed in table 2.3. The laboratory data from the tests with circular and square pier in gravel are used for the comparison.

Figure 5.3.1 compares Franzetti (1982) [eqn. 2.6], Hoffmans and Verheij (1997) [eqn. 2.8] and the new suggested equation [5.1] with the laboratory data of the present study, as non-dimensional time-dependent maximum scour depth, Z_t / D on non-dimensional scour time, t/T.

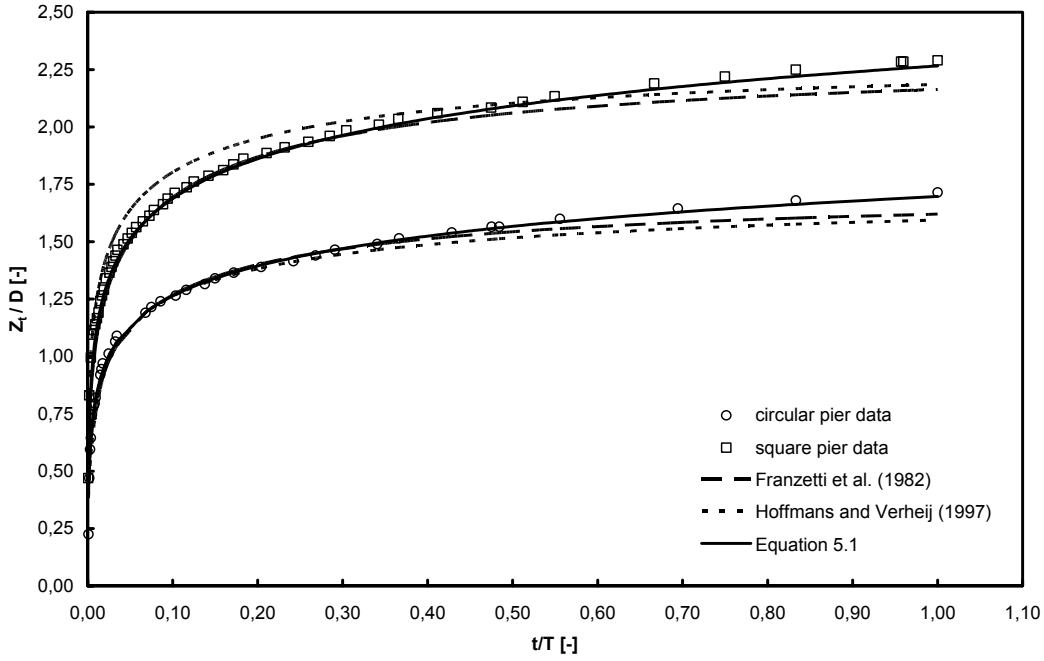

Figure 5.3.1. Comparison of time-dependent maximum scour depth: Franzetti et al. (1982) and Hoffmans and Verheij (1997)

A good agreement was found between the measured and the computed time-dependent maximum scour depths using the equation [5.1] for both circular and square piers. Franzetti (1982) underpredict with small values the measured scour depths around both the circular and square piers during the beginning of scour until t/T ≈ 0.40, and tends to underpredict the final scour depth with a difference of 6%. Hoffmans and Verheij (1997) has the same trend as Franzetti (1982) in the case of circular pier, while it slightly overpredict the measured scour depths at the square pier during the first half of the experimentation time and tends to underpredict the final scour depth.

Figure 5.3.2 compares the laboratory data of the present study and Equation [5.1] with Melville and Chiew (1999) [eqn. 2.9] and Barkdoll (2000) [eqn. 2.10]. For a good comparison with Melville and Chiew (1999) the duration of the experiments should be long than 6 days, as computed from Melville and Chiew [eqn 2.9] depending on our laboratory conditions. Therefore, since the present experiments were run only for duration of 4 days, the equilibrium scour depths were obtained after 6 days by employing the regression analysis and equation [5.1].

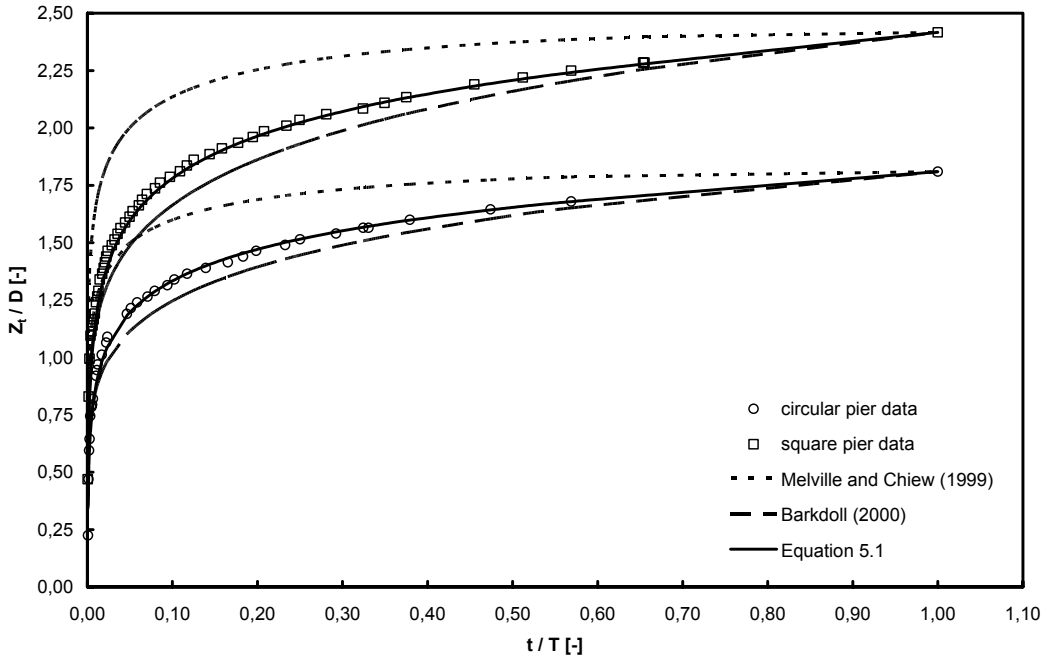

Figure 5.3.2. Comparison of time-dependent maximum scour depth: Melville and Chiew (1999) and Barkdoll (2000), T = 6.10 days as obtained from equation [1.9]

As shown in the figure, Melville and Chiew (1999) overpredict the present measurements during the development of the scour. Although, Barkdoll (2000) underpredict the measured values, is described the present measurements better than Melville and Chiew. The cause for the near-trend may be connected with the fact that Barkdoll's equation was developed from a laboratory data for circular and noncircular piers whereas Melville and Chiew's equation was developed from only the data set of circular pier.

In figure 5.3.3, Zanke (1982a) [eqn. 2.7] and Oliveto and Hager (2002) [eqn. 2.8] are compared with the laboratory data and equation [5.1].

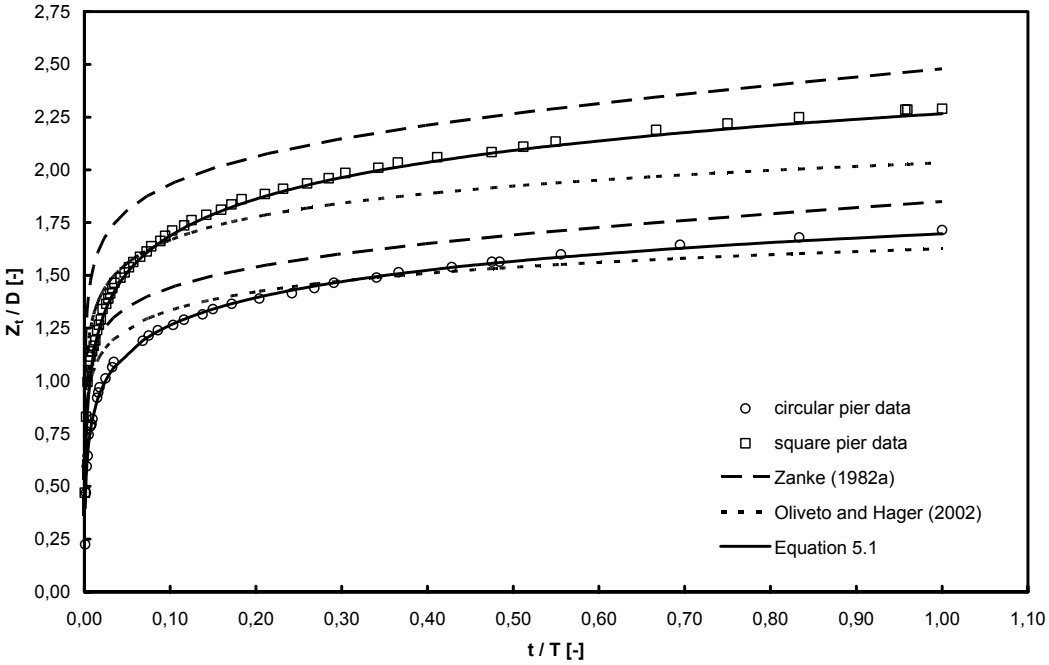

Figure 5.3.3. Comparison of time-dependent maximum scour depth: Zanke (1982a) and Oliveto and Hager (2002).

A new pier shape factor of 1.34 was suggested and used depending on the present laboratory results. Oliveto and Hager's (2002) equation overpredict the measured values during the beginning of scour and tend to underpredict the final scour depth.
A good agreement was found between the present data and the modified equation of Zanke (1982a). It has the same trend of the measurements with an accepted overprediction less than 5%. As recommended by Zanke (1982a), a modification of his equation was done by calibrating the increase velocity parameter ω depending on the data of circular and square piers in gravel beds. Equation [5.2] are obtained and used in the calculations.

$$\omega = 0.9013\left(\frac{Z_t}{D}\right)^6 - 6.9008\left(\frac{Z_t}{D}\right)^5 + 19.775\left(\frac{Z_t}{D}\right)^4 - 24.671\left(\frac{Z_t}{D}\right)^3 + 10.658\left(\frac{Z_t}{D}\right)^2 + 1.3891\left(\frac{Z_t}{D}\right) + 2.5001 \qquad [5.2]$$

5.4 TIME DEVELOPMENT OF SCOUR HOLE PROFILES

In the current section, the developing scour profiles in the longitudinal and lateral directions are presented. The radius of the scour hole was measured from the reference point, which was sited on the centreline of the circular and square piers at the original bed level.

Effect of pier shape

Figure 5.4.1 presents longitudinal profiles of developing scour holes along the centreline of the flume for circular, square and rectangular piers in gravel bed. At all piers the shape of scour profiles remained nearly constant during the scour process. Close to all piers, a ring shaped portion is observed. At the upstream, the width of the ring at the circular pier was about 65-85% of that at the square and rectangular piers. While at the downstream its width at the circular and square piers was about 35-50% of that at the rectangular piers. Over this ring, a nearly uniform slope is identified. At the upstream of the piers, a steeper slope was observed in the lower part of the profiles, being steeper at the square pier than the other shapes. While a second concave slope was observed in the upper part of the profile at the pier downstream. Average slopes of scour profiles at the square and rectangular piers are steeper than at the circular pier, changing from averagely 38º at the circular pier to 36º at the other piers at the upstream, and from 19º at the circular and 16º at the square to 13º at the rectangular pier (L/B = 4) at the downstream.

As shown from the profiles plotted inside the piers, the gradient of the scour hole bottom at the square pier is higher than at the circular piers. For rectangular piers, the bottom gradient decreased with increasing the pier length to width ratio L/B.

To the end of the experiments, the overall extension of the scour holes at the square and rectangular piers was averagely 1.50 times that at the circular pier. The extent of the scour hole downstream the pier's pack decreased with L/B ratio, changing from 5.75 times the pier width to 3.75 and 3.5 by increasing L/B from 1 to 2 and 4, respectively. A mound of the eroded sediment from the scour hole was observed downstream the scour holes.

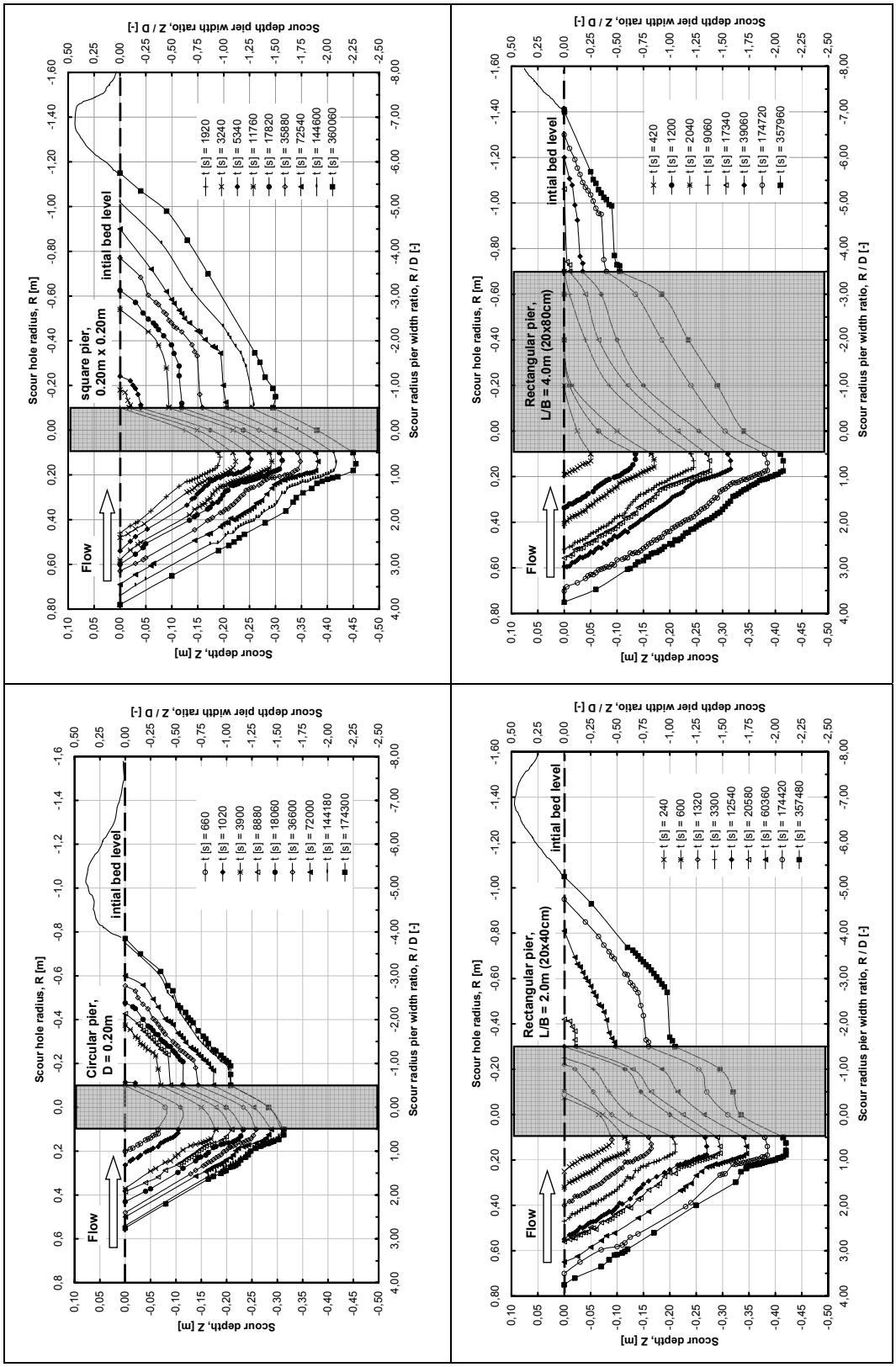

Figure 5.4.1. Scour longitudinal profiles for given times at circular (up-left), square (up-right), rectangular 0.20x0.40 (down-left), rectangular 0.20x0.80 (down-right) piers in gravel [d_{50}= 3.25mm, h/D=1.50 and u/u_{cr} = 0.95].

Figure 5.4.2 shows the lateral profiles of the scour hole for given times, through the centreline of the pier circular and square piers, and through transverse section located 10cm downstream the front face of the rectangular piers. As shown in the figure, the scour profiles are symmetrical about the pier. Similar to the longitudinal profiles, the shape of the transverse profile remained constant during scour development. A ring shaped portion close to the pier face is identified. The width of the ring at the circular pier was about 70% and 50% of that observed at the square and rectangular piers, respectively. Over the ring, a nearly uniform slope is observed. A milder slope was observed in the middle third of the profiles at the rectangular piers. Average side-slopes at the square pier were the steeper. The averaged scour-side-slopes at the circular, square, and rectangular (L/B = 2 and 4) piers were 32, 35, 32 and 30º, respectively. It is shown also that the maximum scour depth observed on the sides of the square pier was always the biggest during scouring development.

To the end of the experiments, the scour hole at the square pier was about 15 % wider and 22.5% deeper than at the circular pier. At the rectangular piers with L/B = 2 and 4, the scour holes were averagely 9% and 22% wider than at the square pier, respectively.

Scour profiles break suggest the action of vortex system with different strengths, vortex strength being lower to the upper part of the scour hole. As shown in the longitudinal profile, clockwise rotation of vortex contributes to side stabilization, explaining the existence of the lower side slope with a higher inclination than the natural repose angle. The wider ring portion at the square and rectangular piers shows that the vortex sizes are bigger than at the circular pier.

The existence of spiral edge vortex at the corners of square pier may be the reason of the deeper scour hole and the steeper slopes than at the circular pier. At the rectangular piers, the interference between the spiral edge vortex and the wake vortex diminishes with L/B, explaining the shallowness of the scour holes and the milder slopes at the rectangular piers.

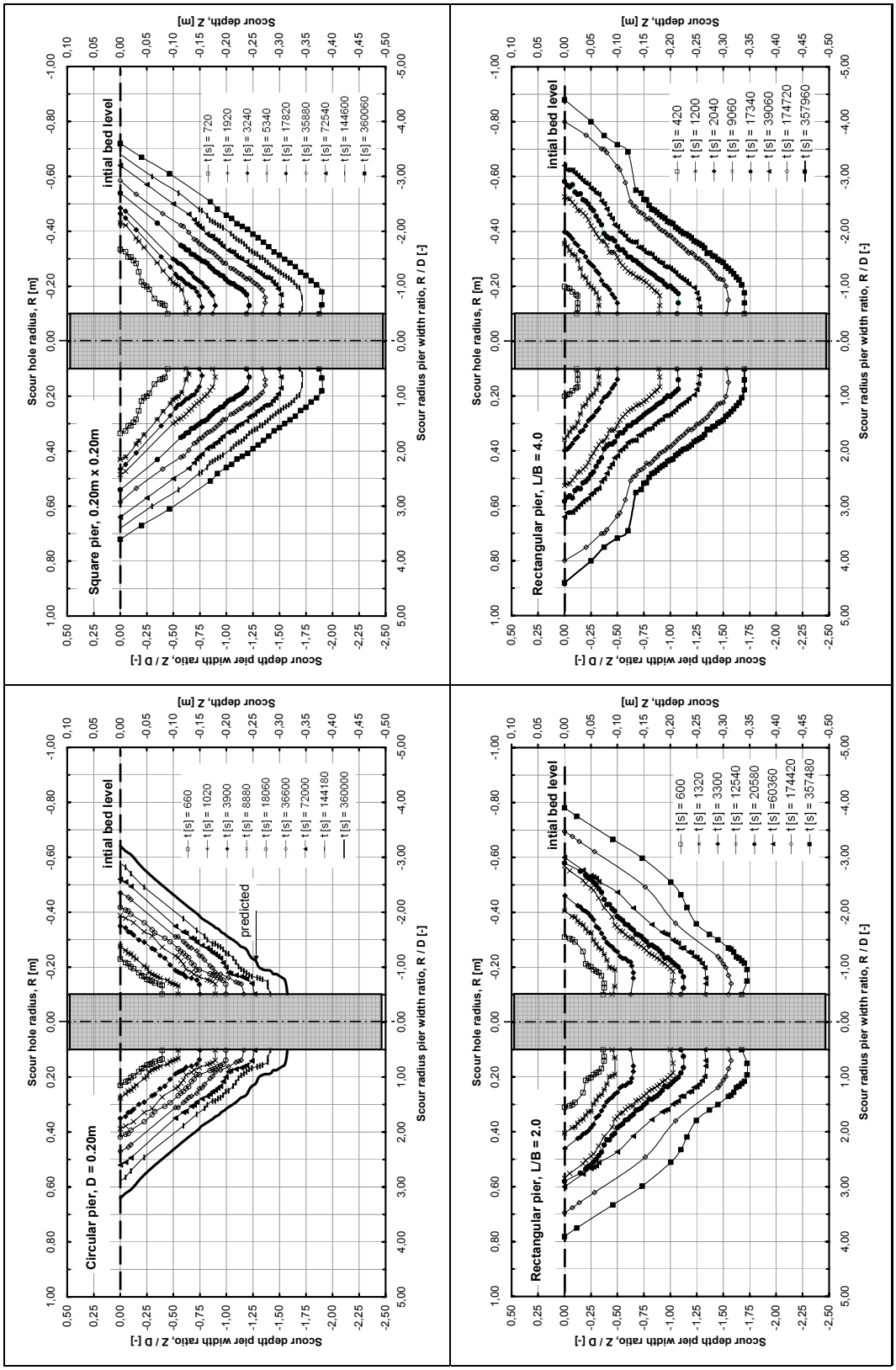

Figure 5.4.2. Scour lateral profiles for given times at circular (up-left), square (up-right), rectangular 0.20x0.40 (down-left), rectangular 0.20x0.80 (down-right) piers in gravel [d_{50}= 3.25mm, h/D=1.50 and u/u_{cr} = 0.95].

Effect of sediment size

In figure 5.4.3, developing longitudinal profiles of scour along the centerline of a square pier as a function of sediment size are presented. The observed shape of scour profiles in sand and gravel beds were generally similar, being nearly constant shape during scour development. Close to the pier, a ring shape portion was observed. The width of the ring in fine/medium and coarse sands was about 70-80% of that observed in fine gravel. Over the ring, a nearly uniform slope was identified. In fine gravel, a steeper slope was observed lower the profiles in the upstream, and a second concave slope was observed in the upper part of the profile in the downstream. Average slopes of scour profiles at the square pier in gravel are steeper than in coarse and fine/medium sands, changing from averagely 36º to 31-30º in at the upstream, and from 16 to 12º at the downstream respectively. Ripple formations were observed downstream the scour hole in fine/medium sand, while mound of the eroded sediment from the scour hole was deposited at the downstream in coarse sand bed.

To the end of the experiments, the longitudinal extension of the scour hole in gravel bed which was about 10 times of the pier width was approximately 1.75 and 3.25 times that observed in coarse and fine/medium sands, respectively.

Transverse profiles of developing scour holes through the centerline of the square pier, for fine/medium sand, coarse sand and fine gravel are plotted. All profiles shape contained a ring shape portion close to the pier followed by a nearly uniform slope. The most pronounced differences between the profiles in sand and gravel bed were the size of the scour holes. The depth and lateral width of the developing scour hole in gravel bed were larger than in sand beds. To the end of the experiments, the width of the scour hole in gravel (about 7.20B) was nearly 1.55 – 1.70 times those observed in coarse (about 4.62B) and fine/medium (about 4.20B) sands, respectively. The maximum scour depths in fine/medium and coarse sands were 70-78% of that observed in gravel. Average side-slopes of the scour hole was steeper than in sands, changing from 35º in gravel to 31-24º in coarse and fine/medium sands, respectively.

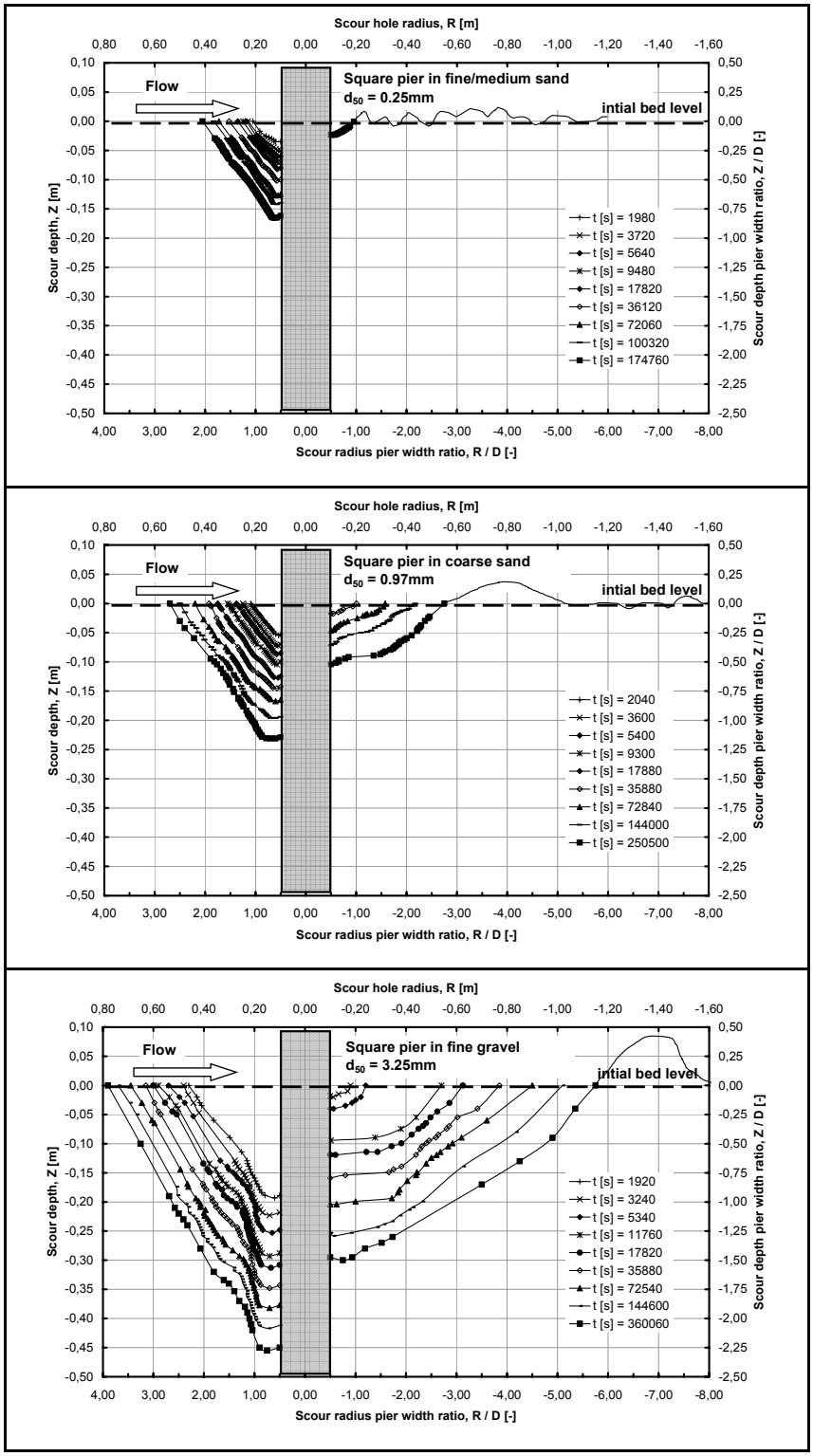

Figure 5.4.3. Scour longitudinal profiles in given times, for square pier in fine/medium sand (upper), coarse sand (middle) and fine gravel (bottom) beds [h/D = 1.50 and u/u_{cr} = 0.95].

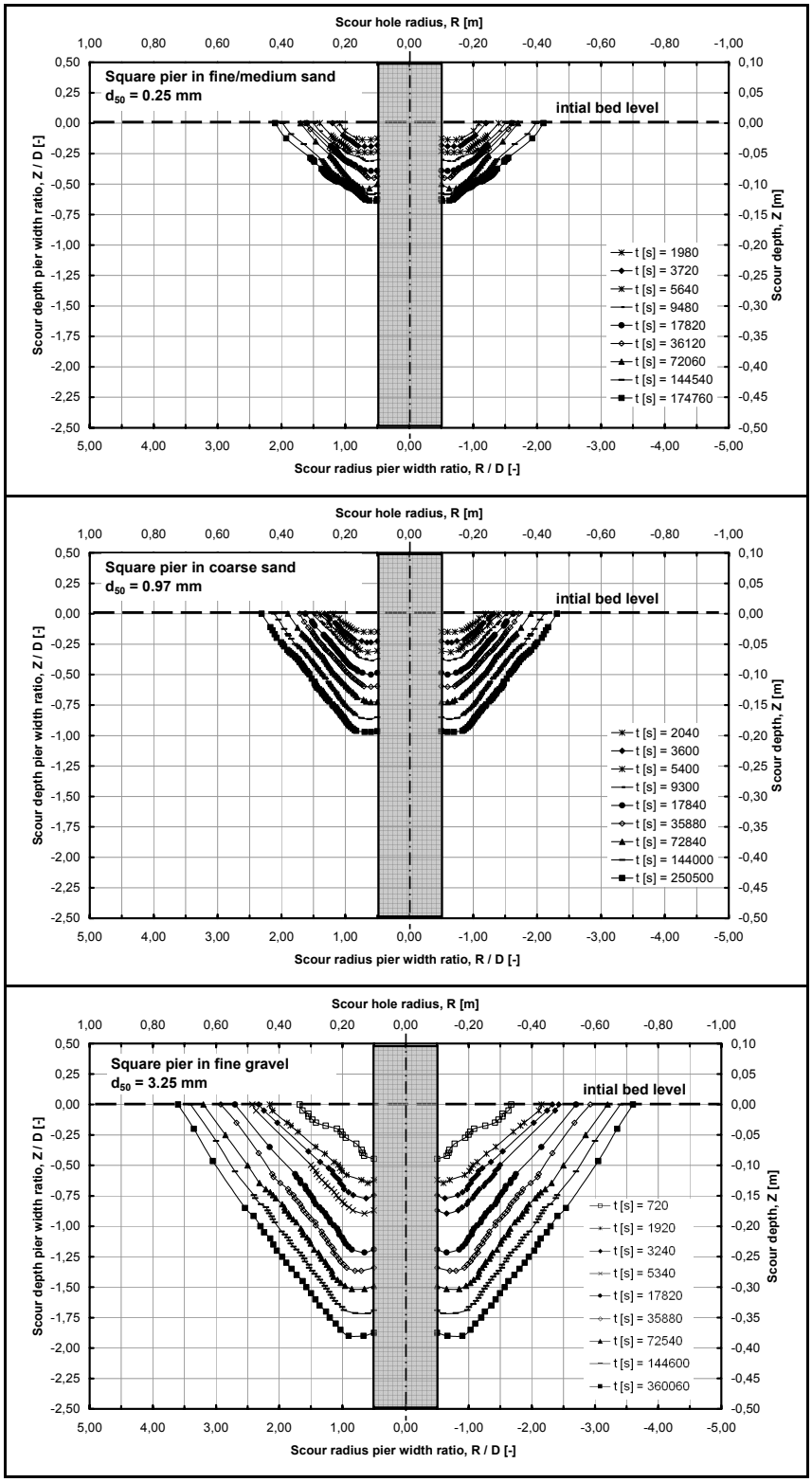

Figure 5.4.4. Scour transverse profiles for given times, for square pier in fine/medium sand (upper), coarse sand (middle) and fine gravel (bottom) beds [h/D = 1.50 and u/u_{cr} = 0.95].

Empirical relation of scour radius

Figure 5.4.5 relates between non-dimensional developing scour depth and radius at azimuthal half-plane with θ = 0º, for different pier shapes and attack angles in gravel (right) and for different sediment materials (left). In the figure, R_{max} and Z_{max} are the maximum developing scour radius and depth. All data which obtained after t/T = 0.01 and 0.02 in gravels and sands were employed, excluding the ring shaped portion. As shown, scour radius at the pier front correlated linearly with corresponding scour depth. All data are well fitted following equation 5.3:

$$\frac{Z}{Z_{\max}} = A \left(\frac{R}{R_{\max}} \right) + B \qquad [5.3]$$

Where: constants A and B are -1.288 and 1.312 for circular and square piers with different angles of attack in gravel bed, and -1.318 and 1.381 for square pier in sand and gravel beds, respectively. Determination coefficients R^2 were 0.98-0.93.

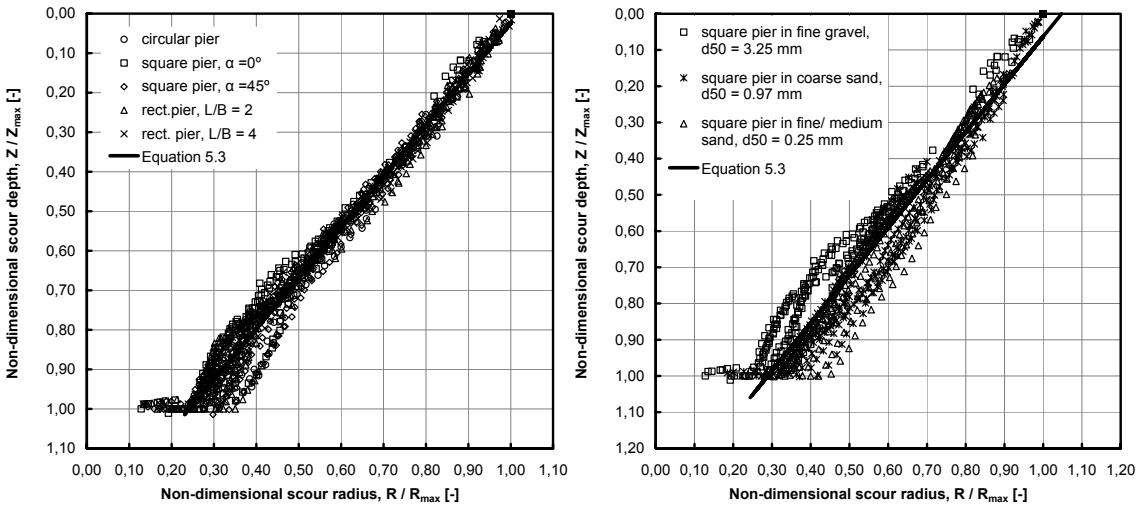

Figure 5.4.5. Non-dimensional scour radius versus non-dimensional scour depth.

5.5 PREDICTION OF EQUILIBRIUM SCOUR DEPTH

New data in the present study are presented and used to show the effect of pier shape and alignment on the equilibrium scour depth. Results are obtained from laboratory experiments which are performed under clear water conditions near the critical velocity, with constant approach flow depth-pier width ratio of 1.50, and constant flow intensity of 0.95.

Effect of experimentation time

The pre-estimated time length of experimentation (e.g. 1, 10, 20 hours, etc) has significant implications on measuring and predicting equilibrium scour depth. Wrong conclusions may reach if an experiment is stopped short of an equilibrium state. Thus, varies definitions of the time to equilibrium have been given in the literature. Table 5.1 shows the effect of definition of equilibrium time on the values of equilibrium scour depths, depending on present laboratory data for circular and square piers in gravel bed. As shown in the table, different experimentation time leads to different equilibrium scour depth vary considerably, depending on what time to equilibrium definition is used. It is also shown that all of the known and listed definitions for equilibrium time are indicating that the equilibrium state is achieved in the current study.

Table 5.1. Effect of definition of time to equilibrium on the prediction of equilibrium scour depth.

Source	Definition of equilibrium time	Z_{eq} [cm] Circular pier	Z_{eq} [cm] Square pier
Ettema (1980)	The time at which the change of scour hole is no more than 1 mm in a timeframe of 4 hours	29.80	41.20
Raudkivi (1986)	After laboratory test duration of 50 hours	31.60	42.20
Melville and Chiew (1999)	The time at which the rate of change of scour depth doesn't exceed 5% of the pier diameter in the succeeding 24 hours period	34.20	45,60
Link (2006)	The time at which the scour rate less than d_{50} per hour	26.80	37.70
Present study	Running time was 100 hrs	34.30	45.80

Figure 5.5.1 relates between relative maximum scour depth $Z_{max,t}/Z_{max,\ 100hrs}$ and time for circular and square piers in gravel, where $Z_{max,t}$ and $Z_{max,\ 100hrs}$ are the maximum scour

depths that obtained after experimentation time t and 100 hours, respectively. As shown, the obtained maximum scour depth after 1 and 10 hours were only about 50 and 75% of $Z_{max,\ 100hrs}$. While the change of scour depth which measured after 75 and 100 hours was only 3%. Depending on this discussions, the pre-determined time of experimentation (e.g.100 hours) was considered in the current study as the reference time. The obtained maximum scour depth at the end of experiments was also taken as the equilibrium scour depth. Nevertheless, the laboratory data showed that a truly equilibrium state is not readily attainable.

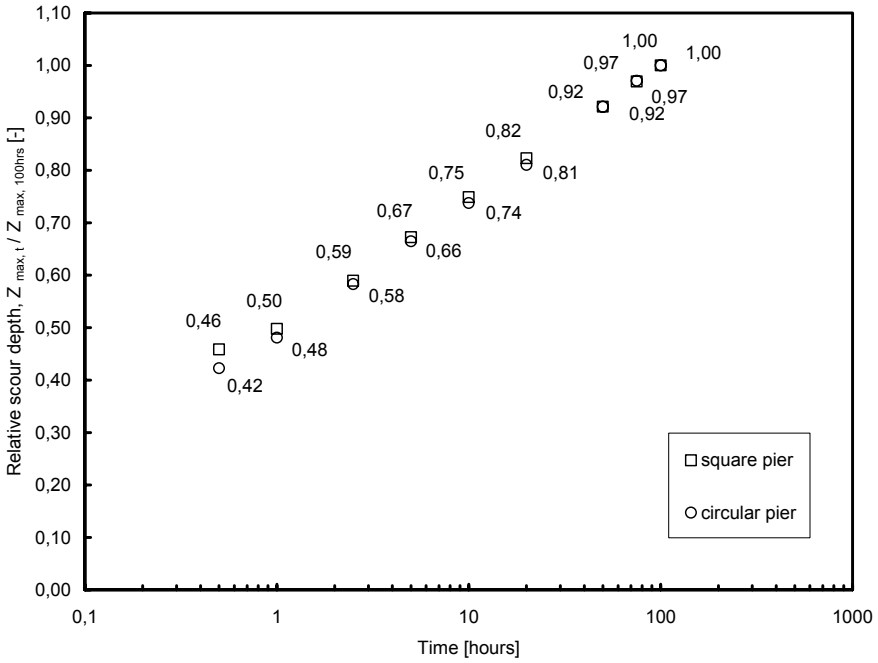

Figure 5.5.1. Effect of experimentation time on prediction of equilibrium scour depth

Effects of pier shape

The effect of pier shape on equilibrium scour depth have been studied by few researchers, such as Tison (1940), Laursen and Toch (1956) and Breusers et al. (1977), coming up with correction shape factors with different values. The usage of these different values results in different pre-predicted scour depth at the same pier shape. Moreover, the same value of shape factor is used to predict scour depth at square and rectangular piers. The data of present study show the effect of pier shape, and differentiate between the square and rectangular piers.

Figure 5.5.2 shows the measured equilibrium scour depth relative to pier width Z_{eq}/D on corresponding measured shape factor k_{sh} (left), and versus pier length-width ratio L/B

(right) , for circular, square and rectangular pier in uniform gravel bed. All piers have the same width D = B = 20cm. The maximum and minimum equilibrium scour depths which are observed at the square and circular piers were about Z_{eq}/D = 2.29 and 1.72, respectively. For rectangular piers, measured scour depths were between those observed at square and circular piers, and equal to 2.10 and 2.08 for L/B = 2 and 4 respectively. The figure gives also new factors to account for square and rectangular piers.

The present data and those from Ettema et al. (1998) are used to show the effect of pier length on the scour depth. Although the used sediment in both studies are different (uniform gravel with d_{50} = 3.25mm in the current study and uniform sand with d_{50} = 0.90mm in Ettema et al. 1998), close agreement between the results is evident. The maximum equilibrium scour depth is attained at the square pier. Although an increased of L/B from 1 (square pier) to 2 results in a decrease of about 9% in the scour depth, changing the pier length-width ratio L/B between 2 and 8 has no significant affect on the equilibrium scour depth. For rectangular pier with L/B = 4, a negligible difference of 1% was found.

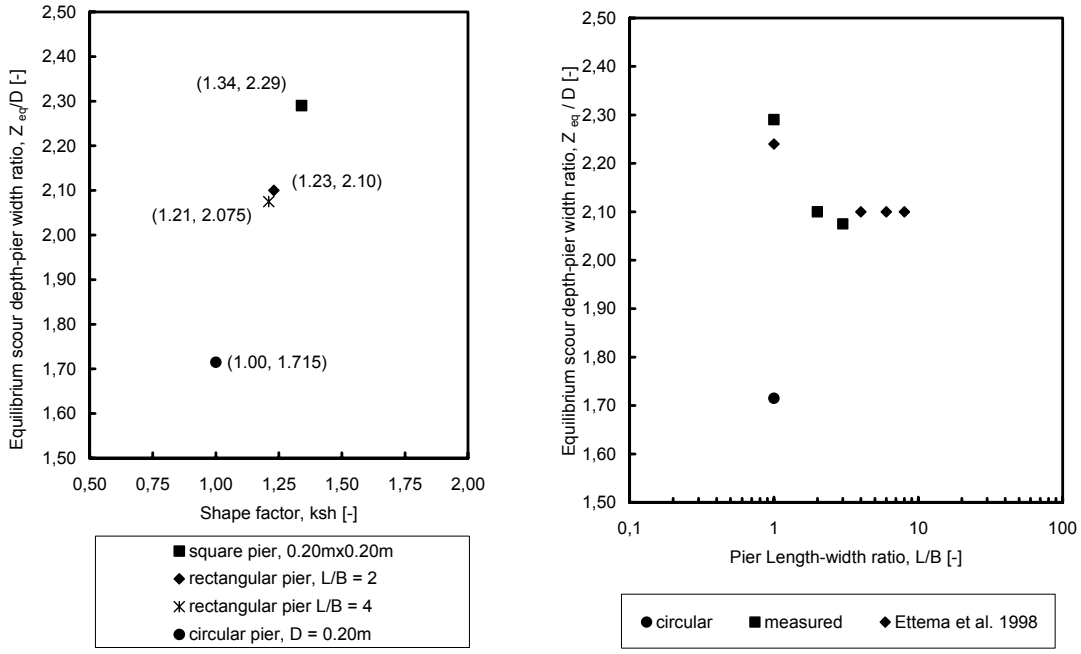

Figure 5.5.2. Equilibrium scour depth versus corresponding shape factor (left) and pier length-width ratio (right), for different pier shapes in gravel bed

Effect of pier alignment

Both the location and the magnitude of equilibrium scour depth are affected by the angle of flow attack. Figure 5.5.3 shows azimuthal half-plane where equilibrium scour depth

was observed on angle of attack. Remarkably, the equilibrium scour depth in the scour hole at the reference time was always located at azimuthal half-plane with θ = α, i.e. on the main flow direction.

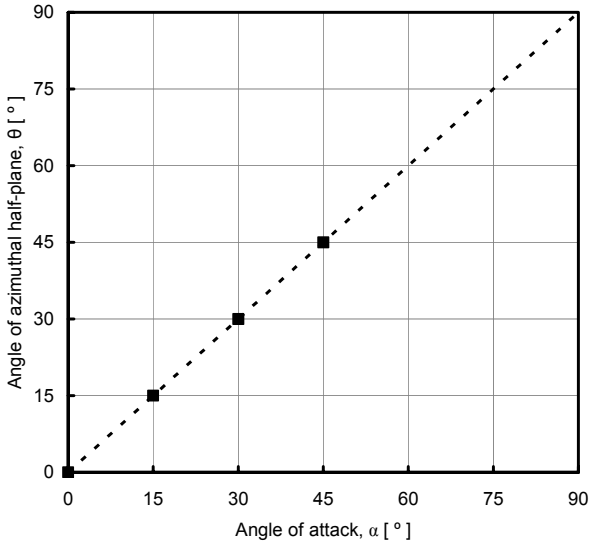

Figure 5.5.3. Effect of pier alignment on the location of equilibrium scour depth.

In figure 5.5.4, the measured and computed [with eqn. 2.4] correction factors versus the angle of attack are presented. In all cases, pier length-width ratio was L/B = 1. Even when pier length in skewed piers increases the effective width (perpendicular to the main flow direction) which is expected to cause a direct increase in scour depth (according to Laursen and Toch 's data for L/B =2 - 16), in case of square piers the angle of attack cause a resulting smaller equilibrium scour depth. Noting that for angles of attack α = 15, 30 and 45º, pier width increased 22.4, 36.6 and 41.4%, but measured scour depth decreases about 7, 9 and 12% with respect to the aligned case with α = 0º, respectively. Thus, It is expected that a rectangular pier with a certain combination of $2 > L/B > 1$ and $\alpha \neq 0$ will present an identical maximum scour depth as a square pier with $L/B = 1$ and $\alpha = 0$. Equation 2.4 is developed and valid also for rectangular piers with L/B = 2 - 16, that explains the wide differences between the measure and computed values.
The suggested angle of attack factors is agreed with the trend of Lausen and Toch's curves, in both $Z_{eq}(\alpha = 90^o)/Z_{eq}(\alpha = 0^o) < L/B$, as also noted by Ettema et al. (1998). Thus, the current results are useful for extension of Laursen's and Toch's curve fot angle of attack.

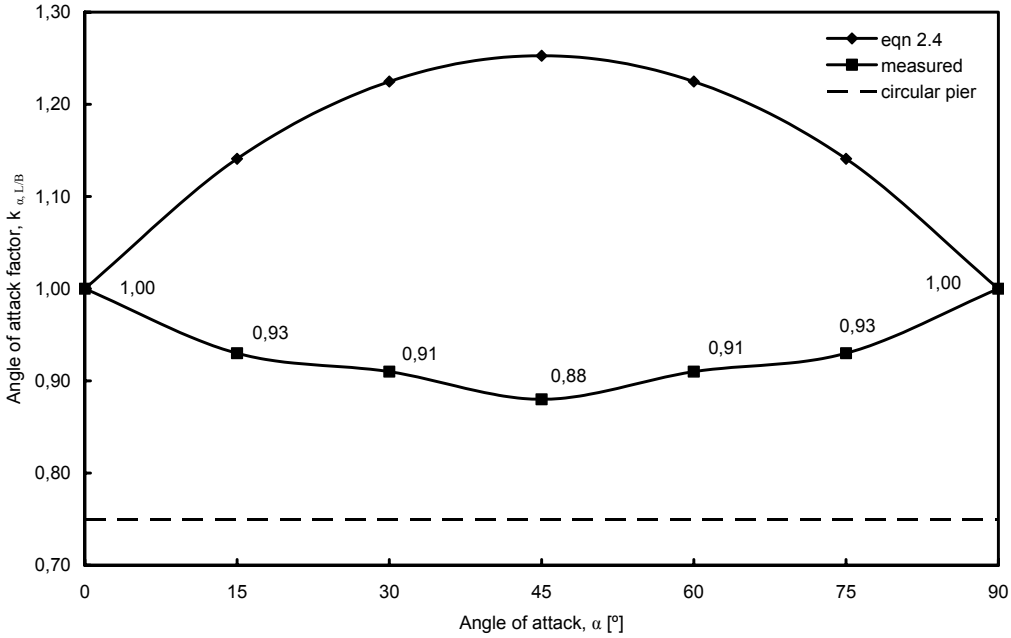

Figure 5.5.4 Measured and computed correction factor on angle of attack
[square pier, L/B = 1, d_{50} = 3.25mm, h / D =1.5, u/u_{cr} = 0.95]

Effect of sediment size

Figure 5.5.5 shows equilibrium scour depth-pier width ratio Z_{eq}/D as a function of sediment coarseness ratio D/d_{50}, for circular and square piers founded in three uniform cohesionless sediment sizes with d_{50} = 0.25, 0.97 and 3.25mm. The data from present study and from Raikar and Dey (2005b) are employed. As shown, equilibrium scour depth firstly increases with increase in sediment coarseness ratio until D/d_{50} ~ 30, then decreases significantly again with increase D/d_{50}. For very large values of D/d_{50}, equilibrium scour depth seems to be independent of D/d_{50}.

The current results are useful to improve current relations for sediment size effect, whose consider no effect of sediment size on scour depth when D/d_{50} > 25 or 50 (Raikar and Dey 2005a, Ettema 1980, Chiew 1984). This limit of sediment coarseness ratio was suggested depending on experimental results that were conducted for short time, comparing with the present study. For example, Chiew (1984) conducted experiment for 4-20 hours, that being not enough to reach the equilibrium and to discover the difference between scour depths for different sediment sizes. A second reason may the tested values of D/d_{50}, that were limited to small values. In Raikar and Dey (2005a) and (2005b), all

used values of D/d_{50} was less than 30. In Chiew (1984), testing some large values of D/d_{50} show a decrease in the scour depth when D/d_{50} increased from 50 to 187.5 (maximum used D/d_{50}) for clear water scour conditions.

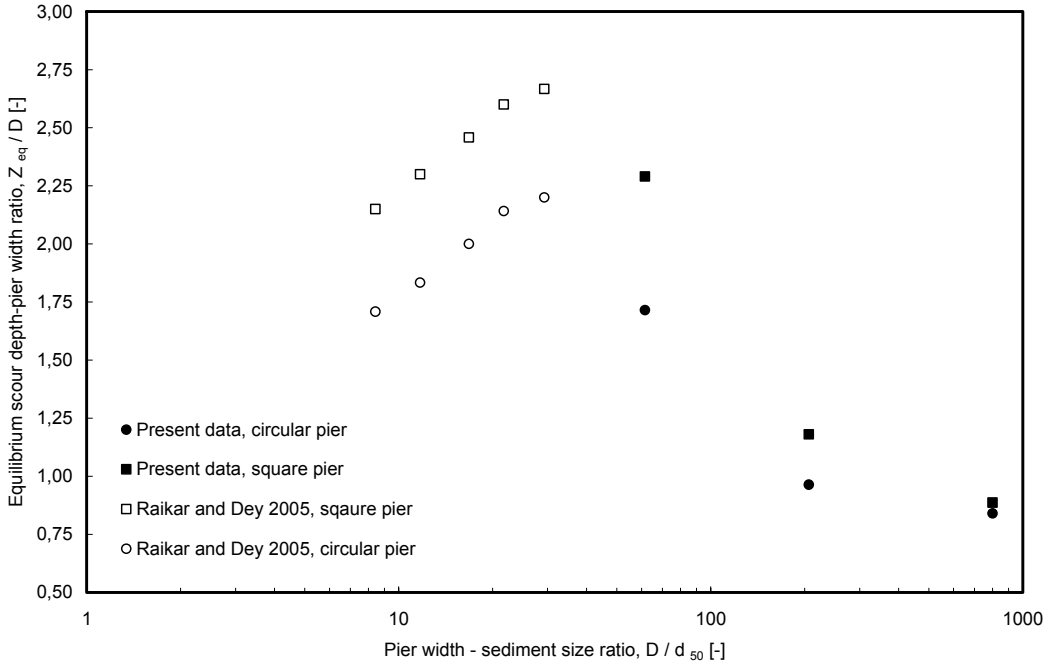

Figure 5.5.5 Effect of relative sediment size on equilibrium scour depth
[circular and square piers, u/u_{cr} = 0.95, h/D = 1.50 - 2.00]

A regression analysis was applied to the own data and those of Raikar and Dey (2005b), resulting in two relations between D/d_{50} and Z_{eq}/D as follows:

$$\frac{Z_{eq}}{D} = 0.416\ln\left(\frac{D}{d_{50}}\right) + 0.903 \quad , \frac{D}{d_{50}} \le 30$$

$$\frac{Z_{eq}}{D} = \frac{1.80}{\left(0.018\,D/d_{50} - 0.16\right)^2} + 0.85 \quad , \frac{D}{d_{50}} > 30 \qquad [5.6]$$

Figure 5.5.6 shows the correlation data of measured data and equation 5.6. As shown in the figure, Z_{eq}/D correlated well to D/d_{50} following a logarithmic and a potential relationships with determinations coefficients equal to R^2 = 0.986 and 0.954 respectively. Correction shape factor of the square pier of k_{sh} =1.33 was used.

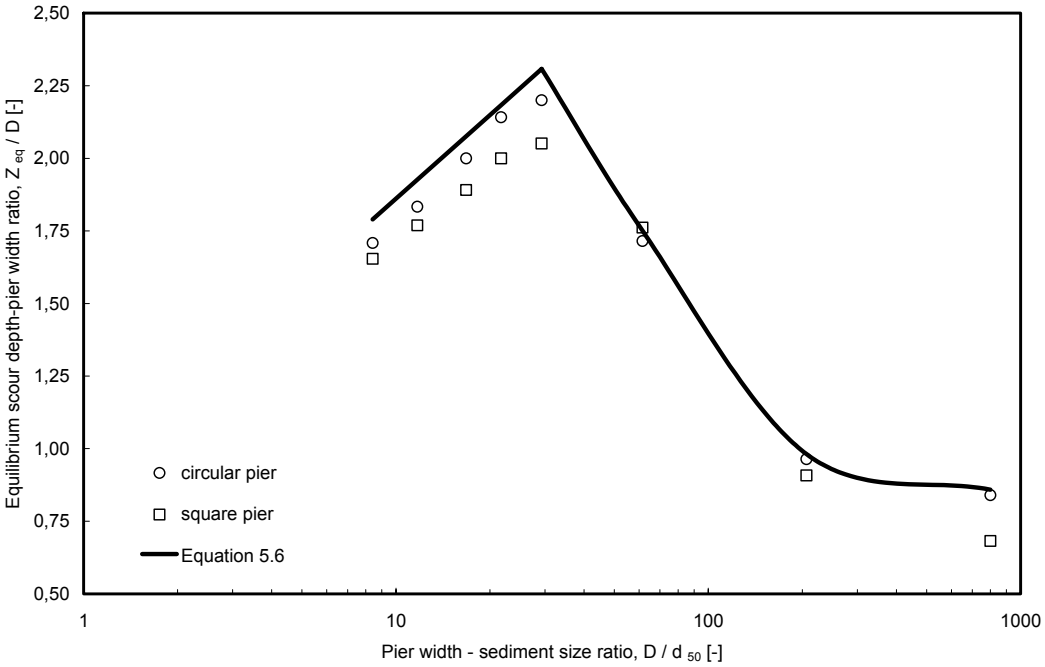

Figure 5.5.6 Correlation of laboratory data and equation 5.6

Evaluation of Equilibrium scour formulas

In an effort to analyse the data of present study further, several of the common prediction equations [table 2.5] were used to calculate the equilibrium scour depth to evaluate their usefulness. This evaluation focused on the ability of the equations to predict the equilibrium scour depth based on the experiments conditions used in the current study. All laboratory data for different pier shapes and alignment and for three different sediment sizes are used in the evaluation.

Figure 5.5.7 compares between computed equilibrium scour depth from the prediction equations and those observed in this study. In the figure, original k's refer to correction factors suggested by the authors of the equations, while new k's are those obtained in the present study. The plots show considerable poorer predictivity of the equations when the original correction shape and alignment factors were used. Some equations (Neil 1964, Breusers 1977, Melville 1997) give constant values for all tested cases, and the others (Richardson et al. 1975, Zanke 1982, Hoffmans and Verheij 1997) show trends away from the line of equality, indicating that they do not properly represent the local scour process that occur in the tested cases. The figures show also that the ability of the equations to accurately predict the scour depth are extensively improve by using the new correction factors which given in this study. A careful consideration on the figures results in the following:

- Some equations don't include corrections factor for pier shape and alignment, or they include corrections for only a few pier shapes.
- Almost all equations don't distinguish between scour at square and rectangular piers.
- There is no equation that takes in consideration the effect of angle of attack on scour at the square pier.
- Equations of Neil's (1964) and Breusers et al. (1977) show the best agreement with the measurements after the effect of angle of attack of attack of square pier (new $k_{\alpha,L/B}$) is considered, and different shape factor for square and rectangular piers are employed.
- In Zanke (1982), a well agreement between the computed and measured values is observed, when new values of ω are computed (equation 5.2) and used, depending on the measurements as recommended by the author.
- Using of Melville's (1997) original equation gives the same scour depths in all cases because the same shape factor (1.00) are used for circular, square and rectangular piers. Further, neither the effect of angle of attack with square piers nor the effect of sediment coarseness ratio when $D/d_{50} > 25$ are consider.
- When the new k's are applied in Melville's (1997) equation, the computed values agreed better the measured with overprediction.
- Although the agreement of measured and computed from Hoffmans and Verheij (1997) scour depths are improved when the new k's used, they still underpredict the measurements.
- With few underpredictions, the predictivity of CSU's equation is improved when the news k's used significantly, especially when different shape factors used for square and rectangular piers, and also in the cases of square with different attack angles.

It can be concluded that the usage of different shape factors for square and rectangular piers results in considerable improvement of the ability of all equations to accurate predict the equilibrium scour depth. Adding a new correction factors for angle of attack also aim to accurate the predicted scour depths in the case of square pier.

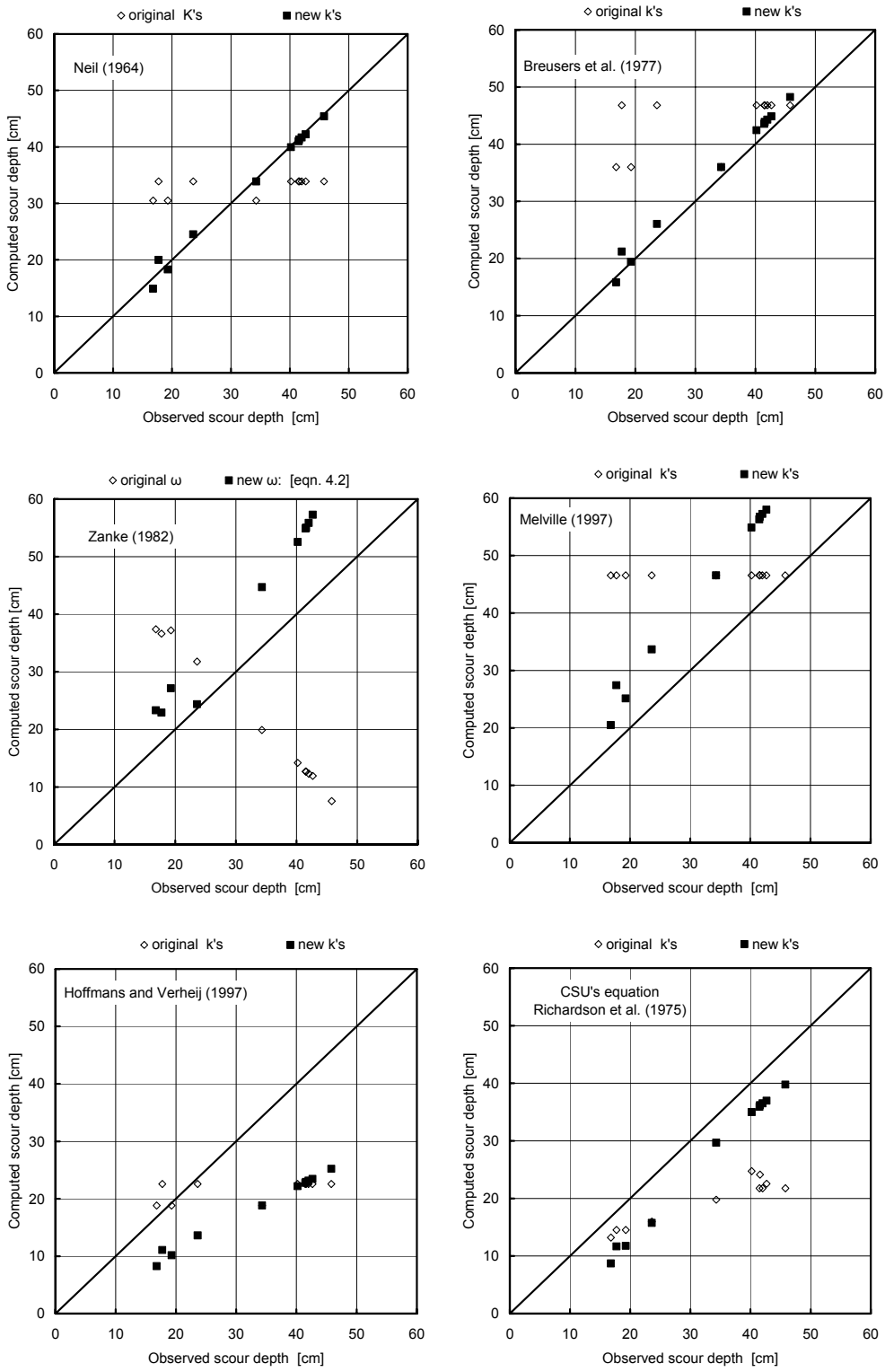

Figure 5.5.7. Computed versus observed equilibrium scour depth, for selected pier scour prediction equations

5.6 PREDICTION OF SCOUR HOLE VOLUME

Volume of developing scour hole is proportional to the sediment size as well as the pier shape and alignment. Figure 5.6.1 presents developing scour hole volume versus time at circular and square piers, as a function of sediment size (left) and angle of attack (right). Volume of developing scour hole in gravel is larger than in sand, and at the square pier is larger than at the circular pier. The highest scoured volume was observed in gravel when the square pier is aligned with the flow, $\alpha = 0^{o}$, and decreased with angle of attack. The maximum scoured volume at square pier with $\alpha = 45^{o}$ was about 70% of that observed at square pier with $\alpha = 0^{o}$ at the end of the experiments. The larger the grain size the larger the scoured volume. At the square pier, developing scour volume in gravel was about 7.25-5.75 times that in sand size range.

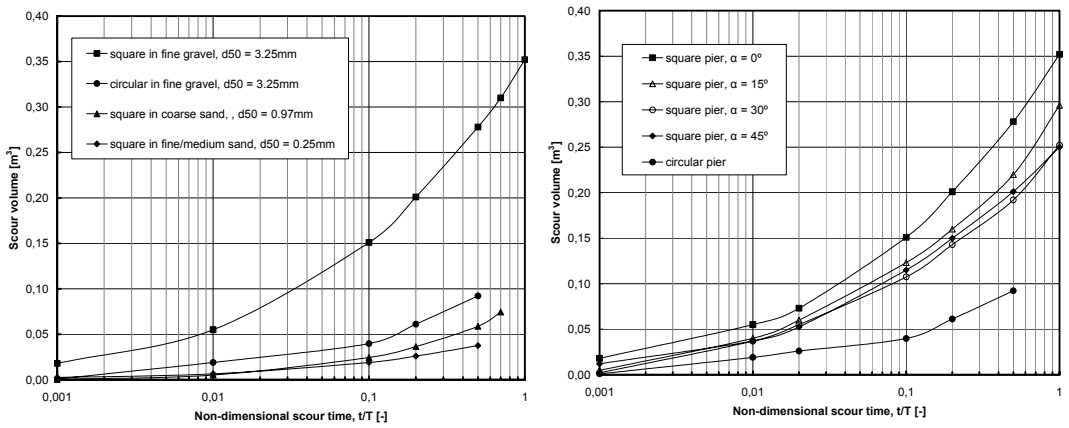

Figure 5.6.1. Developing scour hole volume at circular and square piers, for different sediment sizes (left) and different angles of attack (right).

Figure 5.6.2 shows non-dimensional volume of developing scour holes in gravel over non-dimensional scour time for circular pier and square pier aligned with different angles of flow attack. As shown, 40% of the final maximum scour volume was obtained during only the first 10% of the experimentation time. Scoured volume found to be correlated well with scour time following an exponential relation of the form:

$$\left(\frac{V}{V_{\max}}\right) = x\left(\frac{t}{T}\right)^{y} \qquad [5.7]$$

Where x and y are constants equal to 0.950 and 0.39 respectively. The determination coefficient was $R^2 = 0.923$. V_{max} is defined as the end maximal scour volume, observed at the end of the experiments.

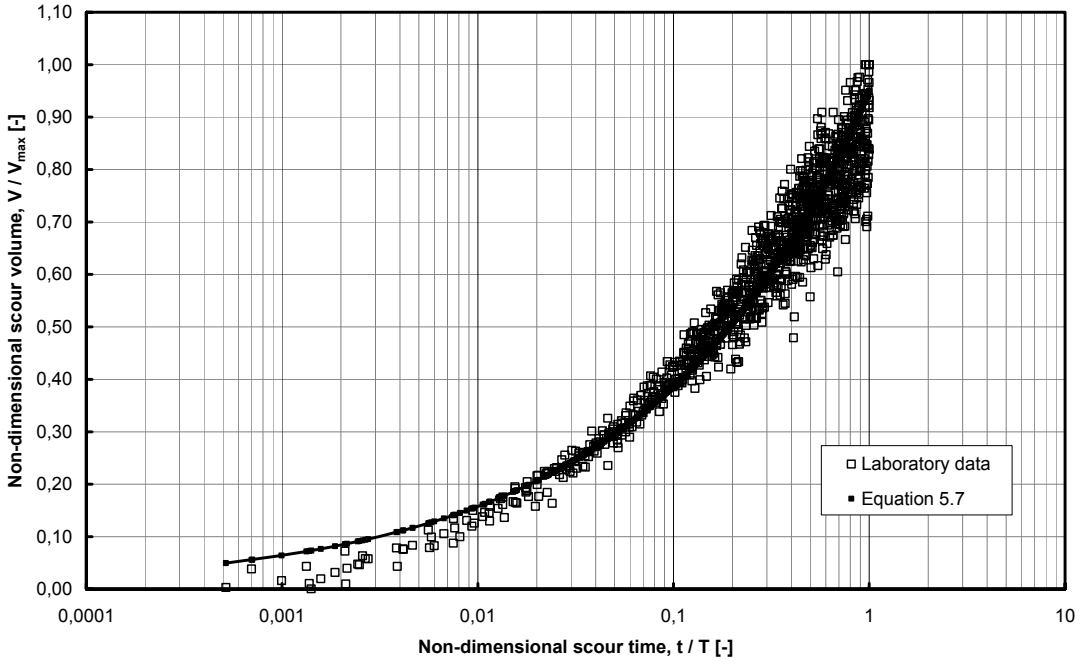

Figure 5.6.2. Non-dimensional scour volume over non-dimensional scour time at circular and square piers in gravel [α = 0, 15, 30, 40º, d_{50}= 3.25mm, h/D=1.50 and u/u_{cr} = 0.95].

Figure 5.6.3 shows non-dimensional volume of developing scour holes in gravel over non-dimensional maximum scour depth in azimuthal half-plane with θ =0º for circular pier and square pier, and for different angles of flow attack. Since scour started at the pier's sides, scoured volume was recorded before maximum scour depth at plane with θ =0º was larger than zero. After scouring reached the pier's front, the general tendency of scoured volume was to correlate with the maximum scour depth following a parabola of the form:

$$\left(\frac{V}{V_{\max}}\right) = 0.340\left(\frac{Z_t}{Z_{\max}}\right)^3 + 0.620\left(\frac{Z_t}{Z_{\max}}\right)^2 - 0.100\left(\frac{Z_t}{Z_{\max}}\right) + 0.012 \qquad [5.8]$$

Where $V_{\max}$ and $Z_{\max}$ are the end maximal scour depth and volume, observed at the end of the experiments. The determination coefficient was $R^2 = 0.938$.

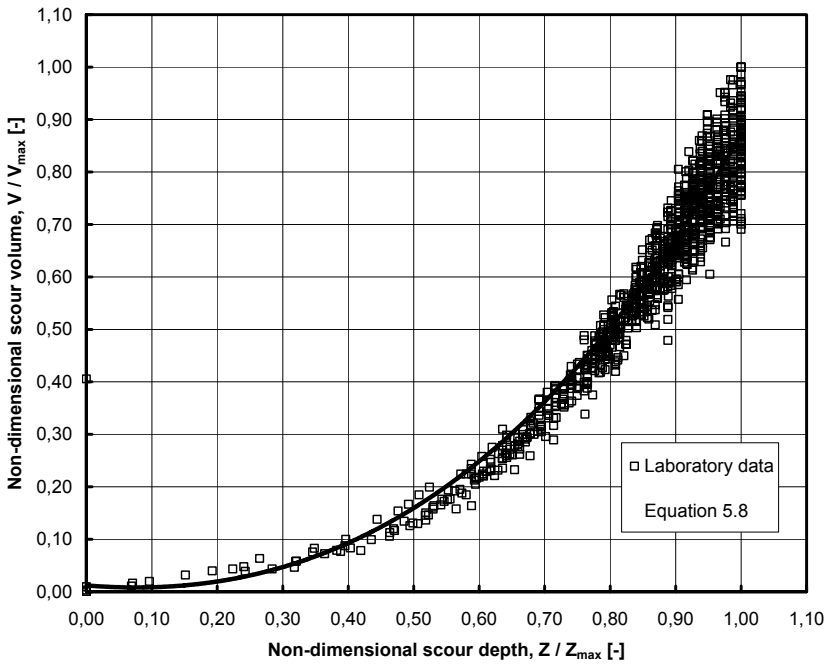

Figure 5.6.3. Non-dimensional volume of developing scour holes on non-dimensional maximum scour depth, for circular and square piers in gravel [α = 0, 15, 30, 45º, d_{50}= 3.25mm, h/D=1.50 and u/u_{cr} = 0.95].

CHAPTER 6
CONCLUSION AND RECOMMENDATIONS

6.1 CONCLUSION

Scour is a natural phenomenon, caused by the erosive action of flowing water over alluvial beds in streams and rivers. It occurs when the critical condition for initiation of sediment transport is exceeded locally, which might happen as a result of natural flow or man-induced flow acceleration due to water works. The leading cause of bridge failure all around the world is bridge scour. This phenomenon has also the major effect on the total construction and maintenance costs. Local scour at piers founded in erodible bed material is a complex three-dimensional phenomenon, as a result of the strong flow-sediment-pier interaction. Notwithstanding the considerable investigations in local scour by many researchers, most studies focused on scour depth at circular pier in alluvial sand beds. An understanding of the mechanism of local scour around piers of different shape and alignment as well as in gravel bed remains far from being complete. However, investigations of the time variations of scour holes geometry not only scour depth, are still in the first stage. This knowledge of geometric features of scour hole provides important information for the design of the bridge foundation size and for the selection of the degree of scour countermeasure.

In this thesis, an extensive experimental investigation of time development of scour hole geometry at piers of different shape and alignment in sediment with different sizes was presented. All experiments were performed under the clear water condition with uniform cohesionless bed materials. The principle objective of the study is the measurement and characterization of spatial (3D) and temporal variation of developing scour holes at piers of different shape and alignment, especially in gravel beds. Subsidiary objectives also included (1) the investigation of turbulent flow field at a square pier in gravel bed and (2) the modification of existent and development of new formulas for the prediction of scour features, such as scour depth, scour radius and scour volume. The evaluation of some of the prediction equations for developing and equilibrium scour depth and the assessment of the occurrence of an equilibrium scour conditions were realized.

A set of long duration scour experiments (about 4 days) were conducted using three uniform cohesionless sediment materials, namely fine gravel, coarse and fine/medium sands. Four shapes of pier, namely circular, square and two rectangular and four angles of attack (α =0, 15, 30 and 45º) were tested.

New non-intrusive, high resolution topography measurement system was developed at the laboratory with an experimental installation using a laser distance sensor (LDS) and

positioning systems. It was used to measure developing scour holes during running experiments from inside the pier. Vertical profiles of scour hole in different azimuthal half-planes around circular and square piers as well as along rectangular piers are taken instantaneously. The analysis and visualization of the measured data were carried out using different software, such as Visual Basic, Active Perl, MATLAB, Excel, Surfer and Tec Plot.

In addition to detect scouring data, point measurements of velocities and turbulence in different elevation from the bed and in different azimuthal half-planes around the square pier were performed with the ADV, allowing the quantitative description of the main flow features in both plane and equilibrium scoured gravel beds.

Spatio-temporal variation of geometric properties of developing scour holes have been analyzed by measuring the scour hole shape, maximum scour depth, scour slopes, and scoured volume. In the following sections the results of the study are concluded:

6.1.1. Developing Scour Hole Shape

The results of current study presented the measured situation of the scour hole shape rather than an inverted scheme. The results showed that the development of scour holes with time varied with pier shape. It is also found that the propagation of scour to the downstream end of the pier is highly dependent on whether or not the pier is aligned with the flow direction. Scour development in gravel is considerably different from the development in sand size ranges.

Further, the following conclusions are obtained from this study:

- Developing scour patterns study showed, that scouring started and progressed fast immediately upon starting the experiments at the sides of the circular pier and at the front corners of the square and rectangular piers. Eventually, scour propagated rather rapidly toward the centerline of the pier's front. In this stage, a mound of the eroded sediment from the scour hole was firstly deposited close to the pier wake, and found to be moving downstream with time. Then the scoured region surrounded the piers. In due time, the deepest point in the scour hole was firstly observed at the pier sides with $\theta = 45^{o}$. When Z/D reached 0.75 - 1.20, it migrated to the centerline of the pier front with $\theta = 0^{o}$ during the first hour in gravel bed, and after 1.30 - 2.30 days running time in sand beds.
- The scour in gravel surrounded the circular, square and rectangular piers when the relative maximum scour depth Z/D reached 0.60, 1.15 and 1.40 respectively. The duration for surrounding the square pier with the scour hole (about one hour) was approximately four times larger that required at the circular pier, increasing significantly to 4-4.60 hours at the rectangular piers with L/B = 2 - 4 respectively.

- In the angle of attack study, the asymmetry of the scour hole in gravel was zero when the square pier aligned with the flow and increased with the angle of attack.
- The larger the angle of attack the shorter the time required to surround the pier with scour, and the longer the time required to moving the deepest point from the far corner of the attack face of the pier to the main flow direction.
- The sediment size tests showed that scouring in gravel bed progresses faster than in sand size ranges. However while scour in gravel surrounded the square pier in one hour only, about seven hours and two days were required in coarse and fine/medium sand beds at the current test series.

6.1.2. Developing Scour Depth

The measurements of time development scour depths in different azimuthal half-planes around piers of different shape and alignment in gravel and sand beds gave the following conclusions:

- The results of long duration scour experiments (about 4 days) showed that, the maximum scour depth developed with different rates during the first 10 - 30% of experimentation time until Z/D reached 1.50 in gravel and 0.50 in sand, faster at the sides than at the front of the piers, faster in gravel than in sand bed, faster at nonaligned than at aligned piers and also faster at square and rectangular than at circular piers. Then, the scour depth developed with nearly the same rate at different piers and in different sediment beds. Thus, wrong conclusions may be drawn if an experiment is canceled at a time shorter than the needed stabilization time.
- The measured maximum scour depths in different azimuthal half-planes showed, that the maximum depth inside the scour hole was firstly observed at the pier sides at the plane with $\theta = 45^{\circ}$, and then moved to the centerline of the piers front. It showed also that the ratio between maximum scour depths at wake and front of the pier ranged between 14 - 66%, increased with the sediment size and decreased with the pier length-width ratio.
- Scouring developed at a decreasing rates in all cases, so that the obtained scour depths during the first 1-3 hours were approximately as deep as in the following about 4 days for different pier shapes.
- For pier shapes study, the highest and lowest scour depths were always observed at the square and circular piers. The observed scour depths at rectangular piers with L/B = 2-4 were smaller than at the square pier. No significant effect of rectangular pier length-width ratio between L/B =2 - 4 was observed.

- The results from the angle of attack study showed, that scour depths at square pier with different angles of attack were higher than at circular pier. Scour rates at nonaligned square pier were higher than at the aligned one during the first 15% of experimental time, resulting in higher scour depth at the nonaligned piers temporally. After stabilization of scour, the developing scour depth at aligned square pier became the largest, decreasing with the angle of attack. That confirms that wrong conclusions will be obtained from experiments with short time length.
- The patterns of developing scour depths (values and location inside scour hole) in gravel were totally different and showed higher scour depths than with the sand size range. Excluding the first 4 hours in experimentation, all measured scour depths developed in fine/medium and coarse sands were about 45-55% times those observed in gravel.
- The time dependent maximum scour depth in sand beds was firstly observed at the pier sides with $\theta = 45^{\circ}$ during the first 1.3-2.3 days of experimentation. Later, it observed at the centerline of pier front at $\theta = 0^{\circ}$. That shows the significant effect of the experiment time length and the location of measuring the depth.
- Depending on all laboratory data from this study and from Link (2006) and Link et al. (2008b), a general empirical relation of the relative maximum developing scour depth was obtained, as follow:

$$\frac{Z_t}{Z_{eq}} = 0.1098\left(\frac{t}{T}\right) + 0.9896 \qquad [6.1]$$

- Furthermore, the laboratory data and obtained relation [6.1] are compared with six well-known prediction equations. A good agreement between the measurements and the suggested equation [6.1] is detected. The pathways of all other equations do not agree with the measurements. A reason for this may be the short time length of the based data experimental work. Franzetti (1982) and Hoffmans and Verheij (1997) overpredict the data during the beginning of experiments and tend to underpredicted the equilibrium scour depth. Melville and Chiew (1999) overpredicted the data with very high values. Barkdoll (2000) and Oliveto and Hager (2002) underpredict the data.
- An adjustment of Zanke's (1982) equation fitted the equation well to the results of the present study. The adjustment were done by calibrating the increased effective velocity parameter ω depending on the experimental data, as follows:

$$\omega = 0.9013\left(\frac{Z_t}{D}\right)^6 - 6.9008\left(\frac{Z_t}{D}\right)^5 + 19.775\left(\frac{Z_t}{D}\right)^4 - 24.671\left(\frac{Z_t}{D}\right)^3 + 10.658\left(\frac{Z_t}{D}\right)^2 + 1.3891\left(\frac{Z_t}{D}\right) + 2.5001 \quad [6.2]$$

6.1.3. Developing Scour Profiles

Measured profiles of developing scour hole in different azimuthal-planes at the piers showed that the shape of scour hole remained nearly constant during scour development. Close to the pier, a ring shaped portion of scour hole was observed. Over the ring, a nearly uniform slope was observed at the pier's front and sides. At the pier wake, a second slope located in the upper part of the scour hole was identified in gravel bed.

The conclusions of developing scour profile study are:

- During experiments, average scour slopes did not exceed the natural repose angle of the sediment particles under water significantly. There was only one exception: a steeper slope was observed in the lower part of the profile in front of the pier in gravel bed.
- An average side-slope of developing scour hole diminishes from upstream to downstream with θ, reaching at the pier wake approximately half of the inclination at the pier front.
- The results of pier shape study showed that steeper scour slopes and higher gradients of the scour hole bottom are observed at the square pier shape. For rectangular piers, the bottom gradient decreases with increasing L/B ratio.
- At the end of pier shape experiments, the longitudinal extent of the scour hole at square and rectangular pier was averagely 50% longer than at circular pier. The width of scour holes at square pier was 22% wider than at circular pier, and found to be increased with the rectangular pier length by 10 and 20% for L/B = 2 and 4, respectively.
- The longitudinal extent and lateral width of scour holes varies significantly with variation of bed material from sand to gravel. At the end of experiments, the longitudinal extent of scour hole in gravel was about 1.75 and 3.25 times those in coarse and fine/medium sands. The width of scour hole in gravel was about 1.55-1.70 times those in coarse and fine/medium sands, respectively.
- Scour slopes break suggest the action of vortex system with different strengths, vortex strength being lower to the upper part of the scour hole. Rotation of vortex towards the slopes contributes to side stabilization, explaining the existence of the lower side slope with a higher inclination than the natural repose angle in front of the piers.

- Developing scour hole radius at the pier front correlates well with developing scour depth following the given linear relation.

$$\frac{Z}{Z_{max}} = A \left(\frac{R}{R_{max}} \right) + B \qquad [6.3]$$

6.1.4. Equilibrium Scour Depth

The present data showed that the pre-estimated time length of experiments affects significantly the obtained equilibrium scour depth. Shape and alignment of a pier affected the magnitude and location of the equilibrium scour depth.

Further, it was found that:

- Discussion of the definition of time to equilibrium from the literature showed that, an equilibrium scour depth determined on some definitions may not be correct as shown via the presented data. Furthermore, it was possible to reach a variety of equilibrium scour depths depending on which definition of time to equilibrium was adopted. Although the definitions showed that the equilibrium scour conditions were achieved in the present work, the laboratory results indicated that a truly equilibrium state was not readily attainable.
- Based on the results of this work and from some results in the literature, it was found that equilibrium scour depth at a square pier shape differs widely from those at a rectangular pier with L/B = 2-8, even though the pier were aligned with the main flow direction. For rectangular piers with L / B = 2-8, the effect of L/B on the equilibrium scour depth was negligible.
- The biggest clear water (equilibrium) scour depth is reached at the square pier shape in gravel over a long duration experiment (4 days), and is approximately equal to 2.30 times the pier width. For rectangular and circular piers in gravel, the maximum equilibrium scour depths were 2.10 and 1.72 times the pier width.
- New correction shape factors for square and rectangular piers were suggested.
- In this study, the effect of pier alignment on magnitude and location of equilibrium scour depth was investigated in detail. The equilibrium scour depth at the square pier was observed always on the main flow direction and identified to decrease with the angle of flow attack. For all attack angles, scour depth at square pier were greater than at circular pier.
- The design angle of attack factors for square pier were obtained in the present study, which were useful to extent Laursen and Toch's design curve which was originally valid for rectangular piers with L/B = 2 -16.

- The analysis of the data for sediment size effect obtained from this study together with data of Raikar and Dey (2005) showed that, the assumption that there is no effect of sediment coarseness ratio D/d_{50} on the scour depth when the ratio exceeds 25-50 is not sound. The investigation showed that the relative equilibrium scour depth Z_{eq}/D which firstly increased with the sediment coarseness ratio D/d_{50}, decreased again when D/d_{50} exceed 30, and seemed to be unaffected at very high values of D/d_{50} (may for $D/d_{50} > 500$).
- Two continuous best-fit prediction equations for relative equilibrium scour depth as a function of D/d_{50} were developed from this study as follows:

$$\frac{Z_{eq}}{D} = 0.416\ln\left(\frac{D}{d_{50}}\right) + 0.903 \quad , \frac{D}{d_{50}} \le 30$$
$$\frac{Z_{eq}}{D} = \frac{1.80}{\left(0.018\,D/d_{50} - 0.16\right)^2 + 1.10} + 0.85 \quad , \frac{D}{d_{50}} > 30 \qquad [6.4]$$

- A comparison between several well-known prediction equations showed that these equations give away trends and a wide range of values comparing with the experiment data when the original shape and angle of attack factors were used. That is because all of the equations don't differentiate between scour at square and rectangular piers and do not consider the effect of the angle of attack for a square pier. Thus, the overall agreement of all equations with the measurements is clearly improved when the new shape and angle of attack factors from the present study employed.
- When the new shape and angle of attack factors are used, Neil's (1964) and Breusers et al.'s (1977) equations showed the best fit to the experimental data. Zanke (1982) and Melville (1997) overestimated the measurement with accepted values. In comparison, CSU's and Hoffmans and Verheij's (1975) underestimated the values.

6.1.5. Scour Hole Volume

The present data allowed the evaluation of volume of developing scour holes at circular and square piers, which embedded in three different uniform cohesionless sediment materials. Also, the effect of flow angle of attack is considered.
The results showed the following:

- The volume of scour hole developed at a decreasing rate with time in all cases, so that the obtained scoured volume during the first experimental day (less than 20%

of experiments time) was approximately the same as the obtained volume until the end of experiments (three more days).

- During the experiments, the maximum volume of developing scour hole was always obtained in the case of square pier aligned with the flow and embedded in fine uniform gravel bed.
- The developing scour hole volume at the square pier with different angles of attack was higher than with the circular pier.
- The larger the angle of attack the smaller the scoured volume during experiments. The maximum scoured volume at square pier aligned with $\alpha = 45^{o}$ was about 70% of that at square pier with $\alpha = 0^{o}$ at the end of the experiment.
- The larger the sediment size the larger the scoured volume during the experimentation time. The obtained maximum scour volume in gravel was about 6 - 7 times larger that in sand size range.
- From these experiments, an empirical relations was developed that relates non-dimensional volume of developing scour hole in gravel beds with non-dimensional scour time for circular and square piers and for different angles of attack. This relation is as follows:

$$\left(\frac{V}{V_{\max}}\right) = x\left(\frac{t}{T}\right)^{y} \qquad [6.5]$$

- The volume of developing scour hole in gravel bed correlated well with the maximum developing scour depth at the pier's front with $\theta = 0^{o}$. Thus, when providing maximum scour depth at the pier's front, the following relation can be used to calculate scour hole volume:

$$\left(\frac{V}{V_{\max}}\right) = 0.340\left(\frac{Z_t}{Z_{\max}}\right)^{3} + 0.620\left(\frac{Z_t}{Z_{\max}}\right)^{2} - 0.100\left(\frac{Z_t}{Z_{\max}}\right) + 0.012 \qquad [6.6]$$

6.1.6. Turbulent Flow Field

The results of the turbulent flow field study showed the spatial distribution of time-averaged velocity components, flow vectors and time-absolute velocity, as well as turbulence intensities components and turbulent kinetic energy.

The conclusions of flow field study are:

- The results showed that the time-average tangential velocity component u increased firstly with increasing θ to a maximum value at $\theta = 90^{o}$, then diminished again with an increase of θ. The large the distance to the bed and the smaller the

distance to the pier, the higher is the value of time-average tangential velocity component.

- The contours of the time-average radial velocity component v showed, that it decreases with decreasing the radial distance and with increasing θ. It also showed the reversal flow due to the flow separations inside the scour hole. The maximum reversal flow was observed at θ = 45º, confirming the existence of a strong horseshoe vortex in front of the pier inside the scour hole.
- The time-average vertical velocity component w was downward in the flow zone and upward near the bed in front of the pier. The downward flow found to be increasing and the upward flow found to be decreasing with decreasing θ and the radial distance from the pier.
- The distribution of the time-average vertical velocity vector $\sqrt{v^2 + w^2}$ showed the characteristics of the horseshoe vortex and the strong downflow inside the scour hole at the pier front and sides. The strong horseshoe vortex was observed at the pier front and found to be decreased with θ. At the pier wake, a swirl motion close to the pier pack was observed, and then the flow became gradually outwards the pier.
- The distribution of the turbulence intensities around the pier was found to be identical. Their magnitudes decreased with the vertical distance from the bed at the pier front and sides. While at the pier wake, the turbulence intensities first increased with the vertical distance to an imaginary line in the middle of the scour hole, then decreased again vertically forming a core of high turbulence over whole of the scour hole.
- The distribution of the turbulent kinetic energy *TKE* was similar to that of the turbulent intensity components. *TKE* values increased with increasing θ and decreasing vertical and radial distances. The effect of turbulence lead to intensive scouring in front of the pier than at the pier wake where upward flow occurred.

6.2 RECOMMENDATIONS

Recommendations regarding possible future work in relation to the present study are as follows:

- The present study represents a preliminary investigation of the variation of scour hole geometry with time as a function of the pier shape, angle of attack and sediment size. Additional systematic studies of the effects of wide range of scour parameters are required to develop a design approach for the scour hole dimensions at bridge piers.

- This research has identified significant effects of pier shape and alignment on the geometric characteristics of a scour hole. Only circular, square and rectangular pier shapes and four angles of attack were tested. Further experiments are required to assess the effect of more particular pier shapes alignment or skewed to the flow, developing new pier shape and alignment adjustment factors.
- The pronounced difference of the time development of scour hole in gravel and sand beds is remarkable via this thesis. Further studies of the effects of different gravel sizes and gradations on the local scour process are needed.
- The turbulent flow field study has given a good idea about the mechanism of local scour at a square pier in gravel bed. Additional measurements of the flow velocities and turbulence around piers of different shape are required to better understand the scour process. These studies are important for the verification of the numerical models which are used to simulate the pier scour
- The current experiments have been explained the scour process and flow field under the effect of unique current action. There are still further researches required to investigate how do the scour hole varies under tidal flow action. A physical hydraulic flow model is needed to study the tidal scour.

REFERENCES

Ali, K., and Karim, O. 2002. Simulation of flow around piers. Journal of Hydraulic Research, IAHR, 40(2): 161-174.

Ataie-Ashtiani, B., and Beheshti, A. 2006. Experimental investigation of clear-water local scour at pile groups. J. Hydr. Engrg., ASCE, 132(10): 1100-1104.

Barbhuiya, A. K., and Dey, S. 2004. Local scour at abutments. Sadhana, Proc. Indian Acad. Sci., 29 (5): 449-476.

Barkdoll, B.B. 2000. Discussion of time scale for local scour at bridge piers by Melville and Chiew. Journal of Hydraulic Engineering, ASCE, 126(10): 793-794.

Birgani, Y.T., Shooshtari, M.M, Adib, A., and Mosavi, A.A. 2010. A new equation for predicting the scour depth around bridge piers. World Applied Science Journal, 9 (2): 151-156.

Breusers, H., Nicollet, G., and Shen, H. 1977. Local scour around cylindrical piers. Journal of Hydraulic Research, IAHR, 15 (3): 211-252.

Breusers, H.N.C., and Raudkivi, A.J. 1991. Scouring. A.A. Balkema, Rotterdam/Brookfield, Netherlands, ISBN 90 6191 983 5.

Butch, G. K. 1996. Scour hole dimensions at selected bridge piers in New York. The North American Water and Environment Congress, ASCE.

Chabert, J., and Engeldinger, P. 1956. Etude des affouillements autour des piles des ponts, (scour around bridge piers). Laboratoire National d'Hydraulique, Chatou, France (in french).

Chiew, Y.M. 1984. Local scour at bridge piers. PhD Thesis. University of Auckland, Auckland, New Zealand.

Dargahi, B. 1987. Flow field and local scouring around a cylinder. Bulletin Nr. TRITA-VBI-137, the Royal Institute of Technology, Stockholm, Sweden.

Dargahi, B. 1989. The turbulent flow around a circular cylinder. Experiments in Fluids. Springer-Verlag, Nr. 8: 1-12.

Dargahi, B. 1990. Controlling mechanism of local scouring. Journal of Hydraulic Engineering, ASCE, 116 (10): 1197-1214.

Dey, S. 1995. Three-dimensional vortex flow field around a circular cylinder in a quasi-equilibrium scour hole. Sadhana, Proc. Indian Acad. Sci., 20 : 771-785.

Dey, S., Bose, S. K., and Sastry, G. L. N. 1995. Clear water scour at circular piers: a model. Journal of Hydraulic Engineering, ASCE, 121 (12): 869–876.

Dey, S. 1997. Local scour at piers, part1: A review of development of research. International Journal of Sediment Research, IJSR, 12(2): 23-46.

References

Dey, S. 1999. Time-variation of scour in the vicinity of circular piers. Proc. Instn. Civ. Engrs., Water & Maritime Engineering, 136 (2): 67-75.

Dey, S., and Barbhuiya, A.K. 2004. Clear-water scour at abutments in thinly armoured beds. Journal of Hydraulic Research, IAHR, 130 (7): 622-634.

Dey, S., and Raikar, R. 2007. Characteristics of Horseshoe Vortex in Developing Scour Holes. Journal of Hydraulic Engineering, ASCE, 133(4): 399-413.

Diab, R., Link, O., and Zanke, U. 2008a. Measurement of developing scour holes in gravel. Proceedings of the Chinese-German Joint Symposium on Hydraulic and Ocean Engineering CGJoint08, Darmstadt, Germany, 24-30 August, Darmstadt University of Technology: 149 – 153.

Diab, R., Link, O., and Zanke, U. 2008b. Measurement of scour hole geometry at a square pier in a gravel bed. Proceedings of the 2nd International Junior Researcher and Engineer Workshop on Hydraulic Structures 2nd IJREWHS'08, Pisa, Italy, 30 July -1st August, University of Pisa: 33-38.

Diab, R., Link, O., and Zanke, U. 2008c. Measuring developing scour holes in gravel. Proceedings of the Fourth International Conference for Scour and erosion ICSE-4, Tokyo, Japan, 5-7 November, Chuo University: 486-490.

Diab, R., Link, O., and Zanke, U. 2009. Experimental investigation of 3D flow field around square pier. Proceedings of the 33rd IAHR Congress, Vancouver, Canada, 9-14 August, University of British Columbia: 5460-5466.

Diab, R., Link, O., and Zanke, U. 2010a. Geometry of developing and equilibrium scour holes at bridge piers in gravel. Can. J. Civ. Eng., NRC, 37 (4): 544-552.

Diab, R., Link, O. and Zanke, U. 2010b. 3D turbulent flow field at square pier in a gravel scour hole. Proceedings of the River Flow 2010 Conference, Braunschweig, Germany, 8-10 September, TU Braunschweig: 691-697.

Diab, R., Link, O., and Zanke, U. 2010c. Time variation of scour hole at square pier in sand bed. Proceedings of the Chinese-German Joint Symposium on Hydraulic and Ocean Engineering CG Joint10, Tianjin, China, 21-28 September, Tianjin University: 361-366.

Dietz, J.W. 1972. Ausbildung von Langen Pfeilern bei Schräganströmung am Beispiel der BAB-Mainbrücke Eddersheim, (Construction of long piers at oblique currents illustrated by the BAB-Main Bridge Eddersheim, systematic model tests on scour formation of piers). Mitteilungsblatt der BAW, 31 : 79-94, Karlsruhe, Germany.

Dumas, C., and Krolack, J. 2002. A geotechnical perspective: design and construction of highway bridge foundations for scour. Proceedings of the First International Conference on Scour of Foundations, Texas A&M University, College Station, USA : 112-119.

References

Ettema, R. 1980. Scour at bridge piers. PhD Thesis. University of Auckland, Auckland, New Zealand.

Ettema, R., Mostafa, E., Melville, B., and Yassin, A. 1998. Local scour at skewed piers. Journal of Hydraulic Engineering, ASCE, 124 (7): 756-459.

Ettema, R., Gokhan, K., and Muste, M. 2006. Similitude of large-scale turbulence in experiments on local scour at cylinders. J. Hydr. Engrg., ASCE, 132 (1): 33-40

Florida Department of Transportation 2005 .Bridge Scour Manual, BSM 2005. State of Florida, USA.

Franzetti, S., Larcan, E., and Mignosa, P. 1981. Erosione localizzata alla base delle pile dei ponti: considerazioni su risultati di un'indagine sperimentale su modello, (Local scour at cylindercal piers: considerations on a laboratori model results). Memorie e Studi dell'Istituto di Idraulica e Costruzioni idrauliche del Politecnico di Milano, 296 (in Italian).

Franzetti, S., Larcan, E., and Mignosa, P. 1982. Influence of tests duration on the evaluation of ultimate scour around circular piers. International Conference on the Hydraulic Modelling of Civil Engineering Structures, organized by BHRA Fluid Engineering, University of Warwick, Coventry, England: 22-24.

Gobert, C., Link, O., Manhart, M., and Zanke, U. 2010. Discussion of Coherent Structures in the Flow Field around a Circular Cylinder with Scour Hole by G. Kirkil, S. Constaninescu and R. Ettema. J. of Hydr. Engrg., ASCE, 136 (1): 82-84.

Graf, W.H. 1995. Local scour at piers. Annu. Repo., Laboratoire de Recherches Hydrauliques, Ecole Polytechnique Fédérale de Lausanne, Lausanne, Switzerland, B33.1-B.33.8.

Graf, W.H. 1996. Fluvial Hydraulics. John Wiley & Sons, N .Y.

Graf, W.H., and Yulistiyanto, B. 1998. Experiments on flow around a cylinder, the velocity and vorticity field. J. Hydraulic Research, IAHR, 36 (4): 637-653.

Graf, W.H., and Istiarto, I. 2002. Flow pattern in a scour hole around a cylinder. Journal of Hydraulic Research, IAHR, 40 (1): 13-20.

Hoffmans, G.J.C.M., and Verheij, H.J. 1997. Scour Manual. A.A. Balkema, Rotterdam, Netherlands.

Jain, S., and Fischer, E. 1980. Scour around bridge piers at high flow velocities. Journal of Hydraulics Division, ASCE, 106 (HY11): 1827-1842.

Johnsons, P. 1992. Reliability-based pier scour engineering. Journal of Hydraulic Engineering, ASCE 118(10): 1344-1358.

Johnes, J.S., and Sheppard, D.M. 2000. Scour at wide bridge piers. Joint Conference on Water Resources Engineering and Water Resources Planning and Management, ASCE, Minneapolis, Minnesota, USA, 10p.

References

Kandasamy, J. K. 1989. Abutment scour. Report No. 458, School of Engineering, University of Auckland, Auckland, New Zealand.

Kirkil, G., Contastantinescu, G., and Ettema, R. 2008. Coherent structures in the flow field around a circular cylinder with scour hole. Journal of Hydraulic Engineering, ASCE, 134 (5): 572-587.

Kothyari, U., Garde, R., and Ranga Raju, K. 1992. Temporal variation of scour around circular bridge piers. J. Hydr. Engrg., ASCE 118 (8): 1091-1106.

Laursen, E., and Toch, A. 1956. Scour around bridge piers and abutments. Bulletin No. 4, Iowa Highway Research Board.

Lee, S. O., and Sturm, T. W. 2009. Effect of sediment size on physical modeling of bridge pier scour. Journal of Hydraulic Engineering, ASCE, 135 (10): 793-802.

Link, O., and Zanke, U. 2006a. Time variation of three dimensional scour geometry. Proceeding of International Conference of River Hydraulics-River Flow, Lisbon Portugal: B3023.

Link, O. 2006b. Untersuchung der Kolkbildung an einem schlanken zylindrischen Pfeiler, . PhD Thesis. Institut für Wasserbau und Wasserwirtschaft, Darmstadt University of Technology. Heft 136 (in German).

Link, O., Gobert, Ch., Manhart, M. y and Zanke, U. 2008a. Effect of the horseshoe vortex system on the geometry of a developing scour hole at a cylinder. Proceedings of the Fourth International Conference for Scour and erosion ICSE-4, Tokyo, Japan, 5-7 November, Chuo University: 162-168.

Link, O., Pfleger, F., and Zanke, U. 2008b. Characteristics of developing scour holes at a sand-embedded cylinder. International J. of Sediment Research, 23(3): 268 – 276.

Manhart, M. 2004. A zonal grid algorithm for DNS of turbulent boundary layers. Computers and Fluids, 33(3): 435-461.

Masjedi, A., Bejestan, M.S., Moti, A., and Taeedi, A. 2010. Time development of local scour at a bridge pier using square collar in a 180 degree flume bend. Journal of American Science, 6(8): 188-195.

Melville, M.W. 1975. Local scour at bridge sites. Project Report No. 117, School of Engineering, University of Auckland, Auckland, New Zealand , 227 p.

Melville, B. W., and Sutherland, A. J. 1988. Design Method for Local Scour at Bridge Piers. Journal of Hydraulic Engineering, ASCE, 114 (10): 1210-1226.

Melville, B.W. 1997. Pier and abutment scour: integrated approach. Journal of Hydraulic Engineering, ASCE, 123(2): 125-136.

Melville, B. W., and Chiew, Y. M. 1999. Time Scale for Local Scour at Bridge Piers. Journal of Hydraulic Engineering, ASCE, 125 (1): 125-136.

References

Melville, B.W., and Coleman, S.E. 2000. Bridge Scour. Water Resources Publication, LLC, ISBN: 1-887-201-18-1.

Mia, Md.F., and Nago, H. 2003. Design method of time-dependent local scour at circular bridge pier. Journal of Hydraulic Engineering, ASCE, 129(6): 420-427.

Molinas, A. 2003. Bridge Scour in Non-uniform Sediment Mixtures and in Cohesive Materials: Synthesis Report. Report Nr. FHWA-RD-03-083.

Mostafa, E. A. 1994. Scour around skewed bridge piers. PhD thesis. Alexandria University, Alexandria, Egypt.

Mueller, D.S. 1996. Local scour at bridge piers in non-uniform sediment under dynamic conditions. PhD thesis. Fort Collins, CO, Colorado State University, USA: 212 p.

Muzzammil, M. and Gangadhariah, T. 2003. The mean characteristics of horseshoe vortex at a cylindrical pier. J. Hydraulic Research, IAHR, 41 (3): 285-297.

Muzzammil, M., Gangadhariaiah, T., and Gupta, A.K. 2004. An experimental investigation of a horseshoe vortex induced by a bridge pier. Water Management Journal, Proceeding of the Institution of Civil Engineers, Thomas Telford Journals, London, 157(2): 109-119.

Nakagawa, H., and Suzuki, K. 1976. Local scour around bridge pier in tidal current. Coastal Engineering in Japan, 19: 89-100

Neill, C.R. 1964. River-bed scour—a review for engineers. Canadian Good Roads Association Technical Publication No. 23, Ottawa, Canada.

Neill, C.R. 1973. Guide for bridge hydraulics. Project Committee on Bridge Hydraulics, Roads and Transportation Associations of Canada. University of Toronto Press and Buffalo: 191p.

Oliveto, G., and Hager, W. 2002. Temporal evolution of clear-water pier and abutment scour. Journal of Hydraulic Engineering, ASCE, 128 (9): 811-820.

Oliveto, G., and Hager, W. 2005. Further results to time-dependent local scour at bridge elements. Journal of Hydraulic Engineering, ASCE, 131 (2): 97-105.

Olsen, N., and Kjellesvic, H. 1998. 3D numerical flow modeling for estimation of maximum local scour depth. J. Hydraulic Research, IAHR, 36(4): 579-590.

Olsen, N., and Melaaen, M. 1993. 3D calculations of scour around cylinders. Journal of Hydraulic Engineering, ASCE, 119(9): 1048-1054.

Raikar, R., and Dey, S. 2005a. Clear-water scour at bridge piers in fine and medium gravel beds. Canadian Journal of Civil Engineering, NRC, 32:775-781.

Raikar, R., and Dey, S. 2005b. Scour of gravel beds at bridge piers and abutments. Water Management, 158: 157-162.

References

Raudkivi, A.J., and Ettema, R. 1977a. Effect of sediment gradation on clear-water scour and measurement of scour depth. Proceeding of 17th Congress IAHR, Baden-Baden 4: 521-527.

Raudkivi, A.J. and Ettema, R. 1977b. Effect of sediment gradation on clear-water scour and measurement of scour depth. Journal of the Hydraulics Division, ASCE, 103 (HY10): 1209-1213.

Raudkivi, A.J., and Ettema, R. 1983. Clear-water scour at cylindrical piers. Journal of Hydraulic Engineering, ASCE, 109 (3): 338-350.

Raudkivi, A.J. 1986. Functional trends of local scour at bridge piers. Journal of the Hydraulics Division, ASCE, 112 (1): 1-13.

Richardson, E.V., Simons, D.B., Karaki, S., Stevens, M.A., and Mahmood, K. 1975. Highways in the River Environment-Hydraulic and Environmental Design Considerations. Training and Design Manual. U.S. Department of Transportation, Federal Highway Administration, Washington, D.C.

Richardson, E.V. 1987. FHWA technical advisory-scour at bridges. Draft report Federal Highways Administration, U.S. Department of Transportation, Federal Highway Administration, Washington, D.C.

Richardson, E.V., Harrison. L.J., Richardson, J.R. and Davis, S.R. 1993. Evaluating Scour at Bridges: 2nd Edition. Publ. No. FHWA HNG-31, HEC-18, Federal Highway Administration, Washington, D.C.

Richardson, E.V., and Abed, L. 1999. Top Width of Pier Scour Holes. Compendium of ASCE Water Resources: 1991-1998, Stream Stability and Scour at Highway Bridges, E.V. Richardson and P.F. Lagasse, (eds), Reston, VA, pp. 311.

Richardson, E.V., Simons, D.B., and Lagasse P.F. 2001. River Engineering for Highway Encroachments: Highways in the River Environment. Publ. No. FHWA NHI 01-004, HEC-6, Federal Highway Administration, Washington, D.C.

Richardson, E.V., and Davis, S.R. 2001. Evaluating scour at bridge, 4th edition. Publ. No. FHWA NHI 01-001, HEC-18, Federal Highway Administration, Washington, D.C.

Richardson, J.R. and Richardson, E.V. 2008. Chapter 10 Bridge Scour Evaluation, in Sedimentation Engineering Processes, Measurements, Modeling, and Practice. Edited by Marcelo H. Garcia, ASCE Manual and Reports on Engineering Practice No. 110., ISBN 13: 978-0-7844-0814-8: 505-542.

Roulund, A., Sumer, M., Fredsøe, J., and Michelsen, J. 2005. Numerical and experimental investigation of flow and scour around a circular pile. Journal of Fluid Mechanics, 534: 351-401.

References

Salahedin, T., Imran, J., and Chaudhry, H. 2004. Numerical modeling of three-dimensional flow field around circular piers. Journal of Hydraulic Engineering, ASCE, 130(2): 91-100.

Sarker, A. 1998. Flow measurement around scoured bridge piers using acoustic-doppler-velocimeter, ADV. Flow Measurement and Instrumentation, Elsevier, 9: 217-227.

Shen, H. W., Schneider, V.R., and Karaki, S. 1969. Local scour around bridge piers. Journal of Hydraulics Division, ASCE, 95(6): 1919-1941

Sheppard; D. M., Ontowirjo, B., and Zhao, G. 1995. Local scour near single piles in steady currents. Proceeding of the first Hydraulics Engineering Conference, San Antonio.

Sheppard, D.M., Odeh, M., and Glasser, T. 2004. Large scale clear-water local pier scour experiments. Journal of Hydraulic Engineering, ASCE, 130 (10): 957-963.

Tison, L.J. 1940. Erosion autour de piles de pont en riviere, (scour around bridge piers in river). Ann. Des Travaux Publics de Beligique, 41 (6): 813-871.

Tison, L.J. 1961. Local scour in rivers. J. Geoph. Res., 66(12): 4427-4232.

Tseng, M-H., Yen, C-L. and Song, C.S. 2000. Computation of three-dimensional flow around square and circular piers. International Journal for Numerical Methods in Fluid, 34: 207-227.

Unger, J., and Hager W. 2005. Discussion to the mean characteristics of horseshoe vortex at a bridge pier. Journal of Hydraulic Research, IAHR, 43(5):585–588.

Unger, J., and Hager, W. 2007. Down-flow and horseshoe vortex characteristics of sediment embedded bridge piers. Experiments in Fluids, 42: 1-19.

Yanmaz, A.M., and Altinbilek H.D. 1991. Study of Time-dependent local scour around bridge piers. Journal of Hydraulic Engineering, ASCE, 117 (10): 1247-1268.

Yanmaz, M., and Ciceckdag, O. 2002. Composite reliability model for local scour around cylindrical bridge piers. Canadian Journal of Civil Engineering, 28: 520-535.

Yanmaz, M., and Köse Ö. 2007. Surface Characteristics of Scouring at Bridge Elements. Turkish J. Eng. and Env. Sci., 31: 127-134.

Yen, Ch., Lai, J., and Chang, W. 2001. Modeling of 3D flow and scouring around circular piers. Proc. Natl. Sci. Counc. ROC(A), 25(1): 17-26.

Zanke, U. 1978a. Zusammenhänge zwischen Strömung und Sedimenttransport, Teil 1: Berechnung des Sedimenttransportes, -allgemeiner Fall-. Mitteilung des Franzius Instituts, TU Hannover, Heft 47: 214 – 345,-ISSN 0340-0077- (in German).

Zanke, U. 1978b. Zusammenhänge zwischen Strömung und Sedimenttransport, Teil 2: Berechnung des Sedimenttransportes hinter befestigten Sohlenstrecken, -Sonderfall zweidimensionaler Kolk-". Mitteilung des Franzius Instituts, TU Hannover, Heft 47: 1 – 95, -ISSN 0340-0077-(in German).

References

Zanke, U. 1982a. Kolke am Pfeiler in richtungskonstanter Strömung und unter Welleneinfluß. Mitteilungen des Franzius-Instituts, TU Hannover. Heft 54: 381-416 (in German).

Zanke, U. 1982b. Grundlagen der Sedimentbewegung. Springer, Verlag, Berlin, Heidelberg, Germany, (in German).

GESAMTVERZEICHNIS

der bisherigen „Technischen Berichte über Ingenieurhydrologie und Hydraulik“ *)

Nr. 1/1965 (vergriffen)
H. Lacher — Über das Kriechverhalten destillierter Bitumina unter Zugrundelegung der Theorie der linearen Viskosität

Nr. 2/1966
J. Bock — Einfluß der Querschnittsform auf die Widerstandsbeiwerte offener Gerinne

Nr. 3/1967 (vergriffen)
P. Unger — Berechnung instationärer Abflußvorgänge in natürlichen Gerinnen unter Verwendung eines von der Gerinneform unabhängigen Rauhigkeitsmaßes

Nr. 4/1968 (vergriffen)
W. Tiedt — Berechnung des laminaren und turbulenten Reibungswiderstandes konzentrischer und exzentrischer Ringspalte

Nr. 5/1969
R. Schröder — Häufigkeitsanalyse hydrologischer Daten
B. Scherer — Unverzerrtes Hele-Shaw-Modell für instationäre Grundwasserströmungen mit freier Oberfläche

Nr. 6/1970
D. Krause — Einfluß der Trassierungselemente auf den Spiegelverlauf in gekrümmten Schussrinnen

Nr. 7/1971
W. Tiedt — Hydrodynamische Untersuchung des Teilfüllungsproblems, Gesetzmäßigkeiten des Abflusses in technisch rauhen Kreisgerinnen bei laminarer und turbulenter Strömung

Nr. 8/1972
M. T. Monzavi — Widerstandsgesetz auf statistischer Basis für extreme natürliche Rauhigkeiten in Druckrohren

Nr. 9/1973
B. Scherer — Die Entwicklung und Anwendung eindimensionaler Modelle der zweidimensionalen Grundwasserbewegungen in Fluß-, Graben- und Drainnähe

Nr. 10/1973 (vergriffen)
diverse Autoren — Sammlung von Kurzberichten 1965 – 1972

*) Bestellungen beim

Institut für Wasserbau und Wasserwirtschaft
Fachgebiet Ingenieurhydrologie und Wasserbewirtschaftung
Petersenstraße 13, D-64287 Darmstadt

Nr. 11/1974 (vergriffen)

E. Zäschke — Widerstandsmindernde Wirkung hochmolekularer Zusätze beim Transport Newtonscher Flüssigkeiten in geschlossenen Leitungen

R. Schröder u. D. Knauf — Über das hydraulische Widerstandsverhalten von Beton- und Stahlbeton-rohren im Übergangsbereich

H. Lacher — Konstruktionshilfe für Strömungsnetze ebener Potentialströmungen mittels Elementarströmungen

H. Lacher u. M. T. Monzavi — Einfluß von Teilfüllungsgrad und von Wanddicke des porösen Rohrmantels auf die Ergiebigkeit von Betonfilterrohren

H. Lacher u. K. J. Ueker — Untersuchung zur Ermittlung der Abflußleistung poröser Betonfilterrohre unter natürlichen Bedingungen

G. Euler u. A. Koussis — Berechnung von Hochwasserabläufen mit Näherungsverfahren und Anwendung

H. Lacher — Neuere Methoden der Wissensvermittlung im Fach „Hydraulik“, erläutert am Lehrbeispiel „Hydrostatik räumlich gekrümmter Oberflächen“

Nr. 12/1974

H. J. Dallwig — Fließformeln und Formbeiwert - eine kritische Untersuchung üblicher Berechnungsmethoden für Gerinneströmungen

R. Schröder — Wirkung periodischer Wandwelligkeiten auf den Strömungswiderstand

Nr. 13/1974 (vergriffen)

D. Belke — Die statistische Analyse von Grundwasserständen mit dem Ziel der Extremwertprognose

Nr. 14/1975 (vergriffen)

G. Euler — Die Simulation der Niederschlagsaufteilung für Hochwasserabfluß-Modelle

Nr. 15/1975

A. Koussis — Ein verbessertes Näherungsverfahren zur Berechnung von Hochwasserabläufen

Nr. 16/1975

G. Lass — Berechnung von Horizontalfilterbrunnen mit beliebig angeordneten Filterrohren

Nr. 17/1976 (vergriffen)

D. Knauf — Die Abflußbildung in schneebedeckten Einzugsgebieten des Mittelgebirges

Nr. 18/1977

H. Bischoff — Die Berechnung von Potentialfeldern mit der Randintegralmethode, dargestellt am Beispiel der ebenen Grundwasserbewegung

Nr. 19/1977

I. David — Grundwasserfassungsanlagen mit Filterrohren

Nr. 20/1977 (vergriffen)

diverse Autoren — Sammlung von Kurzberichten 1972 - 1977

Nr. 21/1978

O. Gieseler — Einfluß der äquivalenten Sandrauhigkeit auf die Lage des Wechselsprungs bei Umlenkung eines frei fallenden runden Flüssigkeitsstrahls an einer ebenen Platte

Nr. 22/1978

R. Schröder	Forschungsarbeiten des Instituts für Hydraulik und Hydrologie
D. Belke u.	Simulation zur Nutzraumoptimierung einer Talsperre
G. Euler u.	Ein detailliertes mathematisches Modell zur Simulation von Hochwasserwellen
R. Wackermann	am Beispiel der Nidda
T. Brandt	Der Austausch von Oberflächen- und Grundwasser
R. Schröder	Gestaltung von Offshore-Bauwerken für die Kühlwasserversorgung thermischer Kraftwerke
H. Lacher u. F. Thiele	Zum Problem des Regenwasserabflusses auf Fahrbahnen
W. Tiedt	Druckspüler/Spülkasten - ein Beitrag zur Hydraulik zweier Spülsysteme der Sanitärtechnik
O. Gieseler	Hydraulische und mechanische Verfahren zur Ermittlung von Rauhigkeiten

Nr. 23/1978

A. Holderbaum	Hydraulische Untersuchung zur Ermittlung der Wasserfilmdicken auf beregneten Fahrbahnoberflächen

Nr. 24/1979

T. Brandt	Modell zur Abflußgangliniensimulation unter besonderer Berücksichtigung des grundwasserbürtigen Abflusses

Nr. 25/1980

N. Könemann	Der wechselseitige Einfluß von Vorland und Flußbett auf das Widerstandsverhalten offener Gerinne mit gegliederten Querschnitten

Nr. 26/1981

R. Wackermann	Ein Rasterverfahren mit flächenvariabler Systemfunktion zur Simulation von Hochwasserganglinien aus großen Einzugsgebieten

Nr. 27/1981

A. Holderbaum	Modellversuche zum Abfluß von Niederschlagswasser auf Verwindungs-Strecken

Nr. 28/1982

H. J. Dallwig	Zur Leistungsfähigkeit von Kelchüberfällen

Nr. 29/1982

R. Schröder	In memoriam Hannes Lacher - Geleitwort
H. Lacher	Über die viskoelastischen Eigenschaften von destilliertem Bitumen
H. Lacher u. R. Schröder	Experimentelle Erfahrungen mit Filterrohren als Grundlage ihrer hydraulischen Bemessung
H. Lacher	Grundwasserabfluß mit freier Oberfläche, Auszug aus dem Textbuch zur Technischen Hydraulik
H. Lacher B. Söhngen H. Bischoff	Anwendung der Randintegralmethode zur Berechnung der Leistungsfähigkeit von teilgefüllten Rohren
H. Lacher	Verallgemeinertes Berechnungsverfahren nach Dupuit-Forchheimer für Grundwasserleiter beliebig hoher Durchlässigkeit
H. Lacher H. Bischoff B. Söhngen	Anwendung der Feldintegralmethode zur Berechnung der Durchströmung von Steinschüttdämmen
F. Zior u. H. Lacher	Ein neues Meßverfahren für die Bestimmung der Oberflächenrauhigkeit von Kanalwandungen
H. Gerdes u. H. Lacher	Die Berechnung dreidimensionaler Grundwasserströmung mit Mitteln der ebenen Potentialtheorie
F. Zior u. H. Lacher	Entwicklung einer konduktometrischen Sonde zur Messung von Wasserfilmdicken auf Fahrbahnoberflächen

Fortsetzung Heft 29

H. Lacher u. E. Zäschke	Schiffahrtsbedingte Wasserdruckausbreitung in Kanalböschungen
F. Thiele u. H. Lacher	Probleme der Straßenentwässerung und neue Bemessungsmethoden Die Berechnung der Ergiebigkeit von Drainagesystemen in horizontal
B. Söhngen, H. Bischoff u. H. Lacher	ausgedehnten Grundwassersystemen Zur Begründung der Konzentrationszeit aus der Sicht der Hydraulik
H. Lacher	Humor im Wasserbaulichen Versuchswesen: Versuchsanordnung zur Bestimmung der äquivalenten Sandrauhigkeit von Steinzeugrohren

Nr. 30/1983

diverse Autoren	Sammlung von Kurzberichten 1978 - 1983

Nr. 31/1983

F. Thiele	Fahrbahnlängsentwässerung im Straßengerinne und ein Entwurf für zukünftige Richtlinien zur Bemessung

Nr. 32/1984

U. Höfer	Beginn der Sedimentbewegung bei Gewässersohlen mit Riffeln oder Dünen

Nr. 33/1985

G. Euler C. Heinzelmann D. Jacobi	Die Berechnung des Schmutzwasserabflusses aus Niederschlägen: Eine vergleichende Darstellung und Wertung der Modellansätze

Nr. 34/1985

H. Gerdes	Berechnung dreidimensionaler Grundwasserströmung mit Mitteln der ebenen Potentialtheorie am Beispiel des Sickerstollens

Nr. 35/1986

diverse Autoren	Stofftransport im Wasser - Darmstädter Wasserbauliches Kolloquium 1985: Zusammenstellung der Referate

Nr. 36/1986

R. Schröder	Diskontinuierliche Abflußvorgänge in Freispiegelrinnen: Randwalzen
R. Schröder	Die turbulente Strömung im freien Wechselsprung: Deckwalze
C. Kraus	Walzenbildung im Kolk

Nr. 37/1987

C. Heinzelmann U. Höfer	Transportbeginn auf geriffelter Sohle unter dem Einfluß einer stationär gleichförmigen Strömung mit überlagerter Schwallwelle

Nr. 38/1987

F. Zior	Regenwasserabfluß auf Fahrbahnoberflächen: experimentelle und theoretische Untersuchungen

Nr. 39/1987

B. Söhngen	Das Formbeiwertkonzept zur Berechnung des Fließwiderstandes in Rohren und Gerinnen

Nr. 40/1988

diverse Autoren	Lösungsansätze zu aktuellen Problemen im Wasserbau - Darmstädter Wasserbauliches Kolloquium 1987: Zusammenstellung der Referate

Nr. 41/1987

G. J. Weiß	Abfluß- und Wasserstandssteuerung in offenen Gerinnen mit Hilfe selbstregulierender Schwimmkörper

Nr. 42/1989
H. Zaiß — Simulation ereignisspezifischer Einflüsse des Niederschlag-Abfluß-Prozesses von Hochwasserereignissen kleiner Einzugsgebiete mit Niederschlag-Abfluß-Modellen

Nr. 43/1990
diverse Autoren — Hydraulik und Hydrologie im Stadtbauwesen - Darmstädter Wasserbauliches Kolloquium 1989: Zusammenstellung der Referate

Nr. 44/1990
H. Wegner — Steuerung für kleine Hochwasserschutzräume

Nr. 45/1991
U. Drechsel — Repräsentanz und Übertragbarkeit von Niederschlagsersatz-belastungen zur Durchführung von Schmutzfrachtberechnungen

Nr. 46/1991
J. Lang — Analyse und Simulation des Feuchtekontinuums auf Straßenoberflächen

Nr. 47/1992
G. J. Weiß — Sohlenbeanspruchung und Sedimenttransport unter Einzelwellen

Nr. 48/1992
C. Heinzelmann — Hydraulische Untersuchung über den Einfluß benthischer Diatomeenfilme auf Strömungswiderstand und Transportbeginn ebener Sandsohlen

Nr. 49/1993
J. Kühlborn — Wachstum und Wanderung von Sedimentriffeln

Nr. 50/1995
M. Schuster — Transportkritische Schubspannungen bei verschiedenen Sohlenzuständen, insbesondere unter Einzelwellenbelastung bei stationärer Grundströmung

Nr. 51/1993 (vergriffen)
diverse Autoren — Dezentraler Hochwasserrückhalt - Darmstädter Wasserbauliches Kolloquium 1992: Zusammenstellung der Referate

Nr. 52/1994
N. Engel — Hydrologische Simulation der Abflußtransformation in Kanalisationsnetzen

Nr. 53/1995
diverse Autoren — Die modellgestützte Bewirtschaftung intensiv genutzter Einzugsgebiete - Darmstädter Wasserbauliches Kolloquium 1994: Zusammenstellung der Referate

Nr. 54/1996
S. Wallisch — Ein mathematischen Modell zur Berechnung der hydromechanischen Beanspruchung von Riffelsohlen

GESAMTVERZEICHNIS (ISSN 0340-4005)
der bisherigen `Wasserbau-Mitteilungen der TH Darmstadt *)
(teilweise Kurztitel)

Heft 1/März 66 (vergriffen)
- Bassler, F. Vorwort des Herausgebers
- Linder, R. Hochwasserentlastung von Staustufen durch Schiffsschleusen
- Bassler, F. Beginnt die Epoche der Gezeitenkraftwerke?
- Elshazli, S. Die Bedeutung der Wasserkraft für die ägyptische Wirtschaft

Heft 2/Juli 67 (vergriffen)
- Uhlig, D. Probleme des landwirtschaftlichen Wasserbaus in Lybien
- Bassler, F. Eindrücke vom ICID-Kongreß in Indien
- Sauer, H.-D. Zentral messendes Wasserstands-Registriergerät für Modelle mit instationärer Strömung
- Bassler, F. Die Nutzung von Meerwasser in der Kattara-Senke/Ägypten

Heft 3/Dez. 68 (vergriffen)
- Müller, J. Weltregister der Pumpspeicherkraftwerke
- Bassler, F. Wasserwirtschaftliche Sonderaufgaben in Entwicklungsländern
- Bayer, E. Die Versuchseinrichtungen des Instituts für Wasserbau und Wasserwirtschaft
- Mäder, Ch. Die Exkursionen des Lehrstuhls für Wasserbau und Wasserwirtschaft
- Bassler, F. Scheme for Qattara Depression/Egypt

Heft 4/Aug. 69
- Bayer, E. Gestaltung der Rampenbauwerke für Flussfähren

Heft 5/Nov. 69
- Sauer, H.-D. Industriewasserentnahme aus schwebstoffreichen Flüssen

Heft 6/Okt. 70
- Schröder, W. Ausbaugefällebemessung alluvialer Bachstrecken nach dem Sandtransportvermögen

Heft 7/Feb. 71
- Müller, J. Auswirkungen eines Unterbeckens für Pumpspeicherung auf die Wasserwirtschaft
- Bassler, F. Nuklearausbruch und Pumpspeicherung als Kostenfaktoren der Wasserkraftanlage in der Kattara-Senke/Ägypten

*) Selbstkostenpreis EURO 20,-- je Heft. Bestellungen beim

Institut für Wasserbau und Wasserwirtschaft, Fachgebiet Wasserbau
Rundeturmstraße 1, D-64283 Darmstadt,
per Fax: 06151/16-3223, per e-mail: zeitler@wb.tu-darmstadt.de

Heft 8/Juli 71

Bassler, F.	10 Jahre Lehre und Forschung in Wasserbau und Wasserwirtschaft an der Technischen Hochschule Darmstadt
Mäder, Ch.	Modellversuche zur Umgestaltung des Mains bei Aschaffenburg
Schmidtke, R.	Projektstudie zur Regelung des Rio Mantaro in der Hochebene von Huancayo/Peru
Schröder, W.	Projektstudie zur Ufersicherung am Amazonas bei Iquitos/Peru
Sulser, P.	Gedanken zu den Exkursionen eines Wasserbaulehrstuhls
Täubert, U.	Modellversuche für Hochwasserentlastungsanlage Staudamm Poza Honda/Ecuador
Uhlig, D.	Das Bewässerungsprojekt Al Hassa/Saudi Arabien
Bassler, F.	Studieneinführung Bauingenieurwesen, Fachgebiet Wasserbau und Wasserwirtschaft

Heft 9/Nov. 71

Mäder, Ch.	Strömungen durch Luftblasenschleier in stehenden und fließenden Gewässern

Heft 10/Aug. 72

Schmidtke, R.	Ein Kostenzurechnungsmodell für wasserwirtschaftliche Mehrzweckprojekte

Heft 11/Dez. 73 (vergriffen)

Sulser, P.	Berührungslose Wasserstandsmessung mittels kontinuierlicher Kondensator-umladung
Börner, R.	Internationale Pumpspeicherbibliographie 1900 bis 1960
Bassler, F.	Solar Depression Power Plant of Qattara/Eqypt
Täubert, U.	Der Abfluß in Schußrinnenversuchen
Bassler, F.	Pumpspeicherkraftwerke an schiffbaren Wasserstraßen u. a.

Heft 12/Apr. 74

Täubert, U.	Wasserwirtschaftliche Systemanalyse des Wärmehaushalts von Flüssen

Heft 13/Dez. 75 (vergriffen)

Bassler, F.	Neue Vorschläge für die Entwicklung der Kattara-Senke/Ägypten
Bassler, F.	New Proposals to Develop Qattara Depression/Egypt
Börner, R.	Moorentwässerung in Finnland
Börner, R.	Internationale Pumpspeicherbibliographie 1961 bis 1965
Gräb, E.	Konstruktion und Umbau einer Kipprinne
Sulser, P.	Die Wasserbau-Exkursionen des Instituts in den Jahren 1970 bis 1975, Forschungsvorhaben und Veröffentlichungen 1970 bis 1975

Heft 14/März 77

Kriesel, E.	Wasserwirtschaftliche Aspekte thermischer Energiequellen

Heft 15/Mai 77

Börner, R.	Einsatzmöglichkeiten der Mehrzweckpumpspeicherung in Entwicklungsländern

Heft 16/Juli 77 (vergriffen)

Franzius, V.	Der Sickerwasserabfluß aus Mülldeponien - Ein mathematisches Modell

Heft 17/ Aug. 77 (vergriffen)

Tönsmann, F.	Verringerung des Feststoffbetriebs in Entnahmebauwerken an Bächen

Heft 18/Dez. 77 (vergriffen)

Bassler, F.	Die Energiequellen Fluss- und Meerwasser
Bassler, F.	Speisung der Schiffahrtskanäle mit Scheitelhaltung
u.a.	
Bassler, F.	100 Jahre Bauingenieurwesen Arab Republic of Egypt : Qattara Depression
Bassler, F.	Tätigkeiten als Ordinarius für Wasserbau und Wasserwirtschaft

Heft 19/Dez. 78

Sulser, P.	Drucklufteinleitung in Flüsse zur Steuerung des Geschiebetransports

Heft 20/Juni 79 (vergriffen)
Friedrich Bassler 70 Jahre/Ansprache und Aufsätze zu seiner Emeritierung

Heft 21/März 81

Döring, M.	Einflüsse der Wassernutzung thermischer Kraftwerke auf Gewässer

Heft 22/Aug. 83

Albert, W.	Solarteich - Kollektor und Wärmespeicher
Gonsowski, P.	Bodenluftkompression bei Wasserinfiltration
Gonsowski, P.	Selbstdichtung von Fließgewässern
Kaiser, W.	Modellversuch HW-Entlastung Sösetalsperre
Wieland, H.	
Krier, H.	Erfahrungen bei Beregnungsanlagen im Hessischen Ried
Krier, H.	Erosionsbeginn bei kohäsiver Wasserlaufsohle
Wieland, H.	Modellversuch zur Hochwasser-Entlastung der Kulmke-Sperre/Harz

Heft 23/Sep. 84 (vergriffen)

Kaiser, W.	Fließwiderstandsverhalten in Gerinnen mit durchströmten Ufergehölzzonen

Heft 24/Feb. 85 (vergriffen)
Darmstädter Wasserbauliches Kolloquium 1984 „Hochwasser am Oberrhein“

Heft 25/Aug. 87

Wieland, H.	Hydraulische Bemessung von Tosbecken für Überfallstrahlen und der Druckbelastung der Sohle

Heft 26/Feb. 87 Darmstädter Wasserbauliches Kolloquium 1986 „Planungsansätze Ökologie - Wasserwirtschaft, so nicht! - wie dann?“

Heft 27/Juli 87

Krier, H.	Zum Langzeiterosionsverhalten kohäsiver Fließgewässersohlen

Heft 28/Sep. 87

Gonsowski, P.	Der Einfluß der Bodenluftkompression auf die vertikale Infiltration von Wasser in Sanden

Heft 29/Dez. 89 Darmstädter Wasserbauliches Kolloquium 1988 `Fließgewässer – Stillgewässer

Heft 30/Dez.89 (vergriffen)

Albert, W.	Die Gebietsverdunstung von Waldstandorten aus der Simulation von Grundwasserganglinien mit klimatischem Bodenwasserhaushaltsmodell

Heft 31/Feb. 90

Weiß. J.	Berücksichtigung der Hysterse der Wasserspannung bei der Berechnung der vertikalen Wasserbewegung in natürlichen Sandböden

Heft 32/März 90 Festschrift zum 60. Geburtstag von Prof. Dr.-Ing. Josef Mock

Heft 33/Aug. 90
Theune, Ch. Hydrological and Economical Aspects of Agronomically Productive Perculation Systems

Heft 34/Dez. 90 (vergriffen)
Darmstädter Wasserbauliches Kolloquium 1990 `Umweltverträglichkeitsprüfung in der Wasserwirtschaft

Heft 35/Nov. 91 (vergriffen)
Nuding, A. Fließwiderstandsverhalten in Gerinnen mit Ufergebüsch - Entwicklung eines Fließgesetzes für Fließgewässer mit und ohne Gehölzufer, unter besonderer Berücksichtigung von Ufergebüsch

Heft 36/Dez. 91 Darmstädter Wasserbauliches Kolloquium 1991 „Boden- und Grundwasserschutz - anwendungsorientierte Forschung und Verfahren“

Heft 37/März 92
Zimmermann, E. Phänomenologische Untersuchungen bei der Erosion einer kohäsiven Sohle

Heft 38/Dez. 93 Darmstädter Wasserbauliches Kolloquium 1993 `Ökologisch orientierte Gewässersanierung und –pflege

Heft 39/Dez. 93
Ruiz Rodriguez, E. Bodenluftströmung in teilgesättigten Böden

Heft 40/Dez. 95 Darmstädter Wasserbauliches Kolloquium 1995 „Hochwassergefahren am Oberrhein“ und Fachseminar „Abflußabhängigkeit der morphologischen und biologischen Verhältnisse von Fließgewässern bei Niedrigwasser“

Heft 41/Juli 99
von der Hude, Die Kapillarsperre als Oberflächenabdichtungssystem von Deponien und Altlasten - Rinnenversuche und Bemessungsregeln

Die Reihe der „Wasserbau-Mitteilungen der TH Darmstadt“ wird zusammen mit den „Technischen Berichten über Ingenieurhydrologie und HydraulikA“ als „Mitteilungen des Instituts für Wasserbau und Wasserwirtschaft der TU Darmstadt“ (ISSN 1430-3434) fortgesetzt. Die neue Nummerierung ergibt sich aus der Summe der Hefte beider Vorgängerreihen.

GESAMTVERZEICHNIS (ISSN 1430-3434) **)

Heft 96/1996 (vergriffen)
Träbing, K. Ökomorphologische Kenngrößen für die Strukturvielfalt von Fließgewässern

Heft 97/1997
Jelinek, D. Die Kapillarsperre als Oberflächenbarriere für Deponien und Altlasten - Langzeitstudien und praktische Erfahrungen in Feldversuchen

Heft 98/1997 Darmstädter Wasserbauliches Kolloquium 1996 `Numerische Simulationen im Wasserbau

Heft 99/1997 Berichte zur Ingenieurhydrologie und Wasserbewirtschaftung

Heft 100/1998
Kilian, T. Abflußcharakteristika und potentiell natürliche Gerinnegrundrißformen hessischer Fließgewässer

Heft 101/1997
Döring, M. Die römische Wasserleitung von Pondel im Val d>Aosta/Italien. Bestandsaufnahme des Bauwerks aus dem Jahre 3 v. Chr.

Heft 102/1998
Schmidt, T.R. Einfluß der Wandrauhigkeitsstruktur auf die Geschwindigkeitsverteilung ausgebildeter, turbulenter Strömungen in Kreisrohren

Heft 103/1998 Darmstädter Wasserbauliches Kolloquium 1997 „Betrieb und Steuerung

von Speichern und Stauhaltungen unter sich ändernden Randbedingungen“

Heft 104/1998
Bettmann, T. Dezentrale Regenwasserbewirtschaftung und deren Auswirkungen auf die Regenwasserbehandlung in urbanen Gewässereinzugsgebieten

Heft 105/1998
Seid, A.H. Modelling the Influence of Shrinkage Cracks on Overland Flow

Heft 106/1999 (Nachdruck)
Zanke, U. Zur Physik von strömungsgetriebenem Sediment (Geschiebetrieb)

Heft 107/1999
Obermann, I. Modellierung des Wasserhaushaltes von Deponien vorbehandelter Siedlungsabfälle

Heft 108/1999 Darmstädter Wasserbauliches Kolloquium 1998
Mischwasserbehandlung - Planung, Prüfung, Vollzug -

Heft 109/2000
Kämpf, M. Fließprozesse in Kapillarsperren zur Oberflächenabdichtung von Deponien und Altlasten - Grundlagen zur hydraulischen Bemessung

Heft 110/2000
Lempert, M. Ein GIS gekoppeltes rasterbasiertes Modell zur Berechnung des Wasserhaushaltes kleiner Einzugsgebiete

Heft 111/2000 (vergriffen)
Darmstädter Wasserbauliche Kolloquium 1999 „Fließ- und Ausbreitungsvorgänge in aquatischen Grenzräumen“

Heft 112/2000 100-Jahr-Feier des Instituts für Wasserbau und Wasserwirtschaft mit Festvortrag von Prof. Dr.-Ing., Dr.-Ing. E.h. J. Plate

Heft 113/2000 (vergriffen)
Mehler, R. Mischwasserbehandlung - Verfahren und Modellierung

Heft 114/2000 (Nachdruck)
Lenk, M. Hydraulische Austauschvorgänge zwischen fließender Welle und Interstitial - Felduntersuchungen in einer Pool-Riffle-Sequenz an der oberen Lahn

Heft 115/2000 (Nachdruck)
Saenger, N. Identifikation von Austauschprozessen zwischen Fließgewässer und hyporheischer Zone

Heft 116/2000
Sieker, H. Generelle Planung der Regenwasserbewirtschaftung in Siedlungsgebieten

Heft 117/2001
Hailu, D. Optimal planning and water management of irrigation systems

Heft 118/2001
Lohr, H. Simulation, Bewertung und Optimierung von Betriebsregeln für wasserwirtschaftliche Speichersysteme

Heft 119/2001
Bente, St. Eine Software-gestützte Methodik zur Voreinschätzung der wasserwirtschaftlichen Auswirkungen von Maßnahmen der naturnahen Regenwasserbewirtschaftung

Heft 120/2001
Zanke, U. Zum Einfluß der Turbulenz auf den Beginn der Sedimentbewegung

Heft 121/2002
Hirschhäuser, T., Zanke, U. Morphologische Langfristprognose für das System Tidebecken-Außensände am Beispiel Sylts und der Dithmarscher Bucht

Heft 122/2002 Darmstädter Wasserbauliches Kolloquium 2000
Integrierte Gewässerbewirtschaftung in Verwaltung, Wissenschaft und Praxis

Heft 123/2002
Kraus, T. Rauheitsänderung durch Biofilmbewuchs in Druckrohrleitungen

Heft 124/2002
Luckner, T. Zum Bewegungsbeginn von Sedimenten

Heft 125/2002
Holfelder, T. Temperaturbeeinflußte Transportprozesse in Kapillarsperren zur Oberflächenabdichtung von Deponien und Altlasten

Heft 126/2003
Mewis, P. Morphodynamisch-numerische Modellierung von Flußkurven

Heft 127/2003
Wetzstein, A. Berechnung von Entlastungsabflüssen an gedrosselten Streichwehren auf der Basis von gemessenen Wasserständen

Heft 128/2003
Hirschhäuser,T. Sedimentologische und biologische Aspekte der morphodynamischen Modellierung von Tidebecken

Heft 129/2003 Darmstädter Wasserbauliches Kolloquium 2003 „Hochwasserschutz“

Heft 130/2003 Darmstädter Wasserbauliches Kolloquium 2001
Aktuelle Themen aus Hydromechanik, Wasserbau und Hydrologie

Heft 131/2003
Witting, M. Simulation von Küstenlängs- und Küstenquertransport im 2DH-morphodynamischen Modell TIMOR3

Heft 132/2003
Krebs, M. Untersuchung instationärer oszillierender Strömungen in buhnenverbauten Flußabschnitten und ihre Bedeutung für morphodynamische Berechnungen

Heft 133/2004
Kudo, Eiji Sustainable Water Management in an Urbanizing River Basin in Japan, Based on Integrated Modeling Technique

Heft 134/2005
Gebrewubet, Y. Numerical Modeling of Koka Reservoir Sedimentation

Heft 135/2006
Schadrac, I. Nouvelle approche méthodologique pour l‘analyse de la sécurité hydrologique des barrages en contexte sahélien soumis à une variabilité climatique

Heft 136/2006
Link, O. Untersuchung der Kolkung an einem schlanken zylindrischen Pfeiler in sandigem Boden

Heft 137/2006
Muschalla, D. Evolutionäre multikriterielle Optimierung komplexer wasserwirtschaftlicher Systeme

Heft 138/2006
Klawitter, A Ein Modellkonzept zur integrativen Betrachtung von Urban- und Ruralhydrologie auf Einzugsgebietsebene

Heft 139/2006 Darmstädter Wasserbauliches Kolloquium / DWA-Seminar 2005 „Feststofftransportmodelle“

Heft 140/2006
Wurpts, A. Numerische Simulation von Dichteeffekten am Beispiel der Umlagerung von Baggergut im Ästuarbereich

Heft 141/2007
Seydell, I. Einlagerung von Feinstoffen in eine Flusssohle und Wasseraustausch zwischen Fluss und Interstitial – Naturuntersuchungen an einer Kiesquerbank der Lahn bei Marburg

Heft 142/2007
Döring, M. Römische Häfen, Aquädukte und Zisternen in Campanien: Bestandsaufnahme der antiken Wasserbauten

Heft 143/2007
Winterscheid, A. Szenariotechnik im Hochwasserrisikomanagement

Heft 144/2008
Zanke, U.C.E. On Applicability of Morphodynamic Acceleration in Morphodynamic Simulations

Heft 145/2009
Schröter, K.A. Contribution to the Uncertainty Analysis of Distributed Hydrological Models

Heft 146/2009
Roland, A. Entwicklung von WWM II -Zur Seegangsmodellierung auf unregelmäßigen Gitternetzen-

Heft 147/2009
Wiesemann, J.-U. Zum Sedimenttransport auf quergeneigter Sohle

Heft 148/2011
Zhou, X. Morphodynamic Response of Yangtze River Estruary to Sea Level Rise and Human Interferences

Heft 149/2011
Diab, R. Experimental Investigation on Scouring around Piers of different Shape and Alignment in Gravel

---

**) Selbstkostenpreis EURO 20,-- je Heft. Bestellungen beim

Institut für Wasserbau und Wasserwirtschaft
Fachgebiet Ingenieurhydrologie und Wasserbewirtschaftung
Petersenstraße 13, D-64287 Darmstadt

oder

Institut für Wasserbau und Wasserwirtschaft, Fachgebiet Wasserbau
Rundeturmstraße 1, D-64283 Darmstadt,
per Fax: 06151/16-3223, per E-Mail: zeitler@wb.tu-darmstadt.de

ISSN-Nr.: 1430-3434

ISBN: 3-936146-29-2